Deformability of cancer cells on 3D microstructured surfaces

Nayana Tusamda Wakhloo

DEFORMABILITY OF CANCER CELLS ON 3D MICROSTRUCTURED SURFACES

DÉFORMABILITÉ DE CELLULES CANCÉREUSES SUR DES SURFACES MICROSTRUCTURÉES EN 3D

Nayana TUSAMDA WAKHLOO

Doctorat de Biophysique

Institut de Science des Matériaux de Mulhouse,
Université de Haute-Alsace, CNRS UMR 7361, Mulhouse

Unité INSERM U1113, Strasbourg

Thèse soutenue le 13 Novembre 2018

Rapporteur	Dr. Julie PLASTINO	Institut Curie, Paris
Rapporteur	Dr. René-Marc MEGE	Institut Jacques Monod
Examinateur	Dr. Matthieu PIEL	Institut Curie, Paris
Examinateur	Dr. Jürgen RÜHE	IMTEK, Freiburg
Examinateur	Dr. Daniel RIVELINE	IGBMC, Université de Strasbourg
Examinateur	Dr. Laurent PIEUCHOT	IS2M, Mulhouse
Co-directeur de these	Dr. Jean-Noël FREUND	INSERM, Strasbourg
Directeur de thèse	Dr. Karine ANSELME	IS2M, Mulhouse

Title: DEFORMABILITY OF CANCER CELLS ON 3D MICROSTRUCTURED SURFACES

ABSTRACT

This thesis deals with understanding the behaviour of different cancer cell types on microstructured topography. We studied the behaviour of osteosarcoma cell line (SaOS-2) on confined micropillar structures and in particular their nuclear deformation. We analysed the role of the cytoskeleton, focal adhesions (FAs), nucleoskeleton (LINC and lamin A) and chromatin in SaOS-2 deformation on micropillar topography. Actomyosin and vimentin intermediate filament were shown to play a crucial role in orchestrating nuclear deformation. We found that FAs arrangement was mostly on side walls of pillars and that the LINC-cytoskeletal connection was essential for the nuclear deformation process but not lamin A. Employing chemo-topography modulations of pillars and a computational simulation model we demonstrated that the pulling down forces and not pushing down forces drive the cellular-nuclear deformation in osteosarcoma cells.

We also studied the nuclear deformation of SaOS-2 on hydrogel micropillars with different stiffness and chemistry. We saw that cell morphology, actin organization and FAs behaviour was modulated by the substrate mechanics and chemistry. To explore the role of cancer origin, we examined the behaviour of various colon carcinomas on various micro-topographies and found that the epithelial origin cancers are less responsive to microscale topography compared to mesenchymal origin cancerous cells. However, their behaviour was affected on large pits which resembled the intestinal crypt and villi arrangement in terms of size.

Keywords: Cell, nucleus, deformation, cancer, topography, rigidity, LINC, actomyosin, vimentin intermediate filaments, forces, focal adhesions, hydrogels, pits, pillars

Titre: DÉFORMABILITÉ DE CELLULES CANCÉREUSES SUR DES SURFACES 3D MICROSTRUCTURÉES

RÉSUMÉ

Cette thèse traite de la compréhension du comportement de différents types de cellules cancéreuses sur des surfaces microstructurées. Nous avons étudié le comportement de cellules issues d'ostéosarcome (SaOS-2) et en particulier leur déformation nucléaire sur des micro-piliers confinés. Nous avons analysé le rôle du cytosquelette, des adhésions focales (AF), du nucléosquelette (LINC et lamin A) et de la chromatine, sur cette déformation. L'actomyosine et les filaments intermédiaires de vimentine jouent un rôle crucial dans l'orchestration de la déformation nucléaire. Nous avons constaté que la disposition des AF était principalement sur les parois latérales des piliers et que la connexion LINC-cytosquelette était essentielle pour le processus de déformation nucléaire contrairement à la lamine A. En utilisant des modulations chimio-topographiques des micro-piliers et un modèle de simulation numérique, nous avons démontré que ce sont les forces de traction et non pas les forces de poussée qui permettent la déformation cellulaire et nucléaire des cellules d'ostéosarcome.

Nous avons également étudié la déformation nucléaire de SaOS-2 sur des micropiliers en hydrogel présentant différentes chimies et rigidités. Nous avons vu que la morphologie cellulaire, l'organisation de l'actine et le comportement des AF étaient modulés par la chimie et la mécanique du substrat. Pour explorer le rôle de l'origine du cancer, nous avons examiné le comportement de divers carcinomes du côlon sur des microtopographies différentes et constaté que les cancers d'origine épithéliale étaient moins sensibles à la microtopographie que les cellules cancéreuses d'origine mésenchymateuse. Par contre, leur comportement était affecté de manière plus visible sur des grandes cavités plus proches en termes de taille de celles des cryptes et villosités intestinales.

Mots-clés: cellule, noyau, déformation, cancer, topographie, rigidité, LINC, actomyosine, filaments intermédiaires de vimentine, forces, adhésions focales, hydrogels, cavités, piliers.

ACKNOWLEDGEMENTS

I would like to express my gratitude to various people that help me complete my PhD work successfully. In my journey towards this degree I have found a teacher, an inspiration, role model and a pillar of support in my supervisor of PhD thesis, Dr. Karine Anselme. I express my heartiest gratitude to her for providing me with all the freedom to pursue my research and constantly guiding, helping and being extremely understanding throughout the thesis. Without her able guidance, this thesis would not have been possible and I shall eternally be grateful to her for her assistance. I would also like to thank my co-supervisors and collaborators Dr. Jean Noel Freund from INSERM for proving the colon cancer cells and giving valuable inputs for thesis and my paper and Dr. Jürgen Rühe at IMTEK for guiding me as well for my paper and in the hydrogel project. I am also thankful to Sebastian Anders for being a supportive collaborator and providing the hydrogels for the thesis. Thanks to Dr. Felix Sima for providing the substrates for colon cancer project. I am greatly thankful to IRTG committee for the conferences, seminar and making me think in broad prospect beyond my thesis topic.

I am really fortunate to have lab members to always mentor and channelled me in the right direction. I have loved working with them as a team these past few years. I would specially like to thank Dr. Isabelle Brigaud to not only mentor me for experiments but for her immense support as a best friend and her always helpful and cheerful behaviour. I deeply thank Dr. Laurent Pieuchot for guiding me in my PhD and also providing me with an opportunity for being a part in his project and paper. I thank Tatiana Petithory for teaching me the confocal microscopy and helping me during my thesis with many other aspects. I would also like to thank Dr. Arnaud Ponche for guidance and input during my thesis. I would like extend my sincere gratitude to Dr. Patricia Davidson for being my jury member during midterm defense and her valuable inputs for my paper and experiments. I would like to thank all the people who helped me for my paper and did computational experiments. These include Florent Badique, Melanie Eichhorn, Maxime Vassaux, Jean-Louis Milan. Their support, encouragement and incredible inputs have been great contributors in the completion of the PhD thesis.

On personal level I would thank all the people who supported me and made my PhD journey easier. It includes my best friends Adeline Marguier and Charline Soraru and their families

for their immense and incredible support during my thesis and my stay in France. They supported me with every aspect of my PhD and personal life during these past few years.

My acknowledgement would be incomplete without thanking the biggest source of my strength, my family. In particular, I would like to deeply thank my family, my father Inderraj Tusamda for being extremely encouraging and supportive, my late mother ManjitKaur Tusamda for her unwavering love and my brother BhupenderSingh Tusamda for always being there for me. I would like to express my gratitude and love to my husband, Tapaswi Wakhloo for his unconditional love, support and patience and my father and mother in law for their understanding and encouragement. I would like to thank God for providing me strength and patience, knowledge, ability to successfully overcome every obstacle and hardship to achieve things in my life.

I would like to dedicate this work to my family- Father Inderraj Tusamda, Late Mother ManjitKaur Tusamda, Brother BhupenderSingh Tusamda and my husband Tapaswi Wakhloo because of whom I would not have been where I am today. I love you all and I am eternally thankful for everything you all did in my life.

Nayana Tusamda. Wakhloo

13. Nov. 2018

INDEX

Title: DEFORMABILITY OF CANCER CELLS ON 3D MICROSTRUCTURED SURFACES II

Titre: DÉFORMABILITÉ DE CELLULES CANCÉREUSES SUR DES SURFACES 3D MICROSTRUCTURÉES IV

ACKNOWLEDGEMENTS VI

Abbreviations XII

RÉSUMÉ DU CHAPITRE 1 - INTRODUCTION 16

CHAPTER 1. INTRODUCTION 20

1.1 CANCER 20
1.2 SPATIAL AWARENESS DURING METASTATIC MIGRATION 21
1.3 ECM CUES AND MIGRATION 22
1.3.1 SOLUBLE FACTORS 22
1.3.2 MECHANICAL CUES- STRESS 24
1.3.3 TOPOGRAPHY CUES 26
1.3.4 RIGIDITY CUES 27
1.4 CELLULAR MECHANOTRANSDUCTION AND MECHANOSENSORS 27
1.4.1 STRESS ACTIVATED CHANNELS 28
1.4.2 INTEGRINS AND THE ASSOCIATED KINASES 28
1.4.3 FOCAL ADHESIONS 29
1.4.4 CYTOSKELETON AND NUCLEUS 31
1.5 BIOMECHANICS OF CYTOSKELETON IN MECHANOTRANSDUCTION 31
1.5.1 MICROFILAMENTS 32
1.5.2 MICROTUBULES 34
1.5.3 INTERMEDIATE FILAMENTS 35
1.6 BIOMECHANICS OF NUCLEUS IN MECHANOTRANSDUCTION 37
1.6.1 NUCLEAR STRUCTURE 38
1.6.1.1 NUCLEAR MEMBRANE AND PORES 38
1.6.1.2 LINC COMPLEX 38
1.6.1.3 NUCLEAR LAMINA 39
1.6.2 NUCLEAR DEFORMATION 41
1.6.2.1 NUCLEUS DEFORMATION DURING MIGRATION 41
1.6.2.2 NUCLEUS DEFORMATION DUE TO STRESS 42
1.6.2.3 INTRACELLULAR COMPONENTS INVOLVED IN NUCLEAR DEFORMATION 42
1.6.2.4 ROLE OF NUCLEUS AS MECHANOSENSOR 43
1.7 CELLULAR TENSEGRITY MODEL 44
1.8 ENGINEERING BIOMATERIALS TO MIMIC EXTRACELLULAR MATRIX- *IN VITRO* MECHANOTRANSDUCTION 46
1.8.1 FABRICATION OF POLYMERS USING LITHOGRAPHY 47
1.8.2 PATTERNING SUBSTRATES- IMPORTANCE OF PILLAR SUBSTRATES TOPOGRAPHY TO STUDY CELL BEHAVIOUR 49
1.9 OUTLOOK AND OBJECTIVE OF THESIS STUDY 52

RÉSUMÉ DU CHAPITRE 2 - MÉCANISMES DE DÉFORMATION DE CELLULES D'OSTÉOSARCOME SUR DES MICRO-PILIERS55

CHAPTER 2. DEFORMATION MECHANISMS OF OSTEOSARCOMA CELLS ON MICROPILLAR ARRAY 59

2.1 BACKGROUND 59
2.2 MANUSCRIPT- PULLING FORCE BY ACTOMYOSIN & LINC TAILORS METASTATIC NUCLEAR DISTORTION IN TOPOGRAPHICALLY-INDUCED SELF-CONFINEMENT 63

RÉSUMÉ DU CHAPITRE 3 - HYDROGELS BIOMIMÉTIQUES – CONTRÔLE DE LA RIGIDITÉ POUR ÉTUDIER LES INTERACTIONS CELLULAIRES 99

CHAPTER 3. BIOMIMETIC HYDROGELS- TUNING STIFFNESS TO INVESTIGATE CELLULAR INTERACTIONS 103

3.1 BACKGROUND 103
3.2 MECHANISM OF CELL BEHAVIOUR ON DIFFERENT RIGIDITIES 106
3.3 NEED OF SUBSTRATES WITH TUNABLE RIGIDITY 107
3.4 HYDROGELS – OVERVIEW 107
3.5 CANCER CELL RESPONSE TO 2D/3D HYDROGEL ENVIRONMENT 108
3.6 OBJECTIVES OF THIS CHAPTER 111
3.7 METHODS 111
3.7.1 SUBSTRATE FABRICATION 111
3.7.2 SUBSTRATE CHEMISTRY COATING 112
3.7.3 YOUNG'S MODULUS MEASUREMENT 113
3.7.4 CELL SEEDING 113
3.7.5 CELL CULTURE 113
3.7.6 IMMUNOSTAINING 114
3.7.6 CONFOCAL IMAGING 114
3.7.7 IMAGE ANALYSIS AND QUANTIFICATION 114
3.7.8 STATISTICAL ANALYSIS 115
3.8 RESULTS AND DISCUSSION 115
3.8.1 CHARACTERIZATION OF TOPOGRAPHY AND CELL BEHAVIOUR ON HYDROGEL POLYMERS 115
3.8.2 FAS ORGANIZATION AND NUCLEAR DEFORMATION ON DIFFERENT RIGIDITY 116
3.8.3 CELL AREA, SPREADING AND ACTIN ORGANIZATION ON DIFFERENT MATRIX RIGIDITY 117
3.8.4 EFFECT OF RIGIDITY ON TAZ 118
3.8.4 CONTROLLING CELL BEHAVIOUR WITH CHEMISTRY MODULATIONS 118
3.9 DISCUSSION 120
3.10 CONCLUSION 124

RÉSUMÉ DU CHAPITRE 4 - COMPORTEMENT DE CELLULES DE CARCINOME DE COLON SUR DES SURFACES MICROSTRUCTURÉES 126

CHAPTER 4. COLON CARCINOMA CELL BEHAVIOUR ON MICROSTRUCTURED SURFACES 130

4.1 INTRODUCTION 130
4.2 COLORECTAL ADENOMA-CARCINOMA SEQUENCE 130
4.3 MECHANISMS OF DEVELOPMENT OF CRCS 131
4.4 GENES MUTATED AND DYSREGULATED IN CRCS 132
4.4.2 TUMOR SUPPRESSOR GENES IN CRCS 132
4.4.2.1 APC GENE 133
4.4.2.2 CDX2 GENE 134
4.5 MECHANOTRANSDUCTION IN CANCER CELLS 135
4.6 EFFECT OF MECHANICAL CUES-RIGIDITY, SHEAR STRESS, STRAIN ON BEHAVIOUR OF CRCS 136

4.7 EFFECT OF TOPOGRAPHY ON BEHAVIOUR OF CRCS AND OTHER EPITHELIAL CELLS 137
4.8 OBJECTIVES OF THIS CHAPTER 139
4.9 METHODS 140
4.9.1 SUBSTRATE FABRICATION 140
4.9.2 CELL CULTURE 145
4.9.3 IMMUNOSTAINING 146
4.9.4 RT-QPCR AND WESTERN BLOT ANALYSIS 147
4.9.5 QUANTIFICATION OF RATIO OF MRNA LEVELS 147
4.9.6 CONFOCAL IMAGING, IMAGE AND STATISTICAL ANALYSIS 147
4.10 RESULTS AND DISCUSSION 147
4.10.1 CHARACTERIZATION OF COLORECTAL CANCER (CRC) CELLS ON FLAT SURFACE (*FIG 4.5*) 147
4.10.2 MRNA EXPRESSION OF NUCLEAR PROTEINS IN CRC CELLS ON FLAT SUBSTRATE 148
4.10.3 MRNA EXPRESSION OF NON-MUSCLE MYOSIN IN CRC CELLS ON FLAT SUBSTRATE 151
4.10.4 FOCAL ADHESIONS, CYTOSKELETON AND E-CADHERIN DISTRIBUTION IN CRC CELLS ON MICROPILLARS 153
4.10.5 NUCLEAR DEFORMATION IN 5 INITIAL CRC CELLS ON MICROPILLARS 156
4.10.6 NUCLEAR DEFORMATION IN APC-/+ AND TG8/TW6 CRC CELLS ON MICROPILLARS 158
4.10.7 LAMIN A/C DISTRIBUTION IN APC-/+ AND TG8/TW6 CELL LINES ON MICROPILLARS 159
..... 160
4.10.8 CRC CELLS ON GROOVE TOPOGRAPHY 161
4.10.9 CRC CELLS ON WELLS/PITS TOPOGRAPHY 169
4.11 CONCLUSION 172

RÉSUMÉ DU CHAPITRE 5 - PERSPECTIVES ***175***

CHAPTER 5. PERSPECTIVES ***178***

5.1 OSTEOSARCOMA CELL RESPONSE TO TOPOGRAPHY 179
5.2 OSTEOSARCOMA CELL RESPONSE TO TOPOGRAPHY SUBSTRATES TUNED TO RIGIDITY AND CHEMISTRY 183
5.3 COLON CARCINOMA CELL BEHAVIOUR ON SUBSTRATES WITH DIFFERENT TOPOGRAPHY 190

References ***194***

ABBREVIATIONS

4.1R	erythrocyte membrane protein band 4.1
ADP	Adenosine di-phosphate
AFM	atomic force microscopy
APC	adenomatous polyposis coli
ARP2/3	actin related protein 2/3
CAMKII	calmodulin-dependent protein kinase II
CBS	Cajal bodies
CDC2	Cyclin-dependent kinase 2
CDC42	Cell division control protein 42
CHO1	CDP-diacylglycerol--serine O-phosphatidyltransferase
CSK	cytoskeletal
DMAA	*N*, *N*-dimethyl acrylamide
DNA	Deoxyribonucleic acid
ECM	Extracellular matrix
EGF	Epidermal Growth factor
EMT	epithelial to mesenchymal transitions
ERK	extracellular signal-regulated kinases
ESCRT III	endosomal sorting complex required for transport III
FAK	focal adhesion kinases
FAS	focal adhesions
FGF	Fibroblast growth factor
FN	fibronectin
FRET	fluorescence resonance energy transfer
GFAP	glial fibrillary acidic protein
GPCRS	G-protein coupled receptors
H3K9	Histone H3 Lysine 9
HESC	human embryonic stem cells
HGF	Hepatocyte Growth factor
IFS	Intermediate filaments
ILK	integrin-linked kinases
INM	inner nuclear membrane
KASH	Klarsicht, ANC-1, Syne Homology
KIFS	Keratins Intermediate filaments
LAP2A	Lamina-associated polypeptide 2 α
LAPS	lamina-associated polypeptides
LBR	Lamin B receptor
LINC	Linker of nucleus cytoskeleton
LMNA	Lamin A
LMNB1	Lamin B1
LMNB2	Lamin B2
MABP	methylacryloyloxybenzophenone
MAN1	Mannosidases alpha class 1
MAPK	mitogen-activated protein kinase
MARS	matrix attachment regions
MDCK	Madin-Darby Canine Kidney
MKLP1	Mitotic kinesin like protein 1
MMP	matrix metalloproteinases

MRNA	Messenger ribo-nucleic acid
MSCS	Mesenchymal Stem Cells
MYC	Myelocytomatosis
NADPH	Nicotinamide adenine dinucleotide phosphate
NF-KB	nuclear factor-κB
NOX2	NADPH oxidase 2
ONM	Outer nuclear membrane
P53	Tumor protein 53
PAA	Poly acrylic acid
PDGF	Platelet derived growth factor
PDMS	Polydimethylsiloxane
PEO	poly ethylene oxide
PGA	poly glycolic acid
PKCE	Protein kinase C - ε
PLA	poly lactic acid
PLGA	poly lactic-co-glycolic acid
PML-NBS	promyelocytic leukemia nuclear bodies
PRB	Retinoblastoma protein
PTEN	Phosphatase and tensin homolog
PVA	poly vinyl alcohol
RAC1	Ras-Related C3 Botulinum Toxin Substrate 1
RAS	Rat sarcoma
RHO A	Ras homolog A
ROCK	Rho Associated Coiled-Coil Containing Protein Kinase
SNRNP	small nuclear-ribonucleoproteins
SOX2	SRY-box 2
SSNA	sodium 4-vinylbenzenesulfonate
ST5	Suppression Of Tumorigenicity 5
SUN	Sad1 And UNC84 Domain Containing
SYNES	synaptic nuclear envelope proteins
TACS	tumor–associated collagen signatures
TAN	transmembrane actin-associated nuclear
TAZ	Tafazzin
TGF	Transforming Growth factor
TIFP	Tissue interstitial fluid pressure
TNM	Tumor-nodes-metastasis
TRCS	Tumor repopulating cells
TRK	tyrosine kinase
VIFS	Vimentin Intermediate filaments
VSMCS	vascular smooth muscle cells
WASP	Wiskott–Aldrich Syndrome protein
WNT	Wingless-Type MMTV Integration Site Family
X-ROS	reactive oxygen species
YAP	yes-associated protein 1
CRC	colorectal cancers
KRAS	V-Ki-Ras2 Kirsten Rat Sarcoma 2 Viral Oncogene Homolog
CIMP	CpG island methylator phenotype
MSI	microsatellite instability
CIN	Chromosomal instability

MGMT	O^6-methylguanine DNA methyltransferase
MLH1	MutL homolog 1
BRAF	v-raf murine sarcoma viral oncogene homolog B1
CDX2	Caudal Type Homeobox 2
CRD-BP	Coding Region Determinant-Binding Protein
EMT	Epithelial to mesenchymal transitions

RÉSUMÉ DU CHAPITRE 1 - INTRODUCTION

Le cancer est une prolifération incontrôlée de cellules conduisant à une tumeur et à sa propagation dans différentes parties du corps par le processus de métastases. La majorité des cancers sont dus à des mutations génétiques ou à des facteurs environnementaux. Le cancer peut présenter différents stades. Le «stade I» implique la formation d'une tumeur par division cellulaire incontrôlée mais qui reste dans son site d'origine. Le «stade II» représente un type de tumeur cancéreuse précoce qui n'a pas poussé profondément dans les tissus natifs et qui est guérissable. Le «stade III» indique une tumeur qui s'est développée profondément dans les tissus voisins et le «stade IV» signifie que le cancer est métastatique et s'est propagé à d'autres parties du corps.

La métastase est l'une des caractéristiques du cancer et est responsable de plus de 90% des décès liés au cancer dans le monde. Les cellules migrent et se propagent à différentes parties du corps en créant une tumeur ailleurs que dans les sites primaires d'origine. Cette migration se fait à travers divers microenvironnements tels que les vaisseaux sanguins, les vaisseaux lymphatiques et les tissus. La migration des cellules tumorales est un processus efficace impliquant des événements coordonnés. L'invasion tissulaire est la première étape où les cellules tumorales envahissent les tissus environnants, entraînant leur libération dans les vaisseaux sanguins et leur activation par le facteur d'activation des plaquettes, par un processus appelé «intravasation». Après l'intravasation, les cellules cancéreuses migrent vers différentes parties du corps en circulant dans le sang. La sortie des cellules en migration des vaisseaux sanguins se fait par un processus appel «extravasation» qui se produit par migration cellulaire active à travers les parois des capillaires. Enfin, les cellules cancéreuses se divisent dans ce nouvel emplacement pour former une tumeur secondaire menant à la métastase.

La capacité des cellules cancéreuses à migrer avec succès dans différents habitats dépend

en partie des forces mécaniques et des interactions physiques que la cellule établit avec son microenvironnement. La matrice extracellulaire peut soit favoriser la progression des cellules invasives, soit au contraire favoriser de leur part un comportement de cellules saines. Au cours des dernières décennies, il a été observé que les indices mécaniques du microenvironnement tumoral, tels que la topographie, la rigidité, le confinement ou l'étirement mécanique, déterminent le comportement des cellules lors de leur migration. Malgré un grand nombre de recherches en cours, le comportement des cellules cancéreuses en réponse à ces signaux reste encore à élucider.

Ces signaux sont «détectés» par les senseurs mécaniques (ou mécanosenseurs) des cellules qui transforment les signaux mécaniques en signaux biochimiques grâce aux voies de mécanotransduction modifiant ainsi le comportement des cellules. Ces signaux biochimiques peuvent induire un remodelage du cytosquelette, du nucléosquelette, et modifier la dynamique des protéines des voies de signalisation. La première ligne de mécanosenseurs est située à la périphérie des cellules au niveau des sites d'adhésion, des jonctions cellule-cellule, des récepteurs membranaires ou des canaux ioniques. L'autre ligne de mécanosenseurs comprend les protéines du cytosquelette, les protéines du nucléosquelette (complexe LINC), la membrane nucléaire et la chromatine. Ces senseurs sont responsables non seulement de l’entrée des signaux mécaniques dans la cellule mais aussi de leur transmission vers l’extérieur de la cellule. Par conséquent, il est essentiel d'élucider le rôle de ces mécanosenseurs dans la modulation du comportement des cellules en réponse à des caractéristiques de l’environnement cellulaire tels que la topographie ou la rigidité.

L'ingénierie tissulaire a émergé il y a plus de vingt ans comme une ère nouvelle et prometteuse dans le domaine de la régénération des organes. Les progrès les plus récents dans ce domaine ont concerné la création de nano- et de micro-topographies pour étudier le comportement des cellules dans un environnement 3D comparable à leur environnement naturel. En particulier, la fabrication de surfaces contrôlées à l'échelle nanométrique et à l'échelle microscopique et l'étude des réponses cellulaires sur ces dernières nous ont permis de mieux comprendre la mécanotransduction induite par les biointerfaces. Les micropiliers se sont révélés être des topographies particulièrement intéressantes notamment dans les recherches sur le comportement des cellules cancéreuses. Les micropiliers se sont avérés affecter le comportement des cellules de nombreuses manières.

Notre laboratoire a commencé à utiliser les micropiliers pour étudier la déformation cellulaire et nucléaire il y a plus de dix ans. Nous avons pu démontrer que cette capacité de déformation était caractéristique des cellules métastatiques par opposition aux cellules saines. Dans cette thèse, nous nous concentrerons sur l'élucidation des mécanismes qui permettent aux cellules métastatiques de déformer leurs noyaux dans un réseau de micropiliers

CHAPTER 1. INTRODUCTION

1.1 CANCER

Cancer is a disease involving abnormal cell growth leading to a tumor or neoplasm and its spreading to different parts of the body. The word 'cancer' is a *Latin* word for crab, as the cancer cells possess finger like projections during spreading. Cancer was first accredited at around 1980 to dysregulation of genes. Since then decades of research have laid down a foundation to unravel the intricate behaviour of different types of cancers. Majority of cancers are caused due to genetic mutations or environmental factors. Neoplastic cells acquire genetic aberrations and epigenetic alterations leading to tumor growth. The genes affected by aberrations can be classified into either "activating" or "inactivating" mutations[1]. Oncogenes that gain a function during mutation fall into activating mutation category. Somatic mutations of oncogenes, also known as 'proto-oncogenes', leads to cancer. RAS, WNT, MYC, ERK and TRK are potent proto-oncogenes. On the contrary, tumor suppressor genes or anti-oncogenes are ones that loose a function during mutation and are categorized as inactivating mutations. These tumor suppressor genes safeguards a cell and inhibits tumor formation. pRb, p53, PTEN, APC, ST5, etc. are examples of anti-oncogenes.

Cancers can be classified depending on the cell type. Cancers arising from epithelial (intestinal, mammary, etc.,) cells are called "carcinomas", whereas cancers of connective tissue (bone, cartilage, etc) are denoted as "sarcomas". "Leukaemia and lymphomas" are cancers attributing to blood cells and "blastoma" are the cancers derived from precursor or embryonic cells. The last category of cancers includes "germ cell tumors" that arise from pluripotent cells mostly in testicles or ovaries. To evaluate the stages of cancer, doctors generally use the "TNM" system for cancer identification. The letter "T-Tumor" describes the size and location of cancer,

letter “N-Nodes” represents the tumor growth in lymph nodes and the letter “M-Metastasis” indicates the cancer progression to other parts of the body. In addition to “TNM” categorization, cancer can also be divided into stages I to IV. Stage I includes early type of cancer tumor which has not grown deeply in the native tissues and is curable. Stage II means that tumor is larger than stage one but hasn’t started to spread around in nearby tissues. Stage III indicates neoplasm which has grown deeply in the nearby tissues and spread to lymph nodes in nearby areas. “Stage IV” means that’s cancer is metastatic and has spread to other parts of body.

1.2 SPATIAL AWARENESS DURING METASTATIC MIGRATION

Metastasis is one of the hallmarks of cancer and is responsible for more than 90% of cancer related deaths worldwide. The cells migrate and spread to different parts of the body creating tumor other than in the primary site of origin. This migration occurs through diverse microenvironments like stroma, blood vessels, vascular systems and the tissues. Migration of the tumor cells is a proficient process of co-ordinated events[2]. Tissue invasion is the initial step where tumor cells invade the surrounding tissue leading to their release in blood vessel by a process called “intravasation”. Following intravasation the cancer cells migrate to different parts of the body by circulating through the blood stream. Exit of migrating cells from blood vessels is brought about by process called “extravasation” which occurs via active cell migration through capillary walls. Finally, the cancer cells start dividing in this new location to form a secondary tumor leading to metastasis (*fig 1.1*). The versatile ability of the cancer cells to migrate successfully through different habitats is in part contingent on the mechanical forces and physical interactions of cell with the microenvironment. Cellular behaviour *in vivo* is influenced and governed by certain stimuli or cues arising from the microenvironment of cells[3]. Over the past few decades it has been observed that

mechanical cues from tumor microenvironment such as topography[4], stiffness[5], confinement[6] or mechanical stretching[7] have dictated the behavioural response of cells during migration. Soft fibrin matrix is proven favourable for culturing highly metastatic melanoma cells[8] and stiff matrix of breast tumor promotes mammary epithelium malignancy[9,10]. Thus it can be concluded that cells are not only spatially aware about their surrounding but also register cues from the ECM and integrate them. Even though these papers provide a wealth of insight, the cellular behaviour of different types of cells in response to these cues still remains to be elucidated. To understand this better, we first need to comprehend the different types of cues effecting cellular behaviour *in vivo*.

1.3 ECM CUES AND MIGRATION

1.3.1 Soluble factors

Soluble cues are the ones that are present in the form of molecular compounds that interact with the cell surface receptors and bring about a change in cellular behaviour. These cues can be further divided into two groups: growth factors and inflammatory mediators[11]. Epidermal Growth factor (EGF), Transforming Growth factor (TGF), Fibroblast growth factor (FGF), Platelet derived growth factor (PDGF) and Hepatocyte Growth factor (HGF) are some examples of soluble growth factors. TGF exists in two different polypeptides- α, β and has been known to induce oncogenic response. TGF is known to be dysregulated in various cancers and has been involved in metastasis and stemness[12]. FGF is known to be required for normal growth of cells *in vivo*, however irregularity in the same is the cause of many diseases. They enhance osteoclast function and contribute to the

formation of metastatic lesions in breast cancer[13].

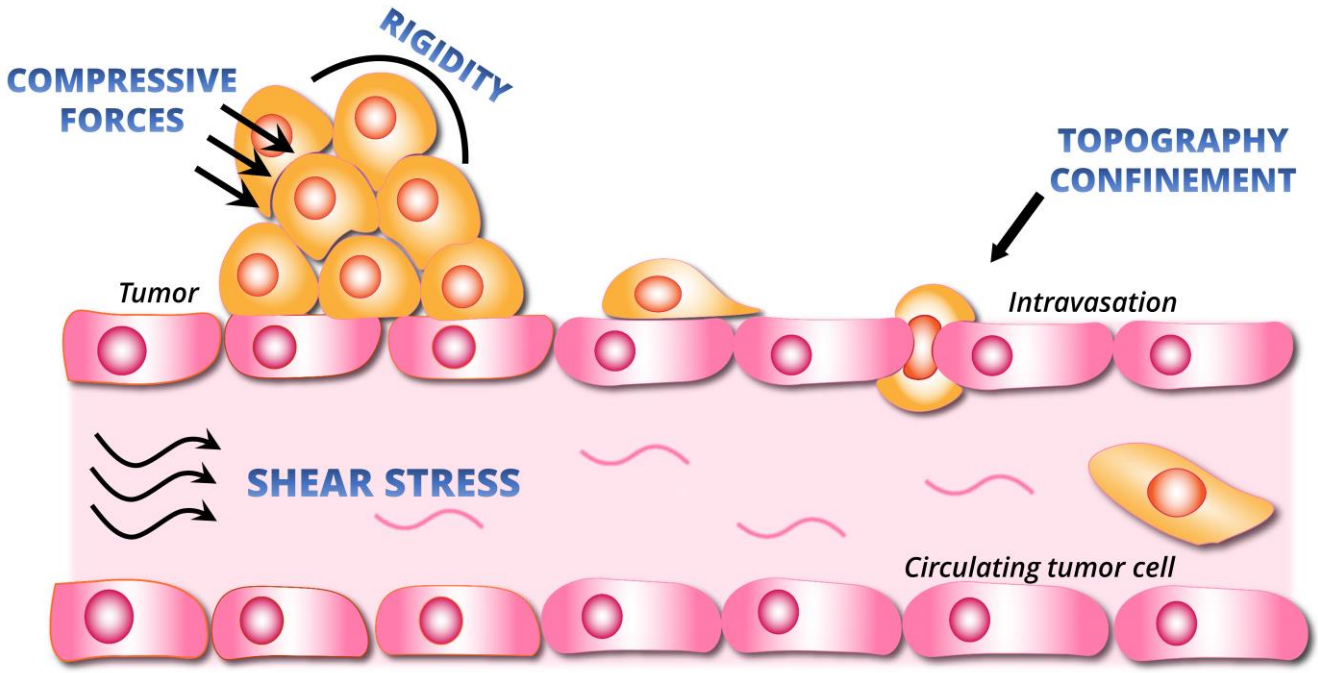

Figure 1.1. *Mechanical cues experienced by cancer cells in in vivo environment. The tumor cell mass itself is known to have rigid environment. Cells growing in tumor also face compressive force while growing in limited space. The metastatic movement requires migration through different topographic confinements. Metastatic cells also experience shear stress during migration through blood vessels or lymphatic or interstitial fluid.*

PDGF is well documented for its role in cell growth and division. It is found to be dysregulated in many cancers like breast, colorectal, lung ovarian, liver, etc[14]. HGF is a paracrine growth factor responsible for growth, motility and morphogenesis and is dysregulated in gastric and lung cancers. Inflammatory mediators include cytokines and chemokines (family of small cytokines), which are responsible for enhancing cell repair and migration. Cytokines are immunomodulating agents responsible for cell signalling. These are specific to the corresponding cell surface receptors and modulate the up and down regulation of various genes. They usually control inflammatory responses but can go awry in chronic infections and induce malignancy[15]. Chemokines are known to act as chemoattractant to navigate cell migration. In cancers cell trafficking in tumor

environment is controlled by chemokines[16]. Interestingly, they have a dual role as many chemokines are also used for immunotherapy.

1.3.2 MECHANICAL CUES- STRESS

There are different types of mechanical cues that the cells encounter, such as tensile, compressive and shear[17] (*fig 1.2*).

- ***Stress***

In physics, stress (σ) is defined as resistance of the object to deform and is generally calculated as the amount of force over a given area (N/m^2) and is expressed in Pascals (Pa). Stress can not only modulate the cellular behaviour of healthy cells but also play an important role in tumor progression and metastasis. It evokes cell response via mechanotransductive pathways that help the cell to sense and convert mechanical signals in biochemical ones.

- ***Tensile stress***

Tensile stress is responsible in expansion of the length of an object. In cells it is responsible for bringing about change in actomyosin contraction in response to surface stiffness *in vitro*. Invasive fronts of cells in collective migration have increased tensile internal stress while travelling through collagenous matrix, thereby propelling the cells and resulting in ECM alignment[18]. These fronts are responsible for creating “paths” for the cells that are following behind.

- ***Shear stress***

Shear stress causes deformation of an object coplanar to the applied stress. Sometimes haemodynamic shear stress is experienced by cancer cells during migration through blood circulatory system[19] or interstitial flow[20] in the ECM of tissue. Moreover, tissue interstitial fluid

pressure (TIFP) is found to be higher in ECM of solid tumors due to dysregulation of lymphatic circulation[21]. This can be a mechanism of the body to destroy invaders and prevent infection or disease. Nevertheless, few circulating cells do survive and are able to create metastasis thereby ensuring cancer progression.

- ***Compression***

Forces like mechanical compression cause the 'squeezing' or compacting of cell bodies. Such a compressive force is known to provoke invasive phenotype in cancer cells[22]. This is because tumor progression in confined spaces exerts a compressive stress on cells and in response the cells might acquire invading phenotype to escape this stress.

- ***External tension (Traction forces)***

Newtonian's 3rd law of physics states that "every action has equal and opposite reaction" and it is applicable to cells as well. If the environment exerts force on cell, the cell also exerts force on ECM. These forces are generally referred to as external tension or traction forces. Cell itself contains an internal stress known as prestress (described further in section 1.7) and during migration this pre-stress is transferred to ECM in the form of traction forces[23]. These forces are responsible for deforming or modulating the ECM around the cell.

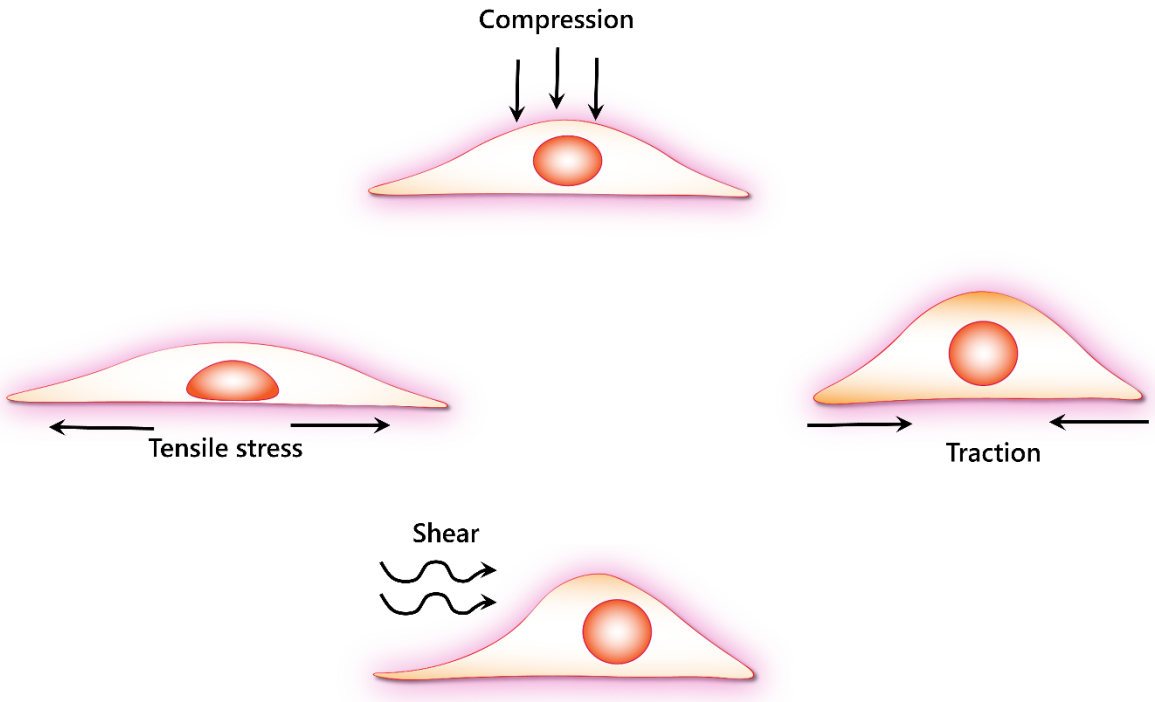

Figure 1.2 *Mechanical stresses experienced by cells. Compression stress due to other cell layers, traction force on extracellular matrix, tensile stress during cell spreading, shear stress during fluid flow.*

1.3.3 TOPOGRAPHY CUES

Topography is defined as the organization of features on an area. These features *in vivo* can be curvatures, confined spaces like pores, collagen fibres, etc. (described in detail in section 1.8.2 and following chapters). 3D matrix *in vivo* creates steric confinements in the form of pores that can impart a physical containment for cell's mechanoresponse[24]. Cell migration is also guided by topography of the underlying matrix[25]. Recently emerged the term "topotaxis" that defines the migration of cells through different topographical features. Interestingly topotaxis depends on interplay between the geometry of the ECM and cell stiffness and is not only applicable to cancer cells but also to healthy cells in processes like wound healing, migration of embryonic cells, etc[26]. The organization of tumor collagen ECM and their dynamic changes, called tumor–associated collagen signatures (TACS), are correlated with metastasis[27]. During normal growth the TACS-1

collagen fibres are arranged in an isotropic arrangement, however they change their conformation to TACS-3, an anisotropic orientation, during tumor progression[28].

1.3.4 RIGIDITY CUES

Rigidity is the stiffness or softness of an object and is a type of passive cue regulating cell behaviour (described in detail in chapter 3). Cell migration *in vivo* is very sensitive to mechanical stiffness of ECM. Cells tend to migrate towards stiff matrix by a process called "durotaxis"[29]. Cancer cells exhibit non-proteolytic migration on relatively soft matrix but a proteolytic migration mode on stiff matrix[5]. Literature suggests that the tumor ECM is stiffer than the healthy counterparts. The turnover of collagen by matrix metalloproteinases (MMPs) is increased during cancer development, leading to a stiff matrix around the tumor[30]. The stiffness is not only the regulator of migration but also causes lineage commitment in mesenchymal stem cells and cancer stem cells[31,32]. Tumor repopulating cells (TRCs) are known to proliferate better in soft gel matrix[33]. TRCs retain their soft structure in order to allow efficient penetration into different tissues and thus possess a unique biochemical feature correlating to rigidity.

1.4 CELLULAR MECHANOTRANSDUCTION AND MECHANOSENSORS

Mechanical cues bring about a change in a cell's behaviour by triggering the mechanotransductive pathways. These pathways are responsible to translate biophysical cues into biochemical ones in order to provoke cellular changes. These biochemical signals can induce remodelling of cytoskeleton, nucleoskeleton protein dynamics or signalling pathways. Cell type and mechanics also plays a role in determining the response of cell to mechanical cues. For example healthy cells respond differently to topography compared to cancerous cells[34–36]. The mechanosensitive mediators of the cell and their mechanics play a vital role in interpreting and bringing about

change in cellular responses. These mediators of the cell are called "mechanosensors" (*fig 1.3*). The first line of mechanosensors are embedded in the cell membrane such as adhesion sites, cell-cell junctions, membrane receptors or ion channels. Other mechanosensors consist of cytoskeletal proteins, nucleoskeletal proteins such as LINC. Changes in gene expressions or in protein structures of those molecules act as mechanosensors that relay or translate mechanical signals in biochemical ones, inside the cell.

1.4.1 STRESS ACTIVATED CHANNELS

Mechanosensitive ion channels or stretch gated ion channels are sensors of touch, hearing, balance, cardiovascular regulation and osmotic homeostasis. These channels are further classified as "cation selective" which are predominant and selective for positive ions, whereas, "anion selective" are less common and have selectivity for negative ions. The best example of stress activated ion channels are the hair of inner ear called stereo-cilia, that transmit signals to central nervous system, allowing us to hear. Shear stress or flow is known to bring about changes in channelling Ca^{2+}, K^{+} and Na^{+} ions and are responsible for bringing about membrane curvature[37] or membrane tension[38]. These channels are highly sensitive to shear stress to as low as 0.01Pa[39]. Details about types of channels and the related mechanisms are discussed excellently in the review by Sanjeev *et al*[40].

1.4.2 INTEGRINS AND THE ASSOCIATED KINASES

Integrins consist of α- and β- subunits and the different combinations of these results in different binding affinities to ECM such as fibronectin, collagen or laminin[41]. 18 α and 8 β-subunits have been identified to form 24 different heterodimer combinations. On the cytoplasmic side, the integrins are connected to focal adhesion complex. These further provide anchorage to F-actin

and guide the mechanotransductive pathways. They are also responsible for exerting traction forces on the ECM, which are channeled from the inside of the cell to outside microenvironment. Kinases such as focal adhesion kinases (FAK) and integrin-linked kinases (ILK) also play a role in mechanotransduction pathways. The mechanical response from the integrins activates several downstream pathways that converge at the activation of mitogen-activated protein kinase (MAPK) phosphorylation or NF-κB activation to bring about mechanotransduction by converting mechanical cues into biochemical ones[42]. Other than these, shear stress in the microenvironments is known to elicit transient increase in Rho A[43] via integrins. Rho A signalling is also linked functionally to MAPK signalling and actin organization[44–46].

1.4.3 FOCAL ADHESIONS

Focal adhesions (FAs) consist of a dynamic scaffold of more than 50 proteins that link the ECM to the actin cytoskeleton. Integrins are the primary modulators of FAs that bring about a change in FAs organization in response to ECM mechanical signals[47,48]. Integrins are connected to the structural protein of FAs called talin which is connected to vinculin, which in turn connects to actin. Vinculin can be recruited at the FAs site in response to mechanical force. Interestingly, Grashoff *et al*., using fluorescence resonance energy transfer (FRET) showed that vinculin is under high tension at newly assembled FAs at leading edge of cell and low tension at disassembling FAs at retracting edge of cells[49]. Other than talin and vinculin, proteins such as α-actinin, filamin, paxillin and tensin also form the structural component of FAs. A stationary FAs exhibits a finite micrometer (1-5μm^2 with lifetime of ~20 min) size. However, as the pulling forces are applied, FAs tend to elongate[50]. A two-spring model theory states that the force at FAs is more in a stiffer environment, thus playing a homeostatic function[51]. Xuan *et al*. show that FAs size increases with decreasing stiffness on

fibrous matrices that might play an important role in tumor progression[52]. Another study shows that FAs increase on decreasing size of nanopillars and exert sufficient forces to bend them[53]. Paxillin phosphorylation is increased in 3D matrix, which in turn increases invasiveness of tumor cells[54,55]. Reduction of stress in ECM reduces the ability of FAs to recruit paxillin. Thus FAs mechanotransduction is a dynamic homeostatic process which self-adjusts itself with respect to rigidity of ECM or intracellular pulling forces[56].

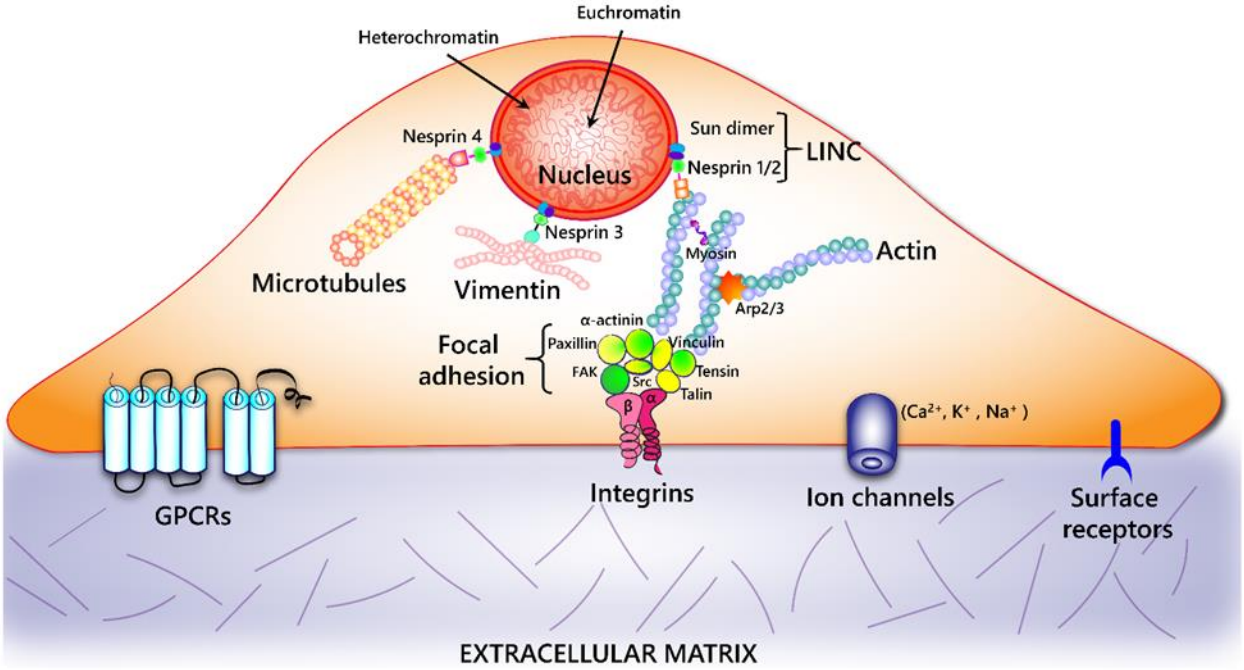

Figure 1.3. *Mechanosensors that 'sense' extracellular matrix cues and bring about cellular and morphological changes. Cell surface receptors like G-protein coupled receptors (GPCRs), integrins, mechanosensing ion channels, cell surface receptors (soluble or chemical molecules) are the ones that bring about 'inside out' or 'outside in' crosstalk in between ECM and cell. Focal adhesions transfer the information to cytoskeletal structures like actin which with their motor protein myosin bring about conformational changes. Arp2/3 brings about nucleation and branching of actin orchestrating actin dynamics. Actin is in turn connected to Sun proteins via nesprins of LINC complex thus organizing nucleus morphology. Different nesprin family members are connected to microtubules and vimentin cytoskeletal components. The euchromatin (loosely arranged) and heterochromatin (tightly arranged) also play important part in guiding the reshaping of nucleus in order to adapt to ECM.*

1.4.4 CYTOSKELETON AND NUCLEUS

Cell maintains its integrity and architecture with the help of cytoskeletal proteins, mainly actin, tubulin and intermediate filaments. Cytoskeleton is a 3D dynamic network that imparts material properties to the cell. Cytoskeleton components contribute to cell stiffness and are also responsible for the viscoelastic properties exhibited by the cell[57]. The cell components are constantly remodelling in order to guide processes like cell migration or division. Recently role of nucleus as a mechanosensor is the topic of great interest[58,59]. Cell is hardwired to nuclear envelope which helps in relaying transformation to the nucleus. Early evidences came from work done by Ingber *et al.* who showed that perturbing actomyosin resulted in nucleus reshaping[60]. In detail description of cytoskeleton and nuclear mechanics is described in section 1.5 and 1.6.

1.5 BIOMECHANICS OF CYTOSKELETON IN MECHANOTRANSDUCTION

Cytoskeleton is a fibrous network of cytoskeletal proteins embedded in the cytoplasm. These proteins are vital for structural integrity and mechanical force generation. Cytoskeletal components form a mesh, that bestow the cell with the calibre to bear the mechanical forces imparted by ECM or cell itself. This ability is greatly due to three cytoskeletal structures- microfilaments, microtubules and intermediate filaments. Together these molecular structures govern the architecture and mechanics of cell and most of them employ “tensegrity” architecture to remodel themselves in order to respond to mechanical forces. Tensegrity architecture is defined by structures that resist tension and compression and balance each other by creating pre-stress (internal tensile stress) or a resting state of isometric tension[61]. Tensegrity theory is usually translated into mathematical terms that aids to define the relationship between cell mechanics and biochemistry of cytoskeleton and their role in mechanotransduction.

1.5.1 MICROFILAMENTS

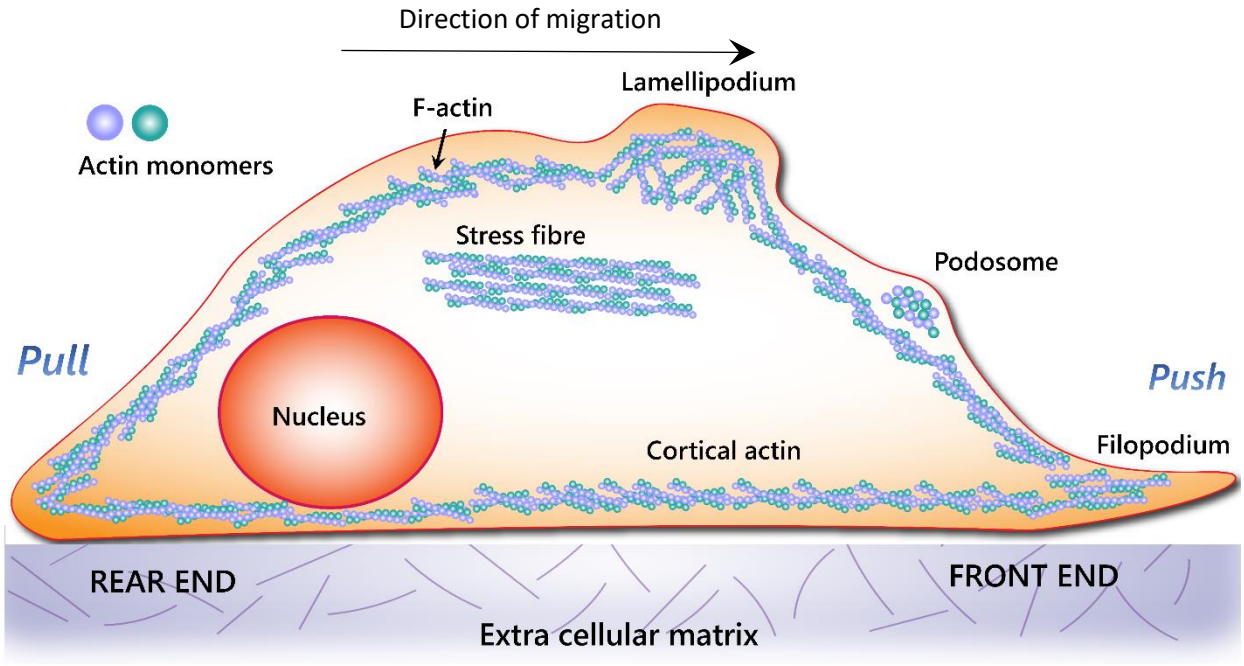

Figure 1.4. *Actin organization in cell. Inspired from[62]. It is the most abundant protein found in the cytoplasm and is organized into cortical actin, filopodium, podosome, lamellipodium and stress fibres. The advancing part is called the front end and the receding part is called the rear end. The front end imparts a pushing force via structures like filopodium and the rear end imparts a pulling force via actomyosin contraction.*

Actin is a globular protein that can polymerize to form 5-9nm thick fibres that impart stiffness to cell structure. They have a persistence length (distance over which they can be linear) of ~10nm. Actin is a polarised polymer (asymmetric in structure) which function as tracks for motor proteins called myosin that have unidirectional movement. Actin remodelling signals are provoked by signalling molecules such as kinases, Rho-family GTPases[63], phosphoinositides or Wiskott–Aldrich Syndrome protein (WASP) proteins[64], which are known to be involved in converting mechanical cues into biochemical cues. These cytoskeletal proteins are further organized into lamellipodia (branched cross-linked structures), filopodia (parallel bundles), invadopodia, podosomes, cortical and cytoplasmic gel (cross-linked) and stress fibres (anti- parallel)[65] (*fig 1.4*).

- ***Lamellipodia***

Lamellipodia are ~0.2μm thick structures that are capable of generating protrusive forces at the leading edge of a migrating cell[66]. Arp2/3 protein is responsible for nucleating new filaments that apply a pushing force at cell membrane, helping the cell to move forward. They create a retrograde flow of actin filaments by employing FAs and thus playing an important role in mechanotransduction.

- ***Filopodia***

Filopodia are ~0.3 μm thick finger-like projections at leading edge that are crosslinked by protein fascin[67]. They can protrude from lamellipodia and play a sensory role during cell migration and cell-cell adhesion formation.

- ***Podosomes***

Podosomes are 0.5-2 μm actin rich, one of the peripheral structures and play a role in both adhesion and degradation in ECM[68]. Podosomes are involved in matrix remodelling in non-cancerous cells such as dendritic cells, macrophages, endothelial cells, vascular smooth muscle cells (VSMCs) and osteoclasts[69].

- ***Invadopodia***

Invadopodia are protruding structures, rich in actin and are involved in degradation of ECM and orchestrating cancer metastasis[70,71]. Invadopodia are very similar in structure to podosomes with the difference that they are smaller than podosomes and play a minor role in ECM degradation during invasion. Invadopodia are generally believed to degrade the matrix more aggressively and protrude further into it than podosomes[69].

- ***Actin cortex***

Actin cortex is a dense network of several hundred nanometres thick that is anchored to cell membrane and is involved in amoeboid like motility. Myosin motors exert contractile forces on this meshwork to maintain cell shape. It plays an important role in processes like cell migration and embryogenesis[72]. Myosin motors exert contractile forces using this meshwork to control cell shape.

- ***Stress fibres***

Stress fibres are bundles of micron structures of ~10-30 actin filaments that are cross-linked via anti-parallelly arranged α-actinin and myosin II proteins. They generate contractile forces with the help of motor protein myosin and are vital for cell adhesion and migration. They are further classified as dorsal, ventral or transverse arcs[73]. Dorsal stress fibres are polymerised by formin and Arp2/3 and cross-liked by α-actinin but do not contain myosin motor proteins hence are not contractile. Ventral stress fibres are attached to FAs on both the ends and contain myosin thus making them contractile[74]. Transverse arcs are localised at edge of the cell due to retrograde flow of actin and are contractile in nature[73].

1.5.2 MICROTUBULES

They are composed of a globular protein called tubulin which is a dimer made of α-tubulin and β-tubulin and are stiffer than actin filaments. Apart from these, another type of tubulin, called γ-tubulin is localised at centrosome and play an important part during cell division by working with separation of chromosomes during cell division and being localised at the two poles of mitotic spindle. Tubulin dimers can undergo rapid assembly and dis-assembly thus aiding the cell adjust to its dynamic microenvironment. Like actin, microtubules are also polarised polymers that pave

way for dynein or kinesis motor proteins. They are radially arranged in cells and function as 'central hubs' and 'highways' for intracellular traffic. They switch between 'rapidly shrinking' and 'stably growing' dynamic instable states which allows them to grow rapidly forming tracks for motor proteins[75]. Microtubules are known to increase intracellular viscosity of myocytes in passive stretching of cardiac muscles[76]. In striated muscles X-ROS (reactive oxygen species generated by NADPH oxidase) is a mechanotransductive pathway by which mechanical stress is transduced by microtubules leading to increased cytoskeletal stiffness that could have therapeutics applications in muscular dystrophy[77]. Fluid shear stress through microtubules is known to activate NADPH oxidase 2 (NOX2) that targets Ca^{2+} channels which in turn activates calmodulin-dependent protein kinase II (CAMKII) to define cytoskeletal stiffness in osteocytes[78]. Over the past few decades there have been increasing evidences that indicate the crosstalk between actin and microtubules. Actin nucleation near plasma membrane is co-ordinated by microtubules and associated proteins[79]. Microtubules are also responsible for spatial distribution of active small GTPases thereby regulating actin cortex organization[80]. Mitotic kinesin like protein 1 (MKLP1) called CDP-diacylglycerol--serine O-phosphatidyltransferase (CHO1) is by far the perfect example of link between actin and microtubules suggesting their interrelated functions[81]. It has two domains, one of which can bind microtubules and the other allows F-actin binding. Thus, all the above examples indicate that even though the role of microtubules in mechanotransduction is not well understood, there are striking evidences proving that microtubules might assist actin in mechanotransduction.

1.5.3 INTERMEDIATE FILAMENTS

These are the least stiff members among the three cytoskeletal members. Intermediate filaments (IFs) form 10nm filaments and are categorized into five types, based on their structure and

sequence[82]. Type I-IV are heteropolymers, localised in cytoplasm and the type V is situated in nucleus. Type I and II keratins are found in epithelial cells and type III IFs are homopolymers of vimentin, desmin, peripherin and glial fibrillary acidic protein (GFAP). Vimentin is found more in fibroblasts and mesenchymal stem cells. Desmin is usually found in smooth, skeletal and cardiac muscles. Peripherin is found in neurons and GFAP in astrocytes and glial cells. Type IV IFs are expressed mostly in nervous system and can only form in association with other IF family members such as desmin or vimentin. Type V are nuclear lamins (A/C, B1 and B2) that form the nucleoskeleton. IFs acts as suspensory cables that interconnects cell cytoskeleton along with nucleoskeleton. IFs help in mechanical coupling between integrins and nucleus[83]. Vimentin IF (VIF) are known to stabilize the internal cell organelles thereby preventing their displacement during cytoplasmic fluctuations[84]. FAs formation, maturation and adhesive strength are promoted by VIFs[85,86]. VIFs also contribute to epithelial to mesenchymal transition in cancer cells thereby modulating the cell mechanics[87]. Integrin recycling, motility and activation is partially regulated by VIFs mediated Protein kinase C - ε type (PKCε) and Cyclin-dependent kinase (Cdc2) phosphorylation signalling pathways. VIFs are also known to stabilize cell-cell junctions thereby aiding the transfer of mechanical loads from one cell to another[88]. Keratins IFs (KIFs) also play a role in mechanotransduction by regulating FAs through PKCε or Akt (also known as protein kinase B) signalling pathways and requiring focal adhesion kinase (FAK) mediated keratin IF organisation[89–91]. IFs phosphorylation can act as reservoirs to sequester stress response or physiological functions. However their hyperphosphorylation can be detrimental or advantageous depending on biological context[92]. Shear stress instigates immediate reorganization of VIFs and KIFs advocating their role in spatial redistribution of cellular force[93,94]. During tensile forces, stress fibres are recruited via KIFs. These KIF recruited stress fibre's contractility is modulated by VIFs in

coordination with Rho proteins[95,96]. IFs possess plasticity acting in their structural conformation which provides viscoelasticity to cell to play a part in stress-mediated responses thereby acting as stress buffers[94,109]. Even though the research on IFs and their role in mechanotransduction is still ongoing, the available evidences advocate distinctly the role played by them in response to mechanosensors in mechanotransductive pathways.

1.6 BIOMECHANICS OF NUCLEUS IN MECHANOTRANSDUCTION

Nucleus is considered as the cellular mastermind or "brain" of cell. DNA synthesis, gene expression leading to protein manufacturing are the primary functions of nucleus. The protein synthesis via transcription and translation entitles the cell to carry out crucial tasks including response to mechanical stimuli. These stimuli can either reach nucleus through cascades of biochemical signalling pathways or through direct force transfer via cytoskeleton. The role of nucleus as a mechanosensor has only emerged recently[58,59]. Mechanically nucleus is 2-10 times stiffer than the cytoplasm[98]. Dahl et al. showed that the nuclear lamina is a network of proteins that act as molecular shock absorbers, as a mechanism to resist damage from mechanical forces[99]. On the contrary, research over the past few decades has also revealed that cancer nuclei are less stiff than their healthy counterparts and are influenced by their mechanical microenvironment[100]. Thus, nuclear envelop has been shown to play an important role in mechanosensing and determining nuclear deformability and plasticity[101]. To understand the nuclear mechanosensing it is important to comprehend the nuclear structure and related proteins and their role in mechanotransduction.

1.6.1 NUCLEAR STRUCTURE

1.6.1.1 NUCLEAR MEMBRANE AND PORES

Nucleus contains two lipid bilayer inner and outer membranes that envelop the nucleus. Outer nuclear membrane (ONM) is continuous with endoplasmic reticulum and inner nuclear membrane (INM) is connected to nuclear lamina. The INM provides attachment sites for chromosomes and help in stabilizing the nuclear structure. The ONM is in connection with the cytoplasm and cytoskeleton. The space between the INM and ONM is ~30-50 nm known as perinuclear space. This space contains proteins embedded in between INM and ONM which form a bridge between the nucleus and cytoskeleton called the LINC (Linker of nucleus cytoskeleton) complex. Other than LINC proteins 74 nuclear membrane proteins have been identified having functions related to import/export, chromatin regulation or nucleo-cytoskeletal coupling[102]. Lamin B receptor (LBR), lamina-associated polypeptides (LAPs), emerin, MAN1, nurim, nesprins, and Sad1p/UNC-84 (SUN) are some of the well identified INM proteins. Loss or miss-localization of these proteins cause a spectrum of diseases called laminopathies[103]. INM and ONM fuse into each other at specific locations forming nuclear pores. These are channels spaced regularly throughout the nuclear membrane in absence of nuclear lamins[104]. These guide the transport of molecule larger than ~40 kDa in and out of nucleus[105].

1.6.1.2 LINC COMPLEX

LINC spans both INM and ONM and helps in transmission of forces across nuclear envelope (*fig 1.5*). INM consists of SUN (Sad1p, UNC-84) proteins and ONM consists of Klarsicht, ANC-1, Syne Homology (KASH) proteins. The SUN proteins are embedded in perinuclear space and are further connected to lamina. SUN are further categorized in SUN1 and SUN2 which are present in somatic

cells and have overlapping functions[106]. Additionally SUN3-5 are only expressed in male germline cells[107]. SUN proteins contain an N-terminal nucleoplasmic transmembrane domain and a coiled-coil luminal domain that ends in trimeric C-terminal head[108]. The SUN C-terminal binds to KASH domains. The first four KASH family members are called nesprins (nuclear envelope spectrin repeat proteins) consisting of several isoforms[109]. Some nesprins are also referred to as (synaptic nuclear envelope proteins) (SYNEs) due to their presence in myonuclei at neuromuscular junctions. Largest isoforms of nesprins called nesprin-1 and -2 bind to actin and also to kinesin and dynein. Nesprin-3 anchors to IFs via plectin and nesprin-4 is connected to microtubules via kinesin-1. Interestingly, nesprins are not only found on the cytoplasmic side but also in the nuclear lamina. Smaller nesprin isoforms such as nesprin-1α and -2β localise to inner nuclear membrane and bind to lamins[110]. LINC complex disruption is known to induce nuclear morphological changes presumably due to loss of compression or cytoskeletal tension[111]. LINC effects on nuclear morphology depending on mechanical cues like substrate stiffness, 2D versus 3D environment and mechanical strain have been demonstrated well over the past few years[112–114]. Other proteins like Samp1, emerin and torsin A are recently found effectors of LINC complex[115–117]. Mutation or downregulation of nesprins is observed in cancers like breast, colorectal, etc[118,119]. Even though these references provide a wealth of insight, the mechanisms of functioning of nesprin and sun proteins still remains to be elucidated.

1.6.1.3 NUCLEAR LAMINA

Nuclear lamina is composed of lamins that are type V IFs and associated proteins forming a dense meshwork. They form parallel dimers of diameter of about 10 nm and are tightly crosslinked with chromatin. They are classified as A type or B type lamins. Lamin A and C are the ones alternatively spliced from *LMNA* gene while *LMNB1* and *LMNB2* produce lamin B1 and B2/B3. Lamins are

responsible for maintaining integrity and mechanical stability of nucleus[120]. Literature suggests that Lamins A/C and not lamin B1 regulate nuclear mechanics[121]. However, lamin B has also shown to partially rescue mechanical defects and are important in nucleus-cytoskeleton anchoring in neurons that lack lamin A , showing the redundancy between functions of lamins[122,123]. Lamin levels are dysregulated in cancer cells.

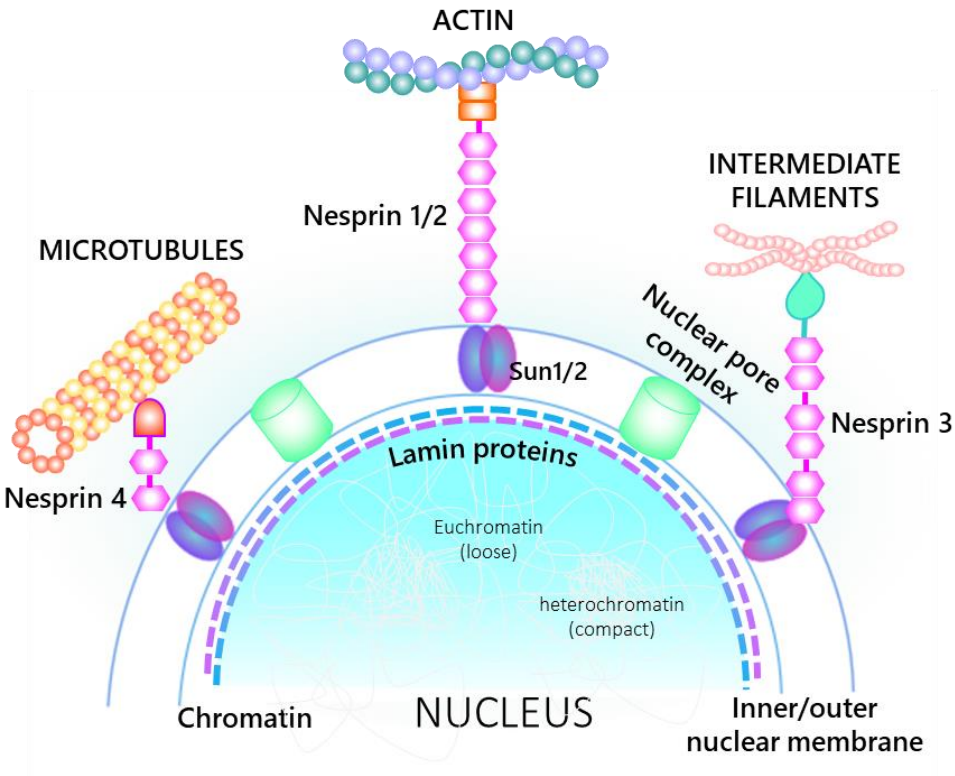

Figure 1.5. *Nucleus organization and connection to the cytoskeletal filaments through LINC. The nucleus and its chromatin are mechanically connected to the plasma membrane and the outer microenvironment. At the nucleus, the mechanically junction is made by the LINC complex. The LINC complex is composed of nesprin proteins on the outer side of the nucleus envelope and the SUN proteins between the two membrane leaflets. The nesprins binds the cytoskeleton components whereas the SUN proteins are linked to the nucleoskeleton protein Lamins, whose distribution and dynamics can effect the distribution of heterochromatin and euchromatin. Thus, the LINC complex is one crucial element of the mechanical continuum that connects the chromatin to the exterior microenvironment.*

Lamin A/C are known to be over-expressed in ovarian, colorectal, prostate and skin cancers whereas under-expressed in basal cell skin carcinomas, leukemia, gastrointestinal and lung cancer[124]. Downregulation of lamins and nesprin might assist the deformability of cancer nucleus

by increasing the flexibility and changing chromatin remodelling, thus aiding in migration[125]. On the other hand, upregulation of lamins might assist in protection of cells from mechanical stress caused due to hydrostatic pressure inside solid tumors.

1.6.2 NUCLEAR DEFORMATION

Nucleus is known to deform or remodel itself in response to extracellular forces. Forces such as stress or compression can result in deformation of nucleus structure. Pioneering work was done by Flaherty et al. in 1972 showing *in vivo* elongation of endothelial nuclei under shear stress due to blood flow[126]. However, increase or decrease of nuclear proteins can also lead to change in nuclear deformation response. For example, lamin A/C deficiency is known to increase nuclear deformation[121]. LINC complex disruption is known to decrease nuclear deformation[112,127]. Growing evidence also shows that composition of nuclear envelope is mutated in cancer cells, thereby providing flexibility to the nucleus. Moreover, cancer cells can be physically distinguished by nuclear morphological deformations in histological tissue sections[128].

1.6.2.1 NUCLEUS DEFORMATION DURING MIGRATION

Nucleus is a stiff organelle of the cell and thus resists deformations. Due to this mechanical property, nucleus becomes a hurdle during cell migration in general and in metastatic conditions. To ease migration through confined spacing, cell usually employ two mechanisms, first is the proteolytic degradation of ECM via MMPs and second is deformation of the cell body and subcellular organelles[129]. If the cell is not able to do either of the two mechanisms it retracts its protrusions and tries to search for an alternative route to bypass the obstacle[130]. Migration through collagen matrices has shown to distort the nucleus (diameter in 3D ranging from 5-15μm[131]) extremely as it passes through ~3 μm constrictions[24]. Neutrophils are fastest migrating

cells and have very less amount of lamins in order to facilitate migration through confined spaces *in vivo*[132]. Lamin A/C deficiency in fibroblasts can lead to reduced cell migration as force transmission between cell cytoskeleton and nucleus is disrupted[133]. During 2D and 3D migration, actin and myosin II aid nucleus translocation with the cell body both pulling and pushing the nucleus[134–136]. Moreover, Arp2/3 complex has been shown to nucleate actin promoting lamin A/C perturbation and aiding the nuclear deformation during migration through narrow constrictions[137]. Striking research revealed that nuclear envelope ruptures during migration through tight spaces and resealing of the same by ESCRT III (endosomal sorting complex required for transport)[138].

1.6.2.2 NUCLEUS DEFORMATION DUE TO STRESS

Nucleus is known to remodel itself in response to mechanical forces and can modulate its mechanics depending upon the mechanical load[139]. Mechanical stress is known to deform nucleus, sometimes leading to its rupture[138] and impacting gene expressions or chromatin structure[140]. Mechanical compression can also change the cellular osmolarity resulting in altered nuclear architecture and chromatin remodulation[141]. Deguchi et al. in 2005 demonstrated that nucleus remodels itself in response to shear stress applied to cell[142]. Endothelial nuclei show elongation and 50% increased stiffness in response to fluid shear stress. Confined spacing can act as mechanical cue and cause nucleus to compress in order to facilitate migration[140]. Compression stress can lead to changes in nuclear shape and height in chondrocytes due to muscle contraction[143].

1.6.2.3 INTRACELLULAR COMPONENTS INVOLVED IN NUCLEAR DEFORMATION

Cellular components such as cytoskeletal or nucleoskeletal proteins also play an important role in

order to deform nucleus. Tensile stress by actomyosin proteins is known to cause nuclear deformation in cells[144]. Large array of actomyosin based transmembrane actin-associated nuclear (TAN) lines apply tensional forces to nesprin-2G to help the nucleus during migration[145]. Actin filaments in the form of stress fibres are also involved in applying compressive pressure on nucleus thus changing its conformation during mechanical stimuli[146]. LINC proteins plays an important role in altering nuclear shape due to mechanical cues such as topographical confinements or mechanical forces such as compressive stress[147] .

1.6.2.4 ROLE OF NUCLEUS AS MECHANOSENSOR

Literature has highlighted the various roles played by the nucleus and other intracellular organelles in mechanotransduction as discussed individually in 1.6.1. One theory suggests that nucleus acts as a piston thereby providing momentum (force required for moving) to the migration of cell through constrictions[135]. This momentum is provided by generating hydrostatic pressure differences in front and rear end of the nucleus[135]. Khatau et al. have shown that sufficient nuclear stiffness is required during the 3D migration of cell[113]. Recently, mechanotransduction has been shown to also trigger transcription pathways that alter the up or down regulation of many proteins[148]. Research also signifies the role of nuclear chromatin in aiding the mechanotransduction and regulation of gene expression[149,150] (*fig. 1.6*). The condensation of chromatin is known to increase the stiffness of nucleus while the decondensation increases nuclear softness[151]. facilitating cancer migration[152]. Moreover, cancer cells are known to have a thick nuclear periphery due to heterochromatin condensation[100,153]. Heterochromatin is connected by a conserved domain to SUN proteins of LINC complex[154,155]. All these bear witness to the fact that nucleus itself does act as a mechanosensor[58,59] thereby guiding migration of cell through

confinements.

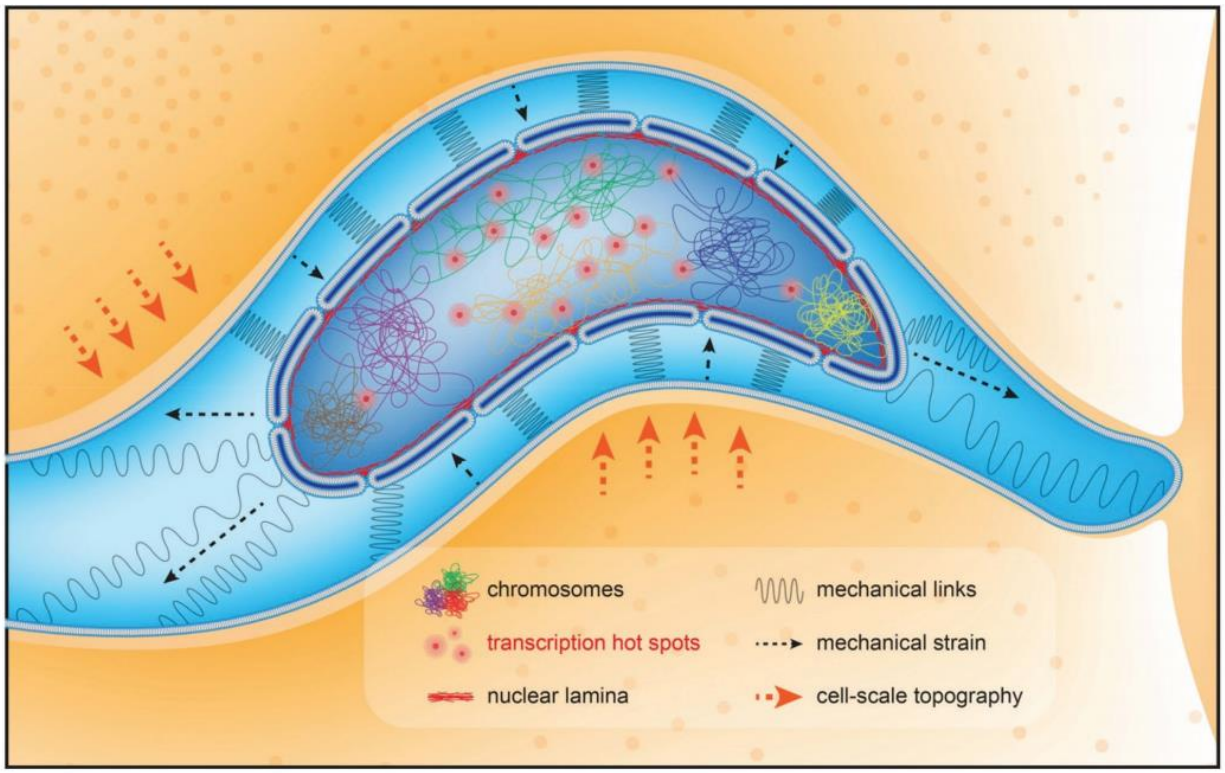

Figure 1.6 *Diagram by Pieuchot.L, from Anselme.K et al. 2018*[59]
Nuclear structure and gene regulation. Loosely organised chromatin (euchromatin) is transcriptionally active. The nucleus is connected to the cytoskeleton via linker of nucleo-cytoskeleton (LINC) proteins (refer to figure 1.5). Deformation in nucleus shape (due to mechanical cues, eg. topography) leads to chromosome reorganisation leading to transcriptional hotspots and thus affecting gene regulation.

1.7 CELLULAR TENSEGRITY MODEL

During mechanotransduction several cytoskeletal (CSK) components orchestrate themselves to bear large mechanical deformations in their shape. Nucleus even though being the stiffest organelle undergoes distortions in order to facilitate cell to pass through constriction and confined spaces *in vivo*. The tensegrity model presumes that CSK and nucleus are hardwired to respond to mechanical forces via cell surface receptors that connect the cell to ECM. Tensegrity illustrates possible model mechanisms of cellular remodulation in response to stress. These models can be classified as continuum and discrete models (*fig. 1.7*).

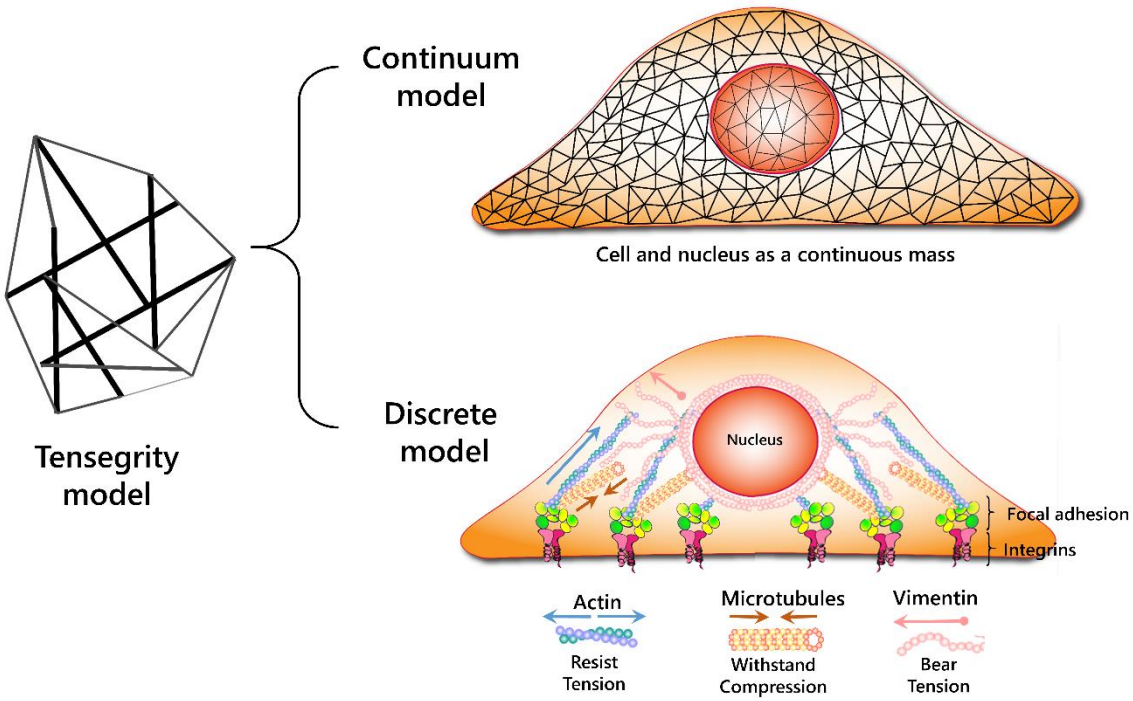

Figure 1.7. *Diagram inspired from Ingber et al.[156] shows two models of cellular tensegrity characterized by continuum model and discrete model. Continuum model considers cell and nucleus as a continuous body of mass responsible for large deformations. Discrete model takes into account individual structures of cell involved in either bearing or resisting forces.*

Continuum mechanics deals with the analysis of mechanical behaviour and kinematics (motion of objects without reference to the forces which cause the motion) of materials which are modelled as continuous mass rather than discrete particles. This explains large scale deformations of cell to microscopic stress-strain relationship that are applicable to whole cell or compartments rather than discrete structures such as CSK elements. Such continuum descriptions can be elastic or viscoelastic. Laws of continuum mechanics are used to evaluate distribution of mechanical stress and deformation of cell. This model can thus help to probe single cell mechanics and evaluate forces sensed by different parts of cell *in vivo* or *in vitro*. *In vitro* these are studied with the techniques like micropipette aspiration[157], microindentation[158], atomic force microscopy (AFM)[159] or magneto-cytometry[160].Discrete model takes into account discrete stress bearing elements of cell[161]. These elements can be of specific length such as actin or microtubules. This model takes

into account the prestress of discrete structures. Tensegrity architecture of cell falls within this model. Research has suggested that stability of cell structure is based on the model that defines cell as a tensed membrane that surrounds viscous cytoplasm. Ingber et al. introduced a different type of stress called “prestress” (pre-existing tensile stress) that is hallmark property displayed by CSK members even before the application of external forces[61]. Rigidity (stiffness) of the cell itself is nearly proportional to the level of prestress that is supported by CSK[162]. This prestress is mostly harboured by microfilaments (actin) and counterbalanced partially by microtubule compression and traction forces applied by the cell on the ECM. Tensegrity model defines actin best to be adapted to resist tension whereas microtubules possess higher moment of inertia aiding them to withstand compression[163]. IFs act as tension cables that play an important role in cell mechanics during large deformations[164]. Tensegrity based models and their importance in mechanotransduction is well documented in cell proliferation, apoptosis, gene expression and many biological functions[165]. Nuclear reshaping in response to force at integrins is also one of the important revelations done based on tensegrity model[166].

1.8 ENGINEERING BIOMATERIALS TO MIMIC EXTRACELLULAR MATRIX- *IN VITRO* MECHANOTRANSDUCTION

In vivo the ECM is engineered into various topographies ranging from nano- to micro- scale. Passive cues such as topography, rigidity or dimensionality cues have been known to affect the cell behaviour in many ways as discussed in section 1.3.2. However, studying the effects of *in vivo* passive cues is an uneasy task and is equipped with challenges. To overcome these hurdles, fabricating biointerfaces have been proven to be a compendious approach to recapitulate the *in*

vivo environment. Moreover, these fabricated surfaces have paved way for tissue engineering and regenerative medicine applications amounting for the development in engineered topographic materials.

1.8.1 FABRICATION OF POLYMERS USING LITHOGRAPHY

There are many polymers that cater to fabrication of wide variety of nano- or micro- structures. Aliphatic polyesters form one of the largest fabricated polymers having biodegradability (property to get decomposed by biological agents) and biocompatibility (property to not elicit immune response or have toxic effects). Moreover, these polyester fabricated surfaces are cell adhesive thereby not requiring the coating of fibronectin or other cell adhesive proteins on the surface. This reduces the cost of cell culturing techniques as cell adhesion proteins are expensive. Most commonly used aliphatic polyesters in regenerative medicine are poly-lactic acid (PLA), poly-glycolic acid (PGA), poly lactic-co-glycolic acid (PLGA) etc. In our work we use PLA polycondensed in L form which is more crystalline than the amorphous D form. It is a hydrophobic polymer owing to –CH3 group with glass transition (Tg) temperature of about 60-70°C[167]. These polymers are fabricated using lithography (Greek *lithos*- stone and *graphein*- write) techniques like photolithography, soft lithography, etc. Photolithography is a selective process allowing the patterning of a design onto the material like silicon wafer. The basic process is as follows (*fig. 1.8*)-

1. Wafer Cleaning and Photoresist Application

In the first step, the wafers are chemically cleaned to get rid of any particulate matter on the surface including traces of organic, ionic, and metallic impurities. After cleaning, silicon dioxide is formed on the surface of the wafer, by exposing it to thermal oxidation. After the formation of the SiO_2 layer, photoresist is applied to the surface of the wafer. High-speed centrifugal whirling of

silicon wafers is the standard method for applying photoresist coatings. This technique, known as "Spin Coating," produces a thin uniform layer of photoresist on the wafer surface.

2. Positive and Negative Photoresist

There are two types of photoresist: positive and negative. For positive resists, the resist is exposed with UV light when the underlying material is to be removed. In these resists, exposure to the UV light changes the chemical structure of the resist so that it becomes more soluble in the developer. The exposed resist is then washed away by the developer solution. The mask, therefore, contains an exact copy of the pattern which is to remain on the wafer.

Negative resists behave in just the opposite manner. Exposure to the UV light causes the negative resist to become polymerized, and more difficult to dissolve. Therefore, the negative resist remains on the surface wherever it is exposed, and the developer solution removes only the unexposed portions. Masks used for negative photoresists, therefore, contain the inverse (or photographic "negative") of the pattern to be transferred.

3. Etching

In etching, a liquid ("wet") or plasma ("dry") chemical agent removes the uppermost layer of the substrate in the areas that are not protected by photoresist.

4. Photoresist removal

After a photoresist is no longer needed, it is removed from the substrate. This usually requires a liquid "resist stripper", which chemically alters the resist so that it no longer adheres to the substrate or by plasma oxidation.

1.8.2 PATTERNING SUBSTRATES- IMPORTANCE OF PILLAR SUBSTRATES TOPOGRAPHY TO STUDY CELL BEHAVIOUR

Fabrication of surfaces at nano- and micro- scale and the cell responses on them have provided us with deep insights of biointerface mediated mechanotransduction (*fig. 1.9*). Grooves of micron-scale are used with the combination of different widths or heights. Cells are known to align themselves along micron-scale grooves leading to change in nuclear shape and volume, which advocates the role of nucleus acting as mechanosensor[168]. Epithelial cancer cells are known to gradually lose 3D geometry recognition on micron-scale grooves allowing them metastatic migration[169]. Micrograting are also known to reduce proliferation through Rho-ROCK myosin pathway of non-cancerous cells contrary to cancerous cells[170]. Large pits are known to inhibit cell migration and smaller pits are known to promote proliferation[171,172]. Micro-wells have also served as biomimetic topography and are known to enhance metabolism in epithelial cancer cells[173]. Nanofiber scaffolds have been shown to effect glioma cells migration[174] and effect stem cell differentiation[175]. Graphene microfibers on the other hand were shown to orient rat and mouse cells[176], regulate neural stem cell differentiation[177].

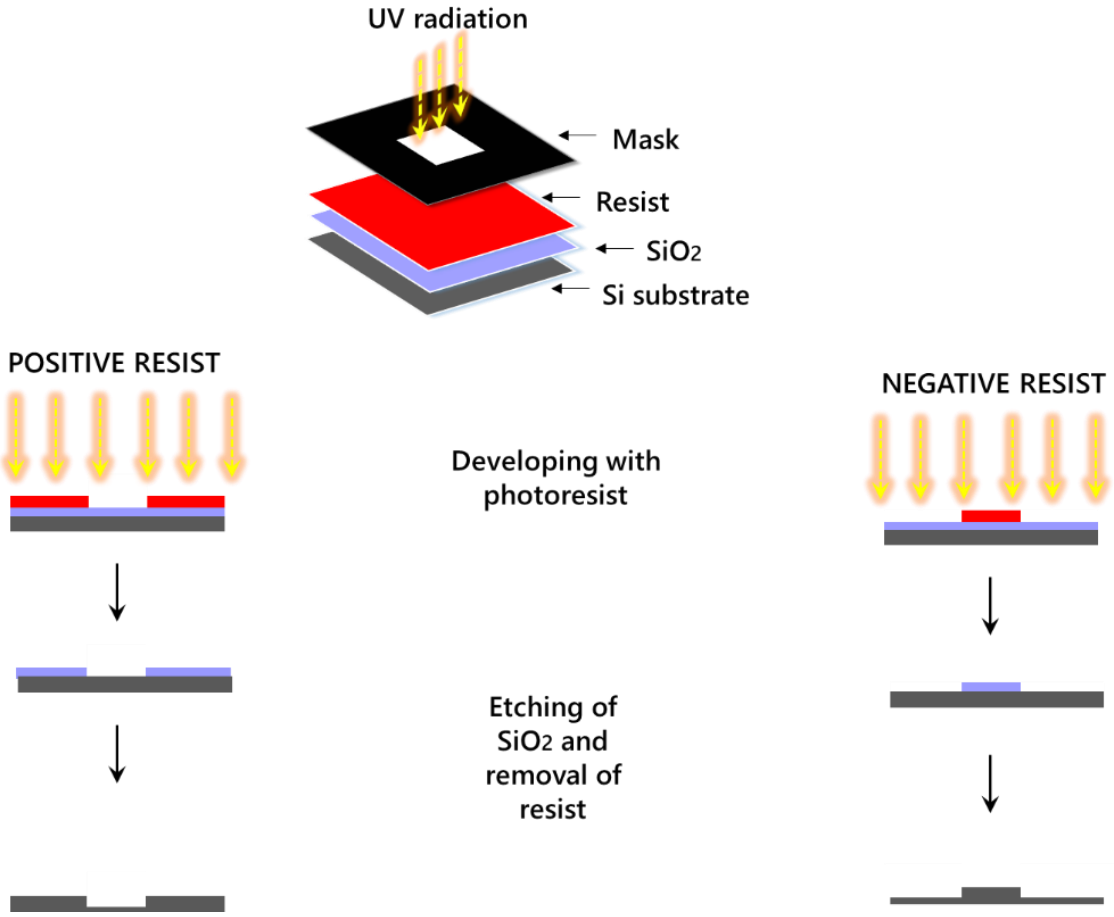

Figure 1.8 *Basic lithography technique. Substrate is coated with resist (positive or negative) and exposed to UV light. The undissolved resist is washed using a developer. The substrate is then etched at areas not protected by photoresist. Lastly, the remaining resist is removed completely using a stripping agent, giving us the desired pattern.*

Apart from all these, micropillars have proven to be the most influential topographies especially in investigation of nucleus deformation. Microposts/columns/pillars have known to effect cell behaviour in many ways. Pillars are known to induce epithelial to mesenchymal transitions (EMT)[178]. Osteoblastic cancer cells (MG63) attempt to phagocytose the pillars via a RhoA/ROCK dependent signalling pathway[179]. PLLA and PLGA micropillars have also emerged as the substrate helping in recognition of cancerous cells from healthy ones depending on their ability to deform their nucleus between pillars[180,181]. Prostate cancer cells were shown to produce

DNA slit structures in their nucleus on pillars[182]. Xiao et al. fabricated micropillar-based microfluidics devices to capture cancer cells by contact with the micropillars[183]. Pillars have also been signified in playing role in topotaxis in aggressive melanoma cells[25]. Apart from cancerous cells, micropillars are known to regulate stem cell behaviour[184], affect astroglial cell arrangement[185] or guide cell migration in fibroblasts[186].

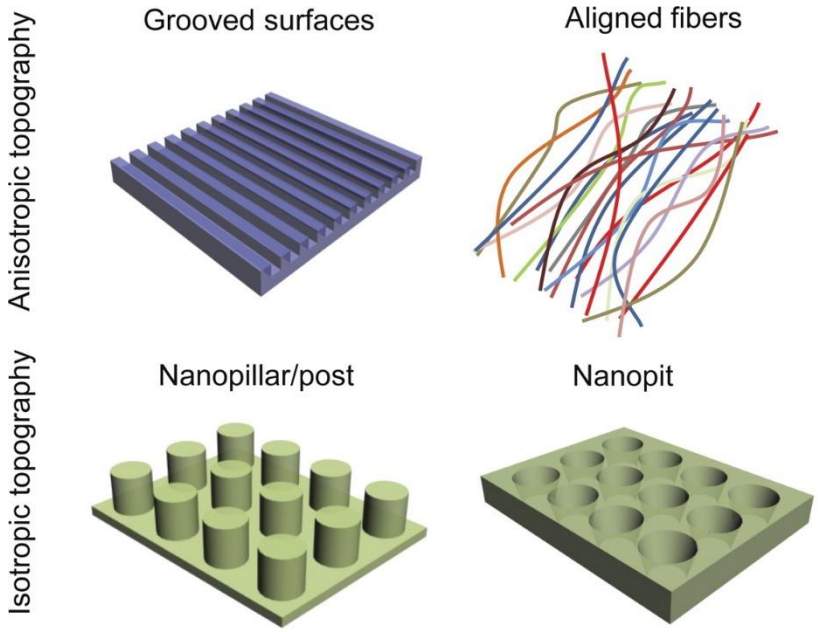

***Figure 1.9**. Adapted from[187]. Different topographical substrates for analyzing cell response. Geometries like pillars, fibers, grooves, curvatures or pits.*

Furthermore, changing the dimension of pillars has proved to be useful for measuring traction forces applied by the cell on the ECM[188]. These forces can be calculated by the bending stiffness or spring constant of the pillars (measuring the difference between the initial and final displacement of the pillars)[189]. Myosin localization on sub-micron pillars is known to cause deflections of the pillars[190]. Disruption of LINC complex is known to reduce forces in perinuclear regions and involvement of actin-cap mediated YAP mechanotransduction pathways in embracing the pillars via traction forces[191]. Epithelial collective migration exerts forces on the edge of the epithelia and

mediated by n-cadherin cell junctions[192–194]. Literature has suggested that traction forces deform the pillars irrespective of their rigidity and are directly proportional to spring constant of pillars[195]. Nevertheless, more FAs are observed on stiff pillars as compared to soft ones correlating with the above fact. This means that's mechanical activity of the cells is steered by matrix rigidity compared to geometry of ECM.

Finally, microfluidics systems fabricated from PDMS and lithography techniques, have also been witnessing cell behaviour, especially in migration of cells through confining regions[196].

These microfluidic systems form an integral structure to study migration functions like chemotaxis (migration along environmental chemical gradient), haptotaxis (migration along substrate bound chemoattractant), durotaxis (migration along the rigidity of substrate) or topotaxis (migration through topographies or confinement)[4,197,198].

1.9 OUTLOOK AND OBJECTIVE OF THESIS STUDY

Mostly what has come to light by previous research, is that the cytoskeletal components relay ECM signals to nucleus that bring about change in nuclear structure. However, what remains to be unravelled is do the cytoskeletal changes via integrin-linked FAs send the signals to nucleus? or does the nucleus itself "mechanosenses" the ECM and regulates the assembly of integrins, FAs and cytoskeleton? We can presume that the latter case might be possible by increasing the mRNA transcription of these proteins (integrin, FAs or cytoskeleton) or by producing some unidentified molecules that signal these proteins to bring about mechanotransduction. Furthermore, cells that have more heterochromatin could assist in strengthening the nucleus and cytoskeletal-LINC bridge which could prevent rupture of these connections in cancer cells, during extreme

compression leading to chromatin condensation, through confined spaces.

Based on these findings, we could assume that the chromatin is decondensed when the nucleus is passing out of confined spaces, thereby making nucleus more elastic[199,200]. Consequently this elasticity could provide a pulling force via LINC at the rear end of the nucleus. We presume that this pulling force could be imagined as retraction of an elastic rubber to its initial state after being stretched apart. Thus, we could hypothesize that changes in stiffness of nucleus, due to chromatin condensation-decondensation, might shift the momentum of the migrating cell from rear end to front, thus aiding the forwarding of cell. It has been shown previously that "exit velocities" of nucleus occur most at the exit of confinement and the cell is propelled by the elastic restoring forces of extracellular matrix once most part of the cell is passed through the confinement[125]. On stiff surfaces, where the substrate is un-deformable, it is more likely that the confinement exit is coupled to nucleus elasticity and the pulling by cytoskeleton[201]. Apart from the chromatin, other nuclear structures also take part in mechanotransduction pathways (as described in section 1.6.1). Hence a lot of questions about how the nucleus deforms still remained unanswered. Therefore, to elucidate how nuclear deformation occurs we propose to use micropillar topography.

Work on pillars started in our lab over the last decade and nucleus deformation of cancerous nuclei in response to micropillar topography was published for the first time by Patricia Davidson et al.[181]. Later on Davidson et al. revealed that the deformation of cells and their nuclei depend on the cell type. The cancerous cells showed maximum deformation compared to healthy and immortalised cells. Badique et al., later evaluated which of the different osteosarcoma cell lines deformed the most. They found that SaOS-2 deformed the most compared to MG-63 and OHS-4. Moreover, they found that the SaOS-2 cells that deformed the most was also the stiffest cell line,

when checked via AFM experiments. This raised many questions as how does this stiff cell line deform? What are the mechanisms entailing the deformation of the SaOS-2 cell and its nucleus? Thus the objective of the thesis work here is to study the role of cytoskeleton and nucleoskeleton in steering nuclear deformation. Moreover, *in vivo* the cells are pushed and pulled in order to facilitate cellular processes like adhesion or migration. To study the deformation of cells at tissue level we analysed the behaviour of epithelial origin colon cancer cells on pillars.

The micropillar substrate that we used for above experiments are PLLA polymers that are very stiff and do not actually represent the magnitude of stiffness of various other tissues. Hence, to be able to mimic the stiffness of the *in vivo* environment, we employed hydrogel pillars which could be modulated not only with mechanics but also topography. Moreover, the hydrogel system we used allowed us to control the cell behaviour with chemistry coating different parts of the pillars.

RÉSUMÉ DU CHAPITRE 2 - MÉCANISMES DE DÉFORMATION DE CELLULES D'OSTÉOSARCOME SUR DES MICRO-PILIERS

Notre laboratoire a été le premier à publier la déformation des noyaux de cellules cancéreuses en réponse à la topographie pilier. D'autres expériences ont révélé que la déformation des cellules et de leurs noyaux dépendait du type de cellule étudié. Les cellules saines se déforment pendant une courte période mais retrouvent rapidement leur structure normale, alors que les cellules immortalisées subissent des déformations limitées et que les cellules cancéreuses subissent des déformations extrêmes. Enfin, des expériences réalisées sur différentes lignées d'ostéosarcomes ont montré que la lignée cellulaire la plus déformable était également la plus rigide. Ces résultats nous ont donc conduit à analyser de manière approfondie la biologie de ces cellules afin de découvrir les mécanismes et les acteurs moléculaires impliqués dans la déformation nucléaire de la lignée cellulaire d'ostéosarcome la plus déformable (SaOS-2). Les questions auxquelles nous voulions répondre étaient: 1) où et comment est organisé le cytosquelette sur les piliers? 2) Quels composants cytosquelettiques sont nécessaires pour guider la déformation nucléaire? 3) Le noyau étant plus rigide que le cytoplasme cellulaire, quel rôle joue le nucléosquelette dans sa déformation? 4) Comment se produit la déformation dans le temps, où sont situées les adhérences focales, comment la chromatine aide-t-elle le noyau à se déformer, comment la cellule se divise-t-elle à l'état déformé? 5) Quelle force entre les forces de traction ou de poussée permet la déformation nucléaire dans la cellule?

Nous avons d'abord analysé la cinétique de la déformation nucléaire puis quantifié la déformation nucléaire ainsi que la localisation des adhésions focales positives à la paxilline le long des micropiliers grâce à la microscopie confocale. Nos observations montrent que la déformation nucléaire augmente avec le temps jusqu'à atteindre un plateau après 24 heures. Au cours de la

déformation, nous avons également observé une compaction de la chromatine qui augmente au cours du temps facilitant la déformation du noyau. Pour percevoir le rôle du cytosquelette dans la dynamique de remodelage nucléaire, nous avons dépolymérisé le cytosquelette des cellules SaOS-2 avec des drogues spécifiques et avons calculé la capacité de déformation nucléaire. Nous avons ainsi observé que les filaments d'actomyosine et de vimentine sont nécessaires à la déformation nucléaire alors que les microtubules ne jouent aucun rôle significatif. Le noyau est connecté aux éléments du cytosquelette via un complexe de protéines appelé Linker du noyau et du cytosquelette (LINC), elles-mêmes connectées aux protéines de la lamina présentes dans l'enveloppe du noyau. Afin de percer le rôle des protéines du complexes LINC, nous avons donc étudié le rôle d'entités du complexe LINC telles que SUN1, SUN2 et nesprin 2 (syne2) et d'une protéine de l'enveloppe nucléaire, la lamine A. Les résultats n'ont montré aucune différence significative dans la capacité de déformation lorsque ces protéines sont inhibées individuellement. Par conséquent, pour élucider définitivement le rôle du complexe LINC, nous avons déconnecté le complexe LINC du cytosquelette en utilisant un plasmide mutant KASH double négatif. En effet, les protéines nesprines sont connectées au cytosquelette et possèdent un domaine conservé de KASH [klarsicht / ANC-1 (ancrage 1) / SYNE (protéine synaptique de l'enveloppe nucléaire)]. Ce mutant plasmidique contient donc le domaine KASH connecté aux protéines nucléaires SUN conservé alors que le domaine de connexion aux éléments du cytosquelette est muté, permettant ainsi de couper la connexion entre le LINC et le cytosquelette. Cette dissociation complète du LINC du cytosquelette diminue significativement la déformation du noyau. Le LINC est également lié au nucléosquelette par l'intermédiaire de protéines nucléaires telles que la lamine A, connue pour jouer un rôle important dans la mécanique cellulaire. Cependant, la diminution des niveaux d'expression de la lamine A par extinction ou leur augmentation par surexpression n'affecte pas

la capacité du noyau à se déformer. Enfin, pour comprendre le rôle dans la déformation du noyau des forces de poussée et de traction dues au cytosquelette, nous avons développé un modèle de simulation chimio-topographique et numérique. Nous avons pu montrer que ce sont les forces de traction qui permettent de déformer la cellule et son noyau et de les confiner complètement dans des espaces inter-piliers de 3 µm. Les données issues de ces modèles démontrent donc la domination des forces de traction sur les forces de poussée dans le confinement du noyau dans les espaces inter-piliers.

CHAPTER 2. DEFORMATION MECHANISMS OF OSTEOSARCOMA CELLS ON MICROPILLAR ARRAY

2.1 BACKGROUND

Tissue engineering has erupted as a new and promising era in the field of implants or organ regeneration, etc. The recent most advances in this field have been the advancement in creating nano- and micro- topographies to have a close look on cell behaviour on *in vivo* comparable 3D environment. There have been many advances in the development of topographies mimicking or providing the *in vivo* landscapes and understanding the behaviour of different types of cells. As described in section 1.8.2 many substrates like grooves, pits, pillars, nanofibers, 3D scaffolds, etc. have been fabricated using lithographic techniques.

Our lab worked on different cell types including osteosarcoma cell lines with different aggressivity on micropillar substrates over the last decade. The aim of our lab initially was to observe the behaviour of various osteoblastic cells on topographic surfaces. Different cell lines were chosen for the same purpose and intriguingly it was observed that the osteosarcoma-derived cancerous cells deform their structure completely in response to micropillar topography. Interestingly the deformed behaviour did not lead to any apoptotic cell death, indicating that the deformation even though severe was not detrimental[181]. Further, experiments revealed that healthy cells deform but for a very short period and they regain their cellular structure thereafter. This signified that the healthy cells are less responsive to topographical cues compared to cancerous cells. In comparison to healthy cells, immortalised cell lines showed very little deformation. However the cancerous cells showed extreme deformation compared to other cells[202]. This proved that being flexible is behaviour of cancerous cells which could probably guide

them to deform themselves during metastatic migration.

To understand the behaviour of the severely deforming osteosarcoma cell lines, three osteosarcoma cell lines (MG63, SaOS-2 and OHS-4) were cultured on these pillars[203]. These cell lines have been previously characterised as model candidates for studying bone tumors[204,205]. Atomic microscopy experiments (AFM) were performed to evaluate the rigidity (Youngs modulus, Pa) of these three cell lines. Interestingly it was observed that SaOS-2 showed the highest Young's modulus, MG-63 showed intermediate and OHS-4 the least. Furthermore, SaOS-2 showed maximum deformation capacity than the rest two candidates, making it the model cell line for further experiments on pillar topography. Other experiments in collaborator's lab revealed that not only the geometry of the pillars but also the dimension play an important role in determining cells behaviour. It was observed that the height less than 5 μm induced comparably less deformation and more than 10 μm induced complete nuclear deformation. This is to be expected as the nucleus itself has a diameter ranging from 8-14 μm depending on cell stage (about to divide or not) and type. Moreover, the spacing in between the pillars also affected the deformation behaviour. Interestingly the SaOs-2 cells were unable to penetrate completely the spacing below 3 μm and the deformation increased with the increase in size of spacing. Therefore, our lab chose pillars with 7 μm height, width and spacings for further experiments.

The question about SaOS-2 deformation that I shall answer in this chapter is: 1) how is the cytoskeletal localization and organization on pillars. 2) Which cytoskeletal components are necessary for guiding nuclear deformation? 3) The nucleus is stiffer than the cell cytoplasm[120], therefore does its own nucleoskeleton play a role in steering deformation? 4) What about kinetics of deformation: how the deformation proceeds over time, where are the focal adhesions situated,

how is chromatin helping the nucleus to deform, how does the cell divide in the deformed state?

5) Which forces navigate the nuclear deformation in the cell, the pulling or pushing down forces?

2.2 Manuscript- Pulling force by actomyosin & LINC tailors metastatic nuclear distortion in topographically-induced self-confinement

Actomyosin anchored to LINC pulls and orchestrates confinement-induced nuclear deformation

Cells pull to squeeze and deform in confinement.

Wakhloo N.T.[a], Anders S.[b], Badique F.[a], Eichhorn M.[b], Brigaud I.[a], Petithory T. [a],Pieuchot L.[a]*,P. Davidson[d], Vassaux M.[c], Milan J.L [c], Freund J.N.[d], Rühe J.[b], Anselme K.[a]

*For correspondence: laurent.pieuchot@uha.fr

[a.] Université de Haute-Alsace, CNRS, IS2M, UMR 7361,F-68100 Mulhouse, France,
[b.] Department of Microsystems Engineering (IMTEK), Albert-Ludwigs-Universität Freiburg, Freiburg, Germany
[c.] Institut des Sciences du Mouvement, Aix-Marseille Université, CNRS UMR7287, Marseille, France
[d.] Institut Curie, CNRS Physico-Chemistry Unit (UMR168), Paris
[e.] INSERM UMR-S1113, Strasbourg, France

ABSTRACT

Deformation of nucleus is a paradoxical event where on one hand it plays a role in physiological processes such as differentiation, immune responses, wound healing and on the other it has adverse effects by providing cellular flexibility for invasion during metastasis. However, the mechanisms underlying the distortion of nucleus - the biggest and stiffest organelle of the cell still remain elusive. Herein we develop an *in vitro* assay based on micropillar confinement and combine live imaging and computational modeling to decipher the mechanisms involved in nuclear deformation during cell confinement. We show that actomyosin, vimentin and nucleo-cytoskeletal interconnections play essential roles in nuclear reshaping. Furthermore, we employ differentially functionalized micropillars to dissect the role of push and pull intracellular forces. We demonstrate that predominantly pulling forces deform and maintain the nucleus within confined spacings contrary to pushing forces. Altogether, we propose a comprehensive mechanism orchestrating nuclear deformation in confinement.

SIGNIFICANCE STATEMENT

Cell deforms itself in various physio-pathological processes such as differentiation, immune responses, wound healing and cancer cell migration. This deformation is accompanied by the morphological changes that affect all cell organelles including nucleus- the biggest and stiffest organelle. The mechanisms underlying this cell-nucleus deformation still remain poorly perceived. To address this we use micropillars based confinement to induce cell-nuclear deformation in cells that readily undergo reshaping. Our results show that cytoskeletal elements such as actomyosin, intermediate filaments and the connection of nucleus to cytoskeleton via LINC complex is essential to distort the nucleus in confinement. Using chemo-topography modulations and computational modelling we found that intracellular pulling forces are more important than pushing to squeeze the nucleus in between micropillar-induced confinement.

BACKGROUND

Cells reside in intricate 3 Dimensional (3D) microenvironments within which they are subjected to various mechanical constraints that modulate their behavior along with their cytoskeleton and organelles[1,2]. For example, human pluripotent stem cells, immune cells, cells during wound healing and cancer cells deform its nuclei during migration through confinement[3–5]. However, the nucleus, which is the largest and stiffest organelle within the cell, represents a physical constraint that limits cell migration in narrow channels[6]. The impact of cell confinement on nuclear deformation and cell mechanics have been extensively studied using rigorous physical methods[7] such as micropipette aspiration[8], micro-indentation[9] or isolating nucleus from cells[10]. Although these techniques have established some new paradigms on cell-nuclear mechanics, they do not reflect how cells spontaneously deform *in vivo*. Precise and simple analytical tools to study how cells deform and maintain themselves within confined environments are still lacking.

Over the last few decades biomaterials have emerged as an extremely versatile tool to engineer and recapitulate tumor microenvironments. Among many biomaterial applications, fabrication of 3D micron-sized pillars have provided more physiologically pertinent frameworks to study nuclear deformation *ex situ*. Contrary to the physical techniques described above, these systems allow direct visualization of nucleus distortion without affecting the nucleus integrity[11–14]. We initially established that osteosarcoma cells spontaneously penetrate 3D micropillars and reshape their nuclei to fit within the topographies whereas healthy cells do not deform and stay above[11,12,15]. These pillar arrays were subsequently used by other researchers to evaluate various cancer cell lines for their ability to deform compared to healthy cells[13], to show differential response of nuclear deformation of embryonic stem cells and induced pluripotent stem cells depending on their differentiation state[16] and to understand the nuclear mechanics of mouse embryonic fibroblast cells[14]. However, the mechanisms and forces underlying nuclear deformation still remains to be elucidated.

Previous studies implied that the nucleus may be pushed from behind or pulled from the front, although it has remained difficult to define precise mechanisms[17]. Our micropillar arrays are able to mimic the invasion of cells into tissues, in a system in which the surfaces can be chemically modified and the cells can easily be treated with drugs and collected for biochemical studies. Importantly, our system allows us to study nuclear deformation caused by the cell, independently

from cell migration. Herein we combine 3D micropillar topography of defined spacing and controlled chemistry with live imaging and *in silico* cell numerical simulation using SaOS-2 cells that previously showed maximum deformation[12], to understand the mechanism by which cells deform their nuclei. We show that nuclear deformation in confinement is orchestrated by pulling forces which are regulated by actomyosin coupled to nucleo-skeleton interconnections (the LINC complex) and is assisted by vimentin.

RESULTS

Nuclear deformation is accompanied with chromatin, cytoskeleton and focal adhesion reorganization:

Kinetics of nuclear deformation and chromatin reorganization

Our previous studies showed that SaOS-2 cells possess a greater ability to deform on micropillars their healthy counterparts[11,15]. Of six different cell lines tested, SaOS-2 osteosarcoma cells displayed the most severe nuclear deformation on poly-L-lactic acid micropillars with 7 µm height, width & space, despite being the stiffest cell line (AFM measurements)[12,15]. The nuclear deformation was quantified by determining the cross-sectional area of nucleus above (undeformed) and below (deformed) the pillars and reporting the proportion below the top of the pillar as the deformation percentage **(S1 and method section).** Using the same fabrication techniques and dimensions of pillars we first investigated the kinetics of nuclear deformation and cell adhesion on micropillars.

The nucleus starts to deform from one hour after the cell contacts the surface and progressively inserts in the interpillar space and finally reaches a stabilized and maximum at 24 hrs (**Fig. 1a,b** and **movie SM1**)**.** Unless otherwise mentioned, all further experiments were performed after 24 hrs of incubation, once nuclear deformation has been achieved and is stable.

We noticed that cells proliferate for days within the pillar arrays, which raised the question of cell division in the confined state[11]. We found that the cells avoided confinement and ascended perpendicularly to the micropillar substrate to perform mitosis (**S2 & SM 2**)[18]. The daughter cells invaded subsequently the structure quickly after cytokinesis, faster than initial cell confinement kinetics, probably because the daughter cells retain FAs from mother cells[19].

Focal adhesion localization during nuclear deformation

Cells adhere to surfaces using integrin mediated focal adhesions (FAs) [20]. We analyzed the FAs localization on pillars by labelling paxillin in cells fixed at different timepoints (**Fig. 1c**). To facilitate the quantification of FAs, we segmented the pillars in top side & top surface, middle and bottom areas and quantified the average number of FAs for each area (details in methods and materials). FAs localize initially to the top part of pillars and gradually disseminate down the lateral sides**.** FA density increases over the initial 6-8 hours and reaches a plateau, concomitantly with the nuclear deformation kinetics. Interestingly, at any time of the process the FAs are preferentially distributed more on the mid-lateral side of pillars compared to bottom and combined top side and surface areas. Altogether, our results show that nuclear deformation progression is correlated with an increase in FA density preferentially on the mid-lateral regions of the interpillar space**.**

Cytoskeletal organization during nuclear deformation

The cytoskeleton plays a crucial role in adapting the cell to its environment[21]. We thus looked at the organization of cytoskeletal components (microfilaments, intermediate filaments (IFs) and microtubules) in deformed SaOS-2 cells. We found that actin and IFs exhibited higher density around the pillar contours whereas microtubules were uniformly spread throughout the cell (**Fig. 1d**)**.** In addition, vimentin IFs accumulated in the center of the cell around the nucleus. The cytoskeleton and FA organization during nuclear deformation is summarized in **Fig. 1e**.

Nuclear deformation is governed by actomyosin and intermediate filaments dynamics.

Next, we dissected the individual contribution of microfilaments (actin), myosin, IF (vimentin) and microtubules (β-tubulin) in the nuclear confinement process. Optimal drug concentrations were determined using standard MTT assay with 50% cell viability (**S3 and methods).** We then used the percentage of nuclear deformation as a readout for nuclear confinement. We found that depolymerizing actin (cytochalasin D, latrunculin B), inhibiting the actin motor protein myosin II activity (blebbistatin, ML 7) as well as depolymerizing IF with acrylamide and 3, 3'-iminodipropionitrile (IDPN) strongly reduced nuclear deformation compared to the control cells (**Fig. 2a and b**)**.** Microtubule depolymerization (colchicine, nocodazole) did not have any effect

on nuclear deformation. Since drugs depolymerizing IF could have cytotoxic effects even when used at optimum concentration[22], we confirmed the results using a gene silencing technique (RNA interference) for vimentin IF specifically. The silencing efficiency was confirmed by RT-qPCR and western blot techniques **(Fig. 2c and d).** Nuclear deformation after vimentin knockdown (KD) was found to be similar to the results obtained with drugs, thereby confirming the role of IF in assisting nuclear deformation on micropillars **(Fig. 2e).** We also performed drug washout control experiments for actin, myosin and vimentin individually to verify the recovery of nuclear deformation when the cytoskeletal polymerization is restored. Our results showed that nuclear deformation was regained over time (2, 5 and 20 hours) after the respective drugs were washed out **(S4).** Thus, our results show that acto-myosin and IF play crucial roles in cell-nuclear confinement contrary to microtubules whose role seems negligible.

Coupling the cytoskeleton to the nucleus through nesprins is necessary for nuclear deformation.

The LINC complex drives the nuclear deformation

The nucleus is bridged to the cytoskeleton by nucleoskeletal proteins which form the LINC (linker of nucleo-cytoskeleton) complex. Cytoskeletal components (Actin, microtubules, IFs) are connected to nesprins, which cross the outer nuclear membrane, and in turn are connected to SUN proteins embedded between inner-outer nuclear membrane[23]. Hence, we next focused on dissecting the role of LINC components in nuclear deformation. We silenced SUN1, SUN2 and syne2 (nesprin2) individually and confirmed the silencing efficiency by immunofluorescence, RT-qPCR and western blot **(Fig. 3a-c).** Our results showed a small, but non-significant reduction in levels of nuclear deformation compared to control cells **(Fig. 3d).** Functional redundancy within SUN and nesprin variants that were not silenced might have played a compensatory role in the process. We attempted to target multiple LINC components using the same RNAi approached but the silencing efficiency was reduced significantly. Thus, we targeted the LINC complex by overexpressing a dominant-negative construct **(Fig. 3e)**. Nesprins have a highly conserved KASH (Klarsicht, ANC-1, Syne homology) domains at their C-termini that bind to SUN proteins while their N-termini bind to different cytoskeletal constituents[23]. A dominant negative-KASH (DN-KASH) mcherry construct has been developed that saturates the binding sites of SUN proteins causing displacement of endogenous nesprin to endoplasmic reticulum[24,25]. It is truncated at the

cytoskeletal binding domain, thereby disconnecting the link between cytoskeleton and nucleus (**Fig. 3f**). Nesprin 2 immunostaining confirmed the delocalization of endogenous nesprins after DN-KASH overexpression (**Fig. 3g**). However, the transfection efficiency varies within the cell population. Hence, we quantified the nuclear deformation of cells in regard to DN-KASH expression levels. We found that both low and high DN-KASH expression levels showed significant reduction in nuclear deformation compared to un-transfected cells (**Fig. 3h**). In addition, cells accumulating the highest DN-KASH levels presented less nucleus deformation in comparison to low DN-KASH expression cells. Altogether, these results highlight the central role of LINC-cytoskeleton coupling in nuclear deformation and cell confinement.

Lamin A plays an insignificant role in nuclear deformation

At the nuclear interior, the LINC complex is connected to lamins that make up the filamentous network underlying the inner nuclear membrane. We therefore asked whether A-type lamins, the major proteins of the nuclear lamina involved in its mechanics, have an effect on SaOS-2 nuclear deformation[26]. We looked at the nuclear deformation using two complementary approaches, by either downregulating (KD) or overexpressing (transfection) lamin A-GFP levels (**Fig. 3i-l**). Surprisingly, neither the increase nor decrease in A-type lamin levels affected the nuclear deformation ability (**Fig. 3m**). We also compared the levels of lamin A with the healthy hMSCs and found no significant difference in the A-type lamin levels. As the healthy cells do not deform compared to SaOS-2, the deformability is not due to A-type lamins. This could also mean that push and pull forces are adapted by the cell to deform the nucleus, independent of the rigidity caused by A-type lamin levels.

Cell adhesion to the lateral sides (but not the top or bottom) of the pillars is necessary for nuclear deformation

Next we wanted to investigate nuclear deformation under additional constraints of dimensions and chemistry. By using these constraints we specifically aimed to address whether the cytoskeleton is pushing down on the nucleus from above, or whether the nucleus is pulled down from below. We thus created three types of surfaces: (1) “all adhesive”, that are completely coated with a cell-adhesive coating (tops and in between the pillars); (2) “top adhesive” pillars, where cells can adhere to the pillar top but not in the space between or the sides of the pillars; and (3) “interpillar

space adhesive" pillars, in which the pillar-tops are cell-repellent but the cells can adhere to the space in between the pillars. To more precisely assess the effects of confined spacings coupled with surface chemistry, we picked pillars of 3 µm spacing, which show least deformation on all adhesive pillars. To allow enough length for the nucleus to squeeze completely (in 3µm spacings) between the top surface repellent pillars we picked 10 µm (**Fig. 4 a**). On "all adhesive" pillars, nuclear deformation reached 30±7% (**Fig. 4 b**). In contrast, on "top adhesive" pillars, no nuclear deformation was observed (0%). Interestingly on "interpillar space adhesive" pillars, the nuclei were completely inserted between the pillars, resulting in a maximum of the nuclear deformation (100%). Such high deformation was not observed even when the pillars were completely adhesive. Altogether, these results show that adhesion to the lateral edges of pillars but not to the top of the pillars is necessary for driving nuclear deformation. Intriguingly, modification of pillar chemistry and topography did not affect hMSCs nuclear deformation indicating that nuclear deformation is a specific trait acquired by the osteosarcoma cells (**S5**). Importantly, our results indicate that the nuclear deformation is due to pulling from the "front" (cell area near bottom of pillars) rather than pushing from "back" (cell area near top of pillars) via actin cap fibers.

In silico cell model analysis of mechanical stress on nucleus during deformation in different conditions

To attain further insight on effect of micropillar topography on mechanical stress on nucleus during strain (deformation) in confinement, we used an assessed *in silico* cell model published by Vassaux et al[27]. It assumes that cell integrity results from the mechanical equilibrium between traction actomyosin contractile network channeled by FAs, compression bearing microtubules assisted by vimentin cables and cytosol[28]. The LINC complex was modeled as connections between the nucleoskeleton and all the three cytoskeletal networks (microfilament, microtubules and IF). Briefly, the nucleus was represented as a dense packing of particles in contact, enclosed by a tensile (stretchable) envelope mimicking the nuclear lamina. The model represents the mechanical stress during nuclear deformation depending on variables such as presence and absence of: i) LINC ii) apical actin cap and iii) pillars dimensions and chemistry modulations. The mechanical stress is assumed to be caused by nuclear components themselves and the cytoskeletal elements (**Fig. 5, S6**).

In the absence of the LINC complex, nuclear deformation and mechanical stress on nucleus are reduced compared to the reference model comprising the LINC complex (~4-fold and 2-fold less respectively) (**Fig. 5a & b**) which recapitulates the cellular biology experiments (**Fig. 3**). This shows that in the absence of LINC complex, the cytoskeleton is unable to transmit forces (observed by least mechanical stress) required for nuclear deformation.

Further, we modeled the pillar dimensions and chemistry constraints to quantify the forces on nucleus. All adhesive pillars serves as a reference for calculation. 1) On "all adhesive" pillars mechanical stress on nucleus during deformation was minimum. 2) On "top adhesive" pillars mechanical stress on nucleus during deformation was least compared to reference surface and 3) On "interpillar space adhesive" nuclear deformation was maximum while the mechanical stress on nucleus doubled compared to the reference surface (**Fig. 5c & d**). All these computational results fit with the biological experiments in **Fig 4**. Maximum mechanical stress on nucleus during complete confinement on interpillar space adhesive pillars (where cell could only attach to the pillars edges and not on the top) indicate that the forces pulling down forces are more essential during nuclear confinement. Besides pulling forces, cells in confined space also experience pushing down forces[14,29,30]. These pushing forces are generated by the apical actin cap. Lastly, we examined the influence of actin cap on both nuclear deformation and mechanical stress caused by the apical cap on nucleus during deformation. We observed that loss of apical actin has no impact on mechanical stress or deformation of nucleus which also coincides with the experimental results (**Fig. 5e & f, S7**). No change in mechanical stress during in absence of actin cap, indicate that the pushing down forces are not significant in deforming the nucleus.

DISCUSSION

Nucleus reshaping is a crucial event in response to cell squeezing in physical cue such as confinement. The recognition of such physical stimuli is done via mechanotransduction - the process by which cells convert mechanical cues from surrounding into biochemical signals. These biochemical signals are relayed to the focal adhesions cell through cell surface receptors such as integrins which leads to restructuring of cell-nuclear architecture[31,32]. This reshaping of the nuclear morphology is a key event in certain physio-pathological processes such as stem cell differentiation, immune responses, wound healing and cancer cell dissemination[3–5]. Thus, the

objective of our study was to comprehend the mechanisms involving deformation of the nucleus- the largest organelle of the cell.

We dissected the role of individual cytoskeletal elements and show that both actomyosin and intermediate filaments (IFs) but not microtubules[14] facilitate nuclear deformation in cancer cells. Actomyosin contractility is known to impact cell-nuclear morphology[12,14,33]. Moreover it has been shown that nucleus adopts a spherical shape when actomyosin activity is perturbed, implying that the nucleus is prestressed[34]. Our results prove that in presence of actin or its motor protein myosin inhibitors the cells are unable to provide flexibility to the cell and nucleus thereby inhibiting the deformation process. Thus, actomyosin are key molecular players involved in cell-nuclear deformation. This is contrary to microtubules[14] which have insignificant effect in this process. Generally microtubules are known to resist deformations. However, confinement is a cue which requires certain cell types to undergo deformation along with its nucleus. Hence, the cell might not use the resistive property of the microtubules to inhibit this distortion process. Nuclear deformation also relies on IF activities such as regulation of intracellular mechanics[35], actin-driven positioning of the nucleus in connection to LINC[36,37] and remodeling of metastatic cytoskeleton[38]. Hence, depletion of IFs could lead to impediment of all these activities thereby reducing nuclear deformation.

Perinuclear cytoskeleton elements are bridged to the nucleus via the LINC complex which in turn is linked to the nuclear lamina and are able to directly transmit forces on the nucleus and modulate chromatin reorganization[39–42]. Thus, absence of the LINC complex disintegrates the bridge between nucleus and cytoskeletal elements such as actin and IFs, thereby disrupting the transmission of forces. Our results corroborate with this hypothesis, proving that LINC complex is imperative in nucleus deformation. A-type lamins are the major determinant of stiffness of the nucleoskeleton. We demonstrated that A-type lamins were insignificant in obstructing nuclear flexibility which is contrary to Hansen et al[14]. This can be attributed first, to the dimension of the pillars that we used and second, to the flexibility of nucleus of cancer cells[43] contrary to the healthy cells used by Hanson et al[43]. We also show that A-type lamin levels in SaOS-2 are similar to healthy hMSCs which do not deform, and therefore the deformability is not due to A-type lamin levels. Furthermore, our *in silico* numerical model predicts that during deformation the cytoskeleton and LINC exerts force on the nucleus. This force could be due to actomyosin

contractility that is known to impart pulling and pushing forces that help the nucleus deformation in confined microenvironment[36].

Cell confinement during metastasis is brought about by forces that either pull or push the nucleus in topographical constraints[17,29,45]. However, the forces predominant in reshaping the nucleus in confinement are still poorly understood. Our chemistry, topography and computational modifications suggest that the nucleus embeds itself completely and experiences most mechanical stress, when it is able to adhere on the lateral edges of the pillars. These forces that are generated by actomyosin dynamics interconnected with FAs, thereby provide a push and pull to help the nucleus deform[29,46]. This could be due to the strong spreading forces exerted by cells on rigid surfaces, in this case our pillar topography[12]. Hence, more FAs are recruited on stiff substrates as more force is required to be distributed across them[47,48]. Our initial results showed that FAs were localized at the mid lateral sides than on the top or bottom part of pillars indicating increased horizontal force for nucleus deformation. This is in accordance with the hypothesis proposed by Hersen and Ladoux., that cells in 3D environment, pull and push in all directions[49] and that depending on substrate rigidity the magnitude of these forces in 3D can vary individually. They proposed that on stiff surfaces (herein micropillars), horizontal forces might increase and vertical ones might decrease. This hypothesis is confirmed by our results where localization of FAs is more on the lateral sides of pillars (leading to horizontal forces and increased cell spreading) rather than on the bottoms of the pillars. Moreover, we saw no influence of vertical pushing forces on nuclear deformation, either by actin cap depletion via lamin A KD or numerical simulations in actin cap tension.

Using a multidisciplinary approach (cell-molecular biology techniques, precise surface chemistry modifications and *in silico* cell modeling) and a cell type that readily deforms in response to confinement, we conclude that-

- Nucleus deformation in confinement is a pulling down mechanism which requires LINC contrary to the pushing down which would not require mechanical LINC connection.
- Deformation of the nucleus by the cell depends more on the cytoskeleton than nuclear stiffness
- Nuclear deformation in topographically-induced confinement is orchestrated with the help of FAs and actomyosin pulling forces mediated by LINC to the nucleus with assistance from IFs (**Fig. 6a,b**).

Furthermore, this conclusion could be extended to understand the cell-nuclear deformation of various cell types (immune cells, stem cells, etc) in response to physical cue such as confinement. Our 3D micropillar array platform provides a simplistic yet ingenious approach to accesses nuclear deformation behaviour of cells separately from migration. This technique could be further exploited to explore the 3D organization of chromosome territories and gene expression patterns modifications and unravel other molecular players/cell signaling pathways related with confinement-induced nuclear deformation.

METHODS

CELL CULTURE:

SaOS-2 osteosarcoma cells (ATCC, USA) were cultured in a humidified incubator at 37 °C and 5% CO_2.
McCoy's 5A Modified medium w/o L-Glutamine was supplemented with streptomycin (0.1 mg/ml) and penicillin (100 U/ml), sterile FBS heat inactivated (15% v/v, Biowest, France) and L-Glutamine (2mM). All products were purchased from Sigma–Aldrich (France) unless specified. For all experiments $1X10^5$/ml cell density was used in 60mm petri dishes.

MICROPILLAR FABRICATION, CELL SEEDING ON PILLAR TOPOGRAPHY, CHEMISTRY MODIFICATION:

PDMS CAST: silicon templates with square micropillars measuring 7µm (height) x 7µm (length) x 7µm (space) were fabricated in IMTEK (Freiburg, Germany). Polydimethylsiloxane (PDMS) (Sylgard 184, Dow Corning, USA) negative replica stamps were produced by uniformly mixing the precursor and curing agent in 10:1 ratio and pouring it over the silicon template glued in an aluminum cup. Following degassing in the vacuum pump for 30 minutes to remove air bubbles, PDMS mixture was cured at 60°C in an oven overnight (ON). Hardened PDMS was then separated from template carefully and used to prepare Poly-L-Lactic acid (PLLA) micropillars.

PLLA FILM: PLLA powder was mixed in chloroform solution and poured in glass petri plate. Uniform PLLA concentration and volume were chosen to keep it constant per unit area of the 10cm glass Petri plate ($0.002g/cm^2$). PLLA film was obtained by allowing the mixture to air dry under fume hood overnight under pressure and then cut into pieces for further use.

PILLAR FABRICATION: Hot embossing was done by heating the PDMS negative replica above the glass transition temperature of PLLA (180°C). The piece of PLLA film was placed over the PDMS template and pressed down manually for approximately 5-10 sec. The assembly containing PDMS-PLLA sandwich was quenched in cold water to vitrify PLLA before demolding.

SAMPLE PREPARATION: Samples were glued using cell compatible aqua-Silicone glue (Den Bravent Sealants, Netherlands) in 60mm Petri plates and then sterilised using 70% ethanol for 10 minutes and dried under laminar air flow.

For more details see[23, 24, 27]

MICROPILLARS DIMENSIONS AND CHEMISTRY MODIFICATIONS:

Polymeric micropillars were fabricated by double replication. As an original, a structured Si wafer was used. The wafer was microstructured with square micropillars with a width of 10 µm, a height

of 10 µm, and spacing of 3 µm. The Silicon wafer was made by the clean room service center of the University of Freiburg (IMTEK). For the first replication step (negative), a commercial PDMS elastomer kit (Sylgard 184, Dow Corning, Midland, USA) was used; base and curing agent were mixed in the ratio of 10:1 (w/w). The mixture was poured over the etched Si wafer and cured at 80 °C for 3 h. The hard PDMS was peeled off the Silicon wafer. The polymer used in the second replication step (positive copy) was obtained by free radical polymerization of n-butyl acrylate (nBA) and 4-(methacryloyloxy) benzophenone (MABP); 5 mol% MABP were used. The resulting P(nBA-co-5%MABP) was dissolved in toluene (100 g/L). A drop of the dissolved polymer was placed on a glass slide (Menzel Gläser cover glasses, round 18 mm, No. 3, VWR, Germany). The PDMS stamp was pressed on top of the dissolved polymer. The combination of all three components (stamp, polymer and glass slide) was crosslinked by UV irradiation (λ = 365 nm, 12.98 J, 90 min). The PDMS stamp was peeled off to liberate the completed microstructured surface. The surface was modified by different methods: To modify the entire surface, spin coating (1000 rpm, 60 sec) with polymer solutions was used either with the cell-repellent (Poly dimethyl acrylamide) P(DMAA-co-5%MABP) (solution in ethanol, 50 g/L), or the cell-attractive (AA-all attractive) P(nBA-co-5%MABP) (solution in toluene, 50 g/L). To modify only the top of the pillars (TA-top attractive, SA-space adhesive), a plane aluminum foil (1 cm× 4 cm) was dip coated (immersion and retraction speed 100 mm/min) with the dissolved polymer. The aluminum foil was then pressed on top of the microstructure and removed directly afterwards. The coated polymer was attached to the surface by UV light crosslinking (λ = 365 nm, 12.98 J, 90 min). For confocal verification of coatings, cell adhesive polymer was tagged with Cyn-5 streptavidin (GE Healthcare, USA) with 1:500 dilution and cell repellent polymer was tagged with Rhodamine B isothiocyanate (Sigma, France) at 1% concentration with the polymer.

DRUG TREATMENT:

All drugs were obtained from Sigma Aldrich (France) unless specified. Concentrations were used as follows: Cytochalasin D (1 µM), Latrunculin B (2 µM), Colchicine (5 µM), Nocodazole (10 µM), 1-(5-Iodonaphthalene-1-sulfonyl)-1H-hexahydro-1,4-diazepine hydrochloride [*ML 7*] (20 µM), Blebbistatin (25 µM), Acrylamide (10 mM) and Iminodipropionitrile [*IDPN*] (2%). The optimum concentration (not cytotoxic) was determined using the standard procedure for MTT colorimetric assay. Cytotoxicity was determined 6 hours after drug treatment. Absorbance was measured at 570nm (normalised at 620nm) using EZ READ 400 Plate reader (Bichrom, UK). Percentage viability graph was plotted (**S5**)**.** Drugs were added in the medium containing cells in suspension and then seeded on pillars for 6 hours. Drug washout experiment was performed at 2, 5 and 20 hours with1X PBS (Gibco, Life technologies, USA).

IMMUNOSTAINING:

Unless specified products were purchased from Sigma, France. Cells were fixed with 4% formaldehyde (Electron Microscopy Sciences, USA) and permeabilized using 0.5% Triton X-100

for 15 min and blocked with 3% bovine serum albumin for 1 hour. Incubation with primary antibodies was done for 1 hour with following antibody concentration: anti-vimentin (1:50; V6630; anti-Mouse), anti-βtubulin (1:200; T4026; anti-Mouse), anti-myosin IIA (1:100; M8064; anti-Rabbit), anti-paxillin (1:250; ab32084; anti-Rabbit; Abcam-UK), anti-pericentrin (1:100; ab4448; anti-Rabbit; Abcam-UK), anti-Histone deacetylase 1 (1:200; H3284; anti-Rabbit), anti-Sun 1 (1:100; M8064; anti-Rabbit), anti-Sun 2 (1:100; M8064; anti-Rabbit), anti-SYNE2 (1:50; HPA003435; Atlas, Sweden), anti-Lamin A (1:500; L1293; anti-Rabbit). After short rinses in 1X PBS, secondary antibodies were incubated for 1 hour using Alexa 488 (1:200; ab150073; anti-Rabbit; Abcam-UK), Alexa 488 (1:200; ab150113; anti-Mouse; Abcam-UK), Alexa 647 (1:200; ab150115; anti-Mouse; Abcam-UK). Confocal acquisitions were done after PBS rinses. Actin-555 (1:20; A34055; Thermoscientific-France) or phalloidin-FITC (Fluorescein-5-isothiocyanate) (0.4µg/ml) were used to label actin and Hoechst (1:1000; 33258; Thermoscientific-France) was used to label nucleus.

TRANSFECTION

Dominant Negative-KASH plasmid DNA was kindly gifted by Dr Nicolas Borghi (Jacques Monod Institute, Paris-France). Lamin A-GFP was used to overexpress lamin A (17653, Addgene, USA). Cells cultured upto 60-70% confluency were transfected with plasmids using Lipofectamine 3000 (Thermoscientific, France) upon manufacturer's recommendations. Culture media used for transfection was deprived of antibiotics. After transfection, cells were seeded for 48-72 hours on pillars before imaging.

For the nuclear deformation of the cell over time, cells were transfected with baculovirus kit for actin-RFP and histone-GFP (BacMan 1.0 and 2.0, Thermoscientific-France). The transfection was carried out according to the manufacturer's protocol. The particle per cell (PPC) value was determined to be 40 for SaOS-2. For histone-GFP kit 1.0, cells were incubated for 4 hours with baculovirus, followed by 2 hours incubation with enhancer at 37 °C with 5% CO_2 in a humidified incubator. For actin-RFP kit 2.0, the cells were directly transfected with the baculovirus and allowed to grow for 16 hours at 37 °C with 5% CO_2 in a humidified incubator.

SiRNA TREATMENTS AND QUANTITATIVE REAL TIME-PCR:

SiRNA used from Thermoscientific- France; were scrambled negative control (AM4613), *SYNE2* (s23330), *SUN2* (s24465), SUN1 (s23629) and *LMNA* (s8221) respectively. Transfection was carried out using Lipofectamine® RNAiMAX Transfection Reagent (Thermoscientific, France) protocol. 10pmol concentration of siRNA was selected for the knockdown. Vimentin siRNA was used at a 40pmol concentration (sc-29522, Santa Cruz Biotechnology, USA). RNA extraction was carried out after 72 hours of KD treatments using RNAeasy micro-kit (Qiagen, France). The quantity and quality of RNA was determined using Nanodrop spectrophotometer (Maestro, Taiwan). Retrotranscription was performed using iQ™ SYBRgreen mastermix (Biorad, Switzerland) in iScript cDNA synthesis instrument (Biorad, Switzerland). The data was normalized against 18S methyltransferase *(emg1)* housekeeping gene. Primers were designed with

melting temperature at 60°C, using primer design algorithm suggested by online using the GenScript Real-time PCR Primer Design algorithm (https://www.genscript.com/tools/real-time-pcr-tagman-primer-design-tool). The qRT-PCR efficiency was determined using LinRegPCR software (Heart failure research centre, Netherland). Expression levels were further analyzed based on ΔΔCT method (n=2). The primer sequences information is given in **S8.** The qPCR program was one cycle at {95 C-30 s}, followed by 39 cycles at {95 C for 5 s} and {60 C for 30 s}. PCR products were then sequentially heated to {65 C for 2 s} and to {95 C for 5 s} to measure the dissociation curve. Experiments were independently repeated at least twice. qPCR efficiency was assessed using the LinRegPCR program (version 2015.2). The expression levels of the genes were analyzed based on the ΔΔCT method, as described by Livak et al. [50].

WESTERN BLOT ANALYSIS:

Unless specified, instruments and supplies were all purchased at Bio-Rad (Germany). Western blot was performed according to the general protocol provided by the Bio-Rad company. Briefly, cell lysis and protein resuspension were achieved in radio immunoprecipitation assay (RIPA) buffer. Total protein amount was then estimated using the colorimetric Micro BCA™ Protein Assay (Thermoscientific-France). 20µg of total protein sample was loaded on a precast Mini-protean TGX stain-free gels and separated according to their size by electrophoresis. Protein gel images for normalization were acquired using ChemiDoc™ Imaging Systems before transfer. Proteins were transferred from the gel to 0.2µm polyvinylidene difluoride (PVDF) pre-activated membranes using the Transfer Blot turbo system. Afterwards, unspecific sites were saturated with 3% BSA (Sigma, France) for 1 hour at room temperature (RT). Primary antibody incubation was performed overnight at 4°C, using the following antibody concentrations: lamin A (1:500, Sigma, France), vimentin (1:200, Sigma, France), SUN1 (1:1000, Abcam-UK), SUN2 (1:100, Sigma, France) and nesprin2 (1:50, Sigma, France). After short rinses, blots were incubated with the Horse Radish Peroxidase (HRP) secondary antibody (1:3000) for 1h at RT. Protein bands were revealed using a chemiluminescent substrate (Clarity™ Western ECL Blotting Substrates) and digitally acquired using the ChemiDoc™ Imaging Systems. Full-sized immunoblots images are given in **S9.**

CONFOCAL IMAGING:

Imaging was done on an upright Carl Zeiss LSM 700 confocal microscope, Germany, using ZEN software. For live imaging z stack were acquired using 63X/1.4 oil; 63X/1.0 VIS-IR water or 20X/1.0 DIC VIS-IR W Plan-Apochromat objective (Zeiss, Germany) equipped with temperature (Okolab, Italy), CO_2/O_2 (Okolab, Italy), and humidity controlled chamber.

IMAGE ANALYSIS AND QUANTIFICATION:

NUCLEAR DEFORMATION AND CHROMATIN CONDENSATION: Cross-sectional images of nuclei were quantified using ImageJ/Fiji (NIH, version 2.0.0-RC-61/1.51n, USA)[51]. The area

below the pillars was considered as deformed and above pillars was considered undeformed. The deformed area was divided by the total cross-sectional area of the nucleus to obtain the percentage of deformation **S1.**

CHROMATIN CONDENSATION: Z-stack of nuclei were acquired with interval constant at 0.15µm. For more details see [52].

FOCAL ADHESION LOCALIZATION ON PILLARS: The height, the number of slices and the interval between slices was kept constant for all independent acquisitions. The image was then thresholded and the resulting particles were analyzed using stack position option in set measurement plugin. Average number of FA in each section was plotted on Y-axis showing the height of pillars and X-axis showing the average number of FA/cell.

***IN SILICO* CELL MODEL:**

The cell model was the one developed and validated previously by authors to analyze in a previous study the influence of the substrate convexity on cell adhesion and nucleus strain[27]. The in silico cell model is widely described in Vassaux et al. In the present study, only the substrate composed of micropillars was implemented and the composition of the model and the adhesion process are same as used in the Vassaux et al paper[27]. To summarize, it is based on the *in silico* cell model concept assumes that cell integrity results from the mechanical equilibrium between the actomyosin contractile network and the compression-bearing microtubules and cytosol. The cell model is an implementation of the tensegrity concept using LMGC90, a multi body contact dynamics software[53,54] to represent the cytoskeleton of the cell as a multi interaction system that can rearrange when the cell move and deforms. In the cell model the cytoskeleton results from networks of tensile cables and compressive springs or contacts which link the 10 000 spherical particles that compose the cell model (**S6**)**.**The constitutive equations governing tensile pre-stressed cables and compressive spring or contact interactions are extensively described in Vassaux et al[27]. Computations using the cell model are solved when each particle verifies the mechanical equilibrium between external and interaction forces and the inertial force. Every particle is given a special role to represent in the model the various sub-structures of the cell. For instance, the nucleus is represented as a dense packing of particles in contact enclosed by a tensile envelop (stretchable membrane) reproducing nuclear lamina. Identically the cytosol is represented as a dense packing of particles enclosed by the tensile (stretchable) cell membrane. Stress fibers are considered as longitudinal structures of aligned particles which are linked by highly contractile cables and link the focal adhesion points while shorter actomyosin filaments are represented by a diffuse network of contractile cables. Intermediate filaments are reproduced by loose cables surrounding the nucleus. Microtubules which are able to sustain compression are therefore considered as a network of compressive springs that is generated from the centrosome. Focal adhesions are considered as simple fixed anchorage points of the cell model with the substrate. Finally, the micropillars of the substrate were considered as perfectly rigid and the surface was represented by a rigid clusters of overlapping particles.

Cell model adhesion on micropillars was conducted first through a spreading step. The cell model is initially a 30µm-diameter sphere with 15µm-diameter nucleus. It spreads over the micropillars until it reaches a diameter of 60µm, being anchored via 30 main focal adhesions. Then the second step occurred in which the cytoskeleton was remodeled from the additional focal adhesion which are formed at the cell membrane which is in contact to the on the surface of the micropillars. We considered a density a potential adhesion site of 0.25/µm². Between the new focal adhesion, stress fibers are formed and generated an intra-cellular tension.

To reproduce experimental protocol, we simulated cell adhesion on micro pillars of 7µm of height, width and space, in the both cases in which LINC is activated or blocked. Moreover we simulated a variation of actin cortex tension to analyze its contribution in nucleus strain.

Force values were calculated depending upon adhesion conditions, where 1 MPa of stress corresponded to surface distribution of 10^6 N/m².

To verify the nuclear deformation we modeled micro pillars of 10µm of height, width and 3µm space to estimate the influence of adherence location on top, wall of the pillars and the space between them.

STATISTICAL ANALYSIS

All the results were checked for significance by using one way ANOVA test followed by two-tailed Student's *t*-test (unequal variance) for pairwise comparison and Dunnet's test for multiple comparisons, using GraphPad Prism software (GraphPad Software, Inc). The significance value obtained were categorized as $P > 0.05$ for ns (not significant); $P \leq 0.05$* (statistically significant); $P \leq 0.01$** (very statistically significant) and $P \leq 0.001$*** (extremely statistically significant). All the error bars indicate the ± standard deviation of samples.

REFERENCES

1. Kirby, T. J. & Lammerding, J. Cell mechanotransduction: Stretch to express. *Nat. Mater.* **15,** 1227 (2016).

2. Pickup, M. W., Mouw, J. K. & Weaver, V. M. The extracellular matrix modulates the hallmarks of cancer. *EMBO Rep.* **15,** 1243–1253 (2014).

3. Grespan, E. *et al.* Effect of geometrical constraints on human pluripotent stem cell nuclei in pluripotency and differentiation. *Integr. Biol.* **10,** 278–289 (2018).

4. Barzilai, S. *et al.* Leukocytes Breach Endothelial Barriers by Insertion of Nuclear Lobes and Disassembly of Endothelial Actin Filaments. *Cell Rep.* **18,** 685–699 (2017).

5. Safferling, K. *et al.* Wound healing revised: A novel reepithelialization mechanism revealed by in vitro and in silico models. *J Cell Biol* **203,** 691–709 (2013).

6. Calero-Cuenca, F. J., Janota, C. S. & Gomes, E. R. Dealing with the nucleus during cell migration. *Curr. Opin. Cell Biol.* **50,** 35–41 (2018).

7. Ivanovska, I., Swift, J., Harada, T., Pajerowski, J. D. & Discher, D. E. Physical Plasticity of the Nucleus and its Manipulation. *Methods Cell Biol.* **98,** 207–220 (2010).

8. Jafari Bidhendi, A. & Korhonen, R. K. A Finite Element Study of Micropipette Aspiration of Single Cells: Effect of Compressibility. *Comput. Math. Methods Med.* **2012,** (2012).

9. Broers, J. L. V. *et al.* Decreased mechanical stiffness in LMNA-/- cells is caused by defective nucleo-cytoskeletal integrity: implications for the development of laminopathies. *Hum. Mol. Genet.* **13,** 2567–2580 (2004).

10. Graham, D. M. *et al.* Enucleated cells reveal differential roles of the nucleus in cell migration, polarity, and mechanotransduction. *J Cell Biol* jcb.201706097 (2018). doi:10.1083/jcb.201706097

11. Davidson, P. M., Özçelik, H., Hasirci, V., Reiter, G. & Anselme, K. Microstructured Surfaces Cause Severe but Non-Detrimental Deformation of the Cell Nucleus. *Adv. Mater.* **21,** 3586–3590 (2009).

12. Badique, F. *et al.* Directing nuclear deformation on micropillared surfaces by substrate geometry and cytoskeleton organization. *Biomaterials* **34,** 2991–3001 (2013).

13. Ermis, M., Akkaynak, D., Chen, P., Demirci, U. & Hasirci, V. A high throughput approach for analysis of cell nuclear deformability at single cell level. *Sci. Rep.* **6,** 36917 (2016).

14. Hanson, L. *et al.* Vertical nanopillars for *in situ* probing of nuclear mechanics in adherent cells. *Nat. Nanotechnol.* **10,** 554 (2015).

15. Davidson, P. M. *et al.* Topographically induced self-deformation of the nuclei of cells: dependence on cell type and proposed mechanisms. *J. Mater. Sci. Mater. Med.* **21,** 939–946 (2010).

16. Grespan, E. *et al.* Effect of geometrical constraints on human pluripotent stem cell nuclei in pluripotency and differentiation. *Integr. Biol.* **10,** 278–289 (2018).

17. McGregor, A. L., Hsia, C.-R. & Lammerding, J. Squish and squeeze-the nucleus as a physical barrier during migration in confined environments. *Curr. Opin. Cell Biol.* **40,** 32–40 (2016).

18. Sorce, B. *et al.* Mitotic cells contract actomyosin cortex and generate pressure to round against or escape epithelial confinement. *Nat. Commun.* **6,** 8872 (2015).

19. Minc, N., Burgess, D. & Chang, F. INFLUENCE OF CELL GEOMETRY ON DIVISION PLANE POSITIONING. *Cell* **144,** 414–426 (2011).

20. Fraley, S. I. *et al.* A distinctive role for focal adhesion proteins in three-dimensional cell motility. *Nat. Cell Biol.* **12,** 598–604 (2010).

21. Fletcher, D. A. & Mullins, R. D. Cell mechanics and the cytoskeleton. *Nature* **463,** 485–492 (2010).

22. Haudenschild, D. R. *et al.* Vimentin contributes to changes in chondrocyte stiffness in osteoarthritis. *J. Orthop. Res.* **29,** 20–25 (2011).

23. Lombardi, M. L. *et al.* The Interaction between Nesprins and Sun Proteins at the Nuclear Envelope Is Critical for Force Transmission between the Nucleus and Cytoskeleton. *J. Biol. Chem.* **286,** 26743–26753 (2011).

43. Swaminathan, V. *et al.* Mechanical stiffness grades metastatic potential in patient tumor cells and in cancer cell lines. *Cancer Res.* **71,** 5075–5080 (2011).

44. Cao, X. *et al.* A Chemomechanical Model of Matrix and Nuclear Rigidity Regulation of Focal Adhesion Size. *Biophys. J.* **109,** 1807–1817 (2015).

45. Petrie, R. J., Koo, H. & Yamada, K. M. Generation of Compartmentalized Pressure by a Nuclear Piston Governs Cell Motility in 3D Matrix. *Science* **345,** 1062–1065 (2014).

46. Ciobanasu, C., Faivre, B. & Le Clainche, C. Actin Dynamics Associated with Focal Adhesions. *International Journal of Cell Biology* (2012). doi:10.1155/2012/941292

47. Zhou, D. W., Lee, T. T., Weng, S., Fu, J. & García, A. J. Effects of substrate stiffness and actomyosin contractility on coupling between force transmission and vinculin–paxillin recruitment at single focal adhesions. *Mol. Biol. Cell* **28,** 1901–1911 (2017).

48. Trichet, L. *et al.* Evidence of a large-scale mechanosensing mechanism for cellular adaptation to substrate stiffness. *Proc. Natl. Acad. Sci.* **109,** 6933–6938 (2012).

49. Hersen, P. & Ladoux, B. Biophysics: Push it, pull it. *Nature* **470,** 340–341 (2011).

50. Livak, K. J. & Schmittgen, T. D. Analysis of Relative Gene Expression Data Using Real-Time Quantitative PCR and the 2−ΔΔCT Method. *Methods* **25,** 402–408 (2001).

51. Schindelin, J. *et al.* Fiji: an open-source platform for biological-image analysis. *Nat. Methods* **9,** 676–682 (2012).

52. Versaevel, M., Grevesse, T. & Gabriele, S. Spatial coordination between cell and nuclear shape within micropatterned endothelial cells. *Nat. Commun.* **3,** 671 (2012).

53. Jean, M. The non-smooth contact dynamics method. *Comput. Methods Appl. Mech. Eng.* **177,** 235–257 (1999).

54. Dubois, F. & Jean, M. The non smooth contact dynamic method: recent LMGC90 software developments and application. in *Analysis and Simulation of Contact Problems* 375–378 (Springer, Berlin, Heidelberg, 2006). doi:10.1007/3-540-31761-9_44

Acknowledgements

We are grateful to Dr. Nicholas Borghi (Jacques Monod Institute, Paris-France) to provide us with DN-KASH mcherry plasmid and Dr Tanmay Lele (University of Florida,USA) for Lamin-A GFP plasmid. We also thank Dr. Patricia Davidson (Institut Curie) for the helpful suggestions and discussion. The authors would like to acknowledge financial support from Region Alsace, IRTG Soft Matter and Ligue contre le Cancer CCIR-GE (2015).

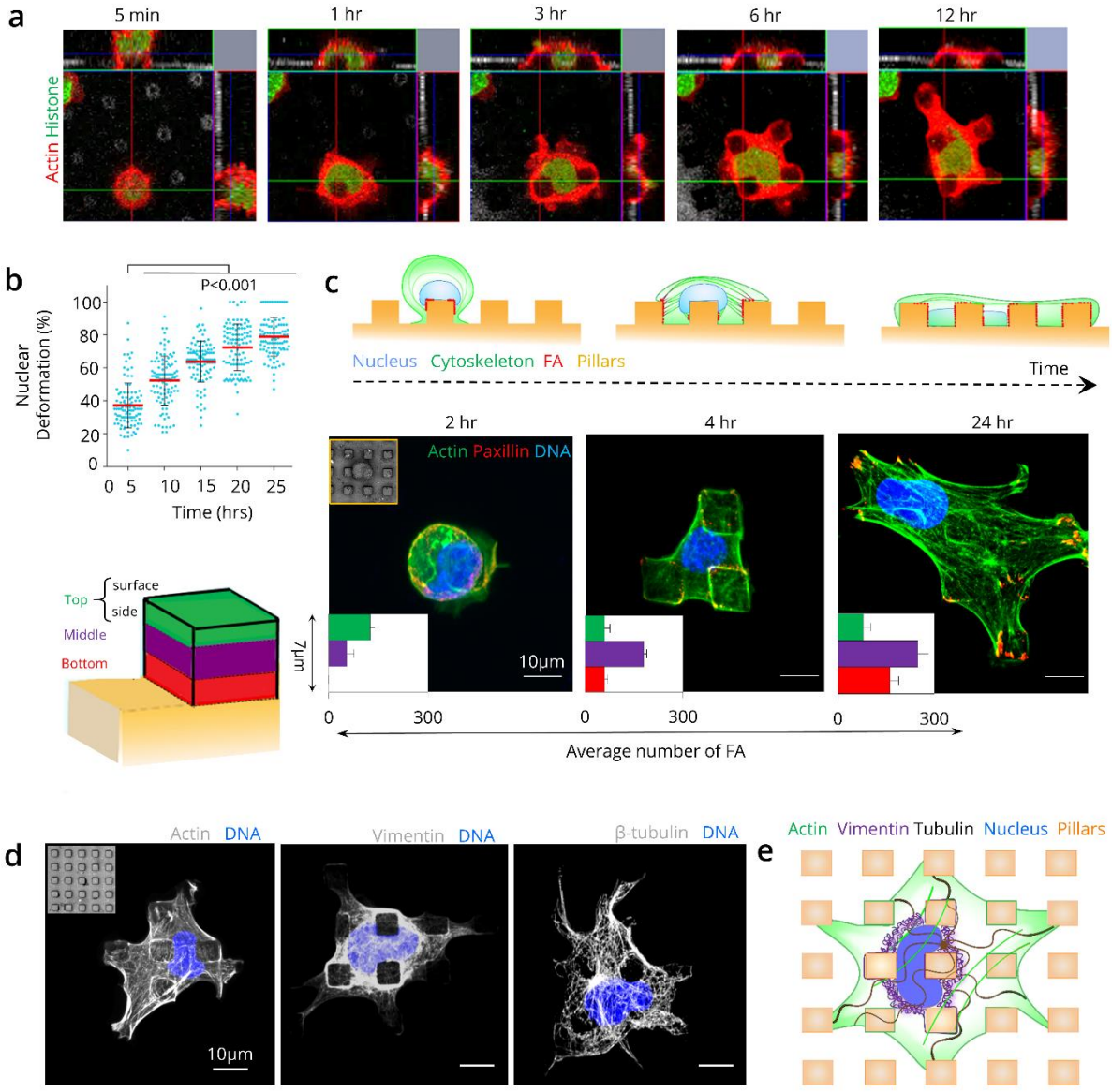

Figure 1. Nuclear deformation involves focal adhesions, chromatin and cytoskeletal dynamics.

a SaOS-2 deformation kinetics on pillars. Time point images extracted from live imaging (SM1). **b** Graph depicting nuclear deformation (%) at 2, 4, 6, 8 and 24 hours respectively (n=50 nuclei at each time point over two independent experiments). **c** Graphical abstract of kinetics of cell adhesion, FAs localization and nuclear deformation on pillars. z-stack projection of SaOS-2 cells immunostained at 2, 4 and 24 hours for Actin (green), paxillin (red) and nucleus (blue). Graphical sketch of 3D pillar divided in top, middle and bottom part for FAs localization quantification. Graphs represent the number of

averaged FAs in top, middle and bottom positions (n=15 at each time point over two experiments). **d** Immunostaining images showing cytoskeleton elements: actin, vimentin and microtubules (grey) and blue nucleus organization on pillars. **e** Graphical sketch resuming cytoskeletal elements organization after nuclear deformation on pillars. Error bars indicate ± s.d; red line represents the median; significance levels were determined by one way ANOVA followed by Dunnet's test for multiple comparison; ***p<0.001, **p<0.01, *p≤ 0.05 and ns=not significant.

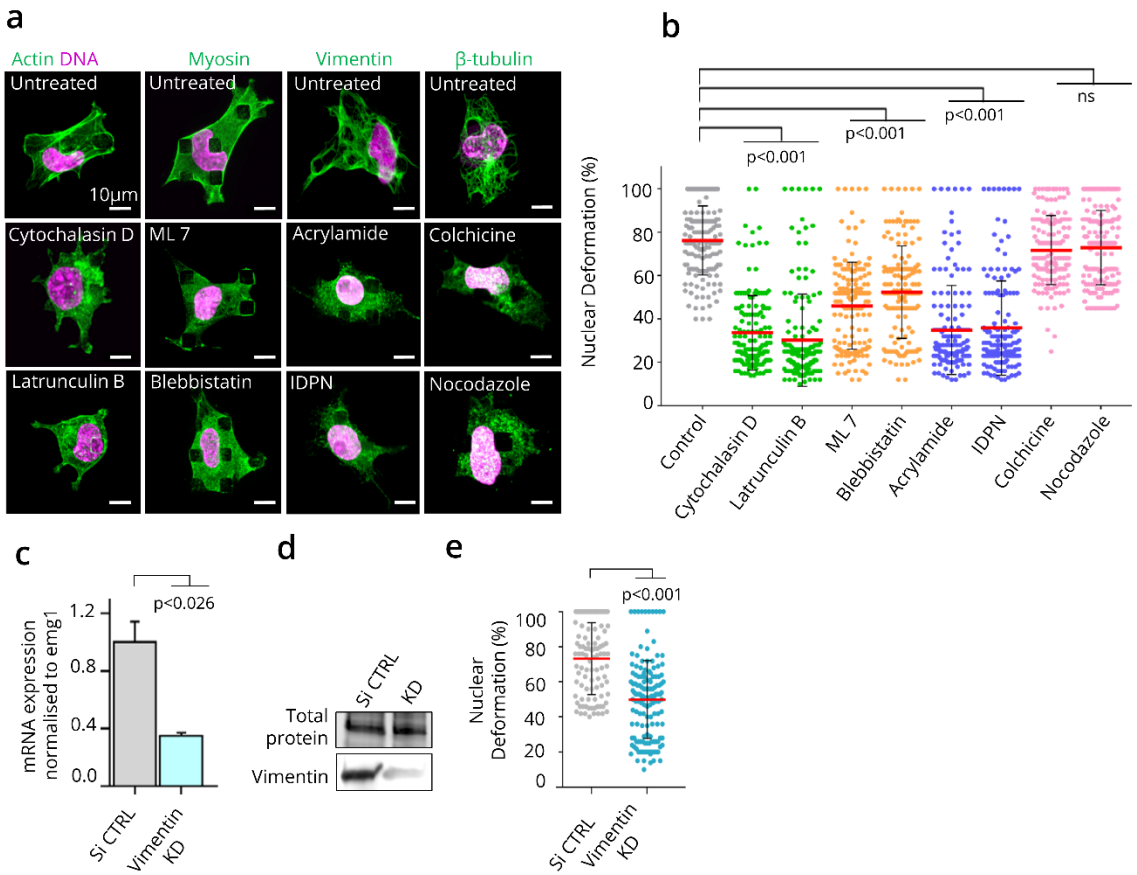

Figure 2. Actomyosin and IF drive nuclear deformation

a Immunostaining of SaOS-2 cells on micropillars at 24 hrs time point after drug treatments. Z stack projection of cells immunostained with actin (green) and nucleus (magenta); myosin IIA (green); vimentin (green), β-tubulin (green). Images were taken after drug treatments targeting actin [cytochalasin D (1µM) and latrunculin (2µM)]; myosin [ML 7 (20µM) and Blebbistatin (25µM)]; vimentin [acrylamide (10mM) and iminodipropionitrile [IDPN] (2%)] and β-tubulin [colchicine (5µM)

and nocodazole (10µM)]. **b** Graph showing nuclear deformation (%) after drug treatment (n=60/drug treatment over two experiments). **c** Vimentin knockdown at RNA level (qPCR) and **d** at protein level (western blot) **e** Graph representing nuclear deformation (%) after vimentin knockdown (n=50/siRNA treatment over two experiments). All experiments were performed independently twice. Red line represents the median. Error bars indicate ± s.d; significance levels were determined by one way ANOVA followed by Dunnet's test for multiple comparison and two-tailed Student's unpaired t test for unequal variance; ***$p<0.001$, **$p<0.01$, *$p\leq 0.05$ and ns=not significant.

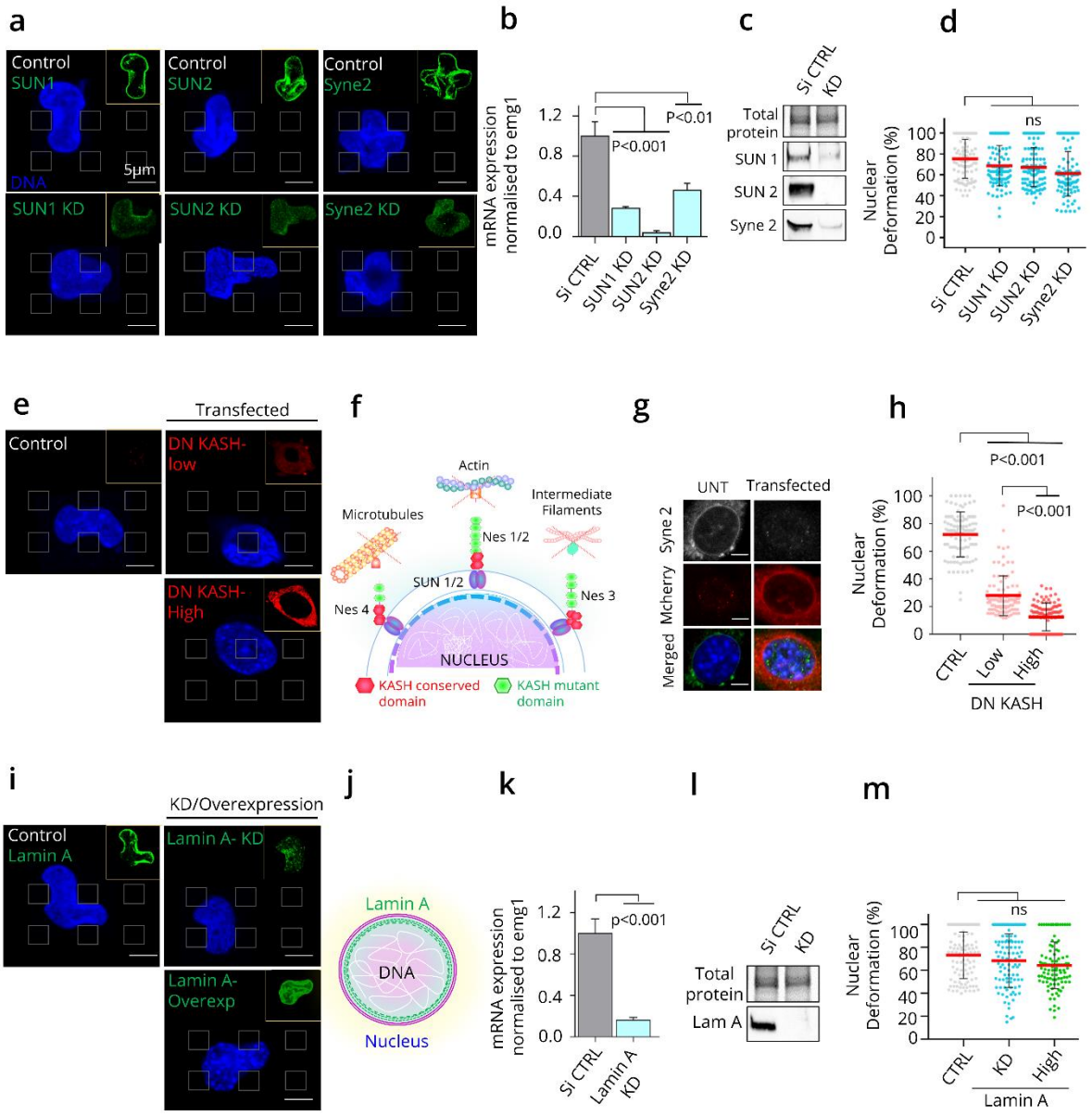

Figure 3. Nuclear deformation requires LINC-cytoskeletal coupling

a SaOS-2 nuclei at 24 hrs time point on micropillars after siRNA treatments. Immunostaining for SUN1, SUN2 and Syne2 (Nesprin2) (green) at right top corner and Hoechst staining for nucleus (blue). All images are Z stack projection. **b** SUN1, SUN2, Syne2 knockdown (KD): at RNA level (qPCR) **c** KD at protein level (western blot). **d** Quantification of nuclear deformation (%) after KD treatments. **e** Confocal images of SaOS-2 transfected with DN-KASH mcherry. **f** Graphical abstract showing disruption of LINC-cytoskeletal connection. **g** Verification of dislocation of endogenous nesprin (grey) by immunofluorescence after DN-KASH transfection. **h** Percentage of nuclear deformation after DN-

KASH transfection. **i** Confocal images of SaOS-2 after lamin A overexpression or KD. **j** Graphical sketch of lamin A distribution in nucleus. **k** Lamin A knockdown (KD): at RNA level (qPCR). **l** KD at protein level (western blot). **m** nuclear deformation after KD and overexpression of lamin A. For all experiments n=50 nuclei over two experiments. Red line represents the median. Error bars indicate ± s.d; significance levels were determined by one way ANOVA followed by Dunnet's test for multiple comparison; ***p<0.001, **p<0.01, *p≤ 0.05 and ns=not significant.

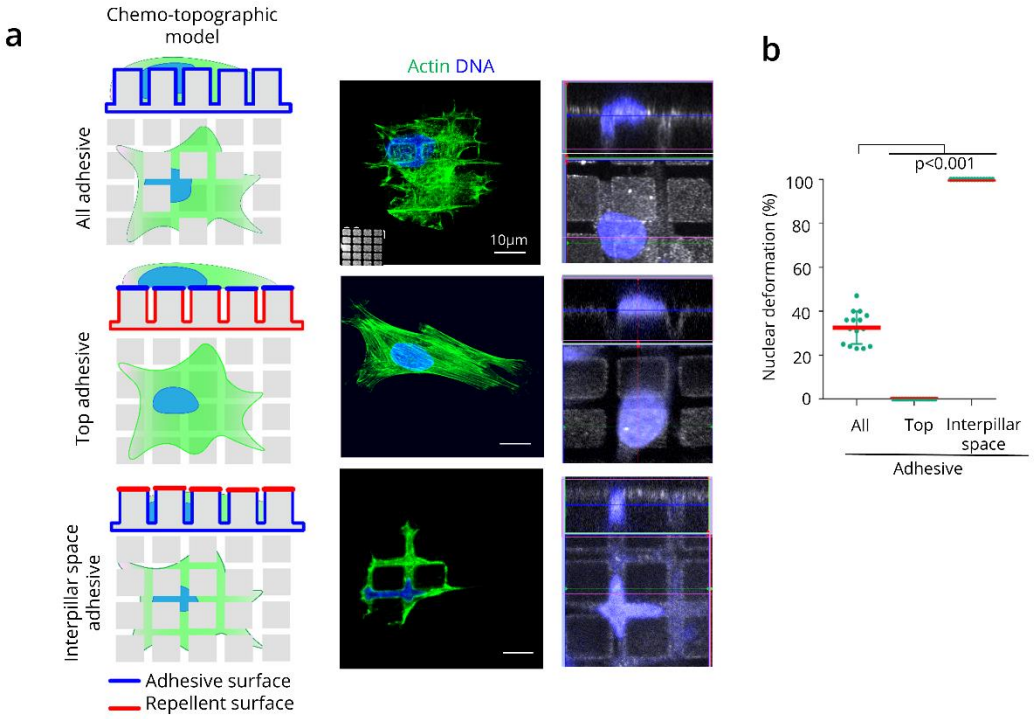

Figure 4. Effect of micropillars chemo-topographic modelling on nuclear deformation

a Sketch representing chemo-topographic alteration of 3/10 µm (space/height) micropillar surface chemistry (Yellow: adhesive, red: repellent coatings). Immunostaining of actin (green), paxillin (red) and nucleus (blue). Orthogonal images of nuclei (blue). **b** graph displaying quantification of corresponding nuclear deformation (%). n=15 nuclei for each surface. All data were compared with all adhesive sample as reference. Error bars indicate ± s.d; significance levels were determined by one way

ANOVA followed by Dunnet's test for multiple comparison; ***p<0.001, **p<0.01, *p≤ 0.05 and ns=not significant.

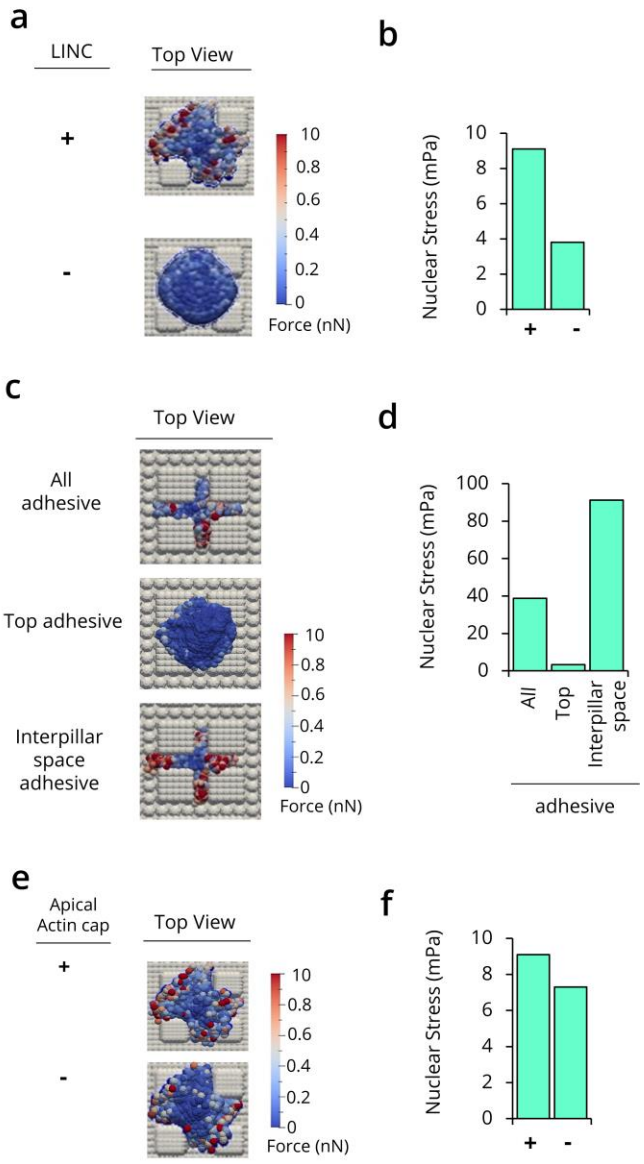

Figure 5. *In silico* cell model to analyze mechanical stress on nucleus during deformation

Computational model images showing the mechanical stress in mPa on pillars with and without LINC (**a & b**), after chemistry and topography surface modifications (**c & d**) and with and without apical actin cap (**e & f**).

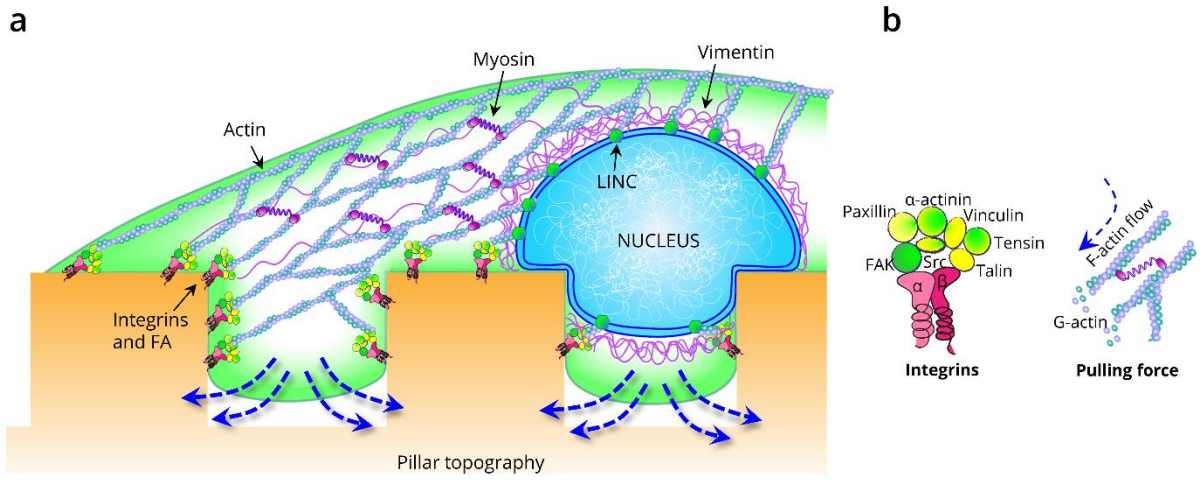

Figure 6. Proposed mechanism underlying nuclear deformation

a FAs mediated actomyosin pulling force, coupled to LINC, drives cell-nuclear deformation on pillar topography. In this system, vimentin IF also assist in nuclear deformation. **b** Focus on FAs assembly along with integrins and F-actin flow mediated by myosin motor protein and actin polymerization.

SUPPLEMENTARY FIGURES

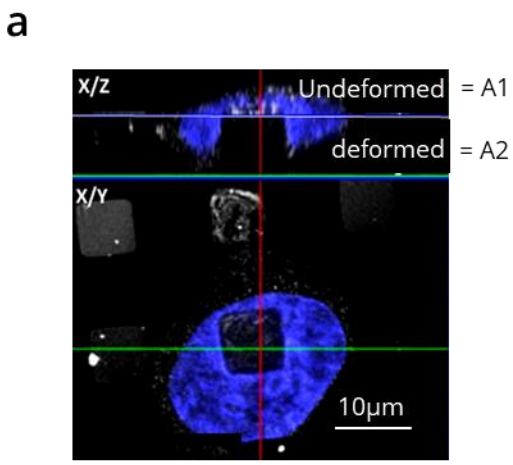

S1: Calculation of nuclear deformation

a Image shows the cross sectional area of nucleus (blue) deformed between the interpillar space. The area above and below pillar is calculated using ImageJ/Fiji. The deformation of nucleus is calculated in percentage by the formula A2/A1+A2*100.

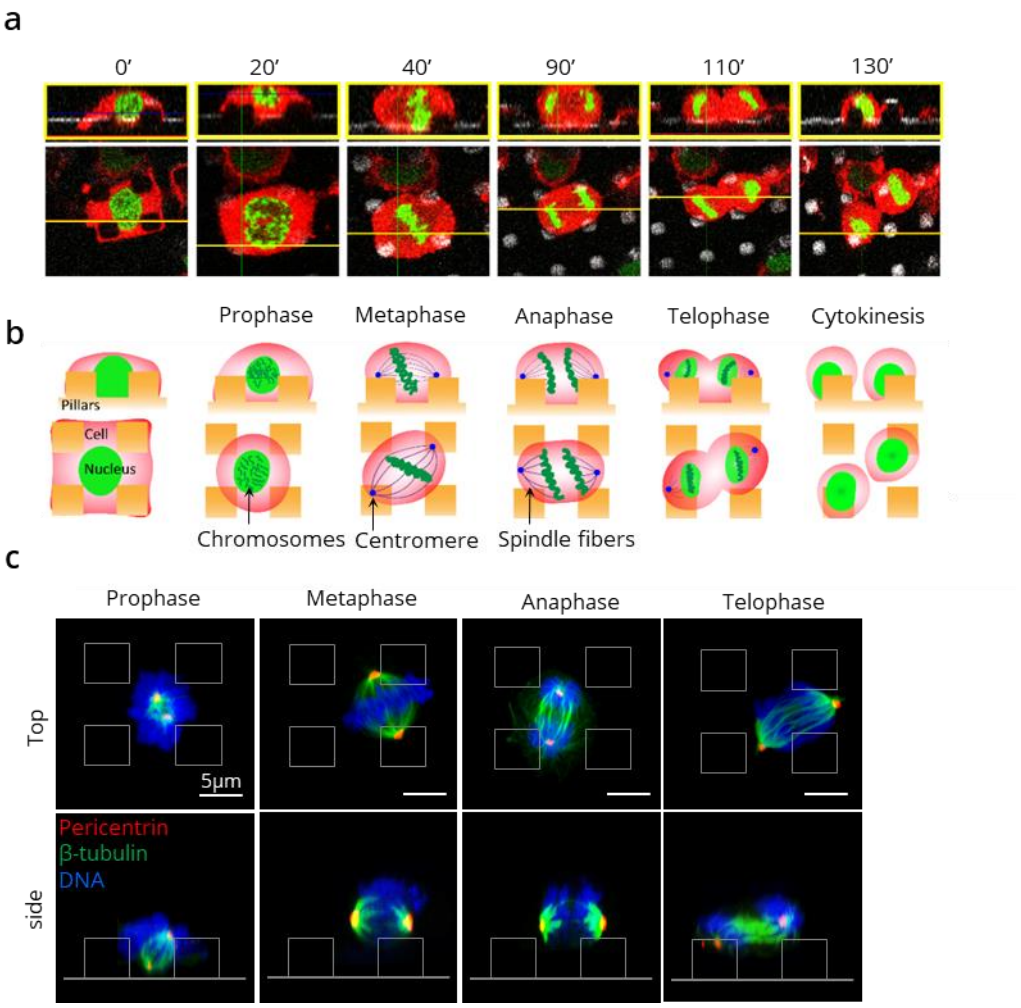

S2: Mitosis on pillars

a Orthogonal view of the SaOS-2 cell dividing on the micro-pillars with time, transfected with histone actin-RFP and histone-GFP. **b** The drawing illustrates the mitotic phases performed by SaOS-2 on pillars. **c** Confocal z stack projection images showing mitotic phases and centromere position during division (pericentrin-red, β-tubulin-green and DNA-blue).

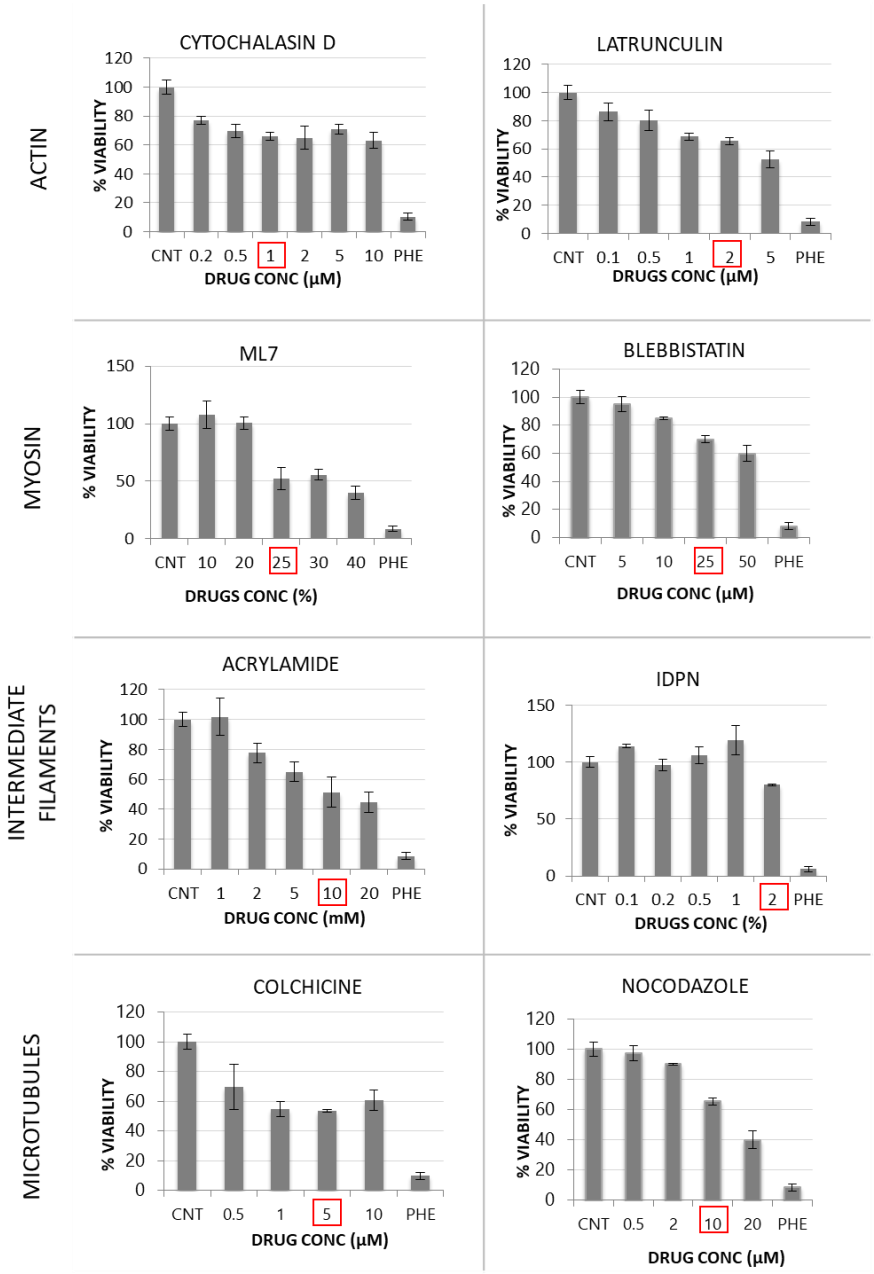

S3: MTT assay

Graph showing the MTT viability test and the respective concentrations chosen (red box). Error bars represent ±s.d resulting from three replicates over two experiments.

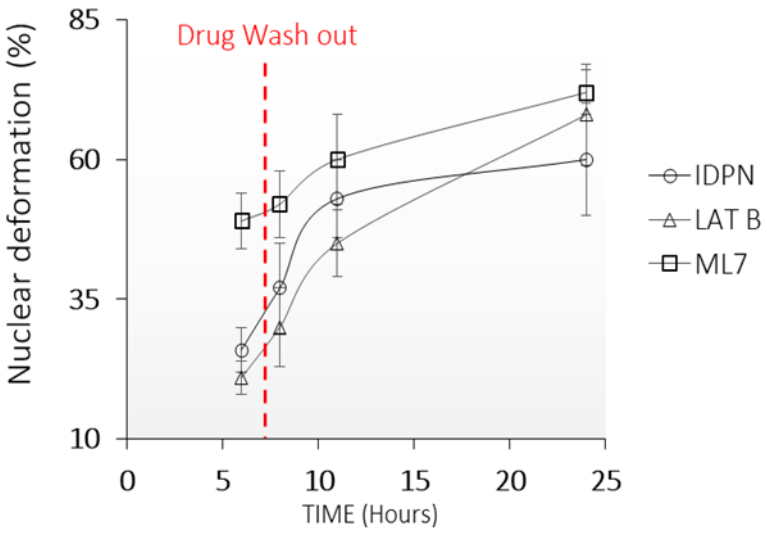

S4: Nuclear deformation is restored after drug washout

Graph showing the retention of nucleus deformation at 2, 5 and 20 hours after drug washout (n=15 cells per drug treatment and time point). Error bars represent ±s.d.

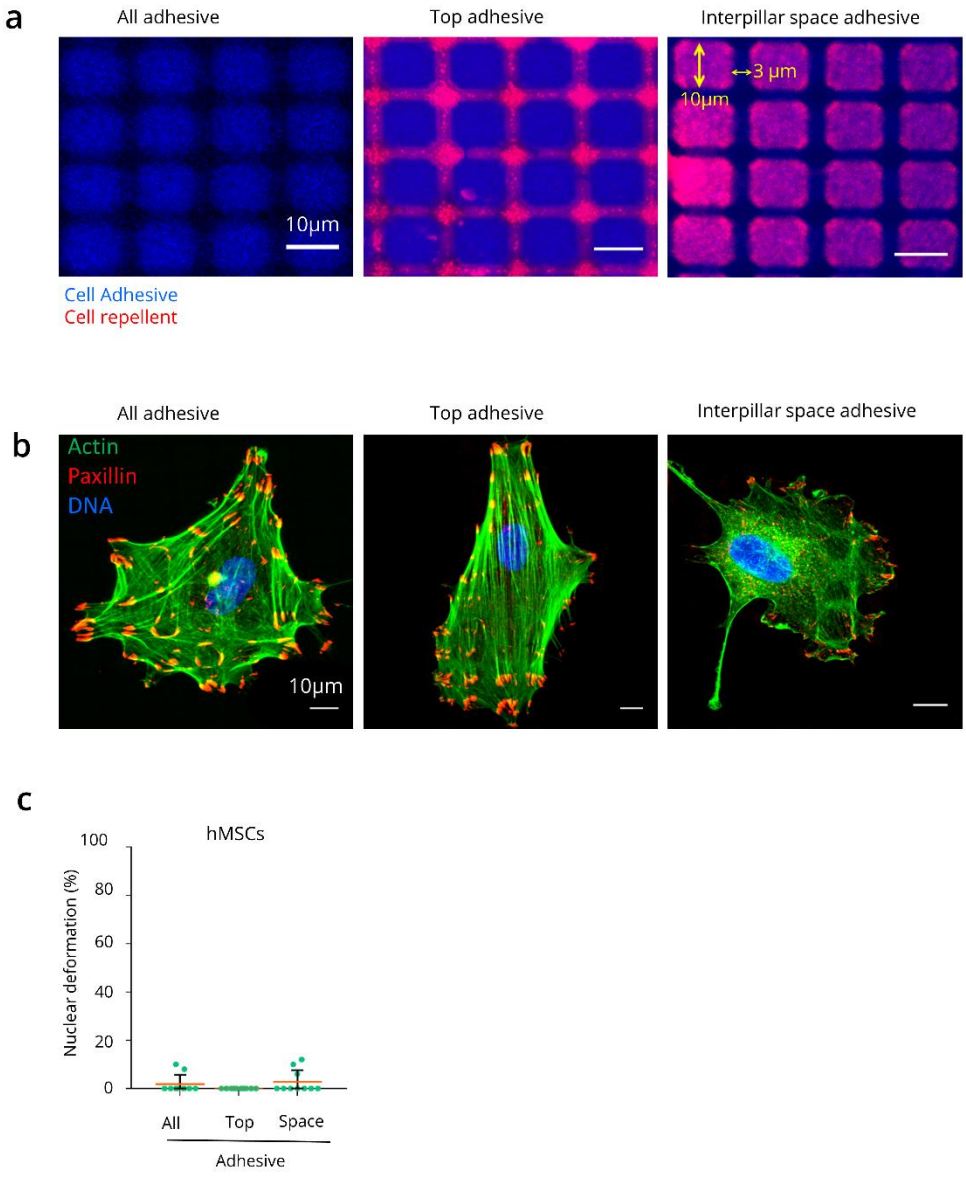

S5: Validation of chemistry coatings and hMSC behaviour on chemo-topographic variations

a Images showing modified surfaces: blue-cell adhesive and red-cell repellent surface. **b**. hMSC cells on modified surfaces, immunostained for actin-green, paxillin-red and nucleus-blue. **c** Graph of percentage of nuclear deformation of hMSC nuclei on different surfaces (n=10 for each surface). Error bars represent ±s.d.

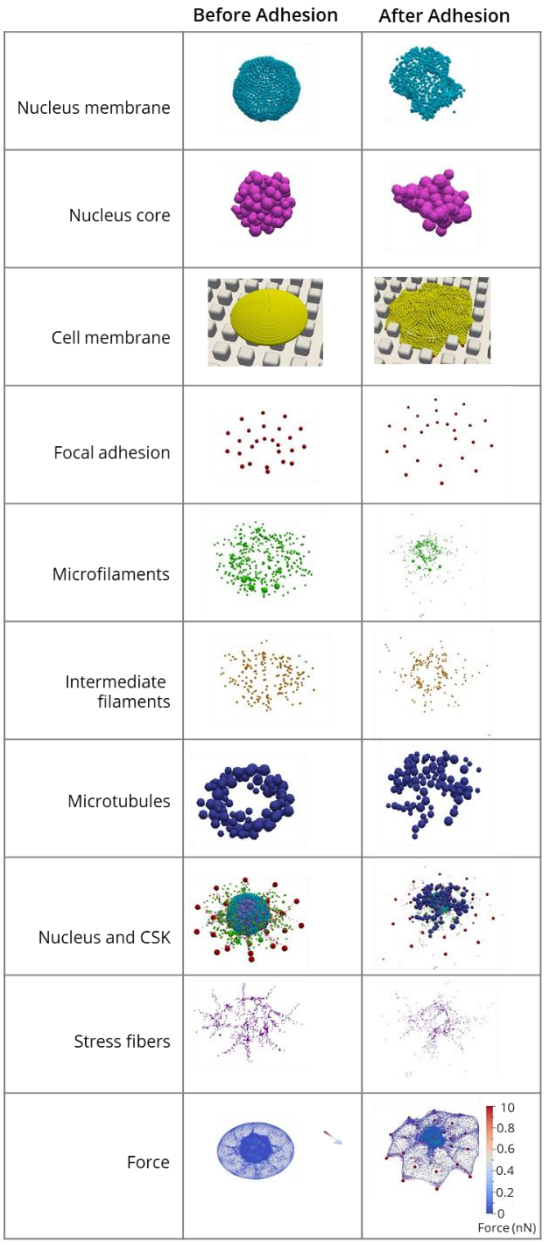

S6: Figure showing elements used in in-silico cell model simulation.

Different elements used in in silico model simulation to calculate mechanical stress on nucleus during deformation

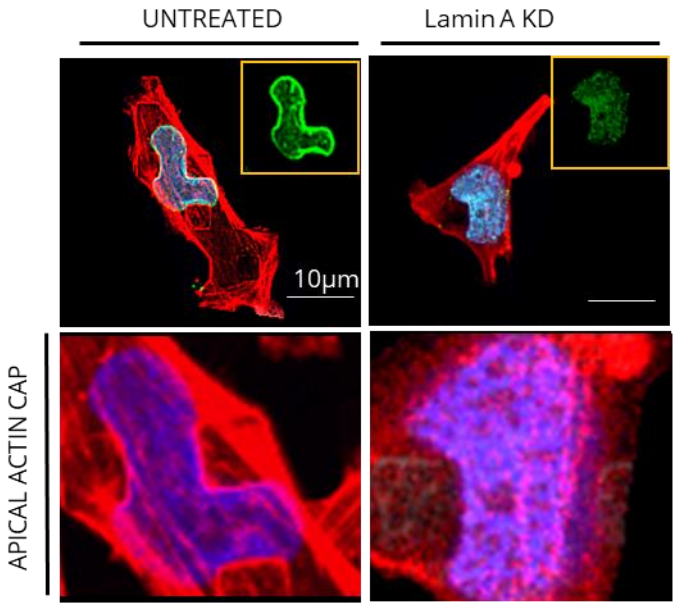

S7: Actin cap reduction by lamin A KD.

Overview and zoom images showing lamin A immunostaining of untreated and control SaOS-2 cells on pillars.

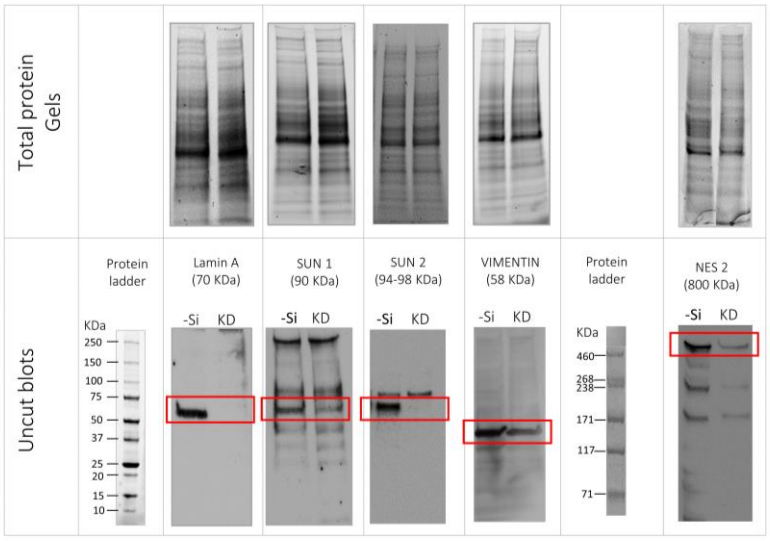

S9: Western blot

Total protein gel images for KD of lamin A, SUN1, SUN2, nesprin 2 and vimentin used for protein normalization and corresponding immunoblots.

2.3 Conclusion

We employed micropillar array topography to understand the mechanism of nuclear deformation in SaOS-2 osteosarcoma cells. Nuclear deformation of cancer cells was seen to increase with time and reach a plateau at 24 hours. Most of the average number of FAs were seen at the lateral part of the pillars, less on top part of the pillars and none in the bottom space between pillars. We observed that nuclear deformation was accompanied by chromatin condensation. In analysis of cytoskeletal components, we observed that actin and vimentin intermediate filament (VIF) was more strongly organised around pillar topography compared to microtubules which were uniformly distributed. Perturbation of the cytoskeletal components such as actin, myosin, VIF and microtubules showed that nuclear deformation decreased significantly when actomyosin and VIF were depolymerised by drugs. Microtubules on the other hand did not show a significant change in nuclear deformation behaviour. Investigation of the role of nucleoskeletal components showed that lamin A plays no significant role in affecting nuclear deformation of SaOS-2 cells. Nucleo-cytoskeletal components such as members of the LINC complex individually showed no effect on nuclear distortion. However, completely disrupting the link between nucleo-cytoskeleton decreased the nuclear deformation significantly. We developed a chemo-topography and computational model to examine the role of different forces (push and pull) assisting the nuclear reshaping on micropillars. We found that pulling down forces play a predominant role in squeezing the nucleus in between pillars contrary to the pushing down forces. Our computational analysis showed that stress on nucleus is more in presence of LINC complex and when the pulling down forces are playing a predominant role. Overall, our study on nuclear deformation on micropillars makes our understanding about the mechanisms of nuclear deformation more clear.

RÉSUMÉ DU CHAPITRE 3 - HYDROGELS BIOMIMÉTIQUES – CONTRÔLE DE LA RIGIDITÉ POUR ÉTUDIER LES INTERACTIONS CELLULAIRES

L'environnement cellulaire *in vivo* est constitué de tissus qui présentent un comportement viscoélastique. Il existe une gamme de rigidité dans notre corps, allant du cerveau, le tissu le plus mou à l'os, le tissu le plus rigide. L'amplitude de l'élasticité ou de la rigidité cellulaire qui va d'environ 100 Pa (neurone) à environ 40 kPa (ostéocytes) dépend des tissus desquels les cellules sont dérivées. Cependant, la rigidité des matériaux de culture, comme le plastique ou le verre, se situe dans la gamme des gigapascals qui est très éloignée de celle des tissus vivants. Ainsi, ces supports de culture cellulaire présentent aux cellules un environnement mécanique non physiologique.

Il a été montré que la rigidité de leur environnement affecte les composants de la cellule, telles que la forme et la dynamique des adhésions focales ou l'organisation du cytosquelette. La cellule exerce une certaine force de traction sur son substrat pour adhérer. Pendant ce phénomène de traction, elle ressent une certaine résistance de la part de la surface. Elle ressentira plus de résistance si la surface est rigide que si la surface est molle.

Les cellules cancéreuses présentent une réponse hétérogène à la rigidité. L'environnement tumoral lui-même est considéré comme rigide par rapport aux environnements sains. Cette propriété est due à la croissance de tissu fibreux entourant la tumeur par un processus appelé «desmoplasie». On sait que le microenvironnement affecte l'activité des cellules cancéreuses du sein. La morphologie, la prolifération, la formation de groupes cellulaires et la migration cellulaire sont affectées dans la gamme de rigidité retrouvée dans le cancer du sein. Une étude intéressante a montré que les cellules cancéreuses sont plus molles que leurs homologues saines. De plus, les cellules saines «détectent» la rigidité de la surface alors que les cellules cancéreuses n'y répondent

pas. Cela explique la facilité avec laquelle les cellules cancéreuses migrent à travers des parties du corps dont la rigidité varie. Ainsi, les cellules sont équipées pour détecter non seulement la topographie mais aussi la rigidité de la surface et ainsi moduler leur comportement.

Le substrat avec micropiliers que nous avons utilisé pour les expériences précédentes (chapitre 2) est très rigide par rapport à l'environnement cellulaire *in vivo*. Par conséquent, pour retrouver la gamme de rigidité rencontrée par les cellules métastatiques en migration, nous avons utilisé des piliers d'hydrogel à rigidité variable et controllable, afin d'observer le comportement des cellules métastatiques et la déformation de leurs noyaux. Les hydrogels sont des polymères hydrophiles réticulés par des liaisons physiques ou chimiques qui présentent des propriétés à la fois solides et liquides. Ils peuvent adsorber les liquides ou les fluides biologiques et gonfler sans se dissoudre. Ils peuvent être classés en fonction de leur origine naturelle ou synthétique. Ainsi, la mécanique contrôlable des hydrogels nous a permis d'explorer le confinement de cellules cancéreuses sur des topographies de rigidités variables telles que celles qu'elles peuvent rencontrer lors de la migration métastatique. Les hydrogels synthétiques offrent un avantage dans ce context, contrairement à leurs homologues naturels, car leurs propriétés physiques telles que la mécanique peuvent être contrôlées et régulées plus facilement. Nous avons choisi une gamme de rigidité de 3,7, 7, 12 et 28 KPa afin d'analyser le comportement des cellules sur des surfaces allant des plus souples (3,7 KPa) aux plus rigides (28 KPa). Nous avons constaté que les cellules SaOS-2 était polarisées et s'étalaient plus sur des substrats rigides (28 KPa) que sur les substrats plus mous (3,7 KPa) et intermédiaires (7 et 12 KPa). Les fibres de stress d'actine étaient également plus orientées sur les piliers de 28 KPa. Sur les piliers de 3,7 KPa, les cellules semblaient s'organiser davantage comme sur une surface plane, avec un noyau rond et une morphologie radiale. Les cellules sur les piliers de 7 et 12 KPa montraient un comportement intermédiaire entre 28 et 3,7

KPa. Le nombre par cellule, le rapport d'aspect et la surface des adhésions focales (AF) étaient également affectés par la rigidité. Ils augmentaient avec la rigidité avec un maximum significatif sur les piliers de 28 KPa, et moins significatif sur les piliers de 3,7, 7 et 12 Kpa. Sur les piliers de 3,7 KPa, les AF étaient organisées de manière plus aléatoire sur les piliers alors qu'elles s'organisaient dans l'axe des piliers de rigidité plus importante. Elles étaient aussi alignés le long des fibres de contrainte et du grand axe de la cellule. Nous avons également étudié la déformation du noyau sur les piliers de différentes rigidités et constaté que le noyau était le plus déformé sur les piliers de 28 KPa, comme sur les piliers en PLLA du chapitre 2. Par contre, la déformation diminuait progressivement sur les piliers de 12, 7 et était minimum à 3,7 KPa.

CHAPTER 3. BIOMIMETIC HYDROGELS- TUNING STIFFNESS TO INVESTIGATE CELLULAR INTERACTIONS

3.1 BACKGROUND

In vivo environment consists of tissues, with a range of stiffness from the brain being the softest tissue and bone being the stiffest (*fig. 3.1*). This magnitude of elasticity or stiffness affects cell stiffness that ranges for example from ~100 Pa (neural cell) to ~40 kPa (osteocytes) depending on the tissues from which the cells are derived. However, the stiffness of culture materials like plastic or glass are in the gigapascal range which is farthest from the living tissue. Moreover, the pillars we used were stiff and did not represent the stiffness of various other body tissues.

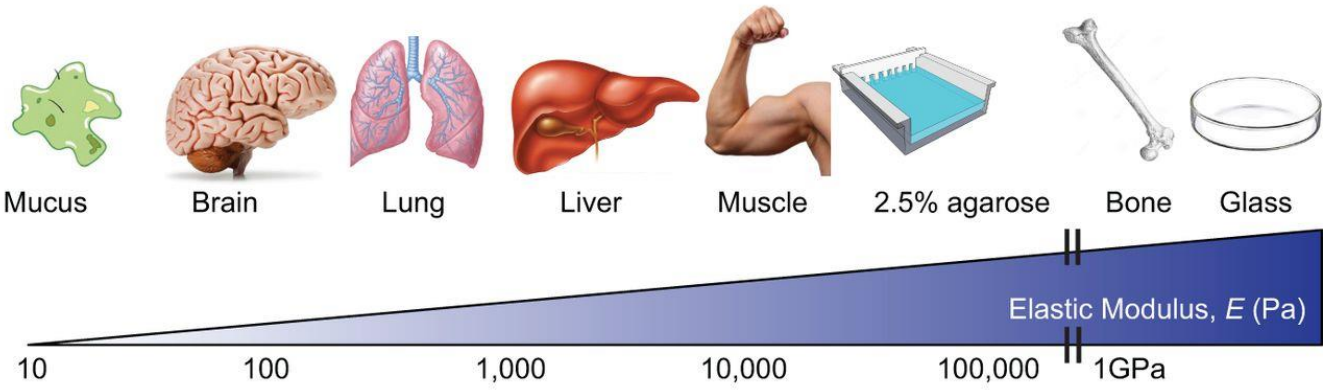

Figure 3.1. *Adapted from Barnes et al. 2017[206]. Mechanical properties of tissues. Young's, or elastic, modulus (E) describes the amount of force required to deform a substance, with units of force/area (N/m^2) or Pascals. E of tissues and cells can be quantified, revealing their relative stiffness. All tissues have distinct intrinsic physical properties, which are important in their structure and function. The stiffest tissues of the body are tooth and bone ($E \geq 10^9$ Pa), muscle tissue is intermediate ($E \geq 10^4$ Pa), and among the softest are lung and brain ($E \leq 4 \times 10^2$ Pa). For reference, a 2.5% agarose gel is approximately 35 kPa, whereas a tissue culture glass is off the scale, in the gigapascal range.*

Rigidity is known to affect the cellular behaviour (details in section 1.3.2.3). Cells on soft matrices are globular and prone to apoptosis whereas stiffness promotes cell adhesion[207]. Literature also suggests that matrix stiffness can also affect the cell differentiation[31]. Cell exerts pulling forces on the substrate in order to adhere. During this pulling phenomenon it experiences resistance from the surface. If the surface is stiff, it is bound to have more resistance than the soft one. Stiff material resists deformation while a soft one is susceptible to deformation. This reflects the elasticity (Young's modulus=E) of the surface. E can be calculated by applying stress to a surface and measuring the resulting deformation in shape (strain). Atomic force microscopy (AFM) is generally used to measure the elasticity of cells.

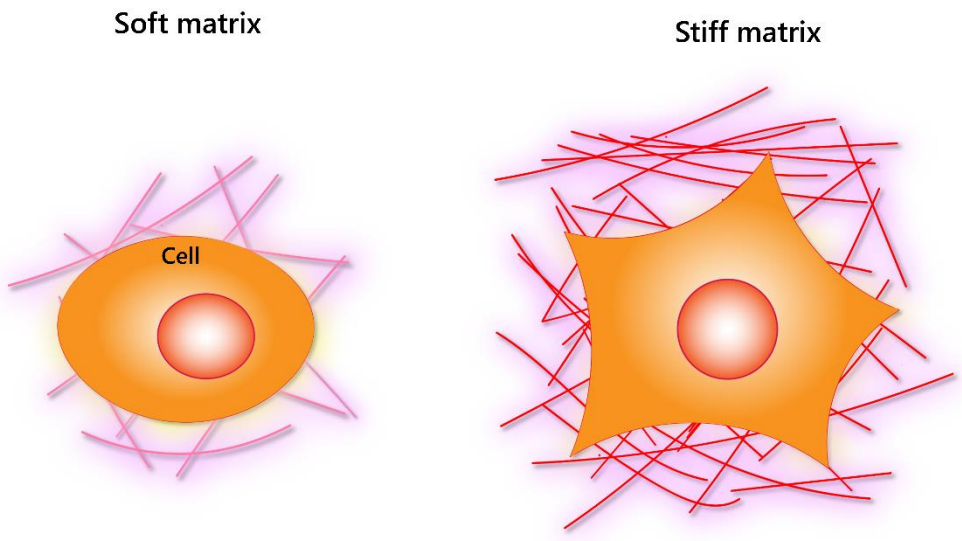

Figure 3.2: *Graphical abstract of cell behaviour on soft and stiff matrix inspired from[208]. Cell spreads less on soft surface as it requires less force to adhere. Cell on stiff matrix requires more force hence spreads more strongly.*

Cells behave different on soft and stiff matrices (*fig. 3.2*). Cancer cells in particular show heterogeneous response to rigidity. Interesting study by Lin et al. showed that cancer cells are softer compared to their healthy counterparts[209]. They further demonstrated that healthy cells

'sense' the rigidity of the surface whereas cancer cells are unresponsive to the same. This indicates the ease with which cancer cell migrate through the body parts ranging in different stiffness. The tumor environment itself is considered stiff compared to healthy ones. This property is due to the growth of fibrous tissue surrounding the tumor by a process called "desmoplasia". The behaviour of cancer cells on the different rigid environments is described below.

- ***Cancer cell behaviour on stiff substrate***

Most of the studies have been done on breast cancer cells and its response to rigidity. Tilghman et al. showed the response of different stages of breast, lung prostate, pancreatic, melanoma cancers cells to rigid surfaces[210]. They divided the growth profiles of cells into 2 categories namely `rigidity-dependent` (breast and lung cancer) and `rigidity-independent` (prostate, pancreatic and melanoma cancer) cell lines. Another study showed that metastatic breast cancer cells cause osteolytic gene expression due to matrix rigidity[211]. The cell morphology, proliferation, cluster formation and migration seems to be affected over a range of stiffness in breast cancer[212,213]. Other studies show an increase in invadosome and lamellae formation in cancer cells due to matrix stiffness[214]. Stiffness also regulates metastatic phenotype by enhancing EMT thus aiding the cells to loose cell-cell adhesion and acquire a mesenchymal phenotype[215]. Moreover, stiff substrates also induce fibronectin (FN) production which can help adhere the cell firmly to the stiff surface by increasing contractility of the cytoskeletal framework.

- ***Cancer cell behaviour on soft (compliant) substrate***

Ovarian cancer cells are known to have enhanced malignancy on soft matrices, involving the Rho-ROCK pathway[216]. Fibrosarcoma cells are known to form invadosome-like protrusions more prominently on soft matrices[217]. Matrix softness is known to regulate plasticity of melanoma tumor

repopulating cells that are critical for cancer progression[218]. On the other hand aggressive cancer cells are generally not responsive to rigidity [209]. Extremely aggressive breast cancer cells undergo apoptosis on soft matrices when rigidity sensing pathways are restored in the cells[219].

- ***Dual cancer cell behaviour on substrate rigidity***

Glioblastoma cells, highly aggressive central nervous system cancer cells, show dual behaviour on range of substrates. Their morphology on soft matrix (close to the brain, 80 Pa) resembles neurons and are largely non-proliferative and display little migration[220]. On soft matrices, they multiply five times faster and their migration increases drastically[220]. Hepatocellular carcinoma proliferation is increased up to 12-fold on 12 kPa versus 1 kPa matrices[221]. Tang et al. showed that human colon carcinoma cells show metastatic like phenotype when cultured on intermediate (21-47 kPa) and very stiff substrates (3.6 GPa) but not on very soft (1 kPa) substrates[222].

3.2 Mechanism of cell behaviour on different rigidities

Cells exert forces on the ECM via integrin mediated FAs and cytoskeletal reorganization[223]. Studies showed that on soft substrates a cell will adhere less as it has to respond to large forces with large deformations[23]. Indeed, the cell is not able to maintain large forces and thus it spreads less on soft surfaces. On stiff surfaces the cell can exert large forces and thus spread more. These forces could be brought about by focal adhesions, actomyosin contractility, stress fibres and other cytoskeletal components. Hence, on stiff surface FAs are larger and exert higher traction forces, actin cytoskeleton is more polarised and stress fibres are organised unidirectionally as compared to soft substrates[224]. Hersen and Ladoux proposed a theory based on previous research that cells interact with the rigid environment using push and pull forces which balance each other so that

the overall force is zero[225]. They explained that cells on 3D soft surfaces push vertically in the region underneath the cell nucleus but pull it obliquely towards the cell centre at the cell's edges. On rigid substrates, they explained that horizontal forces increase and there is a relative decrease in the vertical ones.

3.3 NEED OF SUBSTRATES WITH TUNABLE RIGIDITY

Pioneering work in demonstrating that matrix stiffness is a mechanical cue was done using thin films or hydrogels formed by polyacrylamide[23,226].Since then various substrates have been engineered with different rigidity. PDMS is once such polymer that is used extensively to tune rigidity by controlling the base to curing agent ratio[227]. However, controlling the stiffness of PDMS is a tedious process as it involves long curing times and it is difficult to lower to stiffness to Pascal range. Hence, hydrogels have proved to be excellent polymers in this context. Moreover, they mimic the *in vivo* environment as they contain 80-90% water. Also they can be tuned not just mechanically but also in response to temperature in the case of thermoresponsive ones that allow studying the response to rigidity or topography in various temperatures[228].

Previous work on hydrogels and their tunable properties prove that they can be used to elucidate cell response to substrate mechanics. In our previous chapter we looked at effect of confined topography on metastatic cells. However, we ruled out the rigidity of the substrate. Here, we wanted to observe the behaviour of metastatic cells on arrays of hydrogel pillars with tuned stiffness. This would allow us to perceive the metastatic cell response encountered during migration *in vivo*, through microenvironment with varying stiffness.

3.4 HYDROGELS – OVERVIEW

Hydrogels are hydrophilic polymers that exhibit both solid and liquid like properties owing to their

hydrophilic multiphase mixture. Hydrogels can retain liquids or biological fluids and swell without dissolving. In this swollen state hydrogels display soft and elastic characteristics[229]. The swelling occurs due to osmotic forces driven by the water molecules and the expansion in its structure is resisted by the cohesive forces of the polymer strands. This enables them to preserve their 3D architecture without dissolving. Hydrogels can be categorized based on their origin- natural or synthetic[230]. Natural hydrogels include proteins like collagen, fibrin, gelatin or polysaccharides such as alginate, agarose, chitosan, and hyaluronic acid. Synthetic hydrogels include materials like poly ethylene oxide (PEO), poly acrylic acid (PAA), poly vinyl alcohol (PVA), etc. Hydrogels have proved to be an excellent candidate as biomaterials for biomedical fields due to their high water content and biocompatibility. Their application has been found in contact lenses, wound dressings, drug delivery systems, in diapers as super-absorbents etc[231]. Hydrogels manufactured from natural precursors, recapitulate the physiochemical cues found in the ECM. They possess biochemical cues for cell attachment, growth, migration, etc[232]. On the other hand, synthetic hydrogels can be made cell adhesive by integrating bioactive molecules requires to elicit cell response[233]. Over the past few decades with a rise in studying cell response in 3D environment, hydrogels have also proven to be a worthy candidate to not only mimic biochemical properties of ECM but also passive cues like topography, rigidity, and dimension[234].

3.5 CANCER CELL RESPONSE TO 2D/3D HYDROGEL ENVIRONMENT

Evident by the seminal research over the decades, hydrogels have proven to be excellent biomaterials in mimicking ECM of the cell. They have been used in fabrication of both 2D and 3D structures for cell culturing. Healthy cells generally are subjected a particular environment in which they reside indefinitely. Hence, investigating their response with respect to their native ECM can

be done easily by fabricating the respective landscapes with the help of biomaterials. However, cancerous cells on the other hand are subjected to various environments during their metastatic migration and when spreading tumour in another than the primary site of origin. Moreover, there are various types of cancers that originate in different parts of the body with varying rigidity and topographies. Understanding the behaviour of such cancerous cells requires a bio-mimicking ECM whose mechanics can be easily modulated. Tuning mechanics of hydrogel structures has made it possible to explore the response of cancerous cells to soft/stiff, confined topographic landscapes encountered by them during metastatic migration[235]. Synthetic hydrogels provide an advantage in this context contrary to their natural counterparts as their physical properties such as mechanics, can be controlled and tuned easily. Thus, hydrogels have emerged as 3D biomimetic scaffolds for applications in cancer therapeutics.

3.5.1 TUNING HYDROGEL TOPOGRAPHY

Many techniques have been applied in recent years to fabricate topography with varying geometry. Photolithography is one of the very common micro-patterning technique. It involves polymerization of hydrogel precursor polymer by UV light through a photomask with desired patterns[236]. Lithography technique was used by Seidlits et al. to develop topographical patterns to guide neuronal growth[237]. Many hydrogel based microfluidic chips are manufactured by a similar approach[238]. Electrospinning is a technique where the desire polymer is deposited in the desired direction to manufacture hydrogel fibres which are used as scaffold for biomembranes[239]. Another method involves micromolding, where PDMS stamp with negative replica is used to get the desirable pattern by crosslinking the hydrogel precursor solution by exposure to UV light[240]. For example, Li and Folch used micromolding method to analyse growth paths chosen by axon tips[241]. Hydrogel swelling itself has been utilized to create surface wrinkles as a topographic feature, which

was used by Guvendiren et al. to control stem cell morphology and differentiation[242]. Hydrogels tuned topography such as grating have also been exploited for cell adhesion and polarization[243]. Microplate arrays have been developed to guide human mesenchymal adhesion eventually leading to tissue growth[244]. A quadratic array of hydrogel based micropatterned channels was employed for axon and dendrite outgrowth[245]. Hydrogel based topographies have served to capture and release the cancer cells which could have applications in single cell analysis for personalised therapy[246].

3.5.2 TUNING HYDROGEL RIGIDITY

Human *in vivo* environment is composed of tissues that vary vastly in term of mechanical properties such as rigidity. The brain comprises of the softest tissue and the bone is the hardest. Hence, relying on the topography alone does not recapitulate the *in vivo* environment. Hydrogels, being the most versatile biomaterials, are used extensively to tune mechanics such as stiffness. This can be done by controlling the network crosslink density. To do this either crosslinker or polymer concentration can be increased[247]. Another method involves integration of hydrophobic domains in the polymer in order to control swelling thereby increasing the stiffness[248].

Stiffness has been shown to affect stem cell differentiation with the help of mechanotransduction[249]. Matrix stiffness is known to impact cell adhesion[250], migration[226] and proliferation[251]. 3D matrix stiffness has been shown to influence cancer cell response to toxins[252]. Neural stem cell differentiation was seemed to be affected by decrease in the elastic modulus[251]. In a phenomenon called “durotaxis”, cells have shown to migrate from soft to stiff matrix rigidity[253,254]. Seminal work by Engler et al has shown that hMSCs directed differentiation depends on matrix stiffness[31]. They used hydrogels to modulate the matrix stiffness and found that stem cells underwent neurogenesis at 0.1-1kPa, myogenesis ay 8-17kPa and osteogenesis at 24-40kPa

respectively. Recent work by Lampi et al., has shown that matrix stiffness can govern endothelial single cell and monolayer behaviour[255].

3.6 OBJECTIVES OF THIS CHAPTER

Development of microfabrication techniques has enabled us to fabricate various topographies to closely mimic the *in vivo* environment and provide more physiological conditions to observe cell behaviour. However just designing a geometrical topography, as we did in previous chapter 2, rules out the effects of parameters like rigidity that affect cellular behaviour too. In the previous chapter we combined the technique of topography with dimensionality and chemical alterations without changing the rigidity. We used PLLA pillars that exhibited 485 MPa of stiffness, which is too high and not relevant to mimic *in vivo* environment. Hence to understand the cell response to rigidity, we used herein hydrogels tuned to different stiffnesses to make pillars.

3.7 METHODS

3.7.1 Substrate Fabrication

Substrate fabrication was done at IMTEK-Germany by Sebastian Anders (IRTG SoMAS collaboration). The used polymers were synthesized by a free radical polymerization of *N*, *N*-dimethyl acrylamide (DMAA), sodium 4-vinylbenzenesulfonate (SSNa) and methylacryloyloxybenzophenone (MABP). For the variation of SSNa, different amount of SSNa were incorporated into the polymer. A drop (50 µL) of triethoxybenzophenone silane (3EBP) was spin coated (1000 rpm, 60 sec) on top of a cover glass slide. The glass slide was heated at 120°C for 20 min. The glass slide was washed with ethanol and dried with nitrogen. A Si wafer was micropatterned by the clean room service of the University of Freiburg with lithographical

methods. The PDMS elastomer was mixed with a curing agent in a ratio of 10:1 (v/v). The PDMS solution was poured over the etched Si wafer and was kept under vacuum for 1 h to remove any bubbles. The PDMS (Dow corning, USA) on Si wafer was heated at 120°C for 24 h. The PDMS was peeled of the Si wafer and cut out. For the microstructuring process the polymers were dissolved in water with different 300 mg/mL polymer concentrations. A drop (50 µL) of the dissolved polymer was placed on top of the silanized cover glass. The PDMS stamp was pressed on top of the dissolved polymer. The whole composition (glass slide, polymer and stamp) was crosslinked by UV irradiation (λ = 365 nm) through the glass slide for 5 min. For varying the Young's modulus of the polymer P(DMAA-2.5%SSNa-5%MABP), increasing dose of energy was used to increase the crosslink density, thereby increasing the stiffness. The energy dose of the UV light irradiation was varied between 3 and 30 J/cm². The sample were frozen (-20°C) and the PDMS stamp was removed. The table below represents the resulting Young's modulus and degree of swelling depending on dose of energy.

Dose	3J/cm^2	6 J/cm^2	10 J/cm^2	30 J/cm^2
Degree of swelling	10	9.4	8.2	7
Young's modulus (KPa)	3.7	7.1	12.2	28.1

3.7.2 Substrate chemistry coating

In a first step the swollen (overnight before spin coating) microstructure is spin coated as described above. The swelling before top coating avoids the drying of microstructures during top coating. After this the microstructure is swollen overnight in water again. The top coating process is done at the next day. For that, 50 µL of the dissolved polymer was placed all-over a glass slide. The solvent was evaporated at 120°C. The swollen microstructure was spin coated (1000 rpm, 30 s)

and pressed upside down on the coated glass slide. The whole system was crosslinked by UV irradiation (λ = 365 nm). The microstructure was extracted with ethanol. To analyze the microstructure under the confocal microscope the hydrogel pillars were coated with polymers that were stained with P(DMAA-2.5%SSNa-5%MABP-1%AmS-Fluorescein) in green for cell adhesive and P(DMAA-1%MABP-1%AmS-Rhodamine) in red for cell repellent.

3.7.3 Young's Modulus Measurement

The Young's modulus was measured in a liquid cell filled with water with the help of an atomic force microscope (AMF) at IMTEK-Germany. The polymers were measured in swollen state. The cantilever was calibrated on a Si wafer. The cantilever used was already coated with a hydrogel by the company and fabricated by Surface Science Support (CP-PNPS-PS-C, short, 6.1 µm).

3.7.4 Cell Seeding

Hydrogels were swollen in distilled water for 2-5 min and then washed with 70% ethanol for 10 min. Hydrogel pillars were rinsed thoroughly with sterilised distilled water (3X for 5 min each) after ethanol wash. Samples were glued using aqua-Silicone glue (Den Bravent Sealants, Netherlands) in 60mm Petri plates. Glue was allowed to dry (30 min-1 hour) followed by cell seeding.

3.7.5 Cell Culture

Saos-2 osteosarcoma cells were purchased from ATCC (USA) and cultured using McCoy's 5a modified medium w/o l-glutamine supplemented with 0.1 mg ml-1 streptomycin and 100 u ml−1 of penicillin, 15% (v/v) FBS heat inactivated-sterile (Biowest, France) and 2mm l-glutamine at 37 °C with 5% CO_2 in a humidified incubator. All products were obtained from Sigma–Aldrich (France) unless specified. For experiments $1x10^5$/ml cell density was used.

3.7.6 Immunostaining

Cells were fixed with 4% formaldehyde (Electron Microscopy Sciences, USA), permeabilised using 0.5% Triton X-100 (Sigma, USA) for 15 min and blocked with 3% bovine serum albumin (Sigma, France) for 1 hour. Primary antibody used was anti-paxillin (1:250; ab32084; Rabbit; Abcam-UK), anti-Taz (ab84927; rabbit; Abcam-UK). Actin-555 (1:20; A34055; Thermoscientific-France) or Phalloidin-FITC (Fluorescein-5-isothiocyanate) was used to label actin and Hoechst (1:1000; 33258; Thermoscientific-France) was used to label nucleus. Secondary antibody used was Alexa 488 (1:200; ab150073; anti-Rabbit; Abcam-UK). For tagging pillars, cell adhesive polymer was mixed with cyan 5 dye streptavidin (GE Healthcare, USA) at 1:500 dilution and cell repellent polymer was tagged with Rhodamine B isothiocyanate (Sigma, France) at 1% concentration with the polymer.

3.7.6 Confocal Imaging

A confocal microscope (Zeiss LSM 700 confocal microscope, Germany) equipped with temperature, CO_2/O_2 and humidity controlled chamber (Okolab, Italy) was used for imaging live cells using 63X/1.4 oil, 63X/1.0 VIS-IR water and 20X/1.0 DIC VIS-IR W Plan-Apochromat objectives (Zeiss, Germany) and ZEN software (Zeiss, Germany).

3.7.7 Image Analysis and Quantification

Z-Stacks of the nuclei were acquired to quantify the nucleus deformation in following conditions. Images of the cross-sectional area were obtained using the orthogonal view in ZEN software (Zeiss, France) via confocal imaging. These images were then opened in ImageJ/Fiji (NIH, version 2.0.0-RC-61/1.51n, USA) to quantify the cross-sectional area of nucleus above and below the surface. The area below the pillars was considered as deformed and the area above pillars was considered undeformed. The deformed area was divided by the total cross-sectional area of the nucleus to

obtain the percentage of deformation.

3.7.8 Statistical Analysis

All the results were checked for significance by using one way ANOVA test followed by two-tailed Student's *t*-test (unequal variance) for pairwise comparison and Dunnet's test for multiple comparisons, using GraphPad Prism software (GraphPad Software, Inc). The significance values obtained were categorized as P > 0.05 for ns (not significant); P ≤ 0.05* (statistically significant); P ≤ 0.01** (very statistically significant) and P ≤ 0.001*** (extremely statistically significant). All the error bars indicate the ± standard deviation.

3.8 RESULTS AND DISCUSSION

3.8.1 Characterization of topography and cell behaviour on hydrogel polymers

The dimensions 7µm (height X space X length) have been shown to attain maximum deformation in SaOS-2 osteosarcoma compared to other dimensions[181,203,256]. Moreover, a crosslinked polymer of hydrogel swells (not dissolves) when water enters it and this degree of swelling is a critical parameter that defines how symmetric topography shall be. With such small microstructure, controlling the degree of swelling is difficult to achieve. However, with collaboration in IMTEK, Freiburg (PhD student Sebastian Anders -PhD thesis), we were able to control this property of hydrogels to achieve stable square micropillars with different mechanical modulus (*fig 3.3a)*. Hence we chose the same dimensions and cells to investigate the effect of matrix rigidity combined to topography on cell behaviour. The cell grown on P(DMAA-MABP) pillars showed weak cell adhesion and deformed nuclei in between the pillars(*fig 3.3b).* Moreover, the actin filaments appeared diffused. The cell seemed to be fallen between 2 pillars deforming itself. The cell adhered more strongly on PDMAA-SSNa-MABP pillars (*fig 3.3c*). The cell spread area was more than that on

PDMAA-MABP pillars, covering many pillars. Strong nuclear deformation was observed. Actin was organised around the pillars and stress fibres were seen running in between the pillars.

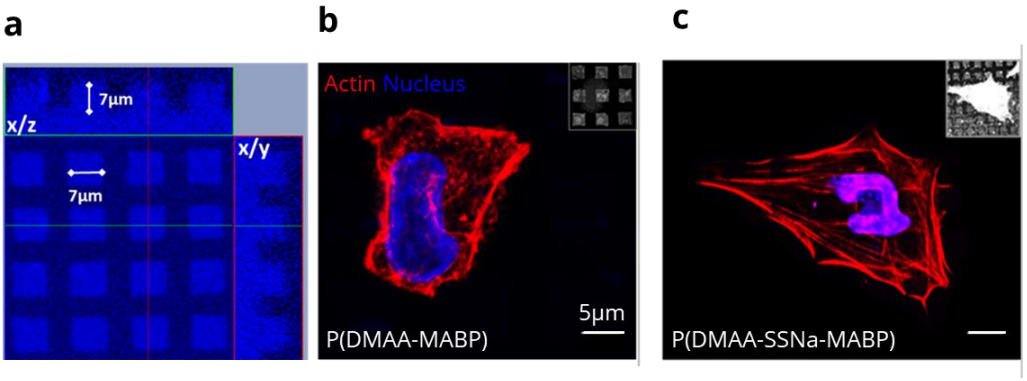

Figure 3.3: a *Fluorescent orthogonal image of hydrogel P(DMAA-2.5% SSNa-5% MABP) showing pillars with 7µm (height/width/pitch) tagged with cyan 5 streptavidin.* ***b*** *Confocal image showing cell poorly adhered on pillars made with P(DMAA-MABP) a cell repellent polymer.* ***c*** *Cell adhered strongly and showed high nuclear deformation on P(DMAA-SSNa-MABP) polymer hydrogel pillars.*

3.8.2 FAs organization and nuclear deformation on different rigidity

We selected 3.7, 7, 12 and 28 KPa range of stiffness to analyse cells on softest (3.7KPa) to stiffest (28KPa) pillars. We saw that the SaOS-2 behaviour changed with the different stiffness (*fig 3.4a*). In our previous chapter 2 we saw that integrin mediated FAs could sense the topography of the surface and pull the cells in between the pillar confinement. Here, we saw that they can not only sense the topography but also the rigidity of the underlying matrix. They respond to the change in stiffness by their organizational behaviour. Focal adhesions (FAs) number, area and aspect ratio increased with stiffness, being significantly maximum on 28 KPa, least on 3.7, 7 and 12 KPa (*fig 3.4d,e & f*). On 3.7 KPa the FAs were organized more randomly on pillars whereas their organization became more along the pillars with increase in stiffness. They were co-aligned along the stress fibres and major axis of cell. We saw that the FAs area and number was lower on 3.7 KPa and highest on 28 KPa. We also checked the nuclear deformation on different surfaces and found that

nucleus deformed the most on 28 KPa, similar to that of PLLA pillars in chapter 2 (*fig 3.4g*). However, the deformation decreased gradually on 12, 7 and was least on 3.7 KPa.

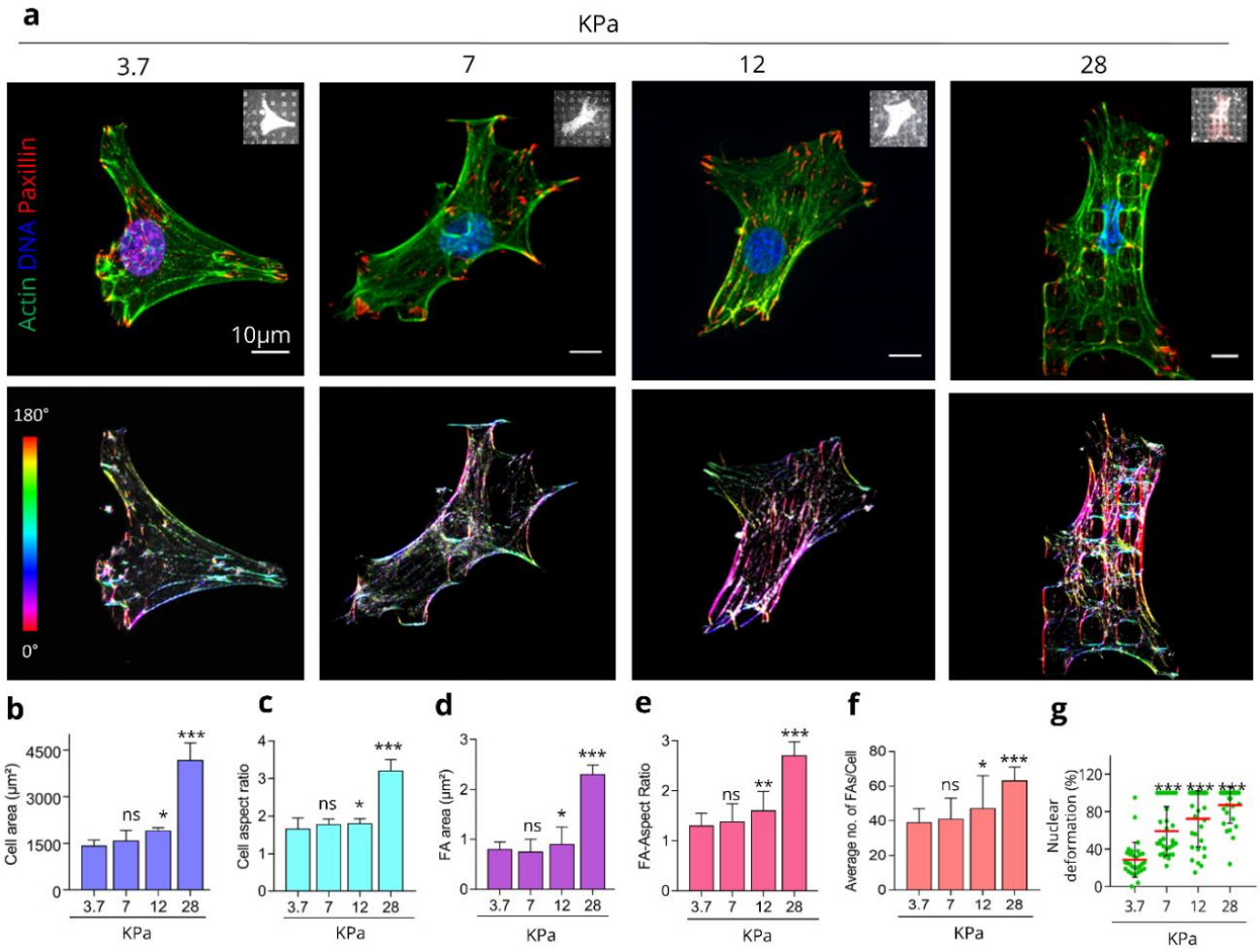

Figure 3.4: a *Confocal images of SaOS-2 cell on pillars with different stiffness showing actin (green), paxillin (red) and nucleus (blue) organization on pillars. Cell area (**b**), cell aspect ratio (**c**), FAs area (**d**), FAs aspect ratio (**e**), 10 measurements were done for calculating average FAs number per cell (**f**) 30 nuclei were analyzed for each rigidity for evaluating nuclear deformation(**g**) on different stiffness. Error bars indicate ± s.d; 3.7 kPa was used as reference to calculate significance; red line represents the median; significance levels were determined by one way ANOVA followed by Dunnet's test for multiple comparison; ***p<0.001, **p<0.01, *p≤ 0.05 and ns=not significant.*

3.8.3 Cell area, spreading and actin organization on different matrix rigidity

The actin stress fibres were least organized and were mostly diffused on 3.7 KPa, whereas their organization increased with stiffness (*fig 3.4)*. Their orientation was more unidirectional (nematic)

on 28 KPa. On 28 KPa cells were completely deformed and polarised, such that their alignment was along the pillars. On 3.7 KPa cells seemed to be organised more like on flat surface, with a round nucleus and radial morphology. The cells on 7 and 12 KPa showed intermediate behaviour between the 28 and 3.7 KPa. The cell area and aspect ratio increased with the stiffness (*fig 3.4b & c*). SaOS-2 cells were spread significantly more on 28 KPa compared to 3.7, 7 and 12 KPa.

3.8.4 Effect of rigidity on TAZ

YAP-TAZ are known to be tightly regulated with cell substrate rigidity and topography[208,257]. TAZ is a protein that acts as mechanosensor and mechanotransducer and is found to modulate its subcellular organization depending on matrix stiffness[258]. It has been known to localise to the cytoplasm on soft matrix and to the nucleus on stiff matrix. Hence next we wanted to investigate the behaviour of TAZ protein on various stiffness coupled to topography. We saw no effect on distribution of TAZ protein on our topography with stiffness (*fig 3.5*). TAZ protein was seen localised to the nucleus in all different stiffness (3.7-28 kPa) substrates.

3.8.4 Controlling cell behaviour with chemistry modulations

It is difficult to overlay different chemistries on hydrogels, especially with topography, as they themselves are porous water logged polymer network. There could be a chance of chemicals leaking into the hydrogel network thereby contaminating the swelling behaviour and crosslinking of hydrogels. Hence, we wanted to observe if the cells could differentiate between various chemistry coatings on hydrogel pillars and whether these coatings affected cell behaviour similar to chapter 2 where we coated the surface of the stiff hydrogels (28 KPa) to either make their tops or interpillar space cell adhesive. We verified the coatings by confocal microscopy (*fig 3.6a & b*).

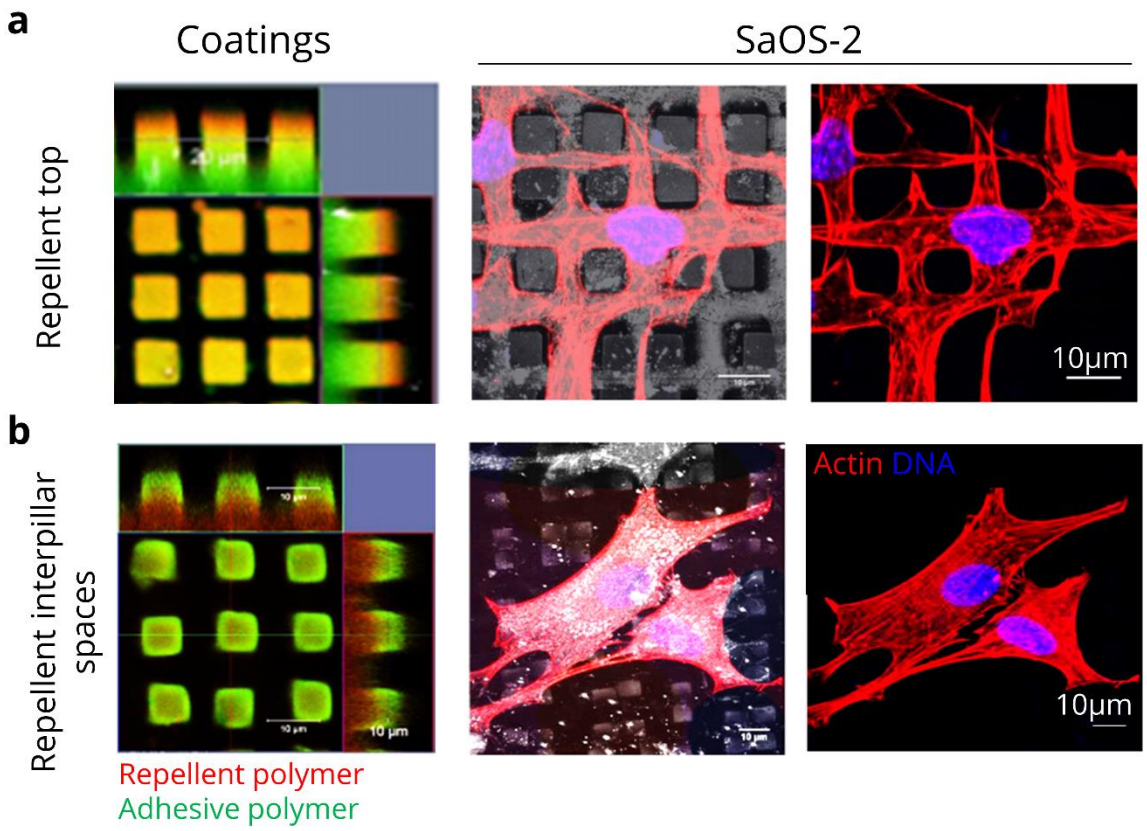

Figure 3.5: *Confocal images of SaOS-2 cell on pillars with different stiffness showing actin (red), TAZ (green) and nucleus (blue).*

We observed that the cells could differentiate between the adhesive parts of pillars based on their coatings, same as they did on PLLA pillars with different chemistries in chapter 2. On cell adhesive tops they did not deform themselves, even though being on hydrogel pillars (*fig 3.6b*). On the other hand, cells on adhesive interpillar space completely embedded themselves in confined spaces of pillar topography (*fig 3.6a*). Altogether, our chemistry coating results demonstrated that hydrogel pillars could be coated with different adhesive or repellent polymers without affecting the hydrogel swelling or crosslinking behaviour. Such coatings could be used to control cell behaviour on hydrogel topography.

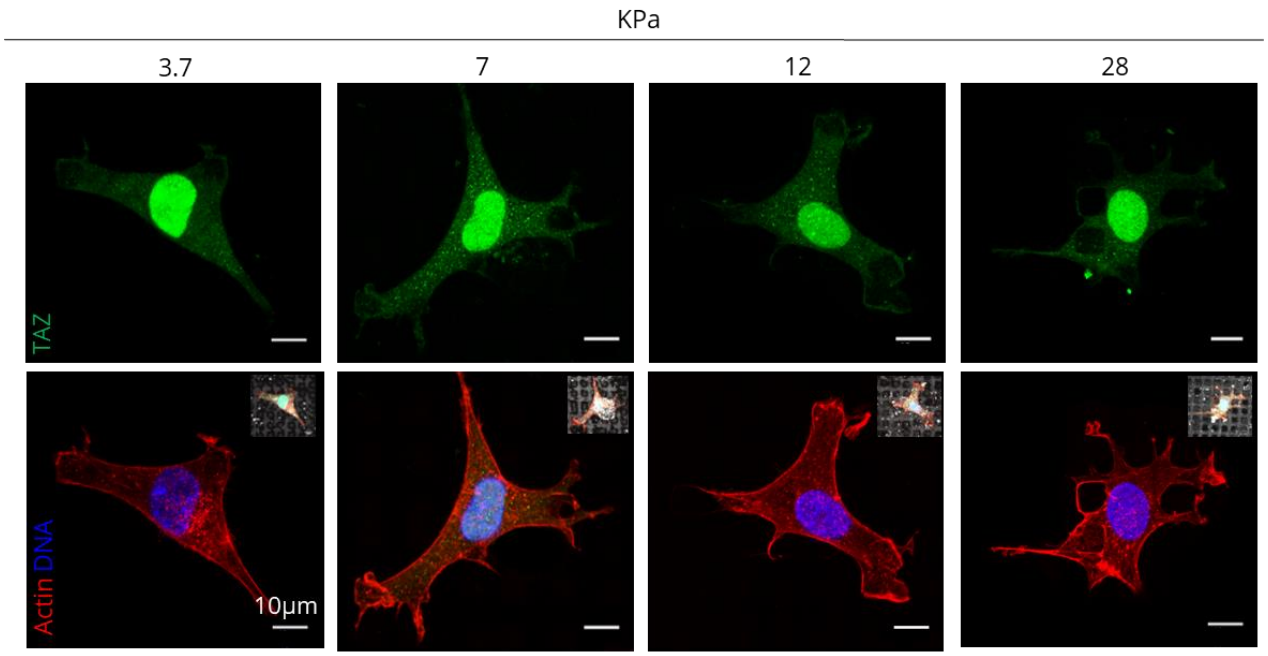

Figure 3.6: *Confocal images of SaOS-2 cell on pillars with different chemistries.* ***a & b*** *Validation of coating was done using confocal microscopy. Cell adhesive polymer P(DMAA-2.5%SSNa-5%MABP-1%AmS-Fluorescein) is in green and the cell repellent P(DMAA-1%MABP-1%AmS-Rhodamine) is in red.* ***a*** *Cell completely confined on repellent tops.* ***b*** *Cell on the top of pillars on interpillar space repellent coatings.*

3.9 Discussion

Hydrogels based on poly-dimethylacyrlamide (PDMAA) have been used in several biomedical applications and are used as cell repellent coatings[259]. However, they can be modified by using crosslinking agents such as benzophenone methacrylate (MABP), to make them cell adhesive. In general, PDMAA itself is a polymer that prevents adsorption of fibronectin[260]. This might be the reason why we saw less adhesion of cell on this polymer. The nucleus was seen deformed which could be due to passive falling down of the cellular part including nucleus in between the pillar spaces. On the contrary, P(DMAA-SSNa), a mixture of water soluble DMAA, the photo-crosslinker MABP and Na-4-styrenesulfonate (SSNa), is a strong polyelectrolyte that favours protein adsorption[259,261]. The nucleus deformation and cell spreading was observed more strongly on

PDMAA-SSNa-MABP. It was similar to that of PLLA pillars used in chapter 2. Hence we selected this polymer for further experiments.

Cells need more force to spread themselves on stiff surface compared to soft ones[225,262]. Hence, more FAs are needed to dispense force across the cell surface area. Moreover, pillars are known to be the pinning points for FAs adhesion[263]. This correlates with the fact that we saw more FAs on stiff micropillars. On the other hand, stiff surfaces promote FAs assembly and therefore the actin cross linking occurs over long time scale[264]. This is why we observed the actin stress fibres more strongly organized on stiff micropillars compared to soft. As the rigidity of the matrix increases the force required for the cell to spread and adhere increases, as it is unable to deform the surface anymore. This could be the reason of increase in cell and FAs area, spreading and nuclear deformation on stiff substrate. On soft surfaces FAs are short lived due to the low friction from the surface[264,265]. Thus they destabilize quickly and actin cytoskeleton becomes cross-linked for a short time scale. Hence, a cell uses less force on softer surfaces as they can deform the matrix and resist deformation themselves. This could explain the decrease in cell and FAs area, aspect ratio and nuclear deformation on soft substrates. These results confirm that FAs are involved in mechanosensing of rigidity of the surface.

Cell spreading is followed by cell polarization[266] which is characterised by increase in cell's aspect ratio and formation of long actomyosin bundles[267]. We observed that actin cytoskeleton was organising itself with the increase in rigidity. Therefore cells on stiff (28 KPa) topography were the most polarized. This is coherent with the results observed by Prager-Khoutorsky et al. in fibroblast on stiff and soft substrates[267]. Concomitantly, Solon et al. showed that there is an increase in cytoskeleton organization, actin bundles and actin cross-linked filaments on different stiffness[268]. Interestingly, they also showed that the cells adjust their stiffness according to the

substrate stiffness and that the same cell type can vary its stiffness to match that of the substrate. Another study from Ladoux et al. found that soft substrates impart less friction, forces and actin organization whereas stiff substrates show polarised cytoskeleton, high friction, forces and stable actin stress fibres formation[269]. They also showed that on intermediate stiffness the assembly of actin fibres develops with increase in stiffness. Gupta et al. found that matrix rigidity controls actin rheology[264]. They showed that actin exhibits bi-phasic rheology on soft-stiff substrates, meaning that actin fibres are organised randomly (isotropic) on soft substrate and unidirectionally (nematic) on stiff substrates. These experiments showed that cell behaviour relies on the underlying matrix. Cell is able to sense not only on the geometry but also the rigidity of surface. This is in accordance with the actin organization that we saw on 3.7 and 28 KPa and the gradual shift in the orientation on 7 and 12 KPa.

Gu et al. showed that even the healthy cells during wound healing, become invasive if exposed to a range of soft matrices[217]. They found that cancer cells on the other hand display invasiveness on range of stiffness. This is in agreement with the cell behaviour we observed on 28KPa surface, where cancerous cell invaded the confined spaces of pillars. Altogether, we showed that cell cytoskeleton can remodel in response to topography tuned with rigidity, where stiff matrix shows stronger cell adhesion than compliant surfaces.

We saw no change in TAZ protein with respect to our topography and range of stiffness. YAP/TAZ proteins have been known to localise in cytoplasm on substrates of 0.7 kPa rigidity[257]. This is less than the rigidity of SaOS-2 cells which is approximately 1 KPa and much less than our lowest rigidity that was 3.7 KPa[203]. Hence, one hypothesis could be that the cell might not consider a substrate compliant until it is softer than its own modulus, to adjust its cytoskeletal rearrangement involving signalling of TAZ protein. Contrary to our results, Dupont et al showed

that cells confined to micropillars with different rigidity, showed TAZ localization in nucleus on stiff and in cytoplasm on elastic pillars[257]. They used height (Pillar diameter 1.83 µm; spacing 4 µm; height of pillars-elastic 0.94 and rigid 12.9 µm) to determine the rigidity which was calculated by the bending stiffness of pillars. In our case we kept the dimensions (7 µm height and diameter) similar throughout the different rigidity of the micropillars. Also we did not observe any bending of the pillars even on soft hydrogel pillars. This could be because cancer cells may be adaptive in terms of force to the rigidity of the substrate more than healthy cells. Moreover, they observed the TAZ behaviour in MSCs (healthy cells) which are known to involve these pathways to differentiate into other cells. In human osteosarcomas these proteins are found to be overexpressed and their depletion leads to inhibition of proliferation and invasion in these cells[270]. Hence based on these finding, another hypothesis could be that cancer cells might not involve mechanisms including YAP-TAZ pathway as their purpose is to invade the ECM and not cell fate commitment. Altogether, we show that pillar topography with different stiffness remained inconsequential to behaviour of TAZ.

There has been an extensive amount of research to study the effect of topography and mechanics of surface. However, the chemical properties which also play an important role in cellular signalling is often overlooked. Surface functionalization of biomaterials is done for application in stem cell culture, tissue engineering and regenerative medecine[271]. Out of the many techniques used for functionalization, adsorption of cell adhesive molecules like fibronectin, laminin, etc. or treatments of surfaces with physical plasma to make the surface hydrophilic are the most often used. However, adhesive molecules such as fibronectin and others are costly techniques and physical plasma are not adapted to wet materials. Other chemical treatments are less considered for the functionalization due to their effects on cell viability. Hence there is a need

to develop polymers that are cost effective and have least negative impact on cell viability. Here we used P(DMAA-2.5%SSNa-5%MABP-1%AmS-Fluorescein) cell adhesive polymer and P(DMAA-1%MABP-1%AmS-Rhodamine) as cell repellent polymer. These chemicals were able to modulate cell behaviour without hampering the cell viability. Moreover, they could be coated on porous water logged substrates such as hydrogels. Thus, these polymers could be used in future to coat other cell repellent substrate and to chemically control the cell behaviour along with topography and rigidity of the surface.

3.10 CONCLUSION

In this chapter we used hydrogels to control the topography, rigidity and chemistry of the engineered micropillars. Our results showed that cell behaviour was affected when the substrates were modulated with different rigidity and chemistries. FAs organization was affected due to different rigidities. On stiff substrates number of FAs was more and they were co-aligned with stress fibres. Soft substrates exhibited less and randomly organised FAs. The aspect ratio of FAs increased with the increase in rigidity. Cell spreading was most on the stiffest substrates (28.7 kPa) and the least on soft substrate (3.4 kPa) and intermediate on 6 and 12 kPa substrates. Cell polarised more on stiff and least on soft substrates. Actin organization was also affected by the rigidity. Stiff substrates showed unidirectional (nematic) organization of stress fibres whereas diffused (isotropic) organization was observed on soft substrates. 6 and 12 kPa showed intermediate actin organization. On calculating the nuclear deformation, we observed that nucleus deformation too increased with the rigidity of substrates. On examining the TAZ protein on different rigidities we saw that there was no effect in TAZ localization. It was localised in the nucleus in all different substrates that we used. To control the cell behaviour, we chemically-coated the

different surfaces of pillars. The top-repellent coating of pillars localised the cells and nucleus in the spaces between the pillars. The space-repellent coating localised the cells on the top part of the pillars. Altogether, we developed a robust system to fabricate substrates tuned with topography rigidity and chemistry and to achieve control of cell response.

RÉSUMÉ DU CHAPITRE 4 - COMPORTEMENT DE CELLULES DE CARCINOME DE COLON SUR DES SURFACES MICROSTRUCTURÉES

Les cancers colorectaux d'origine épithéliale (CC) sont les types de cancers les plus fréquents. L'adénocarcinome (tumeur maligne formée à partir de structures glandulaires du tissu épithélial) est le type le plus commun de CC puisqu'il représente 95% des cas. L'instabilité chromosomique (CIN), le phénotype de méthylateur d'îlot CpG (CIMP) et l'instabilité des microsatellites (MSI) sont les mécanismes par lesquels les CC peuvent survenir. Ces mécanismes impliquent soit une mutation soit une dérégulation des gènes conduisant aux CC. APC et cdx2 sont des gènes suppresseurs de tumeurs qui sont dérégulés dans les CC. La majorité des tumeurs colorectales sporadiques présentent des mutations dans les deux allèles APC. L'APC forme un complexe de destruction avec d'autres protéines qui conduit à une dégradation protéosomale de l'oncogène β-caténine en l'absence de signalisation Wnt. Cdx2 est un gène suppresseur de tumeur dont l'activité est connue pour être diminuée dans la majorité des CC. Il agit comme marqueur pronostique dans les CC de stade II et III. On observe une régulation négative du Cdx2 dans les fronts invasifs des tumeurs des CC. Une myriade de systèmes de culture sont utilisés pour étudier la mécanotransduction cellulaire, notamment des surfaces microstructurées (micropiliers, rainures, puits) ou des systèmes microfluidiques. Cependant, la plupart de ces techniques sont utilisées pour étudier les cellules saines ou des cellules cancéreuses d'origine mésenchymateuse. Moins d'études ont porté sur l'analyse du comportement des CC sur différentes topographies. L'effet de la topographie sur le comportement des cellules issues de CC et les voies de mécanotransduction impliquées restent encore peu connus. L'objectif de cette étude était donc d'étudier le comportement de cellules issues de CC de différents grades et avec des mutations de deux gènes suppresseurs de tumeurs sur différents substrats avec des topographies telles que des piliers ou

des puits. La comparaison de ces lignées cellulaires devait nous permettre d'identifier comment les CC de différents grades se comportent par rapport à la topographie. Cela devait nous aider également à comprendre la différence de comportement entre les cancers d'origine épithéliale et les cancers d'origine mésenchymateuse.

Des lignées cellulaires de CC provenant de cancers de différents stades (HT29, SW480, TC7, DLD1 et HCT116) et des lignées cellulaires transformées avec un gène APC sauvage restauré (SW480 APC-/+) ou avec une expression inductible du gène cdx2 (HT29 TG8/TW6) ont été cultivées et caractérisées. Les niveaux d'expression d'ARNm de différents gènes du nucléosquelette ont été analysés dans ces lignées cellulaires, lesquels ont montré différents niveaux d'expression des gènes de la lamine A/C, la lamine B1, SUN1 et SUN2 en prenant HT29 comme référence. Nous avons également analysé sur la topographie avec micropiliers la distribution d'une protéine d'adhésion focale, la paxilline, de composants du cytosquelette, l'actine et la tubuline, et d'une protéine des jonctions cellulaires, l'e-cadhérine. Les déformations nucléaires ont été analysées sur les micropiliers que ce soit pour des cellules isolées ou pour des cellules formant des colonies. La déformation nucléaire était plus faible pour les cellules en colonie qu'isolées. Les cellules APC + ont montré plus de déformation que les cellules APC- alors qu'aucune différence significative dans la déformation nucléaire n'a été observée pour les cellules TG8 et TW6. Nous avons comparé les niveaux de lamine A/C par immunofluorescence et avons constaté que les mutants APC présentaient une forte expression de lamine alors que les cellules APC+ montraient une population mixte de cellules à forte et faible expression de lamine. Les cellules TG8 et TW6 ont montré des niveaux inférieurs de lamine A/C que les cellules APC +. Dans le but d'étudier le comportement des CC sur différentes topographies, nous avons ensuite évalué la réponse des cellules CC (TC7, APC -/+ et TG8/TW6) sur des rainures (40 µm de largeur et 8 µm de profondeur).

La plupart des lignées cellulaires n'ont pas réagi à la topographie avec rainures. Par conséquent, nous avons décidé d'observer ensuite le comportement des cellules CC sur une topographie qui ressemble plus en termes de taille à la topographie intestinale formée de cryptes et de villosités. Les cellules TC7, clone de CaCO-2 qui est largement utilisé comme lignée cellulaire modèle d'adénocarcinome, ont montré un comportement différent sur ces topographies de type puits (hauteur, largeur et espace de 150x150x60µm).

CHAPTER 4. COLON CARCINOMA CELL BEHAVIOUR ON MICROSTRUCTURED SURFACES

4.1 INTRODUCTION

Epithelial origin colorectal cancers (CRCs) are more common type of cancers. It is the third most frequently diagnosed cancer after prostate and lung cancer in men (663,000 cases, 10.0%), and the second most common cancer type after breast cancer in women (570,000 cases, 9.4%) worldwide in 2008[272]. Up to to 75% of CRCs occur within the descending, sigmoid colon and rectum, 15% of cases come from cancers located in the caecum and ascending colon, and only 10% CRCs arise in the transverse colon[273,274](*fig 4.1*). However, adenocarcinoma (malignant tumour formed from glandular structures in epithelial tissue) is most common type of CRC as it accounts for 95% cases.

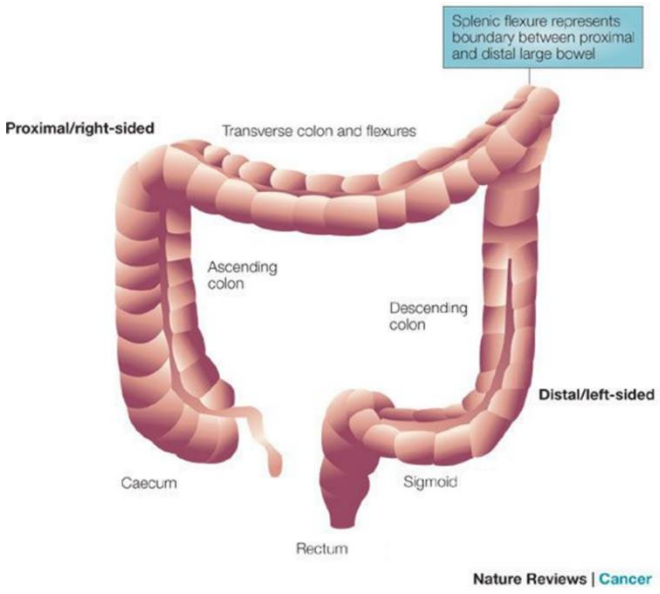

Figure 4.1: *Figure adapted from[275]. Structure of colon.*

4.2 COLORECTAL ADENOMA-CARCINOMA SEQUENCE

Majority of CRCs arise from a polyp (small benign tumor) in a crypt of intestine which further evolves into early adenoma. Adenomas or adenomatous polyps are considered pre-cancerous and

carry high risk leading to CRCs[276]. This adenoma evolves into advanced malignant adenoma which involves mutation of several genes. Adenomas are further classified as sessile serrated adenomas and traditional serrated adenomas[277]. Serrated polyps that arise in right colon (caecum, ascending and transverse colon) show MSI and CIMP mechanism (described in section 4.3) and are forming CRCs. On the contrary, left colon polyps (descending and sigmoid colon and rectum) frequently carry KRAS mutations via CIN pathway (described in section 4.3) and some carry CIMP mutations also end forming CRCs. Thus, in CRCs the evolution of normal epithelium into malignant cancer is called adenoma-carcinoma sequence. This is a stepwise sequence which involves inactivation of tumor suppressor genes (eg p53) or activation of oncogenes (eg KRAS) leading to malignant form of CRC (*fig 4.2*).

4.3 MECHANISMS OF DEVELOPMENT OF CRCs

Chromosomal instability (CIN), CpG island methylator phenotype (CIMP), and microsatellite instability (MSI) are the mechanisms by which the CRCs can arise[278].The CIN pathway, which is prominent in at least 50% of CRCs, involves mutations in adenomatous polyposis coli (APC) followed by mutational activation of KRAS oncogenes and inactivation of p53, a tumor suppressor gene[279] (genes explained in section 4.3 and 4.4 in detail). p53 gene which is localized on the short arm of chromosome 17, is mutated in up to 70% of colorectal cancers[280]. CIMP pathway which accounts for 20-30% of CRCs, consists of hyper methylation of promoter of various tumor suppressor genes such as MGMT and MLH1 and is associated with BRAF mutation[281,282]. MSI pathway, which occurs in about 15% of CRCs is characterised by inactivation of genetic alterations in short repeated sequence[283]. However, these different mechanisms tend to overlap in CRCs (*fig 4.3*)[278].

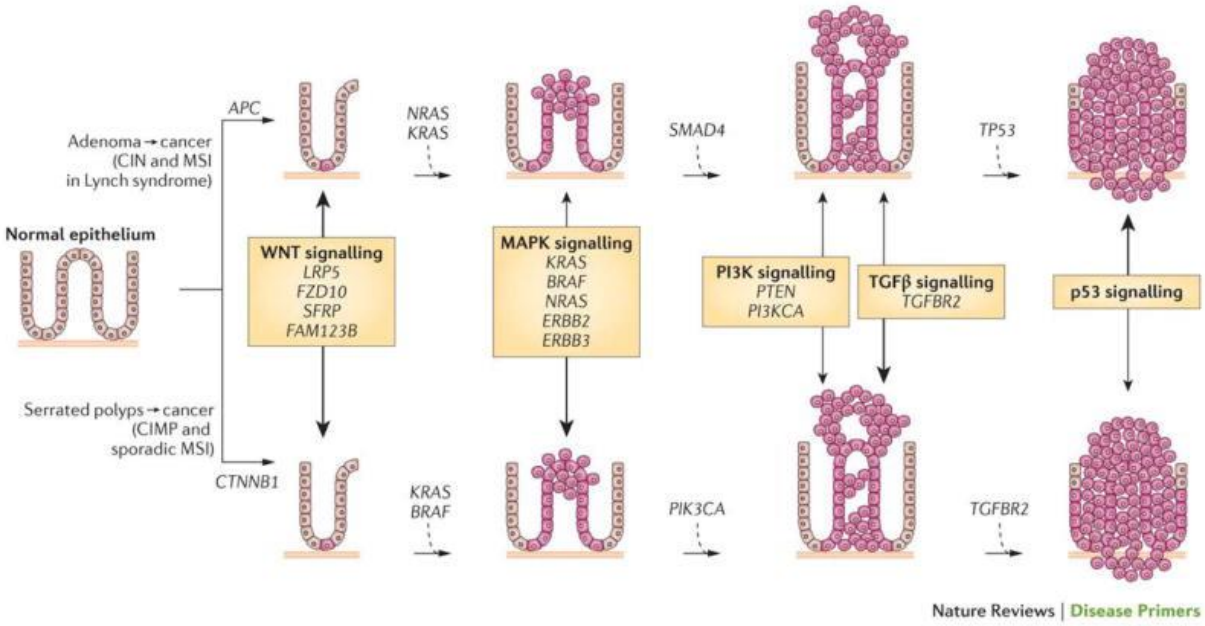

Figure 4.2: *Adapted from*[277]***.****The polyp to colorectal cancer sequences: Currently, two discrete normal colon to colorectal cancer sequences have been identified. Both sequences involve the progression of normal colon epithelial cells to aberrant crypt foci, followed by early and advanced polyps with subsequent progression to early cancer and then advanced cancer. The 'classic' or traditional pathway (top) involves the development of tubular adenomas that can progress to adenocarcinomas. An alternate pathway (bottom) involves serrated polyps and their progression to serrated colorectal cancer has been described in the last 5–10 years. The genes mutated or epigenetically altered are indicated in each sequence; some genes are shared between the two pathways whereas others are unique (for example, BRAF mutations and CpG Island Methylator Phenotype (CIMP) only occur in the serrated pathway). The signalling pathways deregulated during the progression sequence are also shown, with the width of the arrow reflecting the significance of the signalling pathway in tumour formation*

4.4 GENES MUTATED AND DYSREGULATED IN CRCs

4.4.2 Tumor suppressor genes in CRCs

Tumor suppressor genes or anti-oncogenes are ones that loose a function during mutation and are categorized as inactivating mutations[284]. They generally reduce the probability of a cell to become cancerous. However, an inactivating mutation or deletion of such a gene increases the probability of the formation of a tumour. APC and cdx2 are some examples of tumor suppressor genes. Also, we shall be using the cell lines wild type APC restored and cdx2 inducible expression

in CRCs for our experiments.

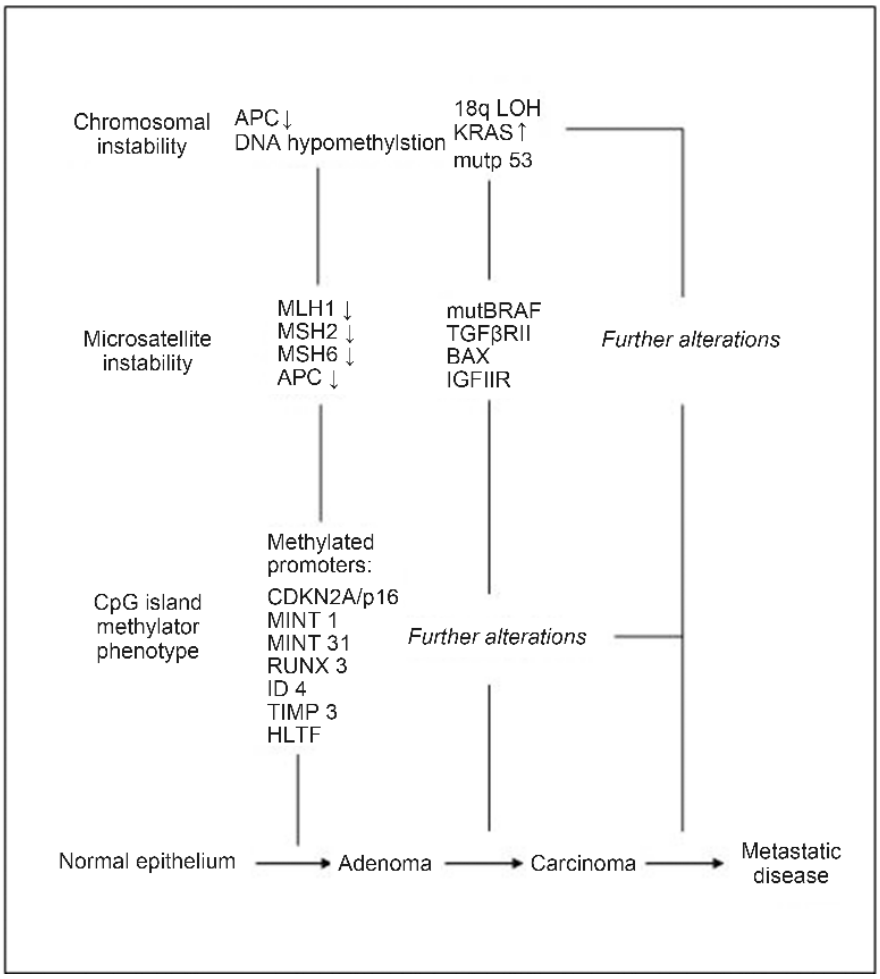

Figure 4.3: *Figure adapted from[278]. Overlapping of mechanisms leading to CRC disease progression.*

4.4.2.1 APC gene

Adenomatous polyposis coli (APC) is a tumor suppressor gene whose mutation can lead to malignant transformation of cells. Majority of sporadic colorectal tumours are found to harbour mutations in both APC alleles[285]. APC forms a destruction complex with other proteins and leads to proteasomal degradation of β-catenin onco-protein in absence of Wnt signalling[286](*fig 4.5*). This loss of APC function therefore leads to accumulation of β-catenin in nucleus and cause expression of target genes such as cyclinD1, c-myc and CRD-BP[287]. APC also has another function to promote microtubules stability[288]. However, the role of deregulation of APC function in the microtubule

context remains poorly understood. Bi-allelic mutation of APC (mutation of both the alleles) along with KRAS and p53 are known to have a prognostic role in tumor evolution[289].

4.4.2.2 Cdx2 gene

Cdx2 is a tumor suppressor gene whose activity is known to be altered in majority of CRCs[290,291]. It acts as a prognostic marker in stage II and stage III CRCs[292]. Cdx2 downregulation is observed in invasive fronts of CRCs tumors[293]. It's encodes homeotic (regulation of anatomical structures) transcription factor for regulation of embryonic development of intestines [294]. APC mutated CRCs were found to be more invasive on loss of cdx2 expression[295]. It is known to enhance e-cadherin trafficking to cell membrane and is also involved in transcription of certain genes involved in cell junctions[296,297]. It is also known to play an important role in migration of cells. Forced expression of cdx2 decreases migration whereas inhibition of cdx2 leads to enhanced migration[295]. Loss of cdx2 gene was observed to increase MMP2 expression[295]. Coskun et al. found that cdx2 is involved in Wnt signalling, where cdx2 is downregulated via TNF-α, which proved its role in tumor promotion in CRCs[298]. Recently, cdx2 was found to increase cellular stiffness involving Rho signalling pathway in CRC cells[299]. Another new study found that CRC cells with cdx2 knockout induce modifications to the tumor microenvironment involving NF-κB pathway activation and loss of APC[300]. Thus these finding prove that cdx2 plays an important role in suppressing metastasis of

CRCs. However the mechanisms involving this anti-metastatic role still remain poorly understood.

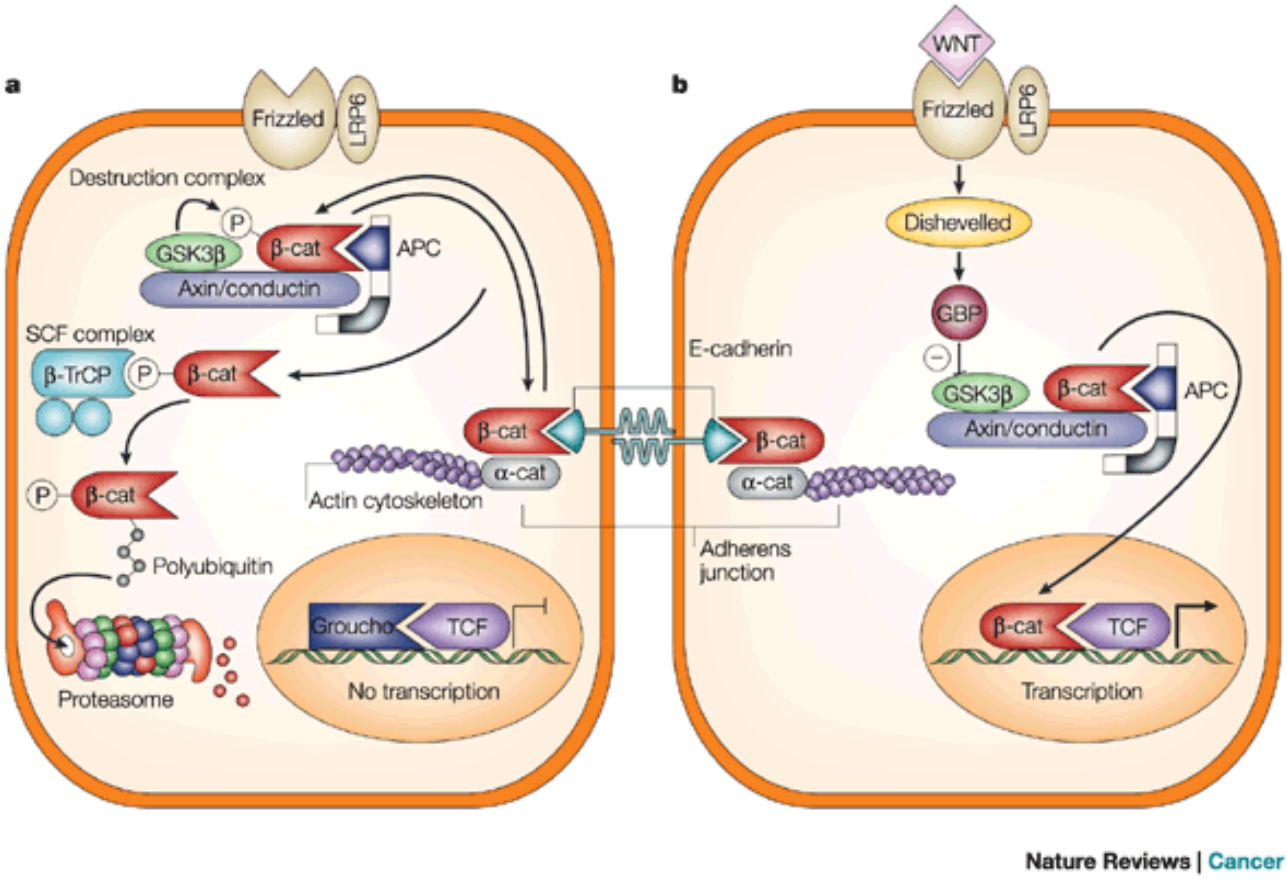

Figure 4.4: *Figure adapted from ,[301,302]. **a** In the absence of a WNT signal, the level of free intracellular β-catenin is minimized by sending it for degradation in the proteasome. Free cytoplasmic β-catenin, which is in equilibrium with β-catenin at adherens junctions, is recruited to a 'destruction complex' containing APC, axin/conductin and glycogen synthase kinase 3β (GSK3β). GSK3β phosphorylates β-catenin, allowing it to be recognized by an SCF complex containing the F-box protein β-TrCP. Other proteins in the SCF complex catalyse the addition of a polyubiquitin chain to β-catenin, allowing β-catenin to be recognized and degraded by the proteasome. Consequently, β-catenin cannot reach the nucleus, and cannot co-activate TCF-responsive genes. Groucho, a corepressor, also prevents the activation of TCF-responsive genes in the absence of β-catenin. **b** In the presence of WNT, its receptor, Frizzled, in complex with LRP6, is activated. This leads to a poorly understood signalling cascade in which Dishevelled activates GBP — an inhibitor of GSK3β. Consequently, β-catenin cannot be targeted for destruction and is free to diffuse into the nucleus, where it acts as a co-activator for TCF-responsive genes.*

4.5 MECHANOTRANSDUCTION IN CANCER CELLS

There is debate about the responsiveness of cancer cells to mechanical cues. Some researchers show that cancer cells are unresponsive to the mechanical stimuli while others show the opposite.

Some cancer cells prefer stiff substrates while other prefer soft and some others are insensitive to rigidity of substrates[210,303,304]. The tumor microenvironment itself becomes stiff in some cancers[212]. In other cancers the core of a tumor is less stiff than its periphery, may be as they contain only cancer cells and little ECM[305,306]. Hence, there is no single mechanism that can be applied as hallmark to every cancer system. Moreover, the invention of 3D model culture systems are paving way for researchers to understand the behaviour of different healthy and cancerous cells in biomimetic environment.

A myriad of culture systems are employed to study the mechanotransduction of cancer cells which include micropillars, grooves, pits/wells, microfluidics, tubular structures, etc. (described below in section 4.5 and 4.6). Other than these, mechanical cues such as stress and strain are also employed to study the response of various cells. However most of these techniques are used to study normal healthy epithelial cells. Fewer studies have focused on analysing the behaviour of CRCs on different topographies, which are summarised in the below sections.

4.6 EFFECT OF MECHANICAL CUES-RIGIDITY, SHEAR STRESS, STRAIN ON BEHAVIOUR OF CRCs

The tumour microenvironment is known to contribute to tumorigenesis due to mechanical forces such as fibrotic stiffness or mechanical pressure caused by the expansion of hyper-proliferative cells in cancer. Mechanotransduction of physical cues from extracellular matrix to initiate intracellular signalling pathways has also been documented in colorectal cancers (CRCs) types. Rigidity of the substrate has shown to affect the behaviour of CRC cells in disease progression. Tang et al showed that CRCs undergoes epithelial to mesenchymal (EMT) transition on lower stiffness[307]. They showed that soft substrates induced transition of adhesive epithelial to rounded

phenotype in low metastatic potential CRC cells. These rounded cells have been shown to have characteristic of metastasis, migration and proliferation. On the other hand, stiffer substrates with 25kPa Young's modulus are known to affect YAP/TAZ proteins to carry out optimal cell survival and proliferation in CRCs[308,309]. Mechanical strain is also known to affect CRCs. 1kPa mechanical strain was shown to induce tumour formation in CRCs with APC mutation[310]. Mechanical strain in APC deficient CRC cells showed an increased number of β-catenin nuclei per crypt, whereas almost no nuclear β-catenin was detected in the wild-type colon epithelium[311]. CRCs are also known to respond to fluids and shear stress and induce mechanotransduction pathways. For example, overexpression of polycystin 1 and 2, proteins present in the plasma membrane and cilia, in CC progression suggests that cells can mechanosense fluids from their dorsal surface[312]. Another study showed that shear stress decreased β-catenin signalling in CRC cells[313].

4.7 EFFECT OF TOPOGRAPHY ON BEHAVIOUR OF CRCs AND OTHER EPITHELIAL CELLS

- ***Various topography effects on CRCs***

Topography effect on CRCs is studied very less. Yeung et al. used matrigel based differentiation of different CRCs to derive cancer stem cells[314]. Koppes et al. replicated the structures of crypts and villi, which was seen inducing differentiation in CRCs by increased alkaline phosphatase activity compared to flat substrate[315]. Another study by Wang et al. showed that biomimetic micro-well topography (similar dimensions to native intestinal topography) enhanced the cell spreading and affected the metabolic activity of CRC cells[173]. CRCs on porous synthetic tissue scaffold with villous structure lead to cellular differentiation similar to native intestine[316]. Confinement is another physical cue that is known to affect CRC cell behaviour. Pachenari et al. showed that confinement by micropipette aspiration caused high deformation of grade IV CRC cells and this deformability

could be used to segregate different grades of CRC[317].

- ***Various topography effects on other epithelial cells***

Mostly the effect of healthy or other epithelial cells has been studied on substrates with grooves topography. Pioneering work by Brunette showed that shallow microgrooves with different depths directed epithelial cell migration and cell elongation[318]. Using microgroove–based topography Kushiro et al. showed that cancerous cells loose geometrical recognition with increasing malignancy probably to ease their migration during metastasis[169]. Microgroove contact-mediated radial migration was seen in corneal epithelial cells[319]. Apical-to-basal polarization of epithelial cells was affected on hydrogel based microgrooves[320]. Wu et al. observed that migration of EMT reduced on cone patterned substrates and increased the most on 5µm grooves[321]. Vedula et al. utilised alternating strips of ECM (FN) to show that keratinocytes maintain the intercellular-bridge to maintain tissue integrity during wound healing[322]. Another study by Saez et al. showed that epithelial cell traction forces are proportional to the substrate rigidity implying that the deformation remains constant irrespective of the rigidity using micropillar array[323]. Further in a similar study using micropillar arrays Roure et al. showed that the maximum traction was observed at the edge of the epithelial layer due to collective migration and the traction forces are more than those of single cells[192]. Xi et al. investigated the behaviour of epithelial cells in tubular confinement and found that actin alignment, cell orientation, tissue organization, and migration modes depend on the extent of tubular confinement and/or curvature[324]. Epithelial cells underwent cytoskeleton remodelling on pores of different sizes and exhibited fluid like behaviour on larger pores[325]. Kim et al. employed micropatterned substrates with convex and concave architectures on immortalised epithelial cells and showed that it affected cell-to-cell contact, focal

adhesions and actin reorganization[326]. Topographic confinement of epithelial clusters in hydrogel microchannels was found to induce epithelial to mesenchymal transition on rigid matrices and affect cytoskeletal polarization[327].

4.8 OBJECTIVES OF THIS CHAPTER

Although all the above research provides us with a wealth of insight of effects of various active and physical cues on epithelial cells, topography effect on behaviour and the involved mechanotransductive pathways in CRCs still remain elusive. Hence the objective of this study was to investigate the behaviour of CRCs from different grades and with mutations of two tumor suppressor genes on different topographic substrates such as pillars and pits. Comparing different grades of CRC cell lines would allow to perceive how CRCs from different stages behave with respect to topography. Also this would help us understand the behavioural difference of epithelial origin cancers compared to mesenchymal origin cancers.

Previous studies in our lab initiated the work on different CRC cells of different grades and observed the behaviour of these cells on pillars[328]. However, the analysis of the behaviour of these cell lines in detail and the entailed mechanisms still need to be understood. Hence we shall employ not only the CRC cells from different grades but also mutant variants of APC gene (mutated in 80% of CRCs) and altered cdx2 expression (in many CRCs) a tumor suppressor gene known to increase cellular stiffness[299,300,329]. This would help us perceive the role of these genes in mechanotransduction of CRCs on topography substrates.

4.9 METHODS

4.9.1 Substrate Fabrication

- ***Pillars***

PLLA pillars were fabricated in the same way as described in methods of chapter 2.

- ***Grooves***

Metal surfaces with the groove topography were provided by Pierre-François Chauvy (Micropat SA, Côtes-de-Montbenon 30, 1003 Lausanne, Switzerland.) Metal surfaces were first replicated by hot embossing (230°C on hot plate) of 35mm polystyrene Petri dishes. Then, liquid PDMS (Sylgard® 184) was casted inside the dishes to generate positive replicates (6H incubation at 80°C). The PDMS replicates were then coated with fibronectin (50μM in PBS). The grooves were 40 μm in width and 8 μm in depth.

- ***Wells/Pits***

Wells were fabricated by Dr Felix Sima (National Institute for Lasers, Plasma, and Radiation Physics (INFLPR); Institute of Atomic Physics; Bucharest V, Romania). The experiments were performed using Foturan photosensitive glass (PG - commercially available from Schott). Foturan is a photo-structurable lithium alumino-silicate glass that accommodate small amounts of Ag_2O (0.05%–0.15%) and Ce_2O_3 (0.01%–0.04%), in principle designed for the UV light-induced selective micro-structuring.

The protocol for obtaining flexible micro-structures in Foturan glass using picosecond (ps) laser is schematically depicted in Figure 4.9.1.1. The process is known as picosecond laser assisted etching (PLAE). First, Laser Direct Write (LDW) was carried out by a ps laser source (Coherent, model

Lumera), delivering pulses of τ_{las}< 10 ps duration and 500 kHz repetition rate. Pulse power was adjusted to few hundreds (300-500) mW for 532 nm VIS pulses. The laser beam was focused onto the sample surface using an aspheric lens of 18 mm focal length in a circular spot of about 4 μm in diameter. The writing speed was set between 0.1 and 1 mm/s depending on the pattern geometrical features. The samples were placed on a customized LDW processing platform consisting of motorized translation stages (PlanarDL Aerotech), having a spatial resolution of few tens of nanometers. The experiments were carried out in a clean room, in air, at atmospheric pressure, and were in-situ monitored with a CCD camera (Thorlabs). By the ps laser irradiation, free electrons are generated by interband excitation based on multiphoton absorption, which reduce Ag ions to precipitate Ag atoms at the laser exposed region.

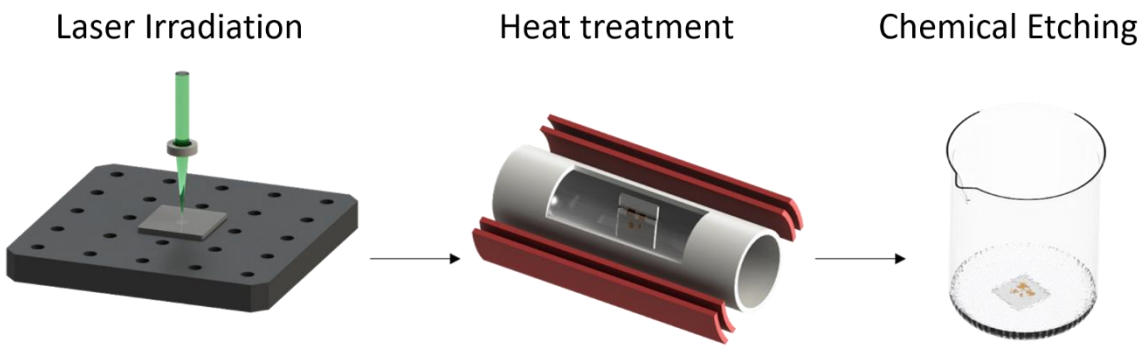

Figure 4.9.1.1: *Schematic of the PLAE process*

In a subsequent step, the laser-exposed glass samples are annealed under control in a programmable furnace (Carbolite, model MTF M1238-250). First, controlled heating with a slope of 5 °C/min up to 500 °C is performed, then the temperature is kept constant for 1 hour in order to cause diffusion of precipitated Ag atoms to grow Ag nanoclusters. Next, the temperature is

increased again with a slope of 3 °C/min up to 605 °C and kept constant for another hour to induce the formation of crystalline lithium meta-silicate phase around the grown Ag nanoclusters which act as nuclei. In the last step, the glass samples are submitted to chemical etching in 8% hydrofluoric acid (HF) solution under ultrasonic condition. During the wet etching process, the grown crystalline phase grown is selectively removed, since it has ca. 50 times higher etching rate as compared with laser unexposed regions. Eventually, micro-structures corresponding to the laser writing trajectory are produced in Foturan glass.

The characterization of the samples was performed in transmission mode by optical microscopy (Leica, model DM4000 B Led). Scanning electron microscopy (SEM) investigations were achieved with an FEI Co. microscope (model Inspect S).

Fabrication of myriad of micro-chambers in PDMS by using photosensitive glass (PG) molds

We have fabricated up to 10000 micro-chambers in PDMS in a single step based on PG mold. First, we apply PLAE in order to create 3D pillars in PG after the chemical etching of laser exposed regions. A VIS ps (<10 ps) laser with 532 nm wavelength and 500 KHz repetition rate was focused on the PG using a aspheric lens with 18 mm focal length. The irradiated area was obtained in a line-by-line scan regime at a power of 600 mW and 1 mm/s scanning speed. The step between lines was set to 10 μm. In *Figure 4.9.1.3* c,d is showed the exposed PG after thermal treatment where the brown color represents modified PG and the white areas reflect the unaffected PG. During the chemical etching in HF the modified PG is etched with a rate of 10 :1 for several minutes. The etching depth is proportional with etching time. In our case, an etching time of 3 minutes is reflected in a pillar height of 30 μm.

We thus obtain molds with 2500 pillars of 150x150x60 μm^3 or even with 10000 of pillars of

50x50x30 μm^3 (Length × width × height). Second, we use the fabricated PG molds to obtain replicas in PDMS, by which reverse patterns are transcribed, i.e., micro-chambers with the same X-Y dimension of glass pillars are formed with a depth corresponding to the glass pillar height. All process is schematically shown in *figure 4.9.1.2*.

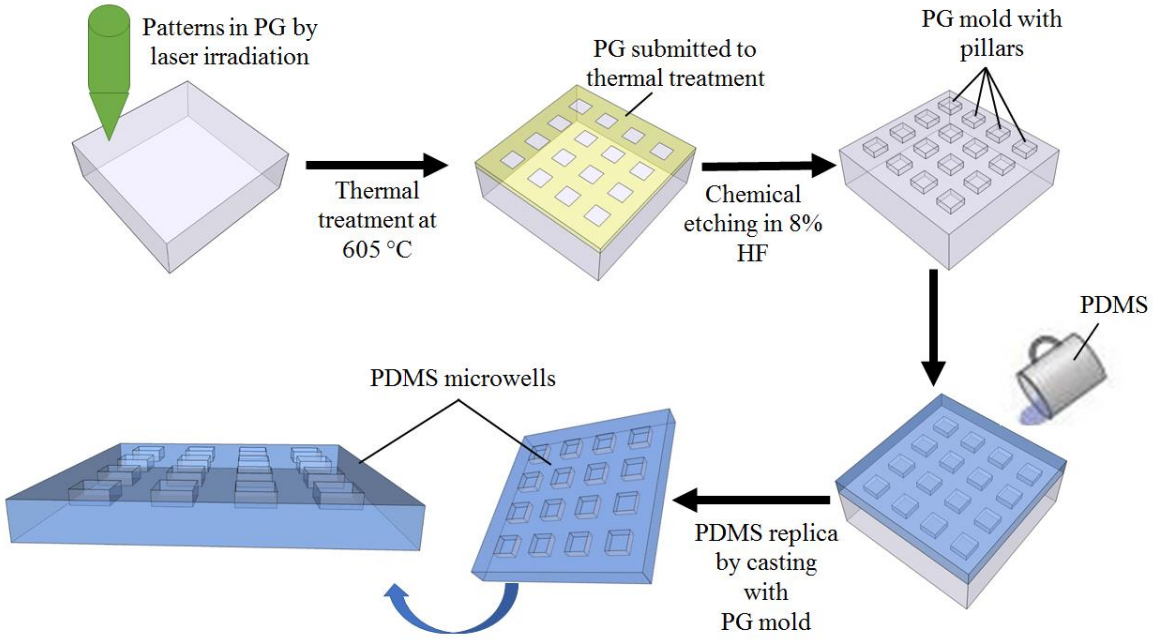

Figure 4.9.1.2: *Schematic of the fabrication procedure of the PG mold and of 3D micro-chambers in PDMS. The mold is obtained after the PG processing protocol described in section Materials and Methods. On the mold surface is dropped a liquid PDMS prepared in 10:1 ratio. The PDMS replica is obtained after 24 hours drying at room temperature by separating the mold from PDMS.*

Sketches and photographs of PG after laser irradiation and thermal treatment are shown in *Figures 4.9.1.3 a,b,* while optical images of the exposed patterns (one layer laser scanning) can be visualised in *Figures 4.9.1.3 c,d*. Similarly, *Figures 4.9.1.3 e,f* depicts the mold sketch and photograph after chemical etching and *Figures 4.9.1.3 g,h* presents magnified images of "f" with different magnifications.

Using such moulding systems one can get controlled and efficient synthesis of thousands micro-chambers having a dimension of 150×150×60 μm^3 (*Figure 4.9.1.4.a*) or 50×50×30 μm^3 (*Figure 4.9.1.4.c*).

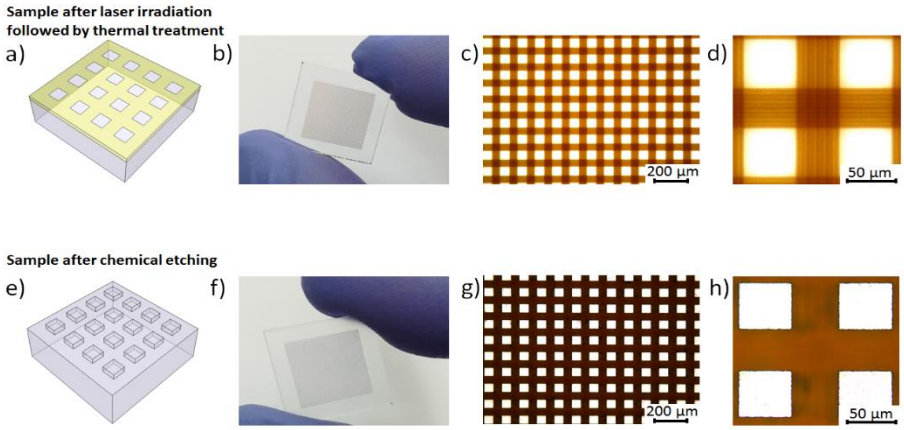

Figure 4.9.1.3: *Fabrication of PG glass mold. PG after laser exposure and thermal treatment: a) Sketch of the irradiated patterns; b) Photograph of the entire sample; c) Optical image of central region; d) Detail view of c). PG after chemical etching; e) 3D mold sketch; f) Photograph of the entire PG mold; g) Optical image of central region; h) Detail view of g).*

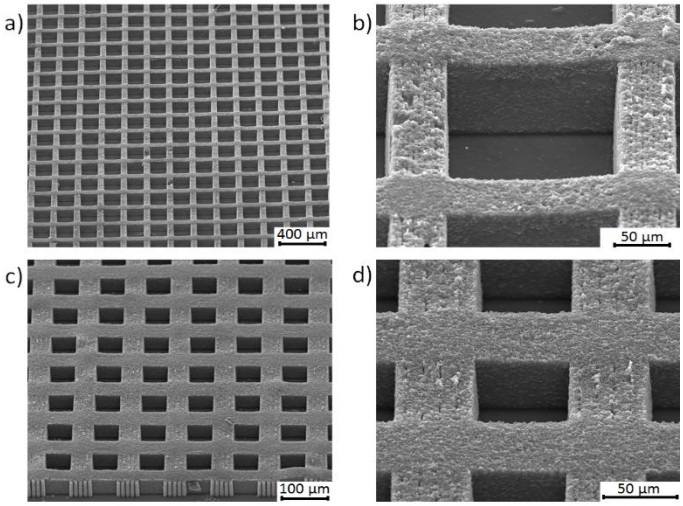

Figure 4.9.1.4: *SEM images of square micro-chambers obtained in PDMS by replication of the PG mold. a) General view of the square micro-wells of 150×150 μm^2 with 60 µm depth separated by a 50 µm thickness wall; b) Detailed view of a); c) General view of the square micro-wells of 50×50 μm^2 with 30 µm depth separated by a 50 µm thickness wall; d)Detailed view of c).*

4.9.2 Cell Culture

All the CRC cells were provided by Dr. Jean Noel Freund laboratory (Inserm U1113, Strasbourg, France). All the cells were cultured in a humidified incubator at 37 °C and 5% CO2. For all experiments 1-3X10^6/ml cell density was used in 60mm petri dishes, unless specified. 5 cell lines from different stages of CRC were used- TC7/CaCO-2; DLD1; HCT116; HT29; SW480.

TC7/CaCO-2 were cultured in Dulbecco's modified eagle medium (Sigma, France) and supplemented with sterile FBS heat inactivated (20% v/v, Biowest, France), 1% penicillin/streptomycin (Sigma, France) and 1% non-essential amino acids (Sigma, France) and 50µl/200ml gentamycin (Sigma, France).

DLD1 were cultured in Dulbecco's modified eagle medium (Sigma, France) and supplemented with sterile FBS heat inactivated (10% v/v, Biowest, France), 1% penicillin/streptomycin (Sigma, France) and 10ml HEPES (Sigma, France).

HCT116, HT29 and SW480 were cultured in Dulbecco's modified eagle medium (Sigma, France) and supplemented with sterile FBS heat inactivated (10% v/v, Biowest, France), 1% penicillin/streptomycin (Sigma, France).

2 cells lines with restored wild type APC and altered cdx2 genes were used with their respective control cell lines (with empty vector)-SW480-APC and SW480-APC CNT; HT-29 TW6 and HT-29 TG8 CNT

SW480-APC and SW480-APC CNT were grown in RPMI 1640 without L-glutamine supplemented with 0.00108% thioglycerol, 0.025 U/ml insulin, 1 mg/L hydrocortisone, sterile FBS heat inactivated (10% v/v, Biowest, France),1% penicillin/streptomycin and 1.5mg/ml G418. All reagents are from Sigma, France unless specified.

HT-29 TW6 and HT-29 TG8 CNT with inducible cdx2 expression were grown in Dulbecco's modified eagle medium supplemented with 5µg/ml blasticidin (Cat. No. R21001; Thermoscientific, France), 100µg/ml zeocin (Cat. No. R25001; Thermoscientific, France) and 1% penicillin/streptomycin. All reagents are from Sigma, France unless specified. Induction of cdx2 was performed by adding doxycycline (1µg/ml, Sigma) to the culture medium. As the cells revived undergo 50% cell death during initial passaging (later on cell death decreases), 3-5X10^6/ml cell density was used in 60mm Petri dishes. For revival of cells, one vial was defrozen and resuspended in 6 ml of medium which was further divided into 3 wells (2ml /well) of 6 well plate. These cells grow better in 6 well plates than T25 flasks while defreezing. Once the cells are confluent in 6 well plate they can be transferred to T25 flask.

4.9.3 Immunostaining

Cells were fixed with 4% formaldehyde (Electron Microscopy Sciences, USA) and permeabilised using 0.5% Triton X-100 (Sigma, USA) for 15 min and blocked with 3% bovine serum albumin (Sigma, France) for 1 hour. Primary antibodies used were lamin a/c (1:250; ab108595; anti-Rabbit; Abcam-UK); anti-paxillin (1:250; ab32084; anti-Rabbit; Abcam-UK); anti-Lamin A (1:500; L1293; anti-Rabbit; Sigma-France), anti-e-cadherin (1:1600; U3254; anti-mouse/rat; Sigma-France) and anti-β tubulin (1:200; T4026; anti-mouse; Sigma-France). Secondary antibodies used were Alexa 488 (1:200; ab150073; anti-Rabbit; Abcam-UK), Alexa 488 (1:200; ab150113; anti-Mouse; Abcam-UK), Alexa 647 (1:200; ab150115; anti-Mouse; Abcam-UK). Actin-555 (1:20; A34055; Thermoscientific-France) or phalloidin-FITC (Fluorescein-5-isothiocyanate) for actin (0.4µg/ml; Sigma-France) was used to label actin and Hoechst (1:1000; 33258; Thermoscientific-France) was used to label nucleus.

4.9.4 RT-qPCR and western blot analysis

RT-qPCR method same as that of chapter 2-methods.

4.9.5 Quantification of ratio of mRNA levels

For the ratio we divided the ΔΔct values of respective genes of interest and plotted it as a logarithmic scale on y axis using GraphPad software.

4.9.6 Confocal imaging, image and statistical analysis

Same as described in methods of chapter 3- 3.5.6; 3.5.7 and 3.5.8.

4.10 RESULTS AND DISCUSSION

4.10.1 Characterization of colorectal cancer (CRC) cells on flat surface (*fig 4.5)*

Our initial experiments included characterization of CRC cell lines individually. Tumorigenic HT29 (grade I) have deleted APC gene and are known to have high glucose consumption rate. They showed round grape shaped colonies like morphology. The HT29-TW6 with inducible expression of cdx2 gene and its control HT29-TG8 showed more epithelial like colonies and fewer round cells. SW480 cells showed 2 populations mainly (>98%) epithelial (E-type) and (>2%) round (R-type) which are described by previous studies[330]. The R-type cells are known to be more malignant variant of E-type cells[330]. Generally APC is deleted in SW480 (APC-) while the wild type APC is restored (APC+) in the mutant cell line of SW480 (grade II). APC- grows slowly compared to APC+ cells. APC- shows more round cells whereas APC+ cells shows more epithelial like morphology. TC7 cells are the clones of CaCO-2 cells (grade II) with homogenous population and higher differentiation properties[331]. They are widely used as model CRC cell line. They too showed few round and most epithelial morphology. DLD1 is stage III CRC cell line with mutated APC gene[288]. They show majority of elongated epithelial cell morphology. HCT116 depending on its strain can range from grade I –

IV and have mutations in KRAS gene[332]. HCT116 showed round and elongated epithelial cell morphology.

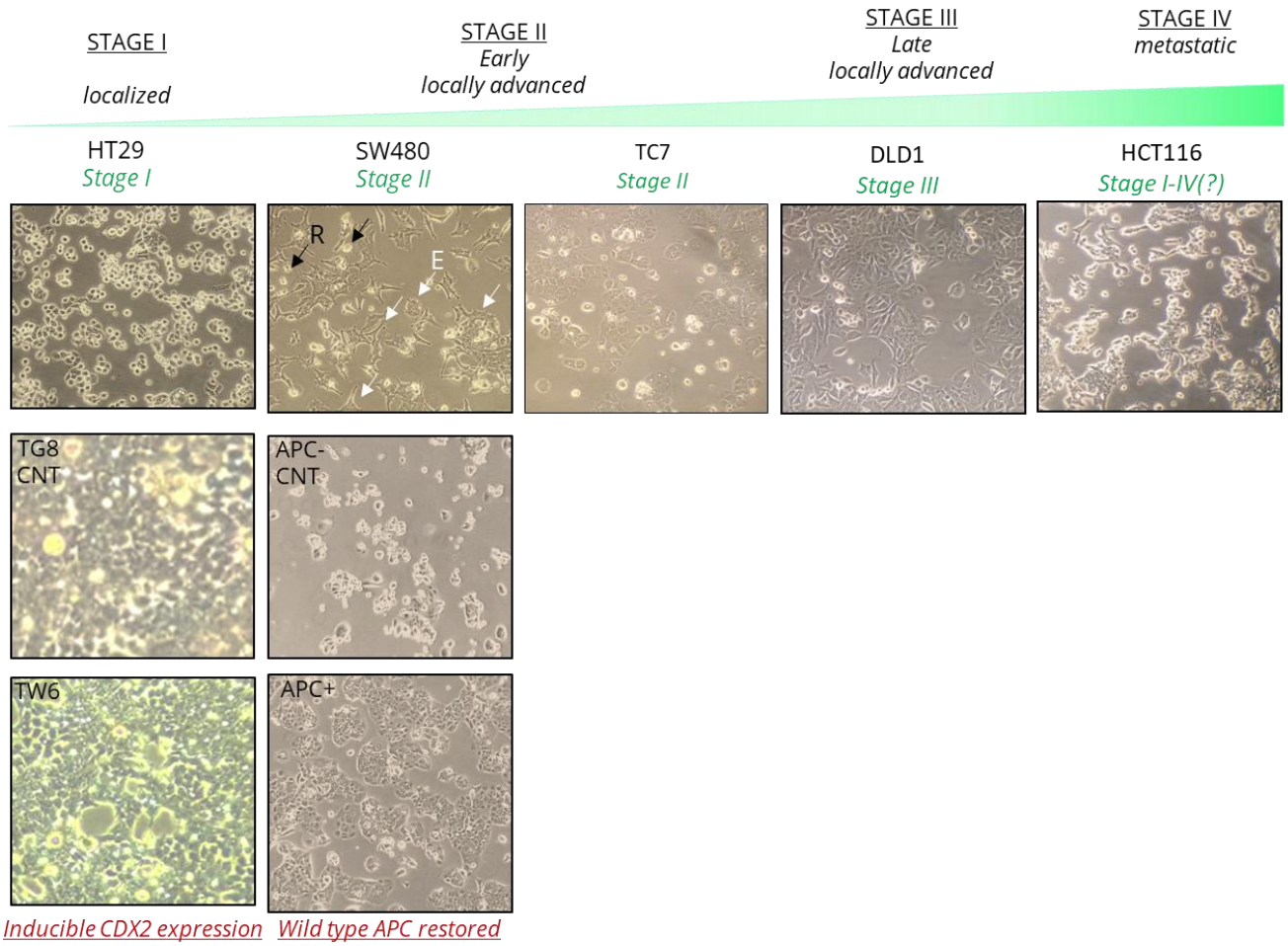

Figure 4.5: *Compound microscope images of CRC cells from different stages and the APC restored and inducible cdx2 cell lines derived from them on T25 flask cultured for 3-5 days.*

4.10.2 mRNA expression of nuclear proteins in CRC cells on flat substrate

The major nucleoskeletal proteins are lamins. There are different types of lamins, but lamin A/C and lamin B1 are the ones that are known to be deregulated in cancer. Lamin A/C expression is down regulated in cells of the colonic crypts except for a few basal crypt cells, which are believed to be stem cells[333]. Lamin A/C is known to affect oncogenes such as β-catenin, which is important regulator of Wnt pathway in colon cells[334]. Its expression is shown to increase invasiveness and stem cell like phenotype in CRC cells, which makes it a risk biomarker in CRCs[335]. EJ et al., showed

that stage II and III CRCs exhibit loss of lamin A/C expression[336]. On the other hand, Lamin B1 is also a key player in epithelial cancers. Its overexpression causes mitotic catastrophe in CRC cells[337]. Lamin B1 expression is also known to stimulate senescence in CRCs[338]. The role of other nuclear proteins such as members of LINC complex-SUN and nesprin proteins in diseases still remains elusive. Epithelial cancers such as breast cancer, have shown global loss of these LINC proteins, leading to cancer progression[339]. SUN2 is known to play a tumor suppressor role in lung cancer[340]. However their role in CRCs is not yet understood. Nesprins are deregulated in cancers including CRCs but their role in the same remains poorly understood[119]. To analyse the mRNA expression of nuclear proteins, we performed the RT-qPCR method on initial 5 cell lines only.

- ***Lamin A/C and lamin B1***

Lamins contribute individually to nuclear mechanics. Lamin A/C are known to enhance nuclear stiffness and stability whereas lamin B is known to be present in phenotypes with soft nucleus[341]. Stoichiometric ratios of lamin A and B have been used by Swift et al., to demonstrate nuclear stiffness that scales with tissue stiffness[342]. Therefore, we applied similar strategy to observe the difference between nuclear lamins and their ratios on flat substrate. The amount of nuclear lamin A/C and lamin B1 was determined using RT-qPCR method. To understand how these genes vary in terms of expression in other cancerous and healthy cells, we also compared the mRNA levels to osteosarcoma (SaOS-2) and healthy human mesenchymal cells (hMSCs). As a reference we used HT29 gene expression (as it is grade I) to compare to other cell types.

We saw significant change in expression of Lamin A/C mRNA compared to HT29. SW480, TC7 and DLD1, which showed no significant change in lamin A/C mRNA levels compared to HT29. HCT116 showed increase levels of lamin A/C. SaOS-2 showed more lamin A/C levels than the CRC cell lines.

hMSCs showed the highest lamin A/C mRNA levels *(fig 4.6. a).*

Lamin B1 was seen more in some CRCs than SaOS-2 and hMSCs. SW480 and TC7 showed less expression of lamin B1 and HCT116 showed more lamin B1 mRNA levels. DLD1 showed the highest expression of lamin B1 amongst all cell lines *(fig 4.6. a)*.

We observed that hMSCs showed most lamin A/C:B1 ratio whereas DLD1 showed that least. TC7 on the other hand showed highest ratio compared to HT29. SW480 and HCT116 did not show any change in the ratio with respect to HT29. SaOS-2 exhibited more lamin A/C:B1 ratio compared to all CRC cell lines. *(fig 4.6. b)*

Swift et al showed that lamin A:B ratios scaled with tissue stiffness[341]. Hence, in accordance to this our data showed that the TC7 showed stiffest nucleus in terms of lamin A/C and B ratio. Healthy hMSC showed most compared to other CRCs (except TC7) and SaOS-2, indicating that these have the stiffest nucleus whereas cancerous nuclei are softer (except TC7). DLD1 showed the least, suggesting that it has softer nucleus.

- ***SUN1, SUN2 and NES2***

SUN1 mRNA expression levels were highest in SW480 and HCT116 whereas least in DLD1. No difference was seen in SUN2 mRNA levels in TC7. SaOS-2 showed high levels of SUN1 as well and least hMSCs. No mRNA significance levels of SUN2 were observed in all cell lines except DLD1 which showed the least expression of SUN2. NES2 levels changed significantly in most cell lines. Generally, levels of NES2 mRNA was decreased in SW480, TC7, DLD1 and HCT116. SaOS-2 showed no difference in NES2 levels and hMSC showed least NES2 levels *(fig 4.6.c)*.

We also compared SUN to lamin proteins ratio. We found that the ratio of SUN proteins in SW480, DLD 1 and HCT116 was higher than lamin ratios. TC7 showed more lamin ratio compared to ratio

of SUN mRNA levels. SaOS-2 on the other hand also showed more lamin ratio compared to SUNs. The SaOS-2 and hMSC showed a trend where more the lamin ratio less was the SUN mRNA ratio. Contrary more the ratio of SUN in SW480, DLD1 and HCT116 less was the ratio of lamins *(fig 4.6.e)*.

All together this data shows that healthy cells showed least SUN ratio compared to all cancerous cell lines. This relation could contribute to the mechanics of the nucleus in these cells. The mechanisms of lamins and SUN contributions in cancerous behaviour in CRCS, still remains to be explored. Also the SUN 1 levels were found to be more in all cells compared to SUN2. NES2 expression levels was also seen decreased in all cells.

4.10.3 mRNA expression of non-muscle myosin in CRC cells on flat substrate

Non-muscle myosin (NM) II is cytoskeletal motor that drives actin architecture and dynamics. There are different subtypes of heavy chains of NM II motors like A, B and C that play an important role in cellular functions. NM IIA depletion is known to decrease 2D migration but increase 3D invasion in CRCs[343]. Apical junctions in epithelial cells are disorganized on depletion of NM IIA[344]. NM IIB is known to play an important role in colonic stem cells survival and pluripotency[345]. NM II A and B have been shown to regulate shape of epithelial cysts in CRC cells[346]. Hence next we checked the levels of NM II A and B in different CRC cell lines.

NM IIA mRNA expression levels was the highest in DLD1 compared to the reference HT29 genes. HCT116 also showed high expression of NM IIA mRNA expression. SW480 and TC7 showed lower expression of NM IIA than HT29. SaOS-2 showed lower amounts of NM IIA whereas hMSC showed not significant change *(fig 4.7.a)*.

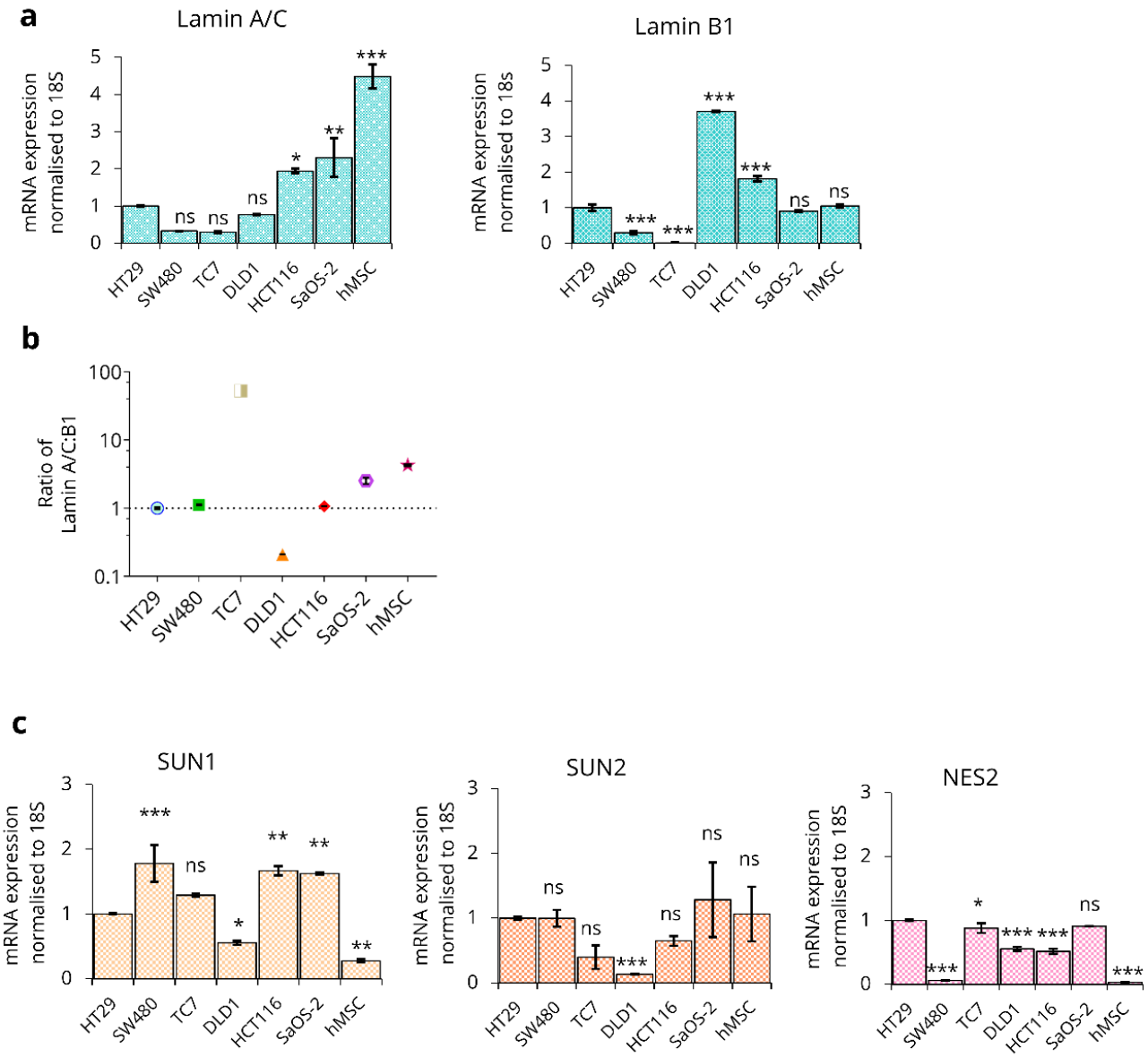

Figure 4.6: *Graphs showing mRNA levels and ratios of different nucleoskeletal genes on flat surface.* ***a*** *mRNA levels of lamin A/C and lamin B1.* ***b*** *Lamin A/C to lamin B1 ratio.* ***c*** *mRNA levels of SUN1, SUN2 and NES2 proteins. n=2 replicates of gene in RT-qPCR experiment. The error bars represent s.d values. HT29 is used as reference. Significance levels were determined by one way ANOVA followed by Dunnet's test for multiple comparison using GraphPad software; ***p<0.001, **p<0.01, *p≤ 0.05 and ns=not significant.*

NM IIB levels in all cell types were significantly different. TC7 showed the least expression of NM IIB mRNA whereas DLD1 showed the highest. SW480 showed significantly less expression and HCT116 showed more than HT29. SaOS-2 also showed significantly lower expression of NM IIB whereas hMSC showed higher levels *(fig 4.7.a)*.

Altogether this data suggests that NM IIA and B show difference in different grades of CRC cells in cancerous cell lines, suggesting they might have a role in either invasiveness, migration or other functions.

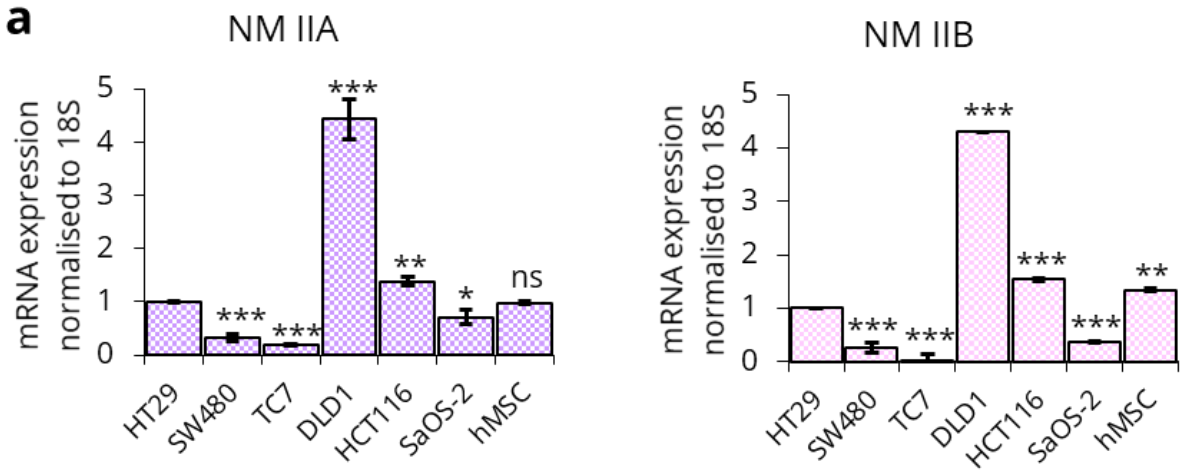

Figure 4.7: *Graphs showing mRNA levels and ratios of NM IIA and IIB genes on flat surface.* ***a*** *mRNA levels of NM IIA and NM IIB. n=2 replicates of gene in RT-qPCR experiment. The error bars represent s.d values. HT29 is used as reference. Significance levels were determined by one way ANOVA followed by Dunnet's test for multiple comparison using GraphPad software; ***p<0.001, **p<0.01, *p≤ 0.05 and ns=not significant.*

4.10.4 Focal adhesions, cytoskeleton and e-cadherin distribution in CRC cells on micropillars

We first wanted to see the organization of focal adhesion, cytoskeletal proteins (actin and tubulin) and cell to cell contact protein (e-cadherin) in CRC cells with different metastatic aggressivity on pillar topography. The aim was to compare the behaviour of different CRCs on topography substrates.

- ***Focal adhesion and actin organization***

Focal adhesions (FAs) are one of the chief players in mechanotransduction of mechanical signals

such as topography. They are known to transmit signals to intracellular proteins such as cytoskeleton to bring about their reorganization in response to topography. Moreover, paxillin is known to promote CRC tumor invasion via ERK activation[347]. Mechanical cue such as pressure is known to activate paxillin and its downstream regulators such as crk, cas and Rac1 to enhance pressure-induced adhesion[348]. Hence we decided to look at focal adhesion protein paxillin and actin cytoskeleton (*fig 4.8*). We stained the cells for paxillin and observed that all the cell lines showed diffused paxillin distribution. Actin however was strongly distributed near the periphery of HT29 and HCT116 cells. Actin in TC7 was seen surrounding the pillars. It was the only cell line showing response to topography geometry compared to other cell lines. On the other hand, SW480 and DLD1 showed diffused actin distribution.

APC-/+ showed diffused but strong paxillin at the periphery of cells contrary to TG8 and TW6 cells which showed just uniform diffused paxillin *(fig 4.9)*. APC- showed strong actin distribution compared to other cells. APC+, TG8 and TW6 showed diffused but more actin organization at the periphery of cells *(fig 4.9)*. Actin in epithelial cells is known to be concentrated near plasma membrane to give structural support to the cell[349]. We saw similar arrangement of actin in CRC cells.

- ***β-tubulin and E-cadherin organization in CRC cells on pillars***

We wanted to observe the distribution of another cytoskeletal protein important in epithelial cells the β-tubulin in the different CRCs cell lines on pillars *(fig 4.10 and 4.11)*[350–353]. On the other hand, e-cadherins are type of cell adhesion molecules (CAM) whose loss is known to promote metastasis of cancer cells. E-cadherin has been known to be a potential biomarker of CRCs[354]. Loss of this protein is known to promote cell migration and invasion in CRCs[355]. Hence we wanted to look at

the distribution of e-cadherin in these CRC cell lines (*fig 4.10 and 4.11*). In SW480 filaments of tubulin are well observed and are visible like that of fibroblasts.

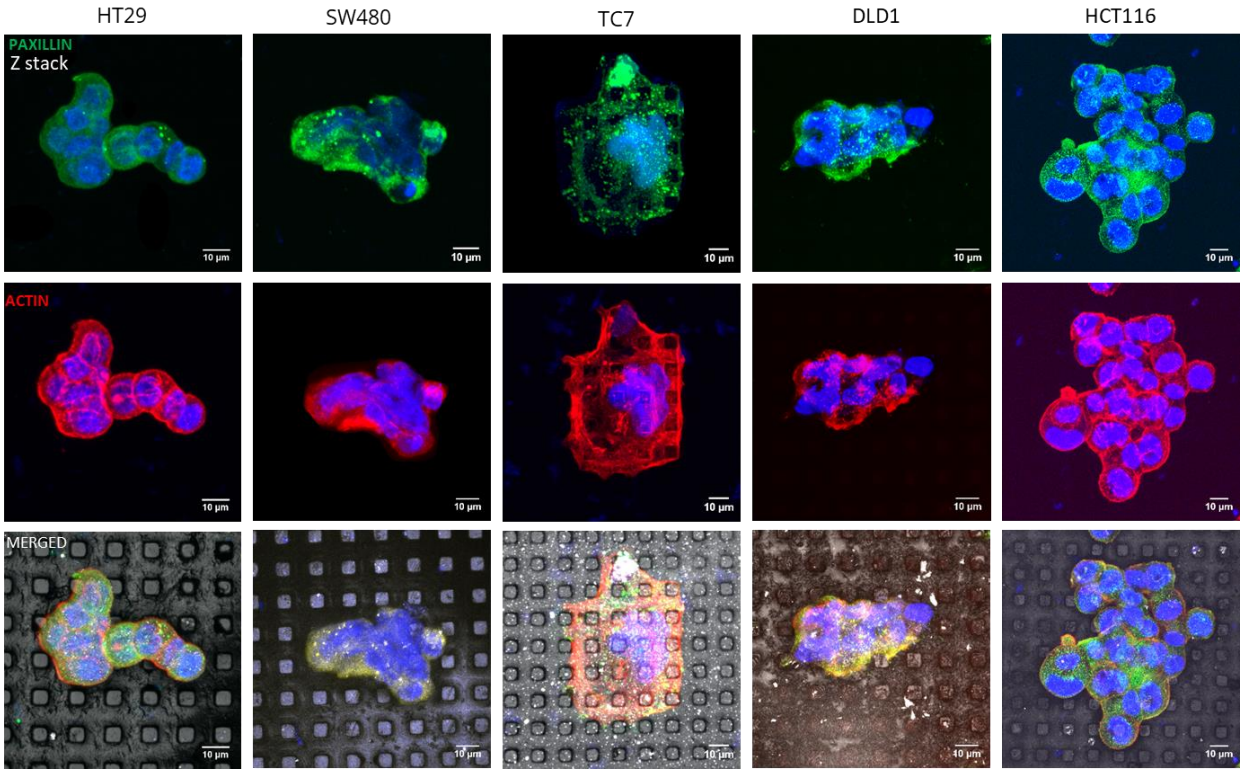

Figure 4.8: *Images of CRC cells immunostained for actin (red), Paxillin (green) and nucleus (blue) on 7µm micropillars. Immunostaining done after 24 hours of seeding 1x10^5 cells in 35mm culture dishes.*

TC7 showed diffused microtubule organization and more localization on the top of the colony. Microtubules in HT29 were observed at the cell periphery similar to e-cadherin distribution. HCT116 and DLD1 showed a diffused tubulin organization. APC-/+ show diffused but strong localization at the periphery of the cells compared to TG8 and TW6 cells that showed diffused tubulin distribution *(fig 4.11)*. SW480 and DLD1 showed uniform distribution of e-cadherin whereas TC7 had diffused distribution of e-cadherin. HT29 exhibited more e-cadherin which was localized at the periphery of each cell and colony. HCT116 had more localization of e-cadherin at the inter-junction of each cell and the colony periphery as well. APC-/+ and TG8/TW6 showed diffused e-cadherin.

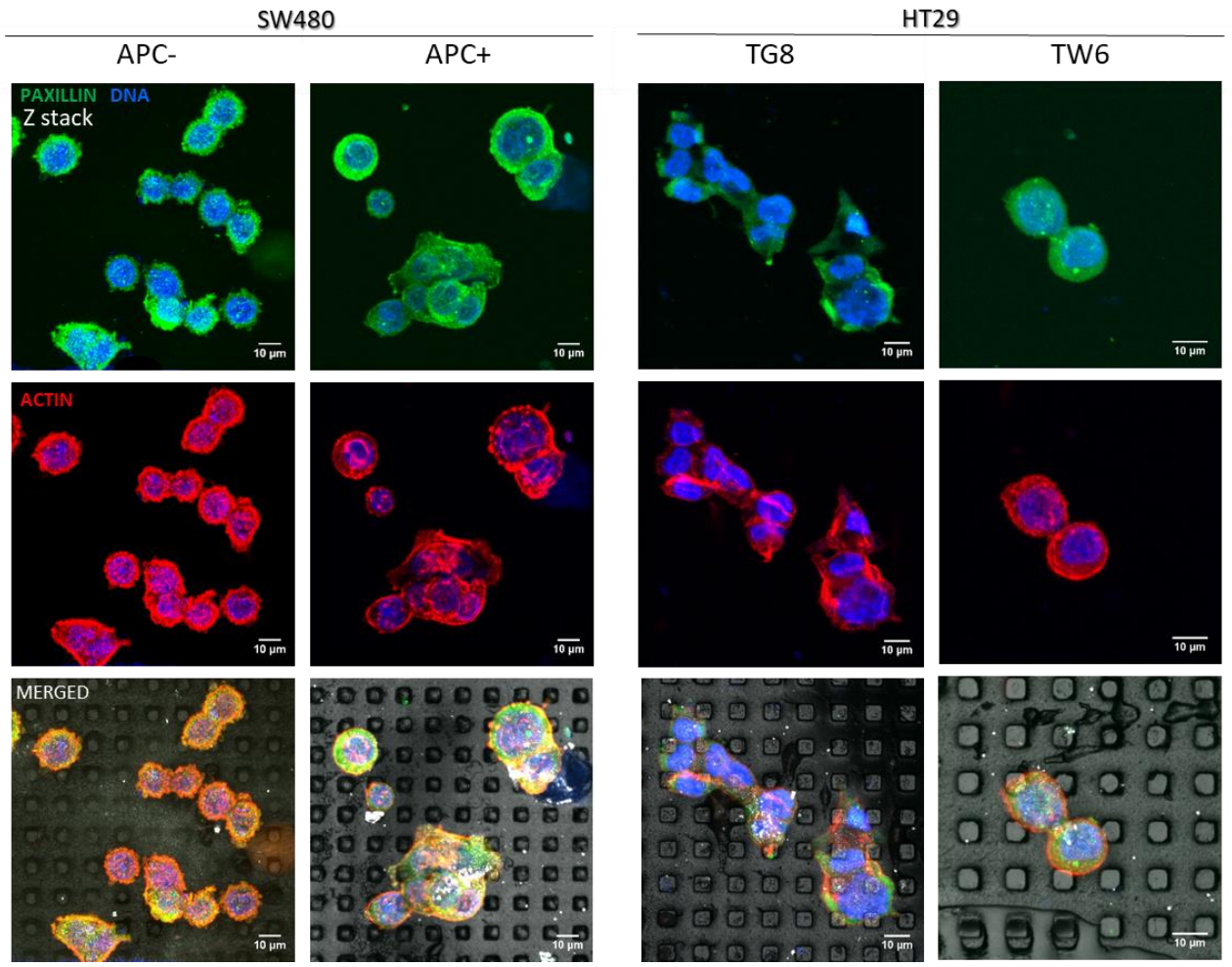

Figure 4.9: *Images of APC mutant and cdx2 inducible expressing CRCs and their control cells immunostained for actin (red), Paxillin (green) and nucleus (blue) on 7µm micropillars. Immunostaining done after 24 hours of seeding 1x10^5 cells in 35mm culture dishes.*

TW6 showed more e-cadherin at cell-cell junction. Moreover, the cell and nucleus looked deformed in APC+ compared to APC- cells. The cells looked more like a '+' showing deformation on pillar topography. Hence the next we checked the nuclear deformation percentage in these cells.

4.10.5 Nuclear deformation in 5 initial CRC cells on micropillars

Next we wanted to observe the effect of topography on nuclear morphology. Hence, we calculated the nuclear deformation in these cells. We calculated separately the nuclear deformation of cells in the 5 CRC cell lines (HT29, SW480, TC7, DLD1 and HCT116) (*fig 4.12*).

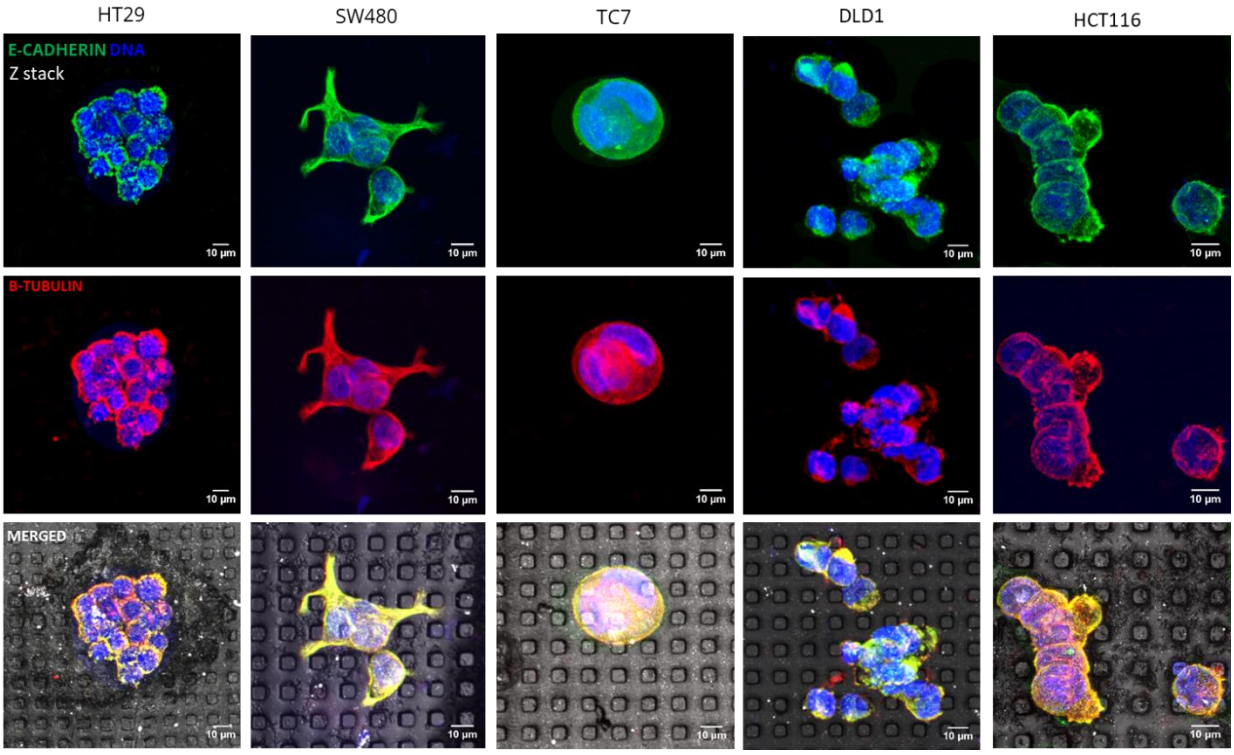

Figure 4.10: *Images of CRC cells immunostained for β-tubulin (red), e-cadherin (green) and nucleus (blue) on 7µm micropillars. Immunostaining done after 24 hours of seeding 1x10^5 cells in 35mm culture dishes.*

We differentiated the colony and separate nuclei in same cultures after 24 hours. Some cell tend to group together and form a colony with multilayers whereas other adhere in a group of single layer of cells or in groups of 2-5 nuclei. We observed that nuclei in colony showed deformation only in layer touching the micropillar substrates, whereas nuclei above this layer showed no deformation. In colony nucleus deformation percentage was seen very less compared to osteosarcoma which showed ~80% of nuclear deformation. However, HT29 and SW480 showed least deformation in colony nuclear deformation whereas TC7, DLD1 and HCT116 showed the most colony nuclear deformation. Separate nuclear deformation showed a completely different behaviour than nuclei in colony. Nuclear deformation was the most in SW480, DLD1 and HCT116 whereas HT29 and TC7 showed least nuclear deformation.

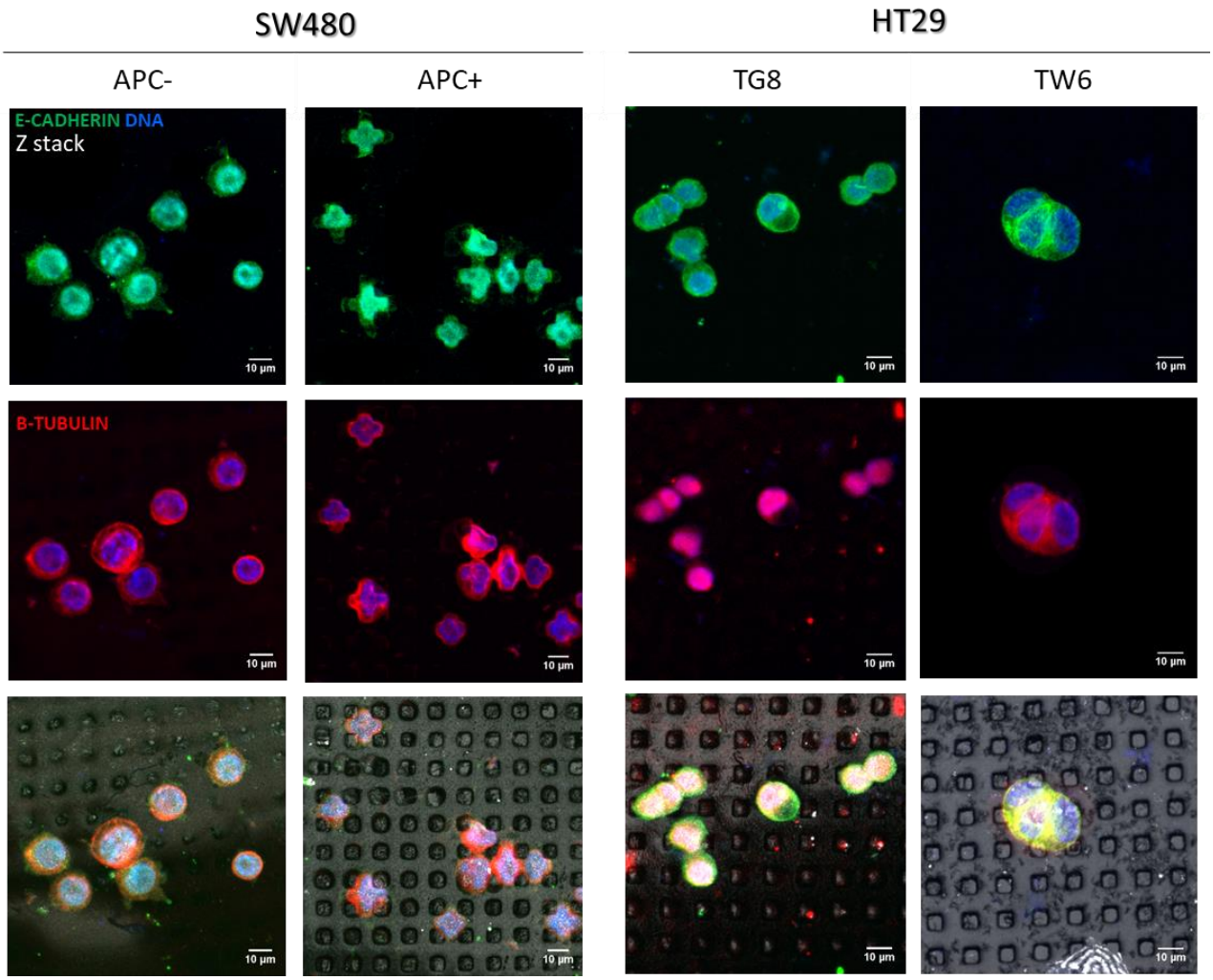

Figure 4.11: *Images of APC mutant and cdx2 inducible expressing CRCs and their control cells immunostained for β-tubulin (red), e-cadherin (green) and nucleus (blue) on 7µm micropillars. Immunostaining done after 24 hours of seeding 1x10^5 cells in 35mm culture dishes.*

Altogether these results showed that separate nuclei show more deformation than in colony. This could be due to the cell-cell contact in colony that protects the nuclei in between the colony from morphological changes. Separate cells have no cell to cell contact so they are easily deformable. Moreover, there was no correlation between the stage of cancer and deformation of nuclei. These results showed that CRC cell lines are less responsive to micropillar topography probably due to their architecture of cell-cell contact.

4.10.6 Nuclear deformation in APC-/+ and TG8/TW6 CRC cells on micropillars

These cell line did not show much cell to cell contact so we did not calculate the nuclear

deformation separately *(fig 4.13)*. We saw that APC- showed less deformation than APC+. Moreover, the parental SW480 (initial) cell line showed most deformation compared to the mutant. This could be attributed to the different cloning of the cell during mutant cell line selection. On the other hand, parental HT29, TG8 and TW6 with inducible expression of cdx2 showed no significant difference in nuclear deformation. Altogether this data showed that these transformed cell lines too are not responsive to micropillar topography.

4.10.7 Lamin A/C distribution in APC-/+ and TG8/TW6 cell lines on micropillars

We were not able to perform mRNA analysis of different nucleoskeletal genes in these cell lines. We performed immunofluorescence of lamin A/C in these cell lines. As described in section 4.9.2 lamin are known to play an important role in deregulation of CRCs.

Lamin A/C in APC- showed uniform distribution whereas APC+ showed high and low levels of lamin A/C in the cell population. Interestingly, deformed cells showed less lamin A/C compared to undeformed cells. TG8 and TW6 on the other hand showed mostly low levels of lamin A/C.

As we saw difference in levels of lamin A/C in APC+ cells, we investigated the nuclear deformation of the cells with low and high expression of lamin A/C. Lamins are known to impart stiffness to the cells[342]. We found that high lamin A/C expressing cell showed significant lower deformation than low lamin A/C cells. APC- cells showed lower deformation than APC+, both with high and low ratios of lamin A/C. Moreover, cancerous cells are known to have a softer nucleus[356]. This softness due to lamins might provide the flexibility to cancerous cells in becoming invasive and in metastatic migrations.

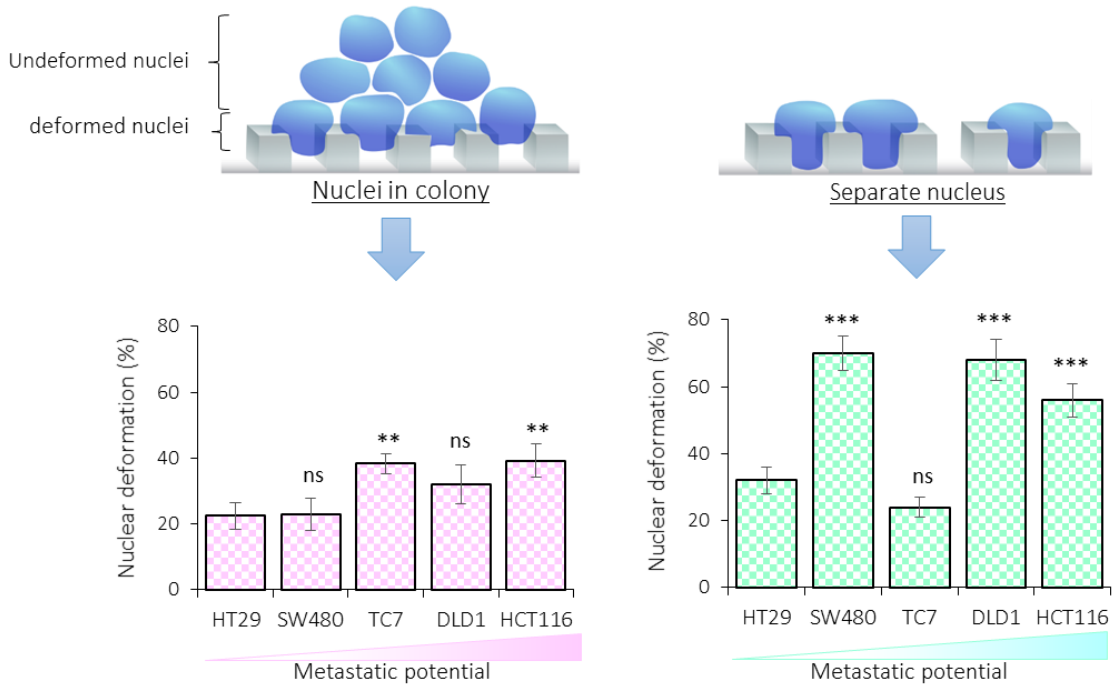

Figure 4.12: *Graphs showing nuclear deformation of CRC cells in colony and separately. n=30 nuclei. The error bars represent s.e.m values. HT29 is used as reference. Significance levels were determined with unpaired Student's t test using online GraphPad software; ***p<0.001, **p<0.01, *p≤ 0.05 and ns=not significant.*

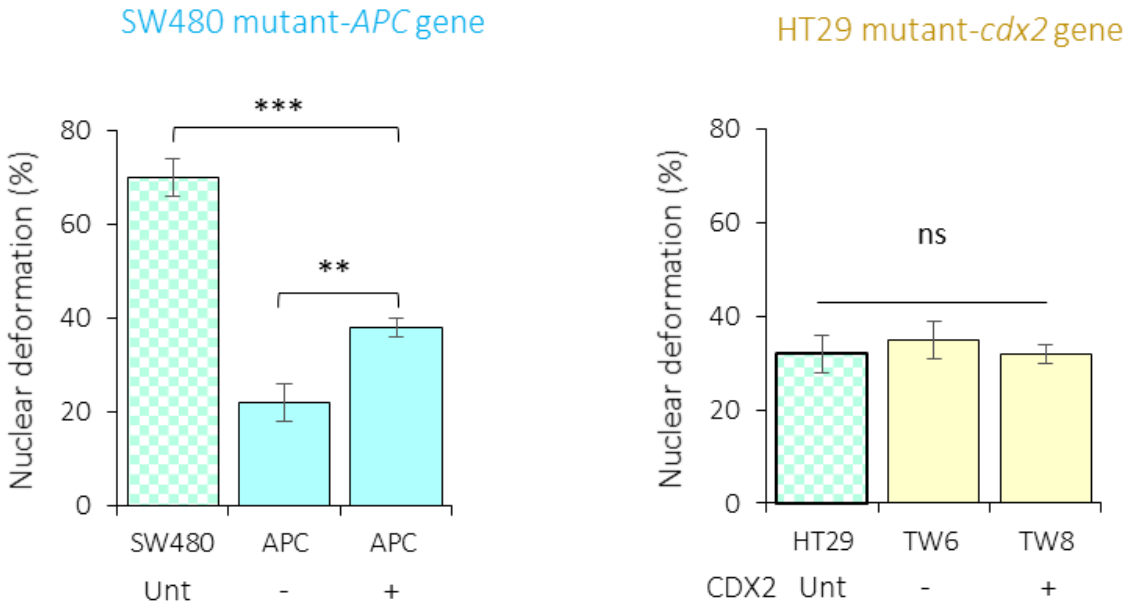

Figure 4.13: *Graphs showing nuclear deformation of APC mutant and cdx2 inducible expressing CRC cells. n=20 nuclei. Error bar represents s.e.m. Significance levels were determined with unpaired Student's t test using online GraphPad software; ***p<0.001, **p<0.01, *p≤ 0.05 and ns=not significant.*

4.10.8 CRC cells on groove topography

As the objective of this chapter was to observe the response of CRC cells on different topographies. Next we checked the behaviour of CRCs on grooves. As described earlier (section 4.6) epithelial cell behaviour is studied generally on groove topography. However, the knowledge of behaviour of CRCs on grooves still remains elusive. Hence we investigated the behaviour of TC7 (model cell line) with transformed cell lines (APC+/- and TG8 and TW6) on grooves with 40 µm of width and 8 µm of depth *(fig 4.15)*. For these experiments we cultured the cells for 72 hours to form monolayer. The topography contained grooves and the boundary outside groove was flat *(fig 4.15)*. Hence we compared the results to flat and groove on the same surface (some sample did not have colonies on the flat part).

TC7 was observed only on grooves as we could not find colonies on flat part of the substrate *(fig 4.16 a-d)*. The cells grew into a multilayer colony (initial cell seeding density was high $1X10^6$/ml in 60mm dishes). The layer touching the grooves was seen following the groove topography. Actin was organised more strongly on apical region. E-cadherin showed diffused organization. Interestingly the multilayer in 3D could be observed in globular organoid like structures *(fig 4.16 d-white arrows)*. Actin in these globular structure was seen more strongly at the periphery of the globules. More e-cadherin was observed in the cell in globule than flat monolayer *(fig 4.16 d-yellow arrows)*.

APC- (CNT) cells showed organised behaviour on grooves topography *(fig 4.17 a-c)*. The cell monolayer on flat showed apical actin organization and diffused e-cadherin *(fig 4.17 a)*. The cells in the depth of the grooves showed elongation and orientation along the grooved substrate. Actin was seen organised on apical regions. E-cadherin was diffused but was more on grooves

compared to flat surface *(fig 4.17 b)*. The 3D top view however showed no strong alignment of the cell layers. APC+ (wild type APC restored) was observed on flat and groove substrates *(fig 4.18 a-c)*. Cells on flat surface showed apical actin organization and diffused e-cadherin *(fig 4.18 a)*. Cell in the depth of grooves were organised along the topography *(fig 4.18 b)*.

TG8 with inducible expression of cdx2 gene showed very few cells (there was a lot of cell death during culture) *(fig 4.19 a-c)*. Cells on flat surface showed more apical actin *(fig 4.19 a)*. Cells however showed no specific orientation to the grooves and showed no special distribution of e-cadherin *(fig 4.19 b)*. Cells were organised into globular colonies with more actin at the periphery of the colonies when observed from 3D top view *(fig 4.19 c)*.

TW6 was observed only on grooved surface, as no cells were found on flat surface *(fig 4.20 a & b)*. The cells were seen in small colonies (lower cell density) mostly aligned in depth of the groove. Actin was seen mostly on colonies growing in the depth of the grooves. E-cadherin was seen diffused.

Altogether, these results showed that the groove topography did not affect the behaviour of the epithelial origin colon cancer cells strongly. This could be due to the dimensions of the grooves topography or the cancerous nature of the cells. However, thus we decided to use a topography more like native environment of the intestinal cells.

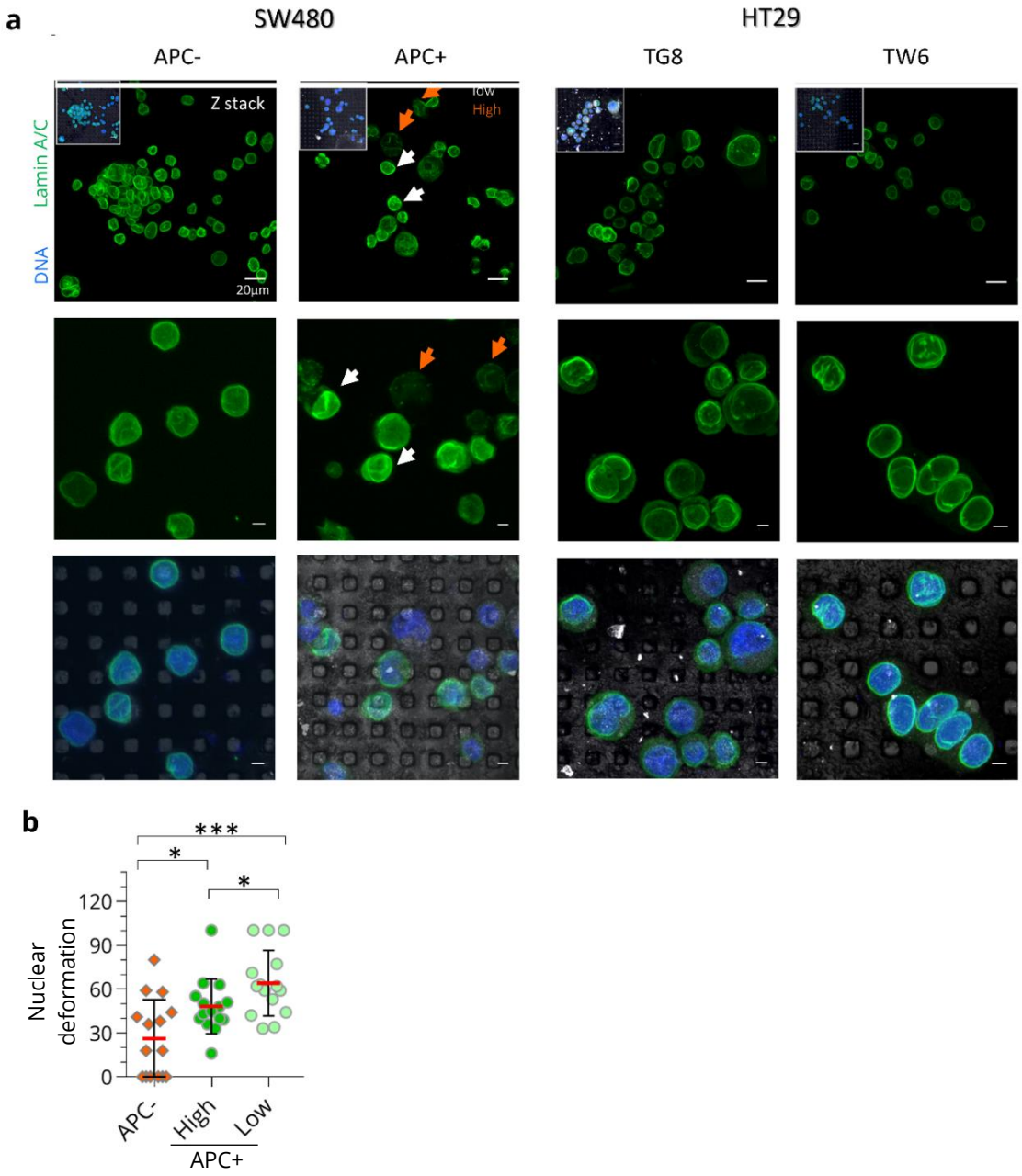

Figure 4.14: *Lamin A/C distribution in APC-/+ and TG8/TW6 CRC cells.* ***a*** *Confocal images showing lamin A/C in transformed cell lines on micropillars. White arrows in APC+ show low lamin A/C levels and orange arrows show high lamin A/C levels.* ***b*** *nuclear deformation in APC- , low (lamin A/C) APC+ and high (lamin A/C) APC+ wild type restored cells. n=15 nuclei. The error bars represent s.d values. Significance levels were determined with unpaired Student's t test using online GraphPad software and for multiple comparisons ANOVA test was followed by Dunnet's test ; ***p<0.001, **p<0.01, *p≤ 0.05 and ns=not*

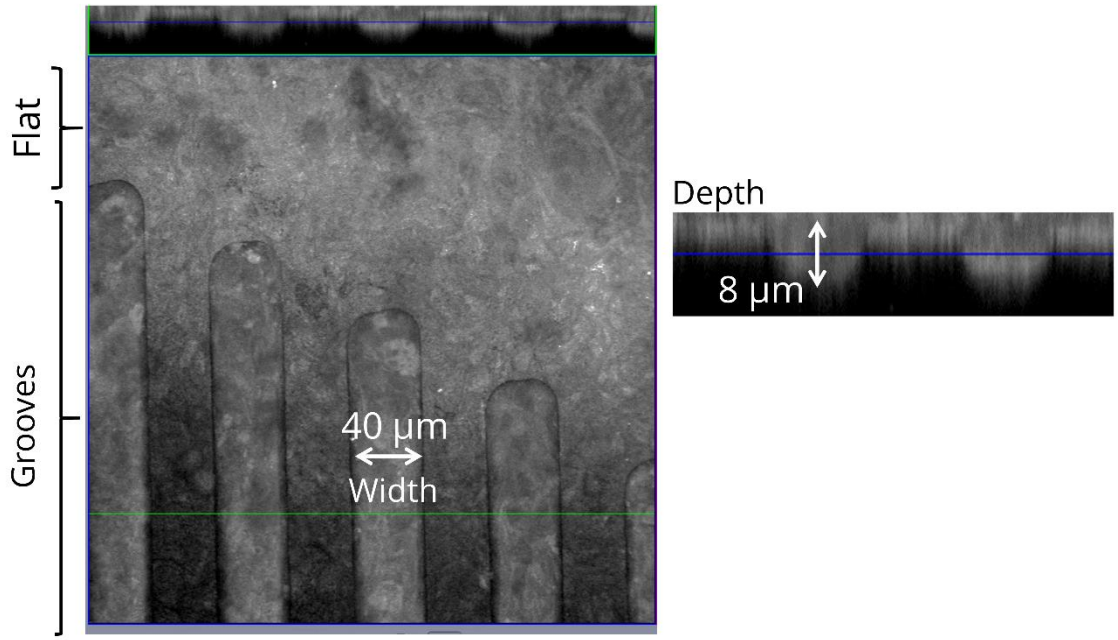

Figure 4.15: *Images of grooves topography (width 40µm and height 8 µm). The cells were compared on flat and grooves on the same substrate.*

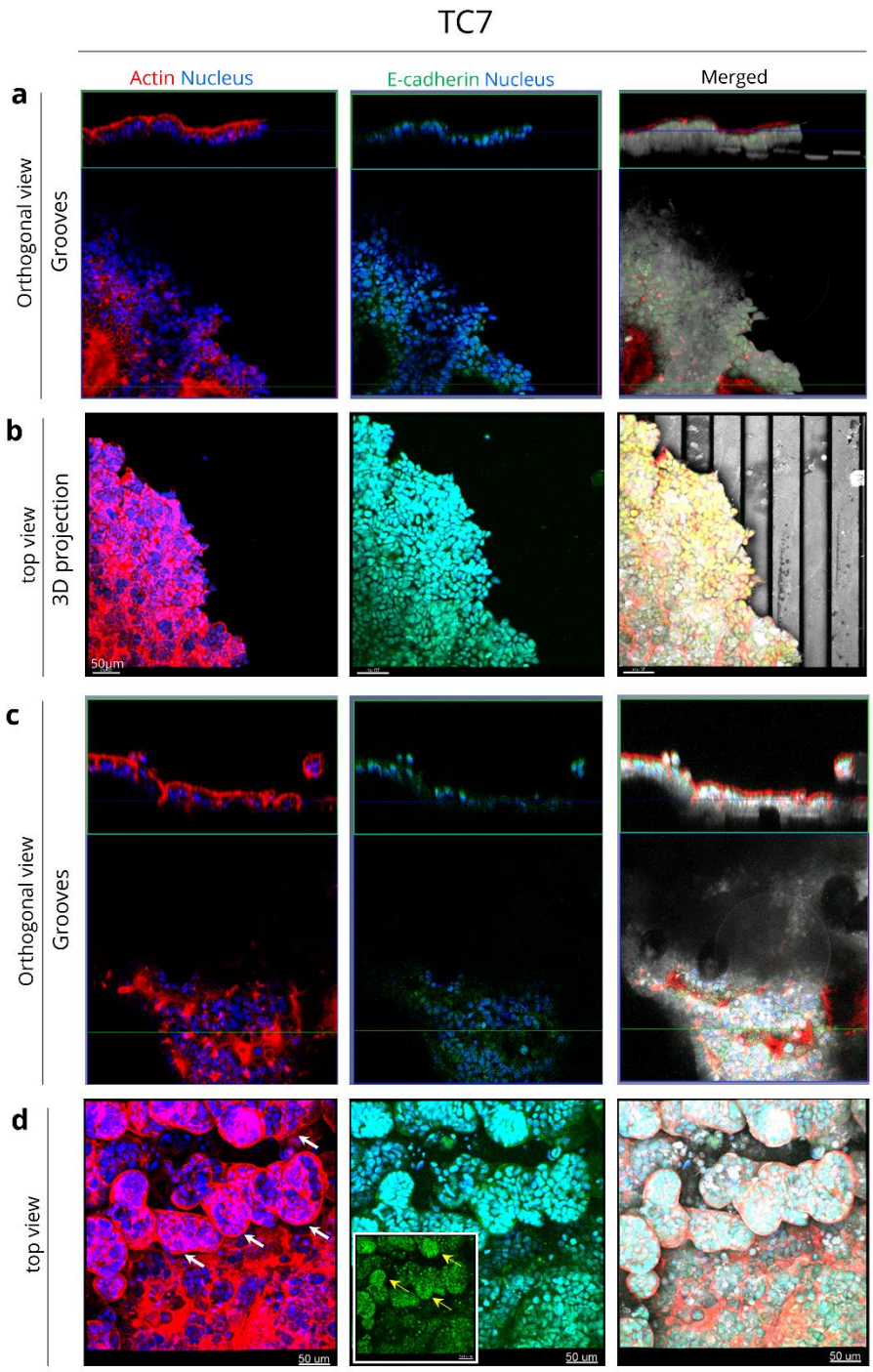

Figure 4.16: *Confocal images of TC7 on grooves after 72 hours.* ***a*** *orthogonal view of actin, e-cadherin and merged images.* ***b*** *3D projection –top view of TC7 on grooves.* ***c*** *Orthogonal view of colony on grooves.* ***d*** *3D z stack projection- top view of cells on grooves. White arrows represent globular colonies. The left down corner small box image shows just e-cadherin without the nucleus and yellow arrows shows globular colonies showing more e-cadherin than flat colonies.*

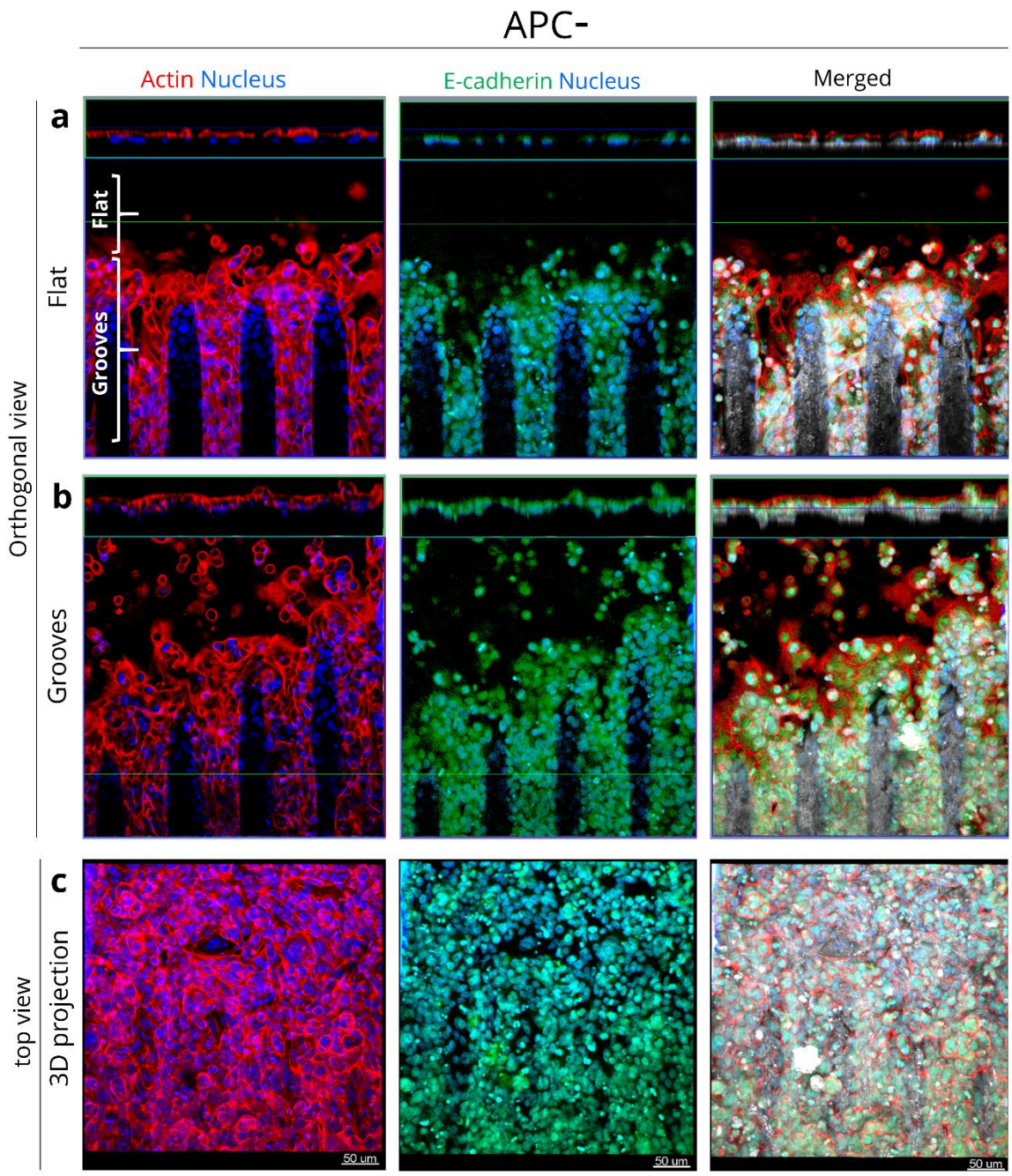

Figure 4.17: *Confocal images of APC- on grooves after 72 hours.* ***a*** *Orthogonal view of actin, e-cadherin and merged images on flat.* ***b*** *Actin, e-cadherin and merged on grooves.* ***c*** *3D projection –top view of APC- on grooves.*

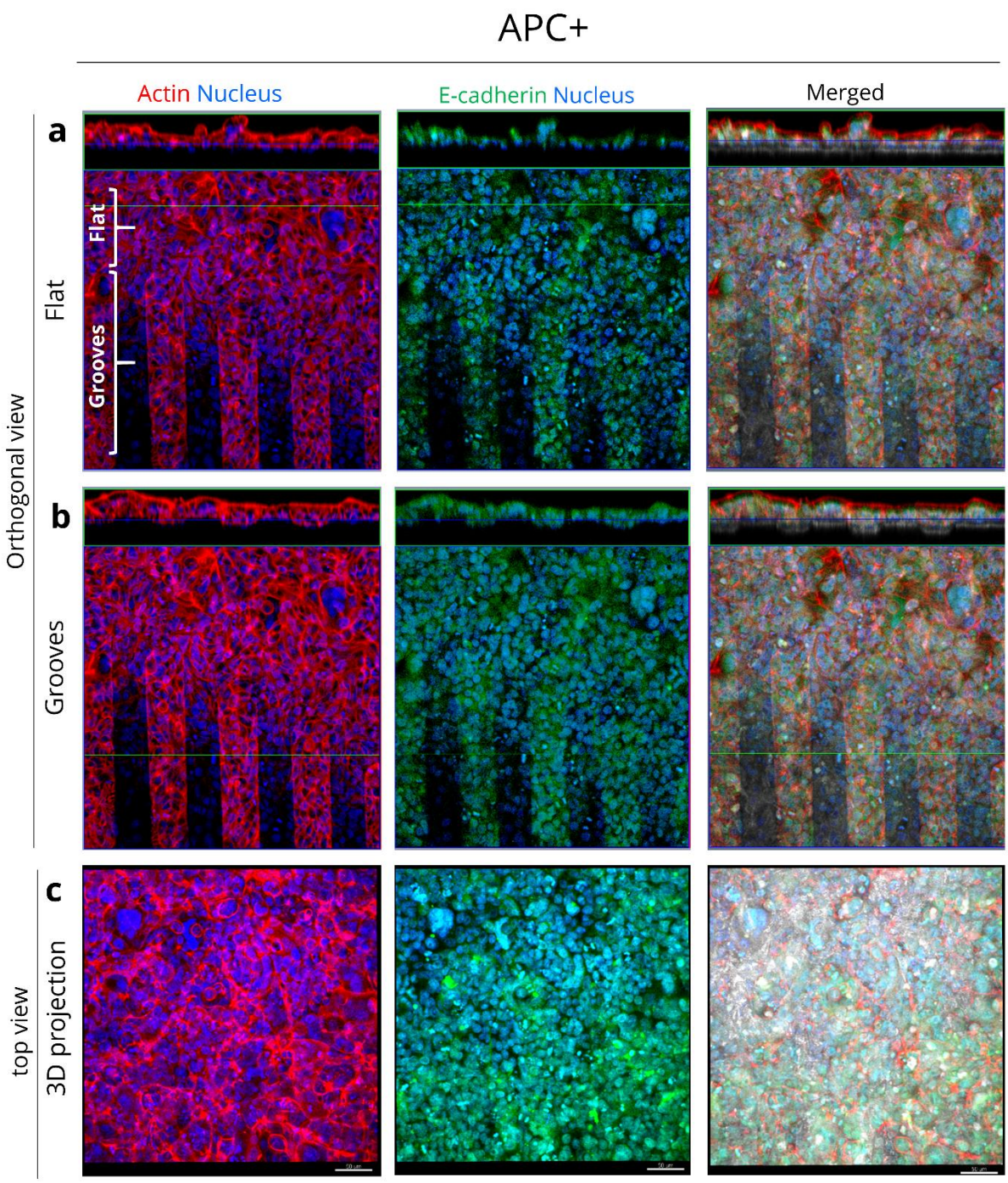

Figure 4.18: *Confocal images of APC+ on grooves after 72 hours.* ***a*** *Orthogonal view of actin, e-cadherin and merged images on flat.* ***b*** *Actin, e-cadherin and merged on grooves.* ***c*** *3D projection –top view of APC+ on grooves.*

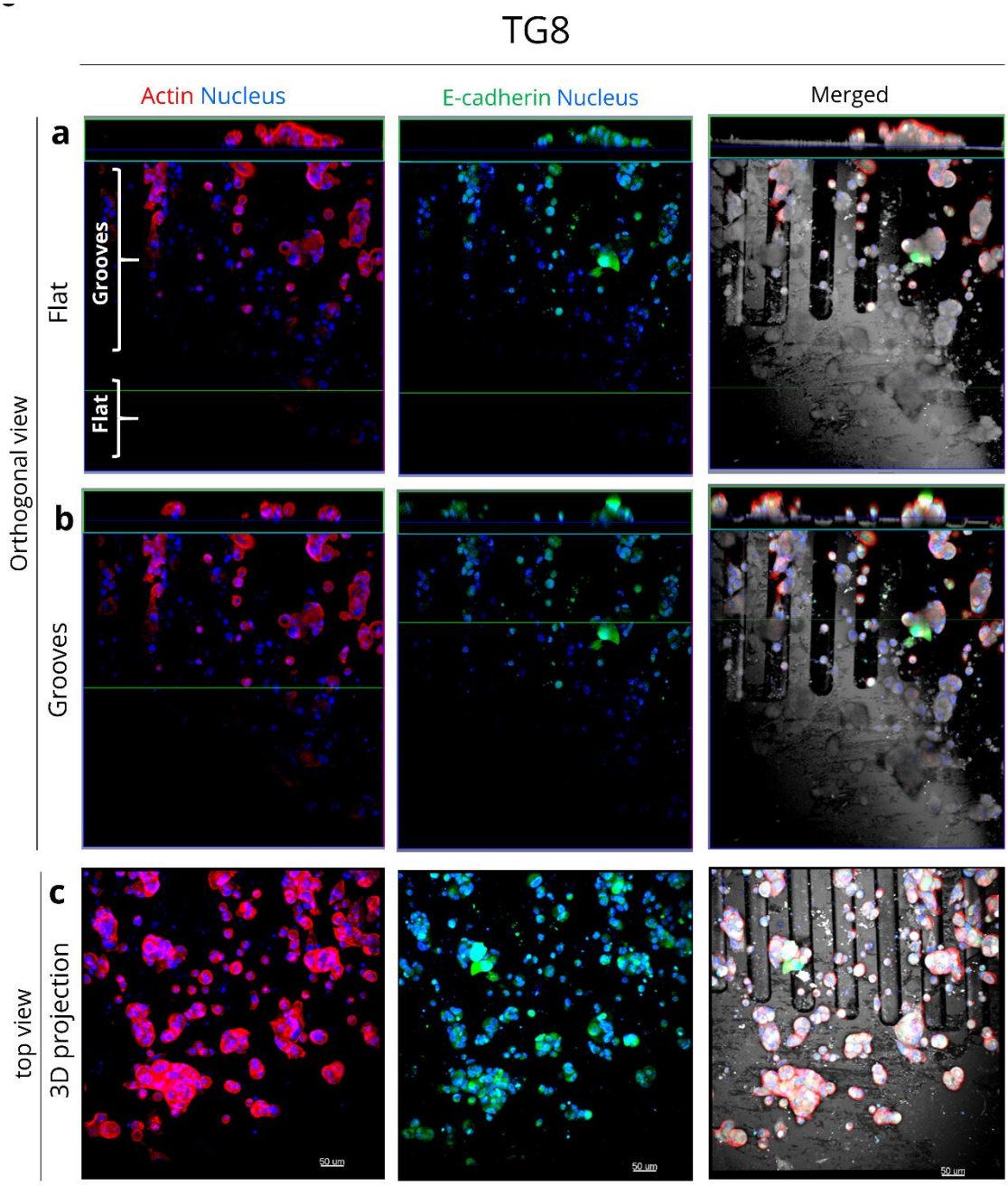

Figure 4.19: *Confocal images of TG8 on grooves after 72 hours.* ***a*** *Orthogonal view of actin, e-cadherin and merged images on flat.* ***b*** *Actin, e-cadherin and merged on grooves.* ***c*** *3D projection –top view of TG8 on grooves.*

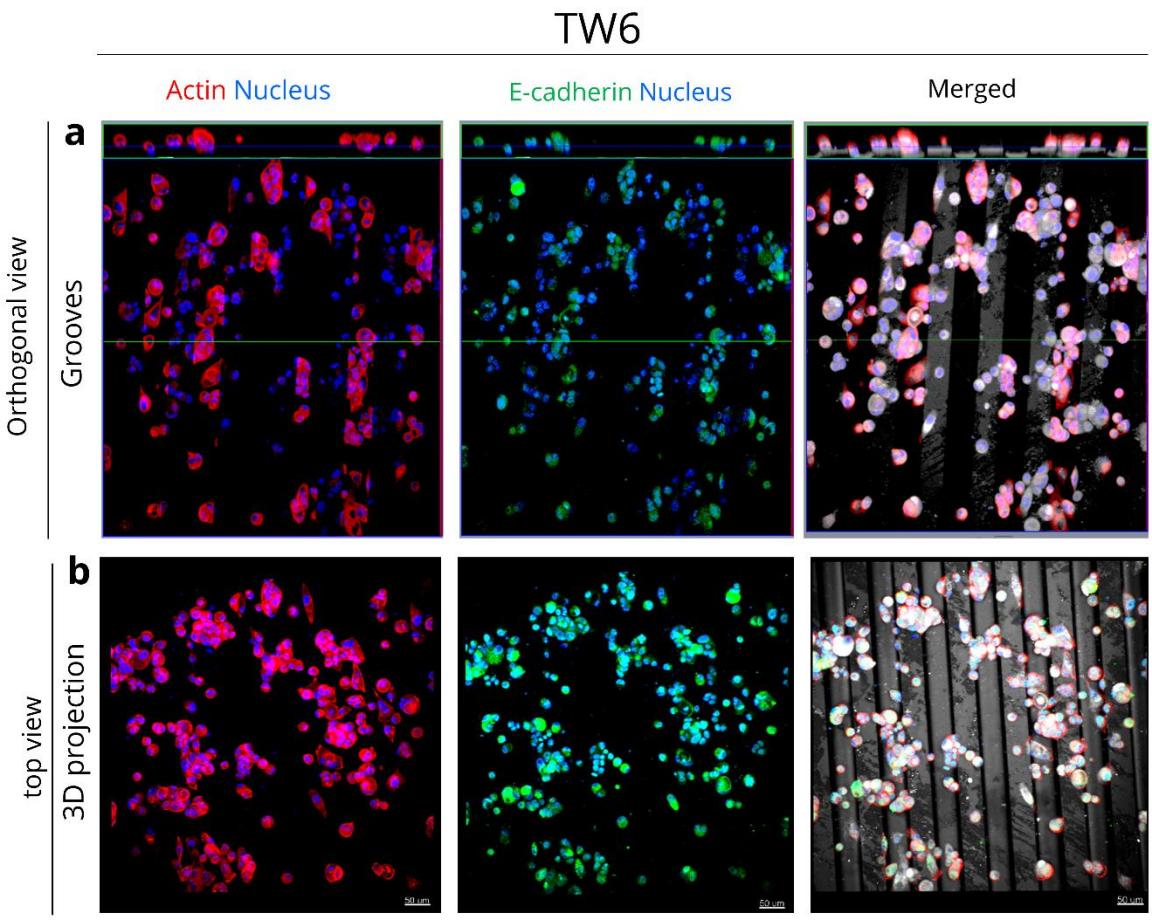

Figure 4.20: *Confocal images of TW6 on grooves after 72 hours.* ***a*** *Actin, e-cadherin and merged on grooves.* ***b*** *3D projection –top view of TW6 on grooves.*

4.10.9 CRC cells on wells/pits topography

We next wanted to observe the effect of well topography on CRC cells. The other objective here was that well represent more closely the crypts and villi of intestine which a native topography of these cells. Hence, we wanted to observe the CRC cells behaviour on such native intestinal biomimetic topography. We started the experiments with TC7, as it is a frequently used model cell line and to evaluate if there is any change in behaviour of these cells before proceeding to other cell lines. We used wells with two different dimensions- 50X50X30µm and 150X150X60µm (lXwxh). Interestingly, we saw that TC7 changed their behaviour on the well/pits topography *(fig 4.21)*. On

50X50X30 wells the TC7 monolayer did not completely descend down in the pits. The layers bended itself on the holes of wells. Actin on the other hand showed apical polarity and was seen as a dense layer over the top of the nuclei. E-cadherin showed no difference in terms of florescence on the well topography. 3D top view projection images showed a normal epithelial sheet with some shallow holes in monolayer *(fig 4.21-top 3D view white arrows)*.

On 150X150X60 wells TC7 completely descended down in the bottom of the wells *(fig 4.22. a)*. The top 3D view showed the cells lining the topography completely. The e-cadherin in the top 3D view was less compared to the top of the wells. Actin was seen completely around the nuclei covering the entire topography *(fig 4.22. b)*. It showed apical to basal polarity. E-cadherin on the other hand was seen more at the top of the wells and least in the bottom of the pits *(fig 4.22.c).*

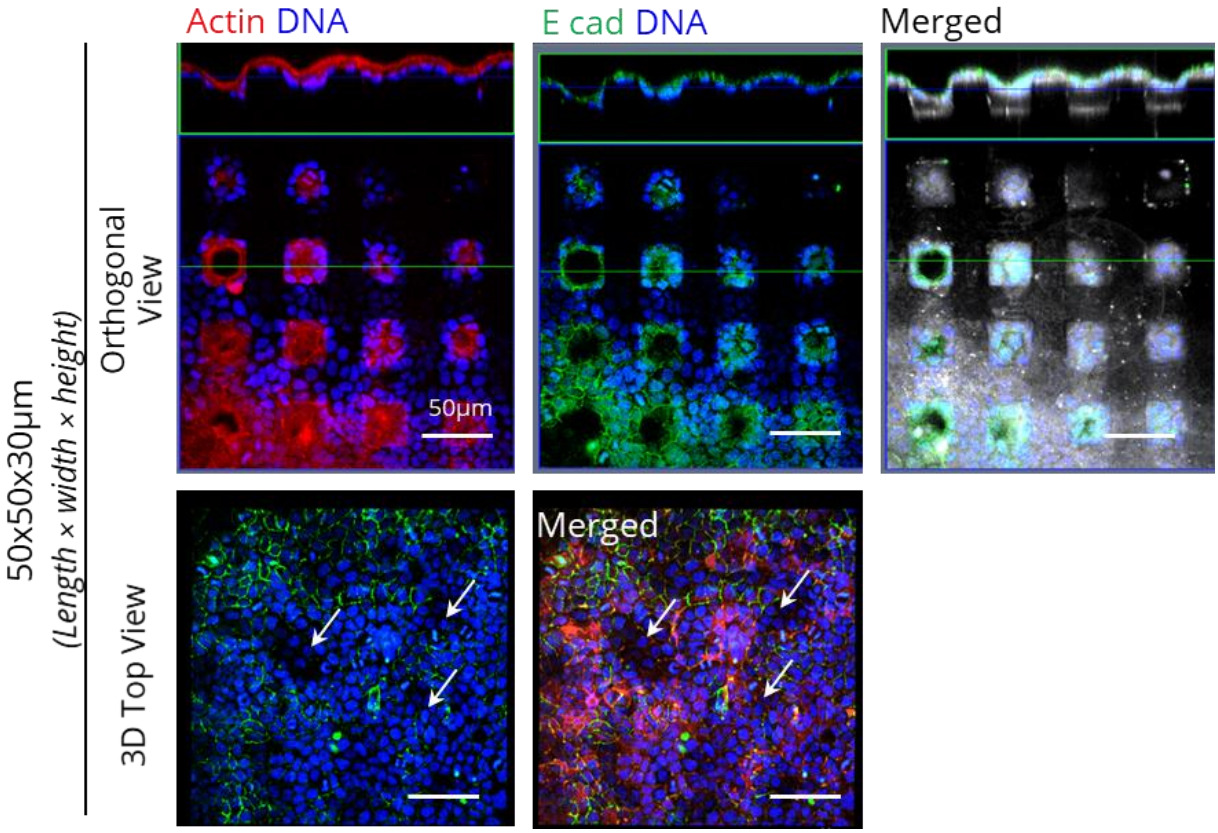

Figure 4.21*:: Images showing TC7 on 50X50X30µm (lxwxh) wells grown for 72hours to form monolayer. Images showing orthogonal and top view of actin and e-cadherin. White arrows show shallow depth in the monolayer observed from top.*

Topologically the intestinal epithelium is arranged in crypts (~120-170 µm in depth & 50 µm in diameter) and villi (~500-1200 µm in height & 100 µm in diameter)[357,358]. The wells of 150X150X60 represent dimensions, close to that of intestinal crypts and villi. This might the reason for the cells to recede completely down at the bottom of the wells. The 50x50x30 wells might be too small for the CRC cells to respond or descend completely down. Wang et al. cultured CaCO-2 cells on topography with pits and saw that cell behaviour was affected by the pit topography. This could also be the reason why CRC cells were not much responsive to the pillar topography with 7 µm dimensions. TC7 cells in the depth of well show less e-cadherin compared to the tops. Previous studies have found that there is switch in cellular pathways when cells move from 2D to 3D[359]. Kim et al. saw a similar effect on e-cadherin in epithelial cells on convex and concave structures[326]. Recently, Salomon et al. also observed a similar behaviour of e-cadherin at the basal part of crypt-villi topography[360].

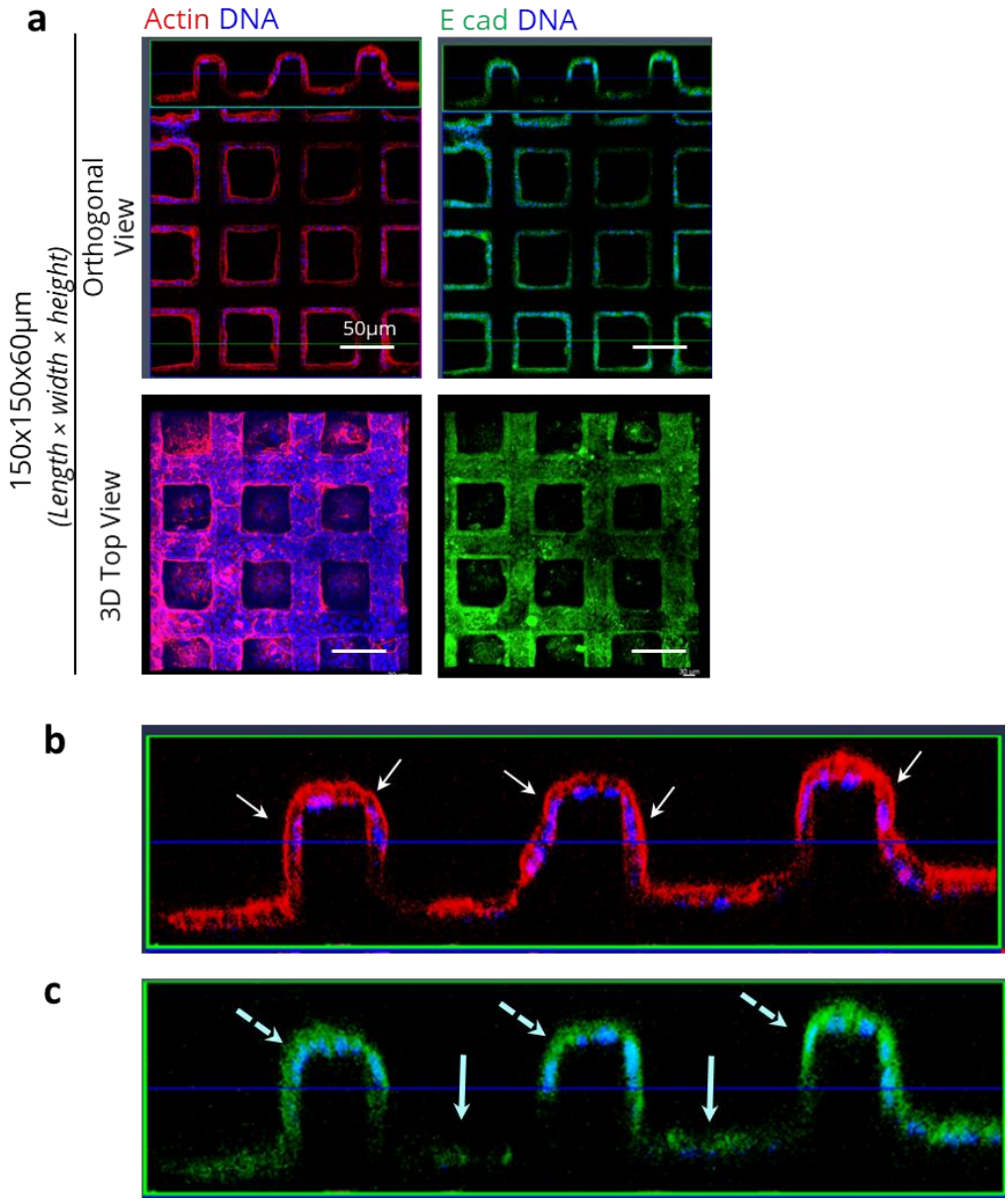

Figure 4.22: *Images showing TC7 on wells on 150X150X60µm (lxwxh) wells grown for 72hours to form monolayer.* ***a*** *Orthogonal and top view of TC7 cells on wells.* ***b*** *Orthogonal view of actin polarization on cells. Arrows show actin on apical region of cells.* ***c*** *Orthogonal view of e-cadherin in cells show low expression (arrow) in bottom of the well and more on the top part (dotted arrow).*

4.11 CONCLUSION

CRC cell lines from different stages of cancer and transformed cell lines with wild type APC restored and inducible cdx2 expression were established and characterised. mRNA expression levels of

different nucleoskeletal genes in HT29, SW480, TC7, DLD1 and HCT116 was done which showed different expression levels of lamin A/C, lamin B1, SUN1 and SUN2 genes compared to HT29 as reference. HCT116 showed highest expression of lamin B1 compared to all other cell lines and to lamin A/C expression. All the 5 initial CRC cells also showed more SUN1 expression than SUN 2. However healthy hMSC cells showed less SUN1 and more SUN2 expression. The behaviour of all cell lines was analysed on micropillars (7 μm height, width and space). Focal adhesion protein paxillin, cytoskeletal proteins actin and tubulin and cell-cell junction protein e-cadherin distribution was analysed in all cells on micropillar topography. Paxillin was seen mostly diffused in all CRC cells whereas actin showed strong localization near the cell periphery of cells on pillars. Only TC7 actin cytoskeleton showed organization around the pillars. Microtubule component tubulin showed more cell peripheral localization like e-cadherin on pillars. SW480 showed more organised tubulin compared to others on micropillars. Nuclear deformation was analysed on micropillars of nuclei in colony and separately. Nuclear deformation was less in in colony than separately. SW480, DLD1 and HCT116 showed most deformation with separate nuclei. APC+ cell and nucleus exhibited more deformed morphology compared to other cell lines. APC+ cells showed more deformation that the APC- cells whereas no significant difference in nuclear deformation was observed for TG8 and TW6 cells. We compared the levels of lamin A/C protein by immunofluorescence and found that APC mutants show high lamin expression and APC + shows a mixed population of high and low expressing lamin cells. TG8 and TW6 showed lower levels of lamin A/C than APC. Due to high low variance in lamin levels in APC we calculated the nuclear deformation separately of nuclei showing high and low lamin A/C levels. We found that high lamin A/C cells show significantly lower deformation than low lamin A/C. APC- cells showed lower deformation levels than APC- low and high lamin A/C level nuclei. With an aim to investigate the

behaviour of CRCs on different topographies we next evaluated the response of CRCs (TC7, APC-/+ and TG8/TW6) cells on groove topography (40 µm width and 8 µm depth). Mostly, all the cell lines did not show much response to the groove topography. The layer of cells touching the topography showed alignment to the grooves. However, on looking the 3D top (z stack projection) view cells showed no relevance to the grooves. Hence next we decided to observe the CRCs cells on topography which closely resembles the intestinal topography of crypt and villi. We first started with the model TC7 cell line to see if showed any significant response. TC7 cells, clone of CaCO-2 which are extensively used as model adenocarcinoma cell lines, showed altered behaviour to well/pits topography. TC7 in wells with dimensions 50x50x30 µm height, width and space, showed less response to topography compared to cells in 150x150x60 dimensions. In 150x150x60 wells the cells receded completely to the bottom. Actin polarization was observed and e-cadherin expression was seen more on the top of the wells compared to the bottom.

These pioneering experiments could be helpful in further investigation of the behaviour of different CRC cell lines on different topographic substrate.

RÉSUMÉ DU CHAPITRE 5 - PERSPECTIVES

L’interaction cellule-surface est un facteur déterminant dans le processus de signalisation cellulaire. L'objectif de cette thèse était de comprendre les réponses de différents types cellulaires et les mécanismes associés vis-à-vis de topographies variées comme des micro-piliers (PLLA et hydrogels de rigidité variable), des rainures et des puits.

Ces résultats ont permis de mettre en évidence que 1) Les cellules utilisent principalement des forces de traction plutôt que de poussée pour adhérer et se déformer entre des micro-piliers confinés. Ces forces sont médiées par des interactions entre les adhésions focales, l'acto-myosine, les filaments intermédiaires de vimentine et le complexe LINC. 2) Les cellules modulent leur réponse sur des substrats hydrogel de propriétés topographiques, mécaniques et chimiques différentes. 3) Les cellules de carcinomes colorectal d'origine épithéliale répondent mal aux topographies micrométriques à petite échelle telles que les micro-piliers et les rainures, mais répondent très fortement à des topographies type puits de dimensions similaires aux cryptes et villosités intestinales.

Dans notre étude sur les cellules d’ostéosarcome, nous avons constaté que l'acto-myosine tire le noyau vers le bas entre les piliers grâce à la mécano-transduction médiée par les adhésions focales. Nous avons également vu que les filaments intermédiaires comme la vimentine sont impliqués dans la déformation du noyau en confinement. Cependant, les mécanismes d’action exacts des filaments de vimentine restent encore mal compris. Nous avons également mis en évidence le rôle des composants du complexe LINC et de la protéine nucléaire lamine A. Cependant, d'autres lamines ou protéines nucléosquelettiques pourraient aussi jouer un rôle dans la mécanique nucléaire et elles doivent encore être étudiées.

Dans notre article, nous avons montré que la déformation du noyau est accompagnée par des modifications dynamiques de la chromatine. Néanmoins, il existe dans le noyau des territoires chromosomiques dont la position est définie. Les déformations nucléaires pourraient donc avoir un impact sur le repositionnement de ces territoires, entraînant des modifications de la transcription des protéines. Par conséquent, de futures expériences devraient étudier (1) le rôle des filaments de vimentine ou de protéines nucléaires autres que la lamine A, (2) la position des chromosomes pendant la déformation, (3) l'analyse transcriptomique des gènes régulés négativement et positivement pendant la déformation. Une autre chose intéressante pourrait être d'observer la cinétique de migration des cellules entre les micro-piliers. Nous pourrions également modifier les dimensions des micro-piliers pour voir comment les cellules migrent ou rompent leur enveloppe nucléaire pendant la déformation.

En ce qui concerne les hydrogels à chimie, topographie et rigidité contrôlée, nous avons pu voir comment les cellules d'ostéosarcome se comportaient en présence de ces trois paramètres. Généralement, les études contrôlent individuellement les paramètres topographiques, chimiques ou mécaniques, ce qui est très différent de l'environnement *in vivo* réel. De plus, la conception de biomatériaux de prochaine génération nécessitera une meilleure compréhension de la manière dont ces propriétés du substrat affectent ensembles le comportement des cellules. Nos systèmes d'hydrogel 3D contrôlables offrent un degré de flexibilité très similaire aux tissus naturels et peuvent être facilement modulés pour obtenir les propriétés mécaniques, topographiques et chimiques souhaitées. Ainsi, les voies de signalisation généralement étudiées sur des substrats de mécaniques variées pourraient être étudiées pour voir s'il y a un changement lorsque la cellule interagit avec un substrat mécaniquement et topographiquement contrôlables.

Nous avons effectué des expériences préliminaires avec des cellules de carcinome colorectal (CRC) présentant différents degrés de cancérisation et des mutations dans les gènes APC et cdx2 sur différentes topographies et analysé les différents niveaux d'expression d'ARNm. Ces niveaux d'ARNm devront être corrélés à l'analyse par Western blot et par immunofluorescence de ces protéines sur la topographie puits. En effet, la topographie puits semble montrer la plus grande réponse cellulaire pour les cellules CRC. Ainsi, les expériences futures pourraient impliquer des modifications de dimensions des puits et également fabriquer des structures imitant les cryptes et les villosités observées in vivo afin étudier le comportement des cellules de CRC. De futures expériences pourraient également concerner le rôle de différentes protéines de jonction cellulaire telles que la β-caténine, l'e-cadhérine, etc. sur la réponse à la topographie en les perturbant individuellement à l'aide de drogues ou de techniques d’extinction de gènes. Enfin, la mécanique des puits pourrait être mieux ajustée à celle des tissus intestinaux, ce qui nous permettrait de comprendre le comportement des cellules de CRC dans un environnement physiologique pertinent.

CHAPTER 5. PERSPECTIVES

Topography has become an integral part of the biomaterials design and various tissue engineering applications. The interface between the substrate and the cell is crucial determinant in the process of cell signalling. The aim of this thesis was to understand the different cell responses to various topographies and to comprehend the mechanisms involving the same. We fabricated topographies such as micropillars, grooves and wells to understand the responses of cancer cell types such as osteosarcomas and different grades and mutants of colon carcinomas. We also accomplished to tune rigidity, topography and chemistry on a single substrate using hydrogels and investigate the combined effect of these factors on osteosarcoma cells.

The research highlights of this thesis are:

- Cells use predominantly pulling forces than pushing, to adhere and deform on confined topographical micropillars (7 μm of height, width, space).
- The pulling of the nucleus in confinement is mediated by interactions between focal adhesions, actomyosin, intermediate filaments (vimentin) and LINC complex.
- Hydrogels can be modulated with different mechanics, topography and chemistry coatings.
- Cells modulate their response taking in account the different cues provided by hydrogel substrates with different topography, mechanics and chemistry. Cell spreading, actin and focal adhesion organization and nuclear deformation of cells is affected by the tuned mechanical, topographical and chemical properties.
- Intestinal epithelial origin colorectal carcinoma cells respond poorly to small-scale micron topographies such as micropillars (7 μm of height, width, space) and grooves (40 μm of width and 8 μm of depth), but respond very strongly to well topography mimicking dimensions (150

μm width and 60 μm depth) of intestinal crypt and villi.

- Lamin A to B ratios scale with the cell type stiffness, which is higher for hMSC and SaOS-2 being the stiff cell types and lower in colorectal cancers being the soft cell types.

5.1 Osteosarcoma cell response to topography

Cell-surface crosstalk is an intricate phenomenon and involved a myriad of cell signalling processes, most of which are still remain to be elucidated. To better understand what could be done in future, the perspectives are described below with respect to concerned topic.

- ***Role of cytoskeleton-Intermediate filaments***

We saw that the actomyosin and intermediate filament vimentin (VIF) play an important part in cell-nucleus deformation on micropillars, whereas microtubules played an insignificant role. Actomyosin role in cell mechanics is extensively studied over the past few decades. However the role of VIFs in cellular mechanotransduction still remains poorly understood. Recently, Keeling et al. showed that vimentin regulates nuclear shape and mechanics and also partakes in chromatin organization[361]. IFs have smaller persistence length (measure of the flexibility) than actin and microtubules making them the most flexible and elastic polymers compared to former two[362–364]. Thus IFs play various roles in cell mechanics such as strengthening of IFs during strain highlights their role as load bearing springs[362]. Also, VIFs are known to have a protective role against compressive stress in fibroblasts[365]. Our results showed that VIFs cages the nucleus, and is arranged at the perinuclear space. Cell organelles including nucleus are known to be stabilised by VIFs, thereby preventing loss of mechanical integrity of cell and its organelles[366]. This role of IFs could suggest that depletion of IFs could lead to destabilization of nuclear shape and thus increase nuclear deformation. Furthermore, IFs are connected to the cytoskeleton via LINC complex protein

nesprin 3[111]. Overexpression of dominant negative nesprin is known to alter the organization of perinuclear IFs[127]. The cell surface receptors such as α/β-integrins, play an important role in mechanosensing of the surface, by relaying signals via FAs to cell cytoskeleton[41]. IFs are linked to β-integrins[86] and not only show dependence on FAs for recruitment sites but also promote formation, maturation and adhesive strength of FAs[87,367]. These findings on IFs, advocate their role more strongly in mechanotransduction and consequently nuclear deformation in response to confinement. However, the exact mechanisms by which the IFs help the nucleus during a confinement still remains to be elucidated. Thus future experiments could revolve more around dissection the mechanotransduction pathway involving IFs.

- ***Role of nucleoskeleton and related proteins***

Herein, we dissected the role of LINC components and nuclear protein lamin A. Discher and colleagues elucidated the role of lamin A as a "mechanostat" responsible of nuclear behaviour[342]. They also showed that lamin A levels increased with the tissue stiffness. However, we did not see any change in nuclear deformation on micropillars with increase or decrease of lamin A. Also, Lamin B1 is required for nuclear integrity and its loss causes severe nuclear blebs in fibroblasts[368]. Moreover, some cells have little or no lamin A/C and in some cell types lamin A/C is not essential[120,369]. Furthermore, lamin A/C depletion only accounts for ~50% decrease in nuclear stiffness[121]. This means that other lamins or nucleoskeletal proteins might play a role in nuclear mechanics which still needs to be un-ravelled. Future experiments could involve dissecting the role of different lamins in cancer nuclear deformation process. However, there are other types of nuclear proteins known to guide cell mechanics. Lamin binding proteins such as LBR, emerin, LAP2α and MAN1 interact with many other proteins to bring about nuclear restructuring in

response to biochemical or biophysical factors[370,371]. Another nuclear binding protein, emerin is responsible for interaction with nesprins and actin. This might suggest its role in nuclear architecture maintenance. In future, exploring the role of such proteins in nucleus deformation could be useful to understand the molecular players involved in preserving nucleus integrity during metastatic deformation events.

- ***Chromatin dynamics***

In our paper we showed that nucleus deformation is accompanied by chromatin dynamics. Chromatin is known to exhibit viscoelastic properties and accompany or drive nuclear reshaping by modulating stiffness[372,373]. Moreover, untethering of chromatin to nuclear membrane leads to high nuclear deformability[155]. Haase et al. showed that nuclear deformation sensitivity to extracellular forces is affected by chromatin organization[374]. Hence, looking at the chromatin dynamics during cancer nucleus deformation can give insight on the role of chromatin in nuclear mechanics. This could be done using fluorescent in situ hybridization (FISH) technique where fluorescent probes can be used to determine specific chromosomal position during or after nuclear deformation. Furthermore, exploring the gene expression changes by transcriptomic analysis over certain time periods, could help fish genes that are significantly involved in cancer deformation kinetics on micropillars.

- ***Signalling pathways***

We saw the role of cytoskeletal proteins whose modulation is brought about by cascades of signalling proteins. For example nuclear factor-κB (NF-κB), is known to translocate from cytoplasm to the nucleus upon mechanical stimulation leading to signalling pathways involving mitogen-activated protein kinase (MAPK), which in turn regulates cytoskeletal dynamics[375]. Elucidating role

of such proteins in metastatic deformation could provide deep insights about the signalling during metastatic cell-nuclear confinement.

- ***Migration kinetics***

It could be interesting to observe the migration kinetics of the cells on micropillars. Here, we studied deformation of nucleus on micropillars, however, it would be intriguing to look at the continuous deformation of the nucleus while cell migration. Migration has been known to involve RAC1, RHO A and CDC42 signalling[6]. Investigation of the roles of these molecules during confined migration could guide us to the underlying mechanisms of metastatic migration. Thus, future experiments by changing the dimensions of pillars, such as reduce spacings, could be employed to see cell migration in extreme confined spaces.

- ***Exploiting micropillar array***

Ermis et al. used the micropillar technique to distinguish cancerous and healthy nuclei[180]. Other study using micropillars revealed that nuclear deformability is highly regulated during differentiation[376]. They showed that during early ectoderm differentiation nuclear deformability is reduced strongly, whereas nuclei keep a deformed shape during early endoderm and intermediate behaviour of nuclei was seen during early mesoderm on micropillars. Another study on mesenchymal stem cell (MSCs) showed a partial deformation and recovery of nuclei on micropillars[377]. Thus, micropillar array could prove to be a valuable model to understand cancer cell invasiveness and the underlying mechanisms. This could help target the cancer invasion by targeting drugs to molecules significantly involved in metastatic migration. Moreover, such arrays could be useful in *in vitro* assays, as their visualization is easy compared to other techniques.

We showed that the different dimensions of pillars could change the deformation

behaviour of metastatic nucleus. Extreme confinement ruptures nuclear lamina and instigates differential expression of genes specifically the ones involved in DNA damage responses[378]. Irianto et al. showed that nuclear lamina damage and DNA double stranded breaks occur during extreme confined migrations[379]. Another similar study showed that constricted migration can deplete DNA repair factors and favour genetic variability in MSCs and bone cancer cell lines[380]. Thus future experiments can be done by changing the dimensions of pillars and understanding the mechanisms of nuclear envelop rupture and the underlying mechanisms. Moreover, pillars with nanoscale dimensions are used to study traction forces[189]. Jung et al. studied traction forces exerted by filopodia using Si-nanopillars[381]. Another study showed that cell morphology regulates the magnitude of traction force generated by cells[382]. Cells on nanopillars, in the absence of myosin IIA mediated force-generating machinery, are known to move with minimal traction forces at the cell periphery[383]. Recently, Shiu et al. showed that perinuclear forces, originating from stress fibres spanning the nucleus of fibroblasts, are significantly higher on nanopillars than the forces acting on peripheral adhesions[191]. Thus changing the micropillar dimension could also reveal the traction forces in migrating cancer cells during confinement.

5.2 Osteosarcoma cell response to topography substrates tuned to rigidity and chemistry

We did preliminary experiments for using hydrogels tuned to topography, chemistry and rigidity in our lab. This could help understand the behaviour of cells with respect to combination of various passive cues such as substrate topography, chemistry and rigidity. The perspectives with respect to each topic are described below:-

- ***Exploiting hydrogels- topography, chemistry and rigidity***

Cell response is guided by many factors such as topography, chemistry and mechanics of its *in vivo* 3D environment. Past few decades have provided us with the wealth of knowledge to understand the myriad of mechanisms of these factors on cell response *in vitro*. Unfortunately, most of the studies target cues like topography or chemistry or rigidity individually, which is not the case in actual *in vivo* environment. Cells *in vivo* come across these all cues more or less simultaneously which induce a feedback in the cells leading to a single response from these combined cues. Thus, practically studying one cue does not explicate the actual cell response found *in vivo*. Moreover, changing the dimensions of cell culture from 2D to 3D has shown significant differences in cell behaviour in response to these dimensions[384,385]. Not only healthy cells but diseased cells such as cancer cells have also shown difference in signalling pathways when cultured in 2D and 3D environment[386]. Changing the geometry of topographical substrates has also shown myriad of different responses in cell behaviour[387]. Changing the mechanics of substrate from soft to stiff has changed the signalling and responses of intercellular cytoskeletal and other proteins[207,388]. Role of molecule mediated cues in regulating cell responses has also been studied extensively[389–392]. Thus, we could presume that studying the response of different cues individually would not shed light on the exact cell response encountered *in vivo*. To overcome this drawback there is a need to fabricate and control different cues like topography, chemistry and mechanics in a single culture model. Next generation biomaterial design needs an improved understanding of how these substrate properties together affect cell behaviour.

Our study provides the use of hydrogel systems in fabricating a substrate whose parameters can be tuned depending on the relative environment *in vivo* of different cells. For that we used PDMAA based hydrogels which not only tune the topography and rigidity of the substrate but also

control the chemistry of the substrates. There are many broad applications of this technique to interpret various cell behaviours. For instance, we used pillar geometry, however there are various topographies that are found *in vivo* that affect cellular behaviour (described in detail in section 1.8.2)[393,394]. Moreover the cells we use were osteosarcoma. There are various cell types-cancerous/healthy (neural, cartilage, intestinal, etc.), whose behaviour could be studied in by recapitulating their native ECM environment using combination of hydrogel-topography and chemistry. The polymers we synthesized for functionalizing the substrate surface could have wide application in controlling the chemistry of surfaces, cost effectively. The polymers used could be altered with ligands or different bioactive compounds. Using these hydrogel coatings in future, one can closely mimic the *in vivo* environment by controlling the topography, rigidity and chemistry of the substrate. This could lead to analyse the cell behaviour close to the *in vivo* milieu.

Moreover, 3D hydrogel system based on tunable properties of topography, chemistry and mechanics could have a broad applications in development of biomaterials. For example, in clinical applications demanding functioning implants may require physiologically relevant scaffolds mimicking the native tissue structure at cell scale level topographical features. Hydrogels have been previously used for drug or growth factor deliver, engineering tissue replacements, etc. Recently they have been also employed as 3D scaffolds to study cell behaviour. Pluripotent stem cells have been shown to undergo lineage commitment when grown in bioactive hydrogel capsules. Moreover, these capsules could be decorated with biologically active ligands to influence cell fate[395]. Tabata et al., developed a 3D hydrogel microchip concept for determining cell fate[396]. Recently, another 3D hydrogel based matrices with mechanical characterization were used for intestinal stem cell and organoid culture[397]. PEG based hydrogel system was used to study migration of cells in 3D matrix tuned with stiffness which showed stiffness dependent migration

pattern[5]. As evident by these studies, 3D hydrogel systems tuned to mechanics or chemistry have been focused on, without taking topography effect on cellular response. *In vivo* cells not only encounter mechanics in 3 dimensions but also topographical geometries that play a key role in determining cell behaviour. Hence, there is a need to manufacture systems that can be modulated with all the 3 components-topography, mechanics and chemistry to closely resemble the *in vivo* milieu. Our tunable 3D hydrogel systems provide a degree of flexibility, very similar to natural tissues and could be easily modulated with desired mechanical, topographical and chemical properties. This technique could be further developed to do porous (probably with the help of porogens) scaffolds of hydrogels with nano-porosity and tuned mechanics. These 3D-tunable hydrogel systems could be used for development of tumor tissue models for better efficacy of anti-cancer drugs, and allow us to better understand cancer cell biology. Finally, there is a need of 3D model culture system that needs to be easy to use and which can be sculpted easily into required topography, mechanics and chemistry. This could minimise the use of human and animal models to reduce the cost of drug delivery process. Diseases originating in different parts of the body could be studied by tuning 3 parameters of the substrate simultaneously in a single culture model system. Altogether, the hydrogels we used could meet this need.

- ***Cellular proteins and signalling pathways***

The cell-ECM surface crosstalk occurs with the integrin adhesion via FAs proteins that activate MAP kinase pathway and various other cascades that respond to difference in rigidity[262]. FAs are used by cells to sense the topography or rigidity of the substrate, whose stabilization on surfaces involve Rho–ROCK pathway. The role of these proteins could be studied in the cells to understand how the deregulation of FAs mediated signalling could affect cancerous cell behaviour on different

rigid-topography-chemistry coupled surfaces. Some cells like hMSC and myocyte cells use RhoA pathway to manage calcium levels in response to substrate rigidity[398,399]. Tan et al. showed that H3K9 demethylation and Sox2 expression are affected by matrix stiffness in tumor repopulation cells[218]. Nucleoskeletal proteins such as lamin A and B are known to be modulated by matrix stiffness[342]. Cytoskeletal protein α-actinin is also known to be involved in rigidity sensing[400]. Collins et al. hypothesized that E-cadherin rigidity sensing guides the transition from initial cell–cell adhesion to more stable contacts in MDCK cells[401]. Tyrosine-kinase-driven signalling pathways have been known to regulate many aspects of cell's ability to respond to mechanical cues such as rigidity[402].

There have been extensive studies on studying the behaviour of cells on different topographies. Many studies however focus more on signalling pathways regulated by surface rigidity. Rho/ROCK[403], FAK[404], RAC1-PI3K[405], YAP/TAZ[308], EGF[406] signalling pathways are studied in regard to matrix stiffness. However, the cell-signalling cascades that bring about these behaviour in response to topographical landscapes are still poorly understood. A few pioneer studies have been addressed here, but the whole picture is far from clear. Dalby et al., performed a RNA sequence analysis for difference in gene expression in fibroblasts on grooved surfaces and found a list of genes up/down regulated in response to this topography. Nevertheless, the signalling pathways that cause the ultimate up/down regulation of these genes still remain poorly understood[407]. In another study, Dalby et al for the first time reported that nano columns affected the clathrin mediated endocytosis due to global redistribution of dynamin and clathrin[408]. Study on nano-cones and flat strips showed that N-BAR protein nadrin-2 accumulates on nano-cone topography compared to flat strips[409]. This implies that the topography of the substrate plays a

key role on inter-cellular signalling in changing protein expressions. Teo et al. showed that nano/micropillars and microgrooves exhibited increased endocytosis of dextran in various cell types[410]. They also found that nanopillars increased the efficacy of inducing plasmid GFP in cells, meaning that the cell signalling pathways in the transcription of the plasmid DNA must be somehow dependent or are regulated with regard to size of topographical features. There are a number of studies showing how the nuclear architecture is affected by topographical features[180,202,203,376,411–413]. Nucleus harbours the genes and transcriptional machinery of the cell. Its deformation must lead to changes in the transcription of genes. However, the cell-signalling pathways leading to the changes in gene expressions still remain elusive. Hence, future studies could revolve more around the signalling pathways relative to topography. Although this does not mean that rigidity could be ruled out. Thus, the signalling pathways studied on different mechanics could be studied on substrate having both mechanical and topographical features to see if there is any change when the cell is on mechanically rigid substrate with topographical features. Our 3D mechanical-topographical-chemical system may serve the best solution with this respect. .

- ***Gene expression and cellular differentiation***

Cell change their gene expression on different rigid substrates, leading to the determination of cell fate. The cells utilise the substrate rigidity to alter different proteins expressions[414]. On the stiffest substrates MSCs expressed early markers of osteogenesis, whereas myogenic markers on intermediate stiffness gels and neuronal markers on the softest gels[31]. Similarly, in another study neural stem cells differentiated into neurons on soft substrates and on stiff substrates into glia, when cultured in media that promoted both lineages[415]. Other studies found that substrate rigidity affected gene expression of pluripotent and differentiation markers in determining human

embryonic stem cells (hESC) fate towards early mesodermal lineages[416]. However, these studies mostly focus on rigidity of the substrate and not topography. There have been very few studies determining the effect of topography on cellular fates. Dalby et al., observed bone differentiation on nanoscale disordered patterns[417]. Colloidal crystal topography is known to lead to differentiation in embryonic stem cells[418]. Cell contractility arising from topography is known to determine hMSC fate[419]. Expression of oct4 (stem cell pluripotency and transcription factor) was seen expressed in human embryonic stem cells on hexagonal nano-topography[420]. Micro and nano patterned grooves showed differentiation of stem cells towards osteogenic and adipogenic lineages[421]. Micron-scale topography induced differentiation is observed in neural stem cell behaviour[422]. As evident by the research, most of the focus is on nanoscale and some on micron scale topographies. However, studying the response of cell scale topography on cell behaviour would enlighten more about the fate of the cells. Moreover with our 3D hydrogel system, the cell-scale topography could be tuned to that of cell-scale stiffness, to interpret the behaviour of stem cells in response to cell-scale features during embryonic development or during differentiation processes. Also, to see the changes in the gene expression transcriptomic analysis like RNA sequencing could shed light on regulation of different genes with respect to different rigid substrates defined with cell scale topography.

- ***Migration of cells on different rigidities***

Cells tend to migrate towards the stiffer region of the substrates which is known as “durotaxis”[423]. Cells are known to migrate faster on soft substrates and slower on stiff substrates[23]. In 2010 Sarvestani et al. found that substrate rigidity affected the anterior and posterior actomyosin contractile forces leading to variation in net traction applied by the cell on substrate[424]. Ng at al. in

2012 found that the cadherin dependent collective migration of cells increased with the substrate rigidity, during epithelial wound healing assay[425]. They further showed that this migration was facilitated by front to back myosin contractility that increased with polarisation of cell on stiff substrate. Evans et al. showed that nerve regeneration that depends upon directed migration of Schwann cells, can be guided by physiologically relevant stiffness gradients[426]. Even though this research provides wealth of insights, the molecular mechanism underlying the durotaxis phenomenon still remain poorly understood. Moreover most of these studies are focused on mechanics of the substrate and do not take topography in account. Topography is known to elicit numerous responses and is bound to reflect on properties of migration in different rigid substrates containing topographical features. Hence, it would be interesting to observe in future the kinetics of cell adhesion and migration on soft, intermediate and stiff substrate with topography to understand better the durotaxis mechanisms in 2.5D or 3D environment.

5.3 Colon carcinoma cell behaviour on substrates with different topography

We performed preliminary experiments with colorectal carcinoma (CRCs) cells on different topographies and analysed different mRNA expression levels in CRCs with different grades of cancer and mutation in APC and cdx2 genes. These results could be used to future experiments that could elucidate the behaviour of CRCs on topographic substrates.

- ***mRNA and protein expression***

We investigated the mRNA levels of different nucleoskeletal and myosin genes in CRC cell lines (HT29, SW480, TC7, DLD1, HCT116) on flat surface. However the mRNA expression does not always express the exact protein levels. Moreover, we did not check these mRNA levels in mutant cell line of CRCs with APC and cdx2 mutations. Hence, future experiments could involve performing RT-

qPCR of the above genes in all different CRCs including mutant cell lines, on topographies such as wells compared to flat surface. This would allow us to understand the deregulated genes in cancer with regard to healthy epithelial cells. The mRNA levels should be correlated with Western blot and immunofluorescence analysis of these proteins on well topography.

- ***Cdx2 induction***

We did experiment with TG8 and TW6 cell lines with inducible expression of cdx2 gene. However this gene is induced only in the presence of doxycycline, without which the cdx2 levels are lower in the cells. TW6 shows high level of cdx2 in presence of doxycycline and TG8 cdx2 expression does not change, thus TG8 acts as a control. Hence, future experiments could involve comparing our results like cytoskeletal or e-cadherin distribution and nuclear deformation of these cells in presence of doxycycline.

- ***Cell behaviour on topography***

Well/pits topography seemed to show most cellular response in the CRC cells. However, we performed this experiment on only 2 dimensions (Widthxdepth µm 50X 30 and 150X60) with only TC7 cell line. The behaviour of other cell lines on these substrates could be performed in future to observe difference in terms of e-cadherin, focal adhesions, actin organization, cell spreading, colony formation, etc. Next, the dimensions of the wells could be changed and a range of depth can be fabricated to see the response of different CRCs to gradual change in dimension such as depth. The topography that we used here are simple wells, however the geometry of the crypts and villi is more different than a well topography. Hence, future studies could focus on fabricating the geometry mimicking the features of intestine, to better understand the cellular responses of different CRCs.

- ***Role of cytoskeletal elements in response to topography***

Cytoskeletal elements are major regulators of cell responses to different cues. CRCs have shown deregulation in actin-cytoskeletal pathway leading to malignant transformation and disease progression of cells[427]. Actin dynamic regulators such as actin-nucleating, depolymerizing and promoting factors have known to be involved in CRCs malignant progression[428]. Microtubules are also known to involved in cancer progression in CRCs[352]. Intermediate filaments like keratin are known to be important in colon homeostasis, differentiation, tumorigenesis and energy metabolisms[429,430]. Hence, future experiments could involve investigating the role of these components on response to topography by perturbing those individually using drugs.

- ***Role of mechanics in CRC cell response***

Our technique on hydrogels combining the topography, rigidity and chemistry could be used on CRCs. The well topography could be tuned and the effect of each parameter in combination to others could be studied in CRC cell lines. Mechanics of the wells could be tuned to that of intestinal tissues which would allow us to understand behaviour of CRC in physiological relevant environment.

References

1. Bunz, F. *Principles of Cancer Genetics*. (Springer Science & Business Media, 2007).
2. Martin, T. A., Ye, L., Sanders, A. J., Lane, J. & Jiang, W. G. *Cancer Invasion and Metastasis: Molecular and Cellular Perspective*. (Landes Bioscience, 2013).
3. Kshitiz, Afzal, J., Chang, H., Goyal, R. & Levchenko, A. Mechanics of Microenvironment as Instructive Cues Guiding Stem Cell Behavior. *Curr Stem Cell Rep* **2**, 62–72 (2016).
4. Park, J., Kim, D.-H. & Levchenko, A. Topotaxis: A New Mechanism of Directed Cell Migration in Topographic ECM Gradients. *Biophysical Journal* **114**, 1257–1263 (2018).
5. Ehrbar, M. *et al.* Elucidating the role of matrix stiffness in 3D cell migration and remodeling. *Biophys. J.* **100**, 284–293 (2011).
6. Paul, C. D., Mistriotis, P. & Konstantopoulos, K. Cancer cell motility: lessons from migration in confined spaces. *Nat Rev Cancer* **17**, 131–140 (2017).
7. Desai, L. P., White, S. R. & Waters, C. M. Cyclic Mechanical Stretch Decreases Cell Migration by Inhibiting Phosphatidylinositol 3-Kinase- and Focal Adhesion Kinase-mediated JNK1 Activation. *J. Biol. Chem.* **285**, 4511–4519 (2010).
8. Liu, J. *et al.* Soft fibrin gels promote selection and growth of tumorigenic cells. *Nature Materials* **11**, 734–741 (2012).
9. Paszek, M. J. *et al.* Tensional homeostasis and the malignant phenotype. *Cancer Cell* **8**, 241–254 (2005).
10. Levental, K. R. *et al.* Matrix crosslinking forces tumor progression by enhancing integrin signaling. *Cell* **139**, 891–906 (2009).
11. Jiang, W. G. *Electric Cell-Substrate Impedance Sensing and Cancer Metastasis*. (Springer Science & Business Media, 2012).
12. Bellomo, C., Caja, L. & Moustakas, A. Transforming growth factor β as regulator of cancer stemness and metastasis. *British Journal of Cancer* **115**, 761–769 (2016).
13. Aukes, K. *et al.* Breast cancer cell-derived fibroblast growth factors enhance osteoclast activity and contribute to the formation of metastatic lesions. *PLOS ONE* **12**, e0185736 (2017).
14. Farooqi, A. A. & Siddik, Z. H. Platelet-derived growth factor (PDGF) signalling in cancer: rapidly emerging signalling landscape. *Cell Biochem Funct* **33**, 257–265 (2015).
15. Landskron, G., De la Fuente, M., Thuwajit, P., Thuwajit, C. & Hermoso, M. A. Chronic Inflammation and Cytokines in the Tumor Microenvironment. *Journal of Immunology Research* **2014**, 1–19 (2014).
16. Nagarsheth, N., Wicha, M. S. & Zou, W. Chemokines in the cancer microenvironment and their relevance in cancer immunotherapy. *Nature Reviews Immunology* **17**, 559–572 (2017).
17. Sugimura, K., Lenne, P.-F. & Graner, F. Measuring forces and stresses in situ in living tissues. *Development* **143**, 186–196 (2016).
18. van Helvert, S. & Friedl, P. Strain Stiffening of Fibrillar Collagen during Individual and Collective Cell Migration Identified by AFM Nanoindentation. *ACS Appl. Mater. Interfaces* **8**, 21946–21955 (2016).
19. Fan, R. *et al.* Circulatory shear flow alters the viability and proliferation of circulating colon cancer cells. *Scientific Reports* **6**, 27073 (2016).
20. Polacheck, W. J., Charest, J. L. & Kamm, R. D. Interstitial flow influences direction of tumor cell migration through competing mechanisms. *PNAS* **108**, 11115–11120 (2011).
21. Leu, A. J., Berk, D. A., Lymboussaki, A., Alitalo, K. & Jain, R. K. Absence of functional lymphatics within a murine sarcoma: a molecular and functional evaluation. *Cancer Res.* **60**, 4324–4327

(2000).
22. Tse, J. M. *et al.* Mechanical compression drives cancer cells toward invasive phenotype. *PNAS* **109**, 911–916 (2012).
23. Lange, J. R. & Fabry, B. Cell and tissue mechanics in cell migration. *Exp Cell Res* **319**, 2418–2423 (2013).
24. Wolf, K. *et al.* Physical limits of cell migration: Control by ECM space and nuclear deformation and tuning by proteolysis and traction force. *J.CELL BIOL., J.CELL.BIOL., The Journal of cell biology, The Journal of cell biology.* **201**, 1069–1084 (2013).
25. Park, J. *et al.* Directed migration of cancer cells guided by the graded texture of the underlying matrix. *Nature Materials* **15**, 792–801 (2016).
26. Park, J., Kim, D.-H. & Levchenko, A. Topotaxis: A New Mechanism of Directed Cell Migration in Topographic ECM Gradients. *Biophys. J.* **114**, 1257–1263 (2018).
27. Provenzano, P. P. *et al.* Collagen reorganization at the tumor-stromal interface facilitates local invasion. *BMC Med* **4**, 38 (2006).
28. Goetz, J. G. *et al.* Biomechanical remodeling of the microenvironment by stromal caveolin-1 favors tumor invasion and metastasis. *Cell* **146**, 148–163 (2011).
29. Plotnikov, S. V. & Waterman, C. M. Guiding cell migration by tugging. *Curr Opin Cell Biol* **25**, (2013).
30. Jodele, S., Blavier, L., Yoon, J. M. & DeClerck, Y. A. Modifying the soil to affect the seed: role of stromal-derived matrix metalloproteinases in cancer progression. *Cancer Metastasis Rev.* **25**, 35–43 (2006).
31. Engler, A. J., Sen, S., Sweeney, H. L. & Discher, D. E. Matrix elasticity directs stem cell lineage specification. *Cell* **126**, 677–689 (2006).
32. Gupta, P. B., Chaffer, C. L. & Weinberg, R. A. Cancer stem cells: mirage or reality? *Nature Medicine* **15**, 1010–1012 (2009).
33. Soft fibrin gels promote selection and growth of tumorigenic cells | Nature Materials. Available at: https://www.nature.com/articles/nmat3361. (Accessed: 6th May 2018)
34. Davidson, P. M. *et al.* Topographically induced self-deformation of the nuclei of cells: dependence on cell type and proposed mechanisms. *J Mater Sci Mater Med* **21**, 939–946 (2010).
35. Ermis, M., Akkaynak, D., Chen, P., Demirci, U. & Hasirci, V. A high throughput approach for analysis of cell nuclear deformability at single cell level. *Scientific Reports* **6**, 36917 (2016).
36. Davidson, P. M. *et al.* Severe Deformations of Malignant Bone and Skin Cells, as well as Aged Cells, on Micropatterned Surfaces. in *Biomaterials Surface Science* 469–489 (Wiley-Blackwell, 2013). doi:10.1002/9783527649600.ch16
37. Bavi, O. *et al.* Influence of Global and Local Membrane Curvature on Mechanosensitive Ion Channels: A Finite Element Approach. *Membranes (Basel)* **6**, (2016).
38. Rasmussen, T. How do mechanosensitive channels sense membrane tension? *Biochem. Soc. Trans.* **44**, 1019–1025 (2016).
39. Charras, G. T., Williams, B. A., Sims, S. M. & Horton, M. A. Estimating the sensitivity of mechanosensitive ion channels to membrane strain and tension. *Biophys. J.* **87**, 2870–2884 (2004).
40. Ranade, S. S., Syeda, R. & Patapoutian, A. Mechanically Activated Ion Channels. *Neuron* **87**, 1162–1179 (2015).
41. Integrins: A family of cell surface receptors: Cell. Available at: https://www.cell.com/cell/pdf/0092-8674(87)90233-

9.pdf?_returnURL=https%3A%2F%2Flinkinghub.elsevier.com%2Fretrieve%2Fpii%2F0092867487902339%3Fshowall%3Dtrue. (Accessed: 7th May 2018)
42. Shyy, J. Y.-J. & Chien, S. Role of Integrins in Endothelial Mechanosensing of Shear Stress. *Circulation Research* **91**, 769–775 (2002).
43. Li, S. *et al.* Distinct roles for the small GTPases Cdc42 and Rho in endothelial responses to shear stress. *J Clin Invest* **103**, 1141–1150 (1999).
44. Marjoram, R. J., Lessey, E. C. & Burridge, K. Regulation of RhoA Activity by Adhesion Molecules and Mechanotransduction. *Curr Mol Med* **14**, 199–208 (2014).
45. Kawamura, S., Miyamoto, S. & Brown, J. H. Initiation and Transduction of Stretch-induced RhoA and Rac1 Activation through Caveolae CYTOSKELETAL REGULATION OF ERK TRANSLOCATION. *J. Biol. Chem.* **278**, 31111–31117 (2003).
46. Khatiwala, C. B., Kim, P. D., Peyton, S. R. & Putnam, A. J. ECM Compliance Regulates Osteogenesis by Influencing MAPK Signaling Downstream of RhoA and ROCK. *J Bone Miner Res* **24**, 886–898 (2009).
47. Wehrle-Haller, B. Structure and function of focal adhesions. *Current Opinion in Cell Biology* **24**, 116–124 (2012).
48. Shemesh, T., Geiger, B., Bershadsky, A. D. & Kozlov, M. M. Focal adhesions as mechanosensors: A physical mechanism. *PNAS* **102**, 12383–12388 (2005).
49. Grashoff, C. *et al.* Measuring mechanical tension across vinculin reveals regulation of focal adhesion dynamics. *Nature* **466**, 263–266 (2010).
50. Geiger, B., Spatz, J. P. & Bershadsky, A. D. Environmental sensing through focal adhesions. *Nat. Rev. Mol. Cell Biol.* **10**, 21–33 (2009).
51. Schwarz, U. S., Erdmann, T. & Bischofs, I. B. Focal adhesions as mechanosensors: The two-spring model. *Biosystems* **83**, 225–232 (2006).
52. Cao, X. *et al.* Multiscale model predicts increasing focal adhesion size with decreasing stiffness in fibrous matrices. *PNAS* **114**, E4549–E4555 (2017).
53. Kuo, C. W., Chueh, D.-Y. & Chen, P. Investigation of size–dependent cell adhesion on nanostructured interfaces. *Journal of Nanobiotechnology* **12**, (2014).
54. Cukierman, E., Pankov, R., Stevens, D. R. & Yamada, K. M. Taking Cell-Matrix Adhesions to the Third Dimension. *Science* **294**, 1708–1712 (2001).
55. Mekhdjian, A. H. *et al.* Integrin-mediated traction force enhances paxillin molecular associations and adhesion dynamics that increase the invasiveness of tumor cells into a three-dimensional extracellular matrix. *MBoC* **28**, 1467–1488 (2017).
56. Bell, S. & Terentjev, E. M. Focal Adhesion Kinase: The Reversible Molecular Mechanosensor. *Biophysical Journal* **112**, 2439–2450 (2017).
57. Hatami-Marbini, H. & Mofrad, M. R. K. Cytoskeletal Mechanics and Cellular Mechanotransduction: A Molecular Perspective. in *Cellular and Biomolecular Mechanics and Mechanobiology* (ed. Gefen, A.) **4**, 3–27 (Springer Berlin Heidelberg, 2010).
58. Kirby, T. J. & Lammerding, J. Emerging views of the nucleus as a cellular mechanosensor. *Nat. Cell Biol.* **20**, 373–381 (2018).
59. Anselme, K., Wakhloo, N. T., Rougerie, P. & Pieuchot, L. Role of the Nucleus as a Sensor of Cell Environment Topography. *Adv Healthc Mater* **7**, e1701154 (2018).
60. Sims, J. R., Karp, S. & Ingber, D. E. Altering the cellular mechanical force balance results in integrated changes in cell, cytoskeletal and nuclear shape. *J. Cell. Sci.* **103 (Pt 4)**, 1215–1222 (1992).

61. Ingber, D. E. Tensegrity I. Cell structure and hierarchical systems biology. *Journal of Cell Science* **116**, 1157–1173 (2003).
62. Taylor, M. P., Koyuncu, O. O. & Enquist, L. W. Subversion of the actin cytoskeleton during viral infection. *Nature Reviews Microbiology* **9**, 427–439 (2011).
63. Provenzano, P. P. & Keely, P. J. Mechanical signaling through the cytoskeleton regulates cell proliferation by coordinated focal adhesion and Rho GTPase signaling. *J. Cell. Sci.* **124**, 1195–1205 (2011).
64. Pollard, T. D. Regulation of actin filament assembly by Arp2/3 complex and formins. *Annu Rev Biophys Biomol Struct* **36**, 451–477 (2007).
65. Blanchoin, L., Boujemaa-Paterski, R., Sykes, C. & Plastino, J. Actin dynamics, architecture, and mechanics in cell motility. *Physiol. Rev.* **94**, 235–263 (2014).
66. Small, J. V., Stradal, T., Vignal, E. & Rottner, K. The lamellipodium: where motility begins. *Trends Cell Biol.* **12**, 112–120 (2002).
67. Mattila, P. K. & Lappalainen, P. Filopodia: molecular architecture and cellular functions. *Nat. Rev. Mol. Cell Biol.* **9**, 446–454 (2008).
68. Chen, Y.-W., Chen, Y.-F., Chiu, W.-T., Chen, H.-C. & Shen, M.-R. STIM1-dependent Ca 2+ signaling regulates podosome formation to facilitate cancer cell invasion. *Scientific Reports* **7**, 11523 (2017).
69. Hoshino, D., Branch, K. M. & Weaver, A. M. Signaling inputs to invadopodia and podosomes. *J Cell Sci* **126**, 2979–2989 (2013).
70. Saykali, B. A. & El-Sibai, M. Invadopodia, Regulation, and Assembly in Cancer Cell Invasion. *Cell Communication & Adhesion* **21**, 207–212 (2014).
71. Eddy, R. J., Weidmann, M. D., Sharma, V. P. & Condeelis, J. S. Tumor Cell Invadopodia: Invasive Protrusions that Orchestrate Metastasis. *Trends in Cell Biology* **27**, 595–607 (2017).
72. Salbreux, G., Charras, G. & Paluch, E. Actin cortex mechanics and cellular morphogenesis. *Trends Cell Biol.* **22**, 536–545 (2012).
73. Hotulainen, P. & Lappalainen, P. Stress fibers are generated by two distinct actin assembly mechanisms in motile cells. *The Journal of Cell Biology* **173**, 383–394 (2006).
74. Tojkander, S., Gateva, G. & Lappalainen, P. Actin stress fibers--assembly, dynamics and biological roles. *J. Cell. Sci.* **125**, 1855–1864 (2012).
75. Mitchison, T. & Kirschner, M. Dynamic instability of microtubule growth. *Nature* **312**, 237–242 (1984).
76. Cooper, G. Cytoskeletal networks and the regulation of cardiac contractility: microtubules, hypertrophy, and cardiac dysfunction. *Am. J. Physiol. Heart Circ. Physiol.* **291**, H1003-1014 (2006).
77. Kerr, J. P. *et al.* Detyrosinated microtubules modulate mechanotransduction in heart and skeletal muscle. *Nature Communications* **6**, 8526 (2015).
78. Lyons, J. S. *et al.* Microtubules tune mechanotransduction through NOX2 and TRPV4 to decrease sclerostin abundance in osteocytes. *Sci. Signal.* **10**, eaan5748 (2017).
79. Martin, S. G., McDonald, W. H., Yates, J. R. & Chang, F. Tea4p links microtubule plus ends with the formin for3p in the establishment of cell polarity. *Dev. Cell* **8**, 479–491 (2005).
80. Siegrist, S. E. & Doe, C. Q. Microtubule-induced cortical cell polarity. *Genes Dev.* **21**, 483–496 (2007).
81. Robinson, D. N. & Spudich, J. A. Mechanics and regulation of cytokinesis. *Curr. Opin. Cell Biol.* **16**, 182–188 (2004).

82. Sanghvi-Shah, R. & Weber, G. F. Intermediate Filaments at the Junction of Mechanotransduction, Migration, and Development. *Front Cell Dev Biol* **5**, (2017).
83. Maniotis, A. J., Chen, C. S. & Ingber, D. E. Demonstration of mechanical connections between integrins, cytoskeletal filaments, and nucleoplasm that stabilize nuclear structure. *PNAS* **94**, 849–854 (1997).
84. Dupin, I., Sakamoto, Y. & Etienne-Manneville, S. Cytoplasmic intermediate filaments mediate actin-driven positioning of the nucleus. *J. Cell. Sci.* **124**, 865–872 (2011).
85. Tsuruta, D. & Jones, J. C. R. The vimentin cytoskeleton regulates focal contact size and adhesion of endothelial cells subjected to shear stress. *J. Cell. Sci.* **116**, 4977–4984 (2003).
86. Bhattacharya, R. *et al.* Recruitment of vimentin to the cell surface by beta3 integrin and plectin mediates adhesion strength. *J. Cell. Sci.* **122**, 1390–1400 (2009).
87. Liu, C.-Y., Lin, H.-H., Tang, M.-J. & Wang, Y.-K. Vimentin contributes to epithelial-mesenchymal transition cancer cell mechanics by mediating cytoskeletal organization and focal adhesion maturation. *Oncotarget* **6**, 15966–15983 (2015).
88. Conway, D. E. *et al.* Fluid shear stress on endothelial cells modulates mechanical tension across VE-cadherin and PECAM-1. *Curr. Biol.* **23**, 1024–1030 (2013).
89. Bordeleau, F., Galarneau, L., Gilbert, S., Loranger, A. & Marceau, N. Keratin 8/18 modulation of protein kinase C-mediated integrin-dependent adhesion and migration of liver epithelial cells. *Mol. Biol. Cell* **21**, 1698–1713 (2010).
90. Sankar, S. *et al.* A novel role for keratin 17 in coordinating oncogenic transformation and cellular adhesion in Ewing sarcoma. *Mol. Cell. Biol.* **33**, 4448–4460 (2013).
91. Bjerke, M. A., Dzamba, B. J., Wang, C. & DeSimone, D. W. FAK is required for tension-dependent organization of collective cell movements in Xenopus mesendoderm. *Dev. Biol.* **394**, 340–356 (2014).
92. Lai, Y. K., Lee, W. C. & Chen, K. D. Vimentin serves as a phosphate sink during the apparent activation of protein kinases by okadaic acid in mammalian cells. *J. Cell. Biochem.* **53**, 161–168 (1993).
93. Helmke, B. P., Thakker, D. B., Goldman, R. D. & Davies, P. F. Spatiotemporal analysis of flow-induced intermediate filament displacement in living endothelial cells. *Biophys. J.* **80**, 184–194 (2001).
94. Sivaramakrishnan, S., DeGiulio, J. V., Lorand, L., Goldman, R. D. & Ridge, K. M. Micromechanical properties of keratin intermediate filament networks. *Proc. Natl. Acad. Sci. U.S.A.* **105**, 889–894 (2008).
95. Fujiwara, S., Ohashi, K., Mashiko, T., Kondo, H. & Mizuno, K. Interplay between Solo and keratin filaments is crucial for mechanical force-induced stress fiber reinforcement. *Mol. Biol. Cell* **27**, 954–966 (2016).
96. Jiu, Y. *et al.* Vimentin intermediate filaments control actin stress fiber assembly through GEF-H1 and RhoA. *J. Cell. Sci.* **130**, 892–902 (2017).
97. Charrier, E. E. & Janmey, P. A. Mechanical properties of intermediate filament proteins. *Methods Enzymol* **568**, 35–57 (2016).
98. Denais, C. & Lammerding, J. Nuclear Mechanics in Cancer. *Adv Exp Med Biol* **773**, 435–470 (2014).
99. Dahl, K. N., Kahn, S. M., Wilson, K. L. & Discher, D. E. The nuclear envelope lamina network has elasticity and a compressibility limit suggestive of a molecular shock absorber. *J. Cell. Sci.* **117**, 4779–4786 (2004).

100. Denais, C. & Lammerding, J. Nuclear Mechanics in Cancer. in *Cancer Biology and the Nuclear Envelope* 435–470 (Springer, New York, NY, 2014). doi:10.1007/978-1-4899-8032-8_20
101. Osmanagic-Myers, S., Dechat, T. & Foisner, R. Lamins at the crossroads of mechanosignaling. *Genes Dev.* **29**, 225–237 (2015).
102. de Las Heras, J. I., Batrakou, D. G. & Schirmer, E. C. Cancer biology and the nuclear envelope: a convoluted relationship. *Semin. Cancer Biol.* **23**, 125–137 (2013).
103. Schreiber, K. H. & Kennedy, B. K. When lamins go bad: nuclear structure and disease. *Cell* **152**, 1365–1375 (2013).
104. Sullivan, T. *et al.* Loss of A-type lamin expression compromises nuclear envelope integrity leading to muscular dystrophy. *J. Cell Biol.* **147**, 913–920 (1999).
105. D'Angelo, M. A. & Hetzer, M. W. Structure, dynamics and function of nuclear pore complexes. *Trends Cell Biol.* **18**, 456–466 (2008).
106. Rothballer, A., Schwartz, T. U. & Kutay, U. LINCing complex functions at the nuclear envelope: what the molecular architecture of the LINC complex can reveal about its function. *Nucleus* **4**, 29–36 (2013).
107. Fridkin, A., Penkner, A., Jantsch, V. & Gruenbaum, Y. SUN-domain and KASH-domain proteins during development, meiosis and disease. *Cell. Mol. Life Sci.* **66**, 1518–1533 (2009).
108. Sosa, B. A., Kutay, U. & Schwartz, T. U. Structural insights into LINC complexes. *Curr. Opin. Struct. Biol.* **23**, 285–291 (2013).
109. Mellad, J. A., Warren, D. T. & Shanahan, C. M. Nesprins LINC the nucleus and cytoskeleton. *Current Opinion in Cell Biology* **23**, 47–54 (2011).
110. Wheeler, M. A. *et al.* Distinct functional domains in nesprin-1alpha and nesprin-2beta bind directly to emerin and both interactions are disrupted in X-linked Emery-Dreifuss muscular dystrophy. *Exp. Cell Res.* **313**, 2845–2857 (2007).
111. Lombardi, M. L. *et al.* The Interaction between Nesprins and Sun Proteins at the Nuclear Envelope Is Critical for Force Transmission between the Nucleus and Cytoskeleton. *J Biol Chem* **286**, 26743–26753 (2011).
112. Anno, T., Sakamoto, N. & Sato, M. Role of nesprin-1 in nuclear deformation in endothelial cells under static and uniaxial stretching conditions. *Biochem. Biophys. Res. Commun.* **424**, 94–99 (2012).
113. Khatau, S. B. *et al.* The distinct roles of the nucleus and nucleus-cytoskeleton connections in three-dimensional cell migration. *Scientific Reports* **2**, 488 (2012).
114. Lovett, D. B., Shekhar, N., Nickerson, J. A., Roux, K. J. & Lele, T. P. Modulation of Nuclear Shape by Substrate Rigidity. *Cell Mol Bioeng* **6**, 230–238 (2013).
115. Gudise, S., Figueroa, R. A., Lindberg, R., Larsson, V. & Hallberg, E. Samp1 is functionally associated with the LINC complex and A-type lamina networks. *J Cell Sci* **124**, 2077–2085 (2011).
116. Nery, F. C. *et al.* TorsinA binds the KASH domain of nesprins and participates in linkage between nuclear envelope and cytoskeleton. *J. Cell. Sci.* **121**, 3476–3486 (2008).
117. Berk, J. M., Tifft, K. E. & Wilson, K. L. The nuclear envelope LEM-domain protein emerin. *Nucleus* **4**, 298–314 (2013).
118. Marmé, A. *et al.* Loss of Drop1 expression already at early tumor stages in a wide range of human carcinomas. *Int. J. Cancer* **123**, 2048–2056 (2008).
119. Sjöblom, T. *et al.* The consensus coding sequences of human breast and colorectal cancers. *Science* **314**, 268–274 (2006).

120. Isermann, P. & Lammerding, J. Nuclear Mechanics and Mechanotransduction in Health and Disease. *Current Biology* **23**, R1113–R1121 (2013).
121. Lammerding, J. *et al.* Lamins A and C but Not Lamin B1 Regulate Nuclear Mechanics. *J. Biol. Chem.* **281**, 25768–25780 (2006).
122. Zuela, N., Bar, D. Z. & Gruenbaum, Y. Lamins in development, tissue maintenance and stress. *EMBO Rep.* **13**, 1070–1078 (2012).
123. Jung, H.-J., Lee, J. M., Yang, S. H., Young, S. G. & Fong, L. G. Nuclear lamins in the brain - new insights into function and regulation. *Mol. Neurobiol.* **47**, 290–301 (2013).
124. Irianto, J., Pfeifer, C. R., Ivanovska, I. L., Swift, J. & Discher, D. E. Nuclear lamins in cancer. *Cell Mol Bioeng* **9**, 258–267 (2016).
125. Friedl, P., Wolf, K. & Lammerding, J. Nuclear mechanics during cell migration. *Curr Opin Cell Biol* **23**, 55–64 (2011).
126. Flaherty, J. T. *et al.* Endothelial nuclear patterns in the canine arterial tree with particular reference to hemodynamic events. *Circ. Res.* **30**, 23–33 (1972).
127. Lombardi, M. L. *et al.* The interaction between nesprins and sun proteins at the nuclear envelope is critical for force transmission between the nucleus and cytoskeleton. *J. Biol. Chem.* **286**, 26743–26753 (2011).
128. Zink, D., Fischer, A. H. & Nickerson, J. A. Nuclear structure in cancer cells. *Nat. Rev. Cancer* **4**, 677–687 (2004).
129. Friedl, P. Prespecification and plasticity: shifting mechanisms of cell migration. *Curr. Opin. Cell Biol.* **16**, 14–23 (2004).
130. Wolf, K., Müller, R., Borgmann, S., Bröcker, E.-B. & Friedl, P. Amoeboid shape change and contact guidance: T-lymphocyte crawling through fibrillar collagen is independent of matrix remodeling by MMPs and other proteases. *Blood* **102**, 3262–3269 (2003).
131. Jaalouk, D. E. & Lammerding, J. Mechanotransduction gone awry. *Nat. Rev. Mol. Cell Biol.* **10**, 63–73 (2009).
132. Rowat, A. C. *et al.* Nuclear envelope composition determines the ability of neutrophil-type cells to passage through micron-scale constrictions. *J. Biol. Chem.* **288**, 8610–8618 (2013).
133. Lee, J. S. H. *et al.* Nuclear lamin A/C deficiency induces defects in cell mechanics, polarization, and migration. *Biophys. J.* **93**, 2542–2552 (2007).
134. Wu, J. *et al.* Actomyosin Pulls to Advance the Nucleus in a Migrating Tissue Cell. *Biophysical Journal* **106**, 7–15 (2014).
135. Petrie, R. J., Koo, H. & Yamada, K. M. Generation of Compartmentalized Pressure by a Nuclear Piston Governs Cell Motility in 3D Matrix. *Science* **345**, 1062–1065 (2014).
136. Cramer, L. P. Forming the cell rear first: breaking cell symmetry to trigger directed cell migration. *Nat. Cell Biol.* **12**, 628–632 (2010).
137. Thiam, H.-R. *et al.* Perinuclear Arp2/3-driven actin polymerization enables nuclear deformation to facilitate cell migration through complex environments. *Nat Commun* **7**, 10997 (2016).
138. Raab, M. *et al.* ESCRT III repairs nuclear envelope ruptures during cell migration to limit DNA damage and cell death. *Science* **352**, 359–362 (2016).
139. Navarro, A. P., Collins, M. A. & Folker, E. S. The nucleus is a conserved mechanosensation and mechanoresponse organelle. *Cytoskeleton* **73**, 59–67 (2016).
140. Denais, C. M. *et al.* Nuclear envelope rupture and repair during cancer cell migration. *Science* **352**, 353–358 (2016).

141. Finan, J. D., Leddy, H. A. & Guilak, F. Osmotic stress alters chromatin condensation and nucleocytoplasmic transport. *Biochem. Biophys. Res. Commun.* **408**, 230–235 (2011).
142. Deguchi, S., Ohashi, T. & Sato, M. Intracellular stress transmission through actin stress fiber network in adherent vascular cells. *Mol Cell Biomech* **2**, 205–216 (2005).
143. Guilak, F. Compression-induced changes in the shape and volume of the chondrocyte nucleus. *J Biomech* **28**, 1529–1541 (1995).
144. Tocco, V. J. *et al.* The nucleus is irreversibly shaped by motion of cell boundaries in cancer and non-cancer cells. *Journal of Cellular Physiology* **233**, 1446–1454 (2018).
145. Luxton, G. W. G., Gomes, E. R., Folker, E. S., Vintinner, E. & Gundersen, G. G. Linear arrays of nuclear envelope proteins harness retrograde actin flow for nuclear movement. *Science* **329**, 956–959 (2010).
146. Khatau, S. B. *et al.* A perinuclear actin cap regulates nuclear shape. *PNAS* **106**, 19017–19022 (2009).
147. Peeters, E. A. G. *et al.* Anisotropic, three-dimensional deformation of single attached cells under compression. *Ann Biomed Eng* **32**, 1443–1452 (2004).
148. Wang, N., Tytell, J. D. & Ingber, D. E. Mechanotransduction at a distance: mechanically coupling the extracellular matrix with the nucleus. *Nature reviews. Molecular cell biology* **10**, 75 (2009).
149. Gerlitz, G. & Bustin, M. Efficient cell migration requires global chromatin condensation. *J Cell Sci* **123**, 2207–2217 (2010).
150. Wang, Y., Nagarajan, M., Uhler, C. & Shivashankar, G. V. Orientation and repositioning of chromosomes correlate with cell geometry-dependent gene expression. *Mol. Biol. Cell* **28**, 1997–2009 (2017).
151. Heo, S.-J. *et al.* Biophysical Regulation of Chromatin Architecture Instills a Mechanical Memory in Mesenchymal Stem Cells. *Sci Rep* **5**, (2015).
152. Gerlitz, G. & Bustin, M. The role of chromatin structure in cell migration. *Trends Cell Biol* **21**, 6–11 (2011).
153. Carone, D. M. & Lawrence, J. B. Heterochromatin Instability in Cancer: From the Barr Body to Satellites and the Nuclear Periphery. *Semin Cancer Biol* **23**, 99–108 (2013).
154. Mattout, A., Cabianca, D. S. & Gasser, S. M. Chromatin states and nuclear organization in development — a view from the nuclear lamina. *Genome Biology* **16**, 174 (2015).
155. Schreiner, S. M., Koo, P. K., Zhao, Y., Mochrie, S. G. J. & King, M. C. The tethering of chromatin to the nuclear envelope supports nuclear mechanics. *Nature Communications* **6**, ncomms8159 (2015).
156. Ingber, D. E. Tensegrity: The Architectural Basis of Cellular Mechanotransduction. *Annual Review of Physiology* **59**, 575–599 (1997).
157. Jafari Bidhendi, A. & Korhonen, R. K. A Finite Element Study of Micropipette Aspiration of Single Cells: Effect of Compressibility. *Comput Math Methods Med* **2012**, (2012).
158. Sakamoto, Y., Buchanan, R. M., Sanchez-Adams, J., Guilak, F. & Sacks, M. S. On the Functional Role of Valve Interstitial Cell Stress Fibers: A Continuum Modeling Approach. *J Biomech Eng* **139**, (2017).
159. Haase, K. & Pelling, A. E. Investigating cell mechanics with atomic force microscopy. *J R Soc Interface* **12**, (2015).
160. Reisbeck, M. *et al.* Magnetic fingerprints of rolling cells for quantitative flow cytometry in whole blood. *Scientific Reports* **6**, 32838 (2016).
161. Ingber, D. E. Cellular mechanotransduction: putting all the pieces together again. *FASEB J.* **20**,

811–827 (2006).
162. Wang, N. *et al.* Mechanical behavior in living cells consistent with the tensegrity model. *PNAS* **98**, 7765–7770 (2001).
163. Mizushima-Sugano, J., Maeda, T. & Miki-Noumura, T. Flexural rigidity of singlet microtubules estimated from statistical analysis of their contour lengths and end-to-end distances. *Biochim. Biophys. Acta* **755**, 257–262 (1983).
164. Wang, N. & Stamenović, D. Contribution of intermediate filaments to cell stiffness, stiffening, and growth. *Am. J. Physiol., Cell Physiol.* **279**, C188-194 (2000).
165. Ingber, D. E., Wang, N. & Stamenović, D. Tensegrity, cellular biophysics, and the mechanics of living systems. *Rep Prog Phys* **77**, 046603 (2014).
166. Wang, N. & Suo, Z. Long-distance propagation of forces in a cell. *Biochem. Biophys. Res. Commun.* **328**, 1133–1138 (2005).
167. Dorgan, J. R., Williams, J. S. & Lewis, D. N. Melt rheology of poly(lactic acid): Entanglement and chain architecture effects. *Journal of Rheology* **43**, 1141–1155 (1999).
168. McKee, C. T., Raghunathan, V. K., Nealey, P. F., Russell, P. & Murphy, C. J. Topographic Modulation of the Orientation and Shape of Cell Nuclei and Their Influence on the Measured Elastic Modulus of Epithelial Cells. *Biophysical Journal* **101**, 2139–2146 (2011).
169. Kushiro, K., Yaginuma, T., Ryo, A. & Takai, M. Differences in Three-Dimensional Geometric Recognition by Non-Cancerous and Cancerous Epithelial Cells on Microgroove-Based Topography. *Scientific Reports* **7**, 4244 (2017).
170. Chaudhuri, P. K., Pan, C. Q., Low, B. C. & Lim, C. T. Topography induces differential sensitivity on cancer cell proliferation via Rho-ROCK-Myosin contractility. *Scientific Reports* **6**, 19672 (2016).
171. Berry, C. C., Campbell, G., Spadiccino, A., Robertson, M. & Curtis, A. S. G. The influence of microscale topography on fibroblast attachment and motility. *Biomaterials* **25**, 5781–5788 (2004).
172. Azatov, M., Sun, X., Suberi, A., Fourkas, J. T. & Upadhyaya, A. Topography on a subcellular scale modulates cellular adhesions and actin stress fiber dynamics in tumor associated fibroblasts. *Phys. Biol.* **14**, 065003 (2017).
173. Wang, L., Murthy, S. K., Fowle, W. H., Barabino, G. A. & Carrier, R. L. Influence of micro-well biomimetic topography on intestinal epithelial Caco-2 cell phenotype. *Biomaterials* **30**, 6825–6834 (2009).
174. Agudelo-Garcia, P. A. *et al.* Glioma Cell Migration on Three-dimensional Nanofiber Scaffolds Is Regulated by Substrate Topography and Abolished by Inhibition of STAT3 Signaling. *Neoplasia* **13**, 831–840 (2011).
175. Kazantseva, J., Ivanov, R., Gasik, M., Neuman, T. & Hussainova, I. Graphene-augmented nanofiber scaffolds demonstrate new features in cells behaviour. *Scientific Reports* **6**, 30150 (2016).
176. Yang, Y. *et al.* Automated fabrication of hydrogel microfibers with tunable diameters for controlled cell alignment. *Biofabrication* **9**, 045009 (2017).
177. Guo, W., Qiu, J., Liu, J. & Liu, H. Graphene microfiber as a scaffold for regulation of neural stem cells differentiation. *Sci Rep* **7**, (2017).
178. Gao, X. *et al.* Regulating cell behaviors on micropillar topographies affected by interfacial energy. *RSC Advances* **5**, 22916–22922 (2015).
179. Moerke, C., Mueller, P. & Nebe, J. B. Sensing of micropillars by osteoblasts involves complex

intracellular signaling. *J Mater Sci: Mater Med* **28**, 171 (2017).
180. Ermis, M., Akkaynak, D., Chen, P., Demirci, U. & Hasirci, V. A high throughput approach for analysis of cell nuclear deformability at single cell level. *Scientific Reports* **6**, 36917 (2016).
181. Davidson, P. M., Özçelik, H., Hasirci, V., Reiter, G. & Anselme, K. Microstructured Surfaces Cause Severe but Non-Detrimental Deformation of the Cell Nucleus. *Adv. Mater.* **21**, 3586–3590 (2009).
182. Seo, B. B. *et al.* Mechanical Contact Characteristics of PC3 Human Prostate Cancer Cells on Complex-Shaped Silicon Micropillars. *Materials (Basel)* **10**, (2017).
183. Xiao, J. *et al.* PDMS micropillar-based microchip for efficient cancer cell capture. *RSC Adv.* **5**, 52161–52166 (2015).
184. Liu, X. *et al.* Subcellular cell geometry on micropillars regulates stem cell differentiation. *Biomaterials* **111**, 27–39 (2016).
185. Turner, A. M. *et al.* Attachment of astroglial cells to microfabricated pillar arrays of different geometries. *J. Biomed. Mater. Res.* **51**, 430–441 (2000).
186. Frey, M. T., Tsai, I. Y., Russell, T. P., Hanks, S. K. & Wang, Y.-L. Cellular responses to substrate topography: role of myosin II and focal adhesion kinase. *Biophys. J.* **90**, 3774–3782 (2006).
187. Kim, D.-H., Provenzano, P. P., Smith, C. L. & Levchenko, A. Matrix nanotopography as a regulator of cell function. *J Cell Biol* **197**, 351–360 (2012).
188. Nagayama, K., Inoue, T., Hamada, Y. & Matsumoto, T. A novel patterned magnetic micropillar array substrate for analysis of cellular mechanical responses. *J Biomech* **65**, 194–202 (2017).
189. Schoen, I., Hu, W., Klotzsch, E. & Vogel, V. Probing Cellular Traction Forces by Micropillar Arrays: Contribution of Substrate Warping to Pillar Deflection. *Nano Lett* **10**, 1823–1830 (2010).
190. Ghassemi, S. *et al.* Cells test substrate rigidity by local contractions on submicrometer pillars. *Proceedings of the National Academy of Sciences* **109**, 5328–5333 (2012).
191. Shiu, J.-Y., Aires, L., Lin, Z. & Vogel, V. Nanopillar force measurements reveal actin-cap-mediated YAP mechanotransduction. *Nature Cell Biology* **20**, 262–271 (2018).
192. Roure, O. du *et al.* Force mapping in epithelial cell migration. *PNAS* **102**, 2390–2395 (2005).
193. Saez, A. *et al.* Traction forces exerted by epithelial cell sheets. *J. Phys.: Condens. Matter* **22**, 194119 (2010).
194. Ganz, A. *et al.* Traction forces exerted through N-cadherin contacts. *Biology of the Cell* **98**, 721–730 (2006).
195. Saez, A., Buguin, A., Silberzan, P. & Ladoux, B. Is the Mechanical Activity of Epithelial Cells Controlled by Deformations or Forces? *Biophysical Journal* **89**, L52–L54 (2005).
196. Velve-Casquillas, G., Le Berre, M., Piel, M. & Tran, P. T. Microfluidic tools for cell biological research. *Nano Today* **5**, 28–47 (2010).
197. Moreno-Arotzena, O., Mendoza, G., Cóndor, M., Rüberg, T. & García-Aznar, J. M. Inducing chemotactic and haptotactic cues in microfluidic devices for three-dimensional in vitro assays. *Biomicrofluidics* **8**, (2014).
198. Hartman, C. D., Isenberg, B. C., Chua, S. G. & Wong, J. Y. Vascular smooth muscle cell durotaxis depends on extracellular matrix composition. *PNAS* **113**, 11190–11195 (2016).
199. Mazumder, A., Roopa, T., Basu, A., Mahadevan, L. & Shivashankar, G. V. Dynamics of Chromatin Decondensation Reveals the Structural Integrity of a Mechanically Prestressed Nucleus. *Biophysical Journal* **95**, 3028–3035 (2008).
200. Petrie, R. J., Harlin, H. M., Korsak, L. I. T. & Yamada, K. M. Activating the nuclear piston mechanism of 3D migration in tumor cells. *J Cell Biol* **216**, 93–100 (2017).

201. Scianna, M. & Preziosi, L. Modeling the influence of nucleus elasticity on cell invasion in fiber networks and microchannels. *Journal of Theoretical Biology* **317**, 394–406 (2013).
202. Davidson, P. M. *et al.* Topographically induced self-deformation of the nuclei of cells: dependence on cell type and proposed mechanisms. *Journal of Materials Science: Materials in Medicine* **21**, 939–946 (2010).
203. Badique, F. *et al.* Directing nuclear deformation on micropillared surfaces by substrate geometry and cytoskeleton organization. *Biomaterials* **34**, 2991–3001 (2013).
204. Ottaviano, L. *et al.* Molecular characterization of commonly used cell lines for bone tumor research: A trans-European EuroBoNet effort. *Genes, Chromosomes and Cancer* **49**, 40–51 (2010).
205. Mohseny, A. B. *et al.* Functional characterization of osteosarcoma cell lines provides representative models to study the human disease. *Laboratory Investigation* **91**, 1195–1205 (2011).
206. Barnes, J. M., Przybyla, L. & Weaver, V. M. Tissue mechanics regulate brain development, homeostasis and disease. *J Cell Sci* **130**, 71–82 (2017).
207. Wells, R. G. The role of matrix stiffness in regulating cell behavior. *Hepatology* **47**, 1394–1400 (2008).
208. Halder, G., Dupont, S. & Piccolo, S. Transduction of mechanical and cytoskeletal cues by YAP and TAZ. *Nature Reviews Molecular Cell Biology* **13**, 591–600 (2012).
209. Lin, H.-H. *et al.* Mechanical phenotype of cancer cells: cell softening and loss of stiffness sensing. *Oncotarget* **6**, 20946–20958 (2015).
210. Tilghman, R. W. *et al.* Matrix Rigidity Regulates Cancer Cell Growth and Cellular Phenotype. *PLoS One* **5**, (2010).
211. Ruppender, N. S. *et al.* Matrix Rigidity Induces Osteolytic Gene Expression of Metastatic Breast Cancer Cells. *PLoS One* **5**, (2010).
212. Cavo, M. *et al.* Microenvironment complexity and matrix stiffness regulate breast cancer cell activity in a 3D in vitro model. *Scientific Reports* **6**, srep35367 (2016).
213. Baker, E. L., Lu, J., Yu, D., Bonnecaze, R. T. & Zaman, M. H. Cancer Cell Stiffness: Integrated Roles of Three-Dimensional Matrix Stiffness and Transforming Potential. *Biophys J* **99**, 2048–2057 (2010).
214. Kai, F., Laklai, H. & Weaver, V. M. Force Matters: Biomechanical Regulation of Cell Invasion and Migration in Disease. *Trends Cell Biol.* **26**, 486–497 (2016).
215. Northey, J. J., Przybyla, L. & Weaver, V. M. Tissue Force Programs Cell Fate and Tumor Aggression. *Cancer Discov* **7**, 1224–1237 (2017).
216. McGrail, D. J., Kieu, Q. M. N. & Dawson, M. R. The malignancy of metastatic ovarian cancer cells is increased on soft matrices through a mechanosensitive Rho–ROCK pathway. *J Cell Sci* **127**, 2621–2626 (2014).
217. Gu, Z. *et al.* Soft matrix is a natural stimulator for cellular invasiveness. *Mol Biol Cell* **25**, 457–469 (2014).
218. Tan, Y. *et al.* Matrix softness regulates plasticity of tumour-repopulating cells via H3K9 demethylation and *Sox2* expression. *Nature Communications* **5**, 4619 (2014).
219. Qin, R., Wolfenson, H., Saxena, M. & Sheetz, M. Tumor suppressor DAPK1 catalyzes adhesion assembly on rigid but anoikis on soft matrices. *bioRxiv* 320739 (2018). doi:10.1101/320739
220. Ulrich, T. A., Pardo, E. M. de J. & Kumar, S. The Mechanical Rigidity of the Extracellular Matrix Regulates the Structure, Motility, and Proliferation of Glioma Cells. *Cancer Res* **69**, 4167–4174

(2009).
221. Schrader, J. *et al.* Matrix stiffness modulates proliferation, chemotherapeutic response, and dormancy in hepatocellular carcinoma cells. *Hepatology* **53**, 1192–1205 (2011).
222. Tang, X. *et al.* Mechanical Force Affects Expression of an In Vitro Metastasis-Like Phenotype in HCT-8 Cells. *Biophysical Journal* **99**, 2460–2469 (2010).
223. Choquet, D., Felsenfeld, D. P. & Sheetz, M. P. Extracellular matrix rigidity causes strengthening of integrin-cytoskeleton linkages. *Cell* **88**, 39–48 (1997).
224. Gupta, M., Doss, B., Lim, C. T., Voituriez, R. & Ladoux, B. Single cell rigidity sensing: A complex relationship between focal adhesion dynamics and large-scale actin cytoskeleton remodeling. *Cell Adh Migr* **10**, 554–567 (2016).
225. Hersen, P. & Ladoux, B. Biophysics: Push it, pull it. *Nature* **470**, 340–341 (2011).
226. Pelham, R. J. & Wang, Y. Cell locomotion and focal adhesions are regulated by substrate flexibility. *PNAS* **94**, 13661–13665 (1997).
227. Wang, Z., Volinsky, A. A. & Gallant, N. D. Crosslinking effect on polydimethylsiloxane elastic modulus measured by custom-built compression instrument. *Journal of Applied Polymer Science* **131**, (2014).
228. Tang, N. *et al.* Thermal Conductivity of PAAm Hydrogel and its Crosslinking Effect. *arXiv:1705.01417 [cond-mat]* (2017).
229. Holback, H., Yeo, Y. & Park, K. 1 - Hydrogel swelling behavior and its biomedical applications. in *Biomedical Hydrogels* (ed. Rimmer, S.) 3–24 (Woodhead Publishing, 2011). doi:10.1533/9780857091383.1.3
230. Chiono, V., Nardo, T. & Ciardelli, G. Chapter 9 - Bioartificial Biomaterials for Regenerative Medicine Applications. in *Regenerative Medicine Applications in Organ Transplantation* (eds. Orlando, G., Lerut, J., Soker, S. & Stratta, R. J.) 113–136 (Academic Press, 2014). doi:10.1016/B978-0-12-398523-1.00009-4
231. Hoffman, A. S. Hydrogels for biomedical applications. *Advanced Drug Delivery Reviews* **64**, 18–23 (2012).
232. Singh, M. R., Patel, S. & Singh, D. Chapter 9 - Natural polymer-based hydrogels as scaffolds for tissue engineering. in *Nanobiomaterials in Soft Tissue Engineering* (ed. Grumezescu, A. M.) 231–260 (William Andrew Publishing, 2016). doi:10.1016/B978-0-323-42865-1.00009-X
233. Rosales, A. M. & Anseth, K. S. The design of reversible hydrogels to capture extracellular matrix dynamics. *Nat Rev Mater* **1**, (2016).
234. Tibbitt, M. W. & Anseth, K. S. Hydrogels as Extracellular Matrix Mimics for 3D Cell Culture. *Biotechnol Bioeng* **103**, 655–663 (2009).
235. Kraning-Rush, C. M. & Reinhart-King, C. A. Controlling matrix stiffness and topography for the study of tumor cell migration. *Cell Adh Migr* **6**, 274–279 (2012).
236. Revzin, A. *et al.* Fabrication of poly(ethylene glycol) hydrogel microstructures using photolithography. *Langmuir* **17**, 5440–5447 (2001).
237. Seidlits, S. K., Schmidt, C. E. & Shear, J. B. High-Resolution Patterning of Hydrogels in Three Dimensions using Direct-Write Photofabrication for Cell Guidance. *Advanced Functional Materials* **19**, 3543–3551 (2009).
238. Miller, J. S. *et al.* Rapid casting of patterned vascular networks for perfusable engineered three-dimensional tissues. *Nat Mater* **11**, 768–774 (2012).
239. González-Henríquez, C. M. & Sarabia-Vallejos, M. A. Electrospinning deposition of hydrogel fibers used as scaffold for biomembranes. Thermal stability of DPPC corroborated by

ellipsometry. *Chemistry and Physics of Lipids* **190**, 51–60 (2015).
240. Yeh, J. *et al.* Micromolding of shape-controlled, harvestable cell-laden hydrogels. *Biomaterials* **27**, 5391–5398 (2006).
241. Li, N. & Folch, A. Integration of topographical and biochemical cues by axons during growth on microfabricated 3-D substrates. *Exp Cell Res* **311**, (2005).
242. Guvendiren, M. & Burdick, J. A. The control of stem cell morphology and differentiation by hydrogel surface wrinkles. *Biomaterials* **31**, 6511–6518 (2010).
243. Choi, C.-H. *et al.* Cell interaction with three-dimensional sharp-tip nanotopography. *Biomaterials* **28**, 1672–1679 (2007).
244. Hu, Y., You, J.-O. & Aizenberg, J. Micropatterned Hydrogel Surface with High-Aspect-Ratio Features for Cell Guidance and Tissue Growth. *ACS Appl. Mater. Interfaces* **8**, 21939–21945 (2016).
245. Larisch, W. *et al.* Proton beam writing of microstructures in Agar gel for patterned cell growth. *Nuclear Instruments and Methods in Physics Research Section B: Beam Interactions with Materials and Atoms* **269**, 2444–2447 (2011).
246. Wang, L., Liu, H., Zhang, F., Li, G. & Wang, S. Smart Thin Hydrogel Coatings Harnessing Hydrophobicity and Topography to Capture and Release Cancer Cells. *Small* **12**, 4697–4701 (2016).
247. Lin, S., Sangaj, N., Razafiarison, T., Zhang, C. & Varghese, S. Influence of physical properties of biomaterials on cellular behavior. *Pharm. Res.* **28**, 1422–1430 (2011).
248. Zhang, C., Aung, A., Liao, L. & Varghese, S. A novel single precursor-based biodegradable hydrogel with enhanced mechanical properties. *Soft Matter* **5**, 3831–3834 (2009).
249. Wozniak, M. A. & Chen, C. S. Mechanotransduction in development: a growing role for contractility. *Nat. Rev. Mol. Cell Biol.* **10**, 34–43 (2009).
250. Lo, C.-M., Wang, H.-B., Dembo, M. & Wang, Y. Cell Movement Is Guided by the Rigidity of the Substrate. *Biophysical Journal* **79**, 144–152 (2000).
251. Banerjee, A. *et al.* The influence of hydrogel modulus on the proliferation and differentiation of encapsulated neural stem cells. *Biomaterials* **30**, 4695–4699 (2009).
252. Zustiak, S. P. *et al.* Three-dimensional matrix stiffness and adhesive ligands affect cancer cell response to toxins. *Biotechnol. Bioeng.* **113**, 443–452 (2016).
253. Hadden, W. J. *et al.* Stem cell migration and mechanotransduction on linear stiffness gradient hydrogels. *PNAS* **114**, 5647–5652 (2017).
254. Lachowski, D. *et al.* Substrate Rigidity Controls Activation and Durotaxis in Pancreatic Stellate Cells. *Scientific Reports* **7**, 2506 (2017).
255. Lampi, M. C., Guvendiren, M., Burdick, J. A. & Reinhart-King, C. A. Photopatterned Hydrogels to Investigate the Endothelial Cell Response to Matrix Stiffness Heterogeneity. *ACS Biomater. Sci. Eng.* **3**, 3007–3016 (2017).
256. Davidson, P. M. *et al.* Topographically induced self-deformation of the nuclei of cells: dependence on cell type and proposed mechanisms. *J Mater Sci: Mater Med* **21**, 939–946 (2010).
257. Dupont, S. *et al.* Role of YAP/TAZ in mechanotransduction. *Nature* **474**, 179–183 (2011).
258. Low, B. C. *et al.* YAP/TAZ as mechanosensors and mechanotransducers in regulating organ size and tumor growth. *FEBS Letters* **588**, 2663–2670 (2014).
259. Wörz, A., Berchtold, B., Moosmann, K., Prucker, O. & Rühe, J. Protein-resistant polymer surfaces. *J. Mater. Chem.* **22**, 19547–19561 (2012).

260. Wörz, A., Berchtold, B., Moosmann, K., Prucker, O. & Rühe, J. Protein-resistant polymer surfaces. *J. Mater. Chem.* **22**, 19547–19561 (2012).
261. Kleber, C., Bruns, M., Lienkamp, K., Rühe, J. & Asplund, M. An interpenetrating, microstructurable and covalently attached conducting polymer hydrogel for neural interfaces. *Acta Biomaterialia* **58**, 365–375 (2017).
262. Discher, D. E., Janmey, P. & Wang, Y. Tissue Cells Feel and Respond to the Stiffness of Their Substrate. *Science* **310**, 1139–1143 (2005).
263. Xie, C. *et al.* Noninvasive Neuron Pinning with Nanopillar Arrays. *Nano Lett.* **10**, 4020–4024 (2010).
264. Gupta, M. *et al.* Adaptive rheology and ordering of cell cytoskeleton govern matrix rigidity sensing. *Nat Commun* **6**, 7525 (2015).
265. Elosegui-Artola, A. *et al.* Rigidity sensing and adaptation through regulation of integrin types. *Nat Mater* **13**, 631–637 (2014).
266. Vasiliev, J. M. Spreading of non-transformed and transformed cells. *Biochim. Biophys. Acta* **780**, 21–65 (1985).
267. Prager-Khoutorsky, M. *et al.* Fibroblast polarization is a matrix-rigidity-dependent process controlled by focal adhesion mechanosensing. *Nature Cell Biology* **13**, 1457–1465 (2011).
268. Solon, J., Levental, I., Sengupta, K., Georges, P. C. & Janmey, P. A. Fibroblast Adaptation and Stiffness Matching to Soft Elastic Substrates. *Biophys J* **93**, 4453–4461 (2007).
269. Ladoux, B., Mège, R.-M. & Trepat, X. Front–Rear Polarization by Mechanical Cues: From Single Cells to Tissues. *Trends Cell Biol* **26**, 420–433 (2016).
270. Zhang, Y.-H., Li, B., Shen, L., Shen, Y. & Chen, X.-D. The role and clinical significance of YES-associated protein 1 in human osteosarcoma. *Int J Immunopathol Pharmacol* **26**, 157–167 (2013).
271. Rana, D. *et al.* Surface functionalization of nanobiomaterials for application in stem cell culture, tissue engineering, and regenerative medicine. *Biotechnology Progress* **32**, 554–567 (2016).
272. Ferlay, J. *et al.* Estimates of worldwide burden of cancer in 2008: GLOBOCAN 2008. *Int. J. Cancer* **127**, 2893–2917 (2010).
273. Cervera, P. & Fléjou, J.-F. Changing pathology with changing drugs: tumors of the gastrointestinal tract. *Pathobiology* **78**, 76–89 (2011).
274. Astin, M., Griffin, T., Neal, R. D., Rose, P. & Hamilton, W. The diagnostic value of symptoms for colorectal cancer in primary care: a systematic review. *Br J Gen Pract* **61**, e231-243 (2011).
275. Davies, R. J., Miller, R. & Coleman, N. Colorectal cancer screening: prospects for molecular stool analysis. *Nature Reviews Cancer* **5**, 199–209 (2005).
276. Delavari, A. *et al.* Characteristics of Colorectal Polyps and Cancer; a Retrospective Review of Colonoscopy Data in Iran. *Middle East J Dig Dis* **6**, 144–150 (2014).
277. Kuipers, E. J. *et al.* COLORECTAL CANCER. *Nat Rev Dis Primers* **1**, 15065 (2015).
278. Tariq, K. & Ghias, K. Colorectal cancer carcinogenesis: a review of mechanisms. *Cancer Biol Med* **13**, 120–135 (2016).
279. Fearon, E. R. & Vogelstein, B. A genetic model for colorectal tumorigenesis. *Cell* **61**, 759–767 (1990).
280. Baker, S. J. *et al.* p53 gene mutations occur in combination with 17p allelic deletions as late events in colorectal tumorigenesis. *Cancer Res.* **50**, 7717–7722 (1990).
281. Weisenberger, D. J. *et al.* CpG island methylator phenotype underlies sporadic microsatellite

instability and is tightly associated with BRAF mutation in colorectal cancer. *Nat. Genet.* **38**, 787–793 (2006).
282. Rhee, Y.-Y., Kim, K.-J. & Kang, G. H. CpG Island Methylator Phenotype-High Colorectal Cancers and Their Prognostic Implications and Relationships with the Serrated Neoplasia Pathway. *Gut Liver* **11**, 38–46 (2017).
283. Sameer, A. S., Nissar, S. & Fatima, K. Mismatch repair pathway: molecules, functions, and role in colorectal carcinogenesis. *Eur. J. Cancer Prev.* **23**, 246–257 (2014).
284. Cooper, G. M. Tumor Suppressor Genes. *The Cell: A Molecular Approach. 2nd edition* (2000).
285. Fodde, R. The APC gene in colorectal cancer. *European Journal of Cancer* **38**, 867–871 (2002).
286. Powell, S. M. *et al.* APC mutations occur early during colorectal tumorigenesis. *Nature* **359**, 235–237 (1992).
287. Noubissi, F. K. *et al.* CRD-BP mediates stabilization of betaTrCP1 and c-myc mRNA in response to beta-catenin signalling. *Nature* **441**, 898–901 (2006).
288. Barth, A. I. M., Caro-Gonzalez, H. Y. & Nelson, W. J. Role of Adenomatous Polyposis Coli (APC) and Microtubules in Directional Cell Migration and Neuronal Polarization. *Semin Cell Dev Biol* **19**, 245–251 (2008).
289. Schell, M. J. *et al.* A multigene mutation classification of 468 colorectal cancers reveals a prognostic role for *APC*. *Nature Communications* **7**, 11743 (2016).
290. Subtil, C. *et al.* Frequent rearrangements and amplification of the CDX2 homeobox gene in human sporadic colorectal cancers with chromosomal instability. *Cancer Letters* **247**, 197–203 (2007).
291. Bonhomme, C. *et al.* The Cdx2 homeobox gene has a tumour suppressor function in the distal colon in addition to a homeotic role during gut development. *Gut* **52**, 1465–1471 (2003).
292. Dalerba, P. *et al.* CDX2 as a Prognostic Biomarker in Stage II and Stage III Colon Cancer. *New England Journal of Medicine* **374**, 211–222 (2016).
293. Brabletz, T. *et al.* Down-Regulation of the Homeodomain Factor Cdx2 in Colorectal Cancer by Collagen Type I: An Active Role for the Tumor Environment in Malignant Tumor Progression. *Cancer Res* **64**, 6973–6977 (2004).
294. Jean-No&euml & l Freund, I. D. Extending the functions of the homeotic transcription factor Cdx2 in the digestive system through nontranscriptional activities. *World Journal of Gastroenterology* **21**, 1436–1443 (2015).
295. Gross, I. *et al.* The intestine-specific homeobox gene *Cdx2* decreases mobility and antagonizes dissemination of colon cancer cells. *Oncogene* **27**, 107–115 (2008).
296. Funakoshi, S., Ezaki, T., Kong, J., Guo, R. J. & Lynch, J. P. Repression of the Desmocollin 2 Gene Expression in Human Colon Cancer Cells Is Relieved by the Homeodomain Transcription Factors Cdx1 and Cdx2. *Mol Cancer Res* **6**, 1478–1490 (2008).
297. Funakoshi, S. *et al.* Intestine-specific transcription factor Cdx2 induces E-cadherin function by enhancing the trafficking of E-cadherin to the cell membrane. *American Journal of Physiology-Gastrointestinal and Liver Physiology* **299**, G1054–G1067 (2010).
298. Coskun, M. *et al.* Involvement of CDX2 in the cross talk between TNF-α and Wnt signaling pathway in the colon cancer cell line Caco-2. *Carcinogenesis* **35**, 1185–1192 (2014).
299. Platet, N. *et al.* The tumor suppressor CDX2 opposes pro-metastatic biomechanical modifications of colon cancer cells through organization of the actin cytoskeleton. *Cancer Letters* **386**, 57–64 (2017).
300. Balbinot, C. *et al.* The Cdx2 homeobox gene suppresses intestinal tumorigenesis through

non–cell-autonomous mechanisms. *J Exp Med* **215**, 911–926 (2018).
301. Fodde, R., Smits, R. & Clevers, H. *APC*, Signal transduction and genetic instability in colorectal cancer. *Nature Reviews Cancer* **1**, 55–67 (2001).
302. Näthke, I. Cytoskeleton out of the cupboard: colon cancer and cytoskeletal changes induced by loss of APC. *Nature Reviews Cancer* **6**, 967–974 (2006).
303. Lam, W. A. *et al.* Extracellular matrix rigidity modulates neuroblastoma cell differentiation and N-myc expression. *Mol. Cancer* **9**, 35 (2010).
304. Wong, S. Y. *et al.* Constitutive activation of myosin-dependent contractility sensitizes glioma tumor-initiating cells to mechanical inputs and reduces tissue invasion. *Cancer Res.* **75**, 1113–1122 (2015).
305. Wang, X. *et al.* Alterations in mechanical properties are associated with prostate cancer progression. *Med. Oncol.* **31**, 876 (2014).
306. Weder, G. *et al.* Increased plasticity of the stiffness of melanoma cells correlates with their acquisition of metastatic properties. *Nanomedicine* **10**, 141–148 (2014).
307. Tang, X. *et al.* A mechanically-induced colon cancer cell population shows increased metastatic potential. *Mol. Cancer* **13**, 131 (2014).
308. Nukuda, A. *et al.* Stiff substrates increase YAP-signaling-mediated matrix metalloproteinase-7 expression. *Oncogenesis* **4**, e165 (2015).
309. Jabbari, E., Sarvestani, S. K., Daneshian, L. & Moeinzadeh, S. Optimum 3D Matrix Stiffness for Maintenance of Cancer Stem Cells Is Dependent on Tissue Origin of Cancer Cells. *PLOS ONE* **10**, e0132377 (2015).
310. Fernández-Sánchez, M. E. *et al.* Mechanical induction of the tumorigenic β-catenin pathway by tumour growth pressure. *Nature* **523**, 92–95 (2015).
311. Whitehead, J. *et al.* Mechanical factors activate beta-catenin-dependent oncogene expression in APC mouse colon. *HFSP J* **2**, 286–294 (2008).
312. Gargalionis, A. N. *et al.* Polycystin-1 and polycystin-2 are involved in the acquisition of aggressive phenotypes in colorectal cancer. *Int. J. Cancer* **136**, 1515–1527 (2015).
313. Avvisato, C. L. *et al.* Mechanical force modulates global gene expression and beta-catenin signaling in colon cancer cells. *J. Cell. Sci.* **120**, 2672–2682 (2007).
314. Yeung, T. M., Gandhi, S. C., Wilding, J. L., Muschel, R. & Bodmer, W. F. Cancer stem cells from colorectal cancer-derived cell lines. *Proc Natl Acad Sci U S A* **107**, 3722–3727 (2010).
315. Koppes, A. N. *et al.* Complex, multi-scale small intestinal topography replicated in cellular growth substrates fabricated via chemical vapor deposition of Parylene C. *Biofabrication* **8**, 035011 (2016).
316. Costello, C. M. *et al.* Synthetic small intestinal scaffolds for improved studies of intestinal differentiation. *Biotechnol. Bioeng.* **111**, 1222–1232 (2014).
317. Pachenari, M. *et al.* Mechanical properties of cancer cytoskeleton depend on actin filaments to microtubules content: Investigating different grades of colon cancer cell lines. *Journal of Biomechanics* **47**, 373–379 (2014).
318. Brunette, D. M. Spreading and orientation of epithelial cells on grooved substrata. *Exp. Cell Res.* **167**, 203–217 (1986).
319. Walczysko, P., Rajnicek, A. & Collinson, J. Contact-mediated control of radial migration of corneal epithelial cells. *Molecular Vision* **22**, 990–1004 (2016).
320. P. Soleas, J., K. Waddell, T. & P. McGuigan, A. Topographically grooved gel inserts for aligning epithelial cells during air–liquid-interface culture. *Biomaterials Science* **3**, 121–133 (2015).

321. Wu, T.-H. *et al.* Migration speed and directionality switch of normal epithelial cells after TGF-β1-induced EMT (tEMT) on micro-structured polydimethylsiloxane (PDMS) substrates with variations in stiffness and topographic patterning. *Cell Communication & Adhesion* **20**, 115–126 (2013).
322. Vedula, S. R. K. *et al.* Epithelial bridges maintain tissue integrity during collective cell migration. *Nature Materials* **13**, 87–96 (2014).
323. Saez, A., Buguin, A., Silberzan, P. & Ladoux, B. Is the Mechanical Activity of Epithelial Cells Controlled by Deformations or Forces? *Biophys J* **89**, L52–L54 (2005).
324. Xi, W., Sonam, S., Beng Saw, T., Ladoux, B. & Teck Lim, C. Emergent patterns of collective cell migration under tubular confinement. *Nat Commun* **8**, 1517 (2017).
325. Rother, J. *et al.* Cytoskeleton remodelling of confluent epithelial cells cultured on porous substrates. *Journal of The Royal Society Interface* **12**, 20141057 (2015).
326. Kim, M.-H., Sawada, Y., Taya, M. & Kino-oka, M. Influence of surface topography on the human epithelial cell response to micropatterned substrates with convex and concave architectures. *J Biol Eng* **8**, 13 (2014).
327. Nasrollahi, S. & Pathak, A. Topographic confinement of epithelial clusters induces epithelial-to-mesenchymal transition in compliant matrices. *Scientific Reports* **6**, 18831 (2016).
328. Davidson, P. The interaction of healthy and cancerous cells with nano- and microtopography; PhD dissertation, Mulhouse, University of Haute-Alsace (2011).
329. Benahmed, F. *et al.* The Microenvironment Controls CDX2 Homeobox Gene Expression in Colorectal Cancer Cells. *Am J Pathol* **170**, 733–744 (2007).
330. Tomita, N. *et al.* Isolation and characterization of a highly malignant variant of the SW480 human colon cancer cell line. *Cancer Res.* **52**, 6840–6847 (1992).
331. Turco, L. *et al.* Caco-2/TC7 cell line characterization for intestinal absorption: how reliable is this in vitro model for the prediction of the oral dose fraction absorbed in human? *Toxicol In Vitro* **25**, 13–20 (2011).
332. Brattain, M. G., Fine, W. D., Khaled, F. M., Thompson, J. & Brattain, D. E. Heterogeneity of Malignant Cells from a Human Colonic Carcinoma. *Cancer Res* **41**, 1751–1756 (1981).
333. Moss, S. F. *et al.* Decreased and aberrant nuclear lamin expression in gastrointestinal tract neoplasms. *Gut* **45**, 723–729 (1999).
334. Markiewicz, E. *et al.* The inner nuclear membrane protein emerin regulates beta-catenin activity by restricting its accumulation in the nucleus. *EMBO J.* **25**, 3275–3285 (2006).
335. Willis, N. D. *et al.* Lamin A/C Is a Risk Biomarker in Colorectal Cancer. *PLoS One* **3**, (2008).
336. Belt, E. J. T. *et al.* Loss of lamin A/C expression in stage II and III colon cancer is associated with disease recurrence. *Eur. J. Cancer* **47**, 1837–1845 (2011).
337. Izdebska, M., Gagat, M. & Grzanka, A. Overexpression of lamin B1 induces mitotic catastrophe in colon cancer LoVo cells and is associated with worse clinical outcomes. *Int J Oncol* **52**, 89–102 (2017).
338. Liu, L. *et al.* β-Asarone induces senescence in colorectal cancer cells by inducing lamin B1 expression. *Phytomedicine* **20**, 512–520 (2013).
339. Matsumoto, A. *et al.* Global loss of a nuclear lamina component, lamin A/C, and LINC complex components SUN1, SUN2, and nesprin-2 in breast cancer. *Cancer Med* **4**, 1547–1557 (2015).
340. Lv, X. *et al.* SUN2 exerts tumor suppressor functions by suppressing the Warburg effect in lung cancer. *Scientific Reports* **5**, 17940 (2015).
341. Swift, J. *et al.* Nuclear lamin-A scales with tissue stiffness and enhances matrix-directed

differentiation. *Science* **341**, 1240104 (2013).
342. Swift, J. *et al.* Nuclear lamin-A scales with tissue stiffness and enhances matrix-directed differentiation. *Science* **341**, 1240104 (2013).
343. Babbin, B. A. *et al.* Non-Muscle Myosin IIA Differentially Regulates Intestinal Epithelial Cell Restitution and Matrix Invasion. *Am J Pathol* **174**, 436–448 (2009).
344. Ivanov, A. I. *et al.* A Unique Role for Nonmuscle Myosin Heavy Chain IIA in Regulation of Epithelial Apical Junctions. *PLOS ONE* **2**, e658 (2007).
345. Zhao, B. *et al.* The non-muscle-myosin-II heavy chain Myh9 mediates colitis-induced epithelium injury by restricting Lgr5+ stem cells. *Nat Commun* **6**, 7166 (2015).
346. Ivanov, A. I. *et al.* Myosin II regulates the shape of three-dimensional intestinal epithelial cysts. *Journal of Cell Science* **121**, 1803–1814 (2008).
347. Huang, C.-C., Wu, D.-W., Lin, P.-L. & Lee, H. Paxillin promotes colorectal tumor invasion and poor patient outcomes via ERK-mediated stabilization of Bcl-2 protein by phosphorylation at Serine 87. *Oncotarget* **6**, 8698–8708 (2015).
348. Downey, C., Craig, D. H. & Basson, M. D. Pressure activates colon cancer cell adhesion via paxillin phosphorylation, Crk, Cas, and Rac1. *Cell Mol Life Sci* **65**, 1446–1457 (2008).
349. Doctor, R. B. The Actin Cytoskeleton in the Apical Domain of Epithelial Cells. in *Advances in Molecular and Cell Biology* **37**, 25–47 (Elsevier, 2006).
350. Zhao, X. *et al.* Class III β-Tubulin in Colorectal Cancer: Tissue Distribution and Clinical Analysis of Chinese Patients. *Med Sci Monit* **22**, 3915–3924 (2016).
351. Jirásek, T., Cipro, S., Musilová, A., Kubecová, M. & Mandys, V. Expression of class III beta-tubulin in colorectal carcinomas: an immunohistochemical study using TU-20 & TuJ-1 antibody. *Indian J. Med. Res.* **129**, 89–94 (2009).
352. Melling, N. *et al.* βIII-tubulin overexpression is linked to left-sided tumor localization and nuclear β-catenin expression in colorectal cancer. *Cancer Treatment Communications* **4**, 96–102 (2015).
353. Wu, S. *et al.* Bis-cyclopropane analog of disorazole C1 is a microtubule-destabilizing agent active in ABCB1-overexpressing human colon cancer cells. *Oncotarget* **6**, (2015).
354. Christou, N. *et al.* E-cadherin: A potential biomarker of colorectal cancer prognosis. *Oncol Lett* **13**, 4571–4576 (2017).
355. Kim, S. A. *et al.* Loss of CDH1 (E-cadherin) expression is associated with infiltrative tumour growth and lymph node metastasis. *Br J Cancer* **114**, 199–206 (2016).
356. Alibert, C., Goud, B. & Manneville, J.-B. Are cancer cells really softer than normal cells? *Biol. Cell* **109**, 167–189 (2017).
357. Weiss, L. *Histology: cell and tissue biology*. (Elsevier Biomedical, 1983).
358. Kahle, W., Leonhardt, H., Platzer, W. & Palmer, E. *Color Atlas and Textbook of Human Anatomy: Internal organs*. (Year Book Medical Publishers, 1978).
359. Ghibaudo, M. *et al.* Substrate Topography Induces a Crossover from 2D to 3D Behavior in Fibroblast Migration. *Biophys J* **97**, 357–368 (2009).
360. Salomon, J. *et al.* Contractile forces at tricellular contacts modulate epithelial organization and monolayer integrity. *Nature Communications* **8**, 13998 (2017).
361. Keeling, M. C., Flores, L. R., Dodhy, A. H., Murray, E. R. & Gavara, N. Actomyosin and vimentin cytoskeletal networks regulate nuclear shape, mechanics and chromatin organization. *Scientific Reports* **7**, 5219 (2017).
362. Pawelzyk, P., Mücke, N., Herrmann, H. & Willenbacher, N. Attractive interactions among

intermediate filaments determine network mechanics in vitro. *PLoS ONE* **9**, e93194 (2014).
363. Janmey, P. A. Mechanical properties of cytoskeletal polymers. *Current opinion in cell biology* **3**, 4–11 (1991).
364. Kreplak, L., Bär, H., Leterrier, J. F., Herrmann, H. & Aebi, U. Exploring the mechanical behavior of single intermediate filaments. *J. Mol. Biol.* **354**, 569–577 (2005).
365. Mendez, M. G., Restle, D. & Janmey, P. A. Vimentin Enhances Cell Elastic Behavior and Protects against Compressive Stress. *Biophys J* **107**, 314–323 (2014).
366. Guo, M. *et al.* The role of vimentin intermediate filaments in cortical and cytoplasmic mechanics. *Biophys. J.* **105**, 1562–1568 (2013).
367. Burgstaller, G., Gregor, M., Winter, L. & Wiche, G. Keeping the vimentin network under control: cell-matrix adhesion-associated plectin 1f affects cell shape and polarity of fibroblasts. *Mol. Biol. Cell* **21**, 3362–3375 (2010).
368. Vergnes, L., Péterfy, M., Bergo, M. O., Young, S. G. & Reue, K. Lamin B1 is required for mouse development and nuclear integrity. *Proc. Natl. Acad. Sci. U.S.A.* **101**, 10428–10433 (2004).
369. Butin-Israeli, V., Adam, S. A., Goldman, A. E. & Goldman, R. D. Nuclear Lamin Functions and Disease. *Trends Genet* **28**, 464–471 (2012).
370. Schirmer, E. C. & Foisner, R. Proteins that associate with lamins: many faces, many functions. *Exp. Cell Res.* **313**, 2167–2179 (2007).
371. Stewart, C. L., Roux, K. J. & Burke, B. Blurring the boundary: the nuclear envelope extends its reach. *Science* **318**, 1408–1412 (2007).
372. Stephens, A. D., Banigan, E. J., Adam, S. A., Goldman, R. D. & Marko, J. F. Chromatin and lamin A determine two different mechanical response regimes of the cell nucleus. *Mol Biol Cell* **28**, 1984–1996 (2017).
373. Schreiner, S. M., Koo, P. K., Zhao, Y., Mochrie, S. G. J. & King, M. C. The tethering of chromatin to the nuclear envelope supports nuclear mechanics. *Nature Communications* **6**, 7159 (2015).
374. Haase, K. *et al.* Extracellular Forces Cause the Nucleus to Deform in a Highly Controlled Anisotropic Manner. *Scientific Reports* **6**, 21300 (2016).
375. Lehoux, S., Castier, Y. & Tedgui, A. Molecular mechanisms of the vascular responses to haemodynamic forces. *J. Intern. Med.* **259**, 381–392 (2006).
376. Grespan, E. *et al.* Effect of geometrical constraints on human pluripotent stem cell nuclei in pluripotency and differentiation. *Integr. Biol.* **10**, 278–289 (2018).
377. Liu, X., Liu, R., Gu, Y. & Ding, J. Nonmonotonic Self-Deformation of Cell Nuclei on Topological Surfaces with Micropillar Array. *ACS Appl. Mater. Interfaces* **9**, 18521–18530 (2017).
378. Le Berre, M., Aubertin, J. & Piel, M. Fine control of nuclear confinement identifies a threshold deformation leading to lamina rupture and induction of specific genes. *Integr Biol (Camb)* **4**, 1406–1414 (2012).
379. Irianto, J. *et al.* Constricted cell migration causes nuclear lamina damage, DNA breaks, and squeeze-out of repair factors. *bioRxiv* 035626 (2015). doi:10.1101/035626
380. Irianto, J. *et al.* DNA Damage Follows Repair Factor Depletion and Portends Genome Variation in Cancer Cells after Pore Migration. *Current Biology* **27**, 210–223 (2017).
381. Jung, U., Kan, T., Kuwana, K., Matsumoto, K. & Shimoyama, I. Si nano-pillars for measuring traction force exerted by filopodia. in *2011 16th International Solid-State Sensors, Actuators and Microsystems Conference* 2754–2757 (2011). doi:10.1109/TRANSDUCERS.2011.5969359
382. Tan, J. L. *et al.* Cells lying on a bed of microneedles: An approach to isolate mechanical force. *PNAS* **100**, 1484–1489 (2003).

383. Jorrisch, M. H., Shih, W. & Yamada, S. Myosin IIA deficient cells migrate efficiently despite reduced traction forces at cell periphery. *Biol Open* **2**, 368–372 (2013).
384. Baker, B. M. & Chen, C. S. Deconstructing the third dimension: how 3D culture microenvironments alter cellular cues. *J. Cell. Sci.* **125**, 3015–3024 (2012).
385. Duval, K. *et al.* Modeling Physiological Events in 2D vs. 3D Cell Culture. *Physiology (Bethesda)* **32**, 266–277 (2017).
386. Riedl, A. *et al.* Comparison of cancer cells in 2D vs 3D culture reveals differences in AKT–mTOR–S6K signaling and drug responses. *J Cell Sci* **130**, 203–218 (2017).
387. Kim, H. N. & Kim, J. Effect of Topographical Feature Size on the Trend of Cell Behaviors. *IEEE Transactions on Nanotechnology* **17**, 377–380 (2018).
388. Goli-Malekabadi, Z., Tafazzoli-Shadpour, M. & Seyedjafari, E. Effects of substrate deformability on cell behaviors: elastic modulus versus thickness. *J. Mech. Med. Biol.* **17**, 1750088 (2017).
389. Chesmel, K. D., Clark, C. C., Brighton, C. T. & Black, J. Cellular responses to chemical and morphologic aspects of biomaterial surfaces. II. The biosynthetic and migratory response of bone cell populations. *J. Biomed. Mater. Res.* **29**, 1101–1110 (1995).
390. van Kooten, T. G., Spijker, H. T. & Busscher, H. J. Plasma-treated polystyrene surfaces: model surfaces for studying cell-biomaterial interactions. *Biomaterials* **25**, 1735–1747 (2004).
391. Hallab, N. J., Bundy, K. J., O'Connor, K., Clark, R. & Moses, R. L. Cell adhesion to biomaterials: correlations between surface charge, surface roughness, adsorbed protein, and cell morphology. *J Long Term Eff Med Implants* **5**, 209–231 (1995).
392. Ventre, M., Causa, F. & Netti, P. A. Determinants of cell–material crosstalk at the interface: towards engineering of cell instructive materials. *J R Soc Interface* **9**, 2017–2032 (2012).
393. Nguyen, A. T., Sathe, S. R. & Yim, E. K. F. From nano to micro: topographical scale and its impact on cell adhesion, morphology and contact guidance. *J. Phys.: Condens. Matter* **28**, 183001 (2016).
394. Anselme, K. & Bigerelle, M. Role of materials surface topography on mammalian cell response. *International Materials Reviews* **56**, 243–266 (2011).
395. Tabata, Y., Horiguchi, I., Lutolf, M. P. & Sakai, Y. Development of bioactive hydrogel capsules for the 3D expansion of pluripotent stem cells in bioreactors. *Biomater. Sci.* **2**, 176–183 (2013).
396. Tabata, Y. & Lutolf, M. P. Multiscale microenvironmental perturbation of pluripotent stem cell fate and self-organization. *Scientific Reports* **7**, 44711 (2017).
397. Gjorevski, N. & Lutolf, M. P. Well-defined matrices for the expansion of intestinal stem cells and organoids. (2017).
398. Jacot, J. G., McCulloch, A. D. & Omens, J. H. Substrate stiffness affects the functional maturation of neonatal rat ventricular myocytes. *Biophys. J.* **95**, 3479–3487 (2008).
399. Kim, T.-J. *et al.* Substrate rigidity regulates Ca2+ oscillation via RhoA pathway in stem cells. *J. Cell. Physiol.* **218**, 285–293 (2009).
400. Meacci, G. *et al.* α-Actinin links extracellular matrix rigidity-sensing contractile units with periodic cell-edge retractions. *Mol Biol Cell* **27**, 3471–3479 (2016).
401. Collins, C., Denisin, A. K., Pruitt, B. L. & Nelson, W. J. Changes in E-cadherin rigidity sensing regulate cell adhesion. *PNAS* 201618676 (2017). doi:10.1073/pnas.1618676114
402. Giannone, G. & Sheetz, M. P. Substrate rigidity and force define form through tyrosine phosphatase and kinase pathways. *Trends Cell Biol.* **16**, 213–223 (2006).
403. Huang, X. *et al.* Matrix stiffness-induced myofibroblast differentiation is mediated by intrinsic mechanotransduction. *Am. J. Respir. Cell Mol. Biol.* **47**, 340–348 (2012).

404. Bae, Y. H. *et al.* A FAK-Cas-Rac-lamellipodin signaling module transduces extracellular matrix stiffness into mechanosensitive cell cycling. *Sci Signal* **7**, ra57 (2014).
405. Chaudhuri, O. *et al.* Extracellular matrix stiffness and composition jointly regulate the induction of malignant phenotypes in mammary epithelium. *Nat Mater* **13**, 970–978 (2014).
406. Kenny, F. N. *et al.* Tissue stiffening promotes keratinocyte proliferation through activation of epidermal growth factor signaling. *J Cell Sci* **131**, jcs215780 (2018).
407. Dalby, M. J., Riehle, M. O., Yarwood, S. J., Wilkinson, C. D. W. & Curtis, A. S. G. Nucleus alignment and cell signaling in fibroblasts: response to a micro-grooved topography. *Experimental Cell Research* **284**, 272–280 (2003).
408. Dalby, M. J. *et al.* Attempted endocytosis of nano-environment produced by colloidal lithography by human fibroblasts. *Exp. Cell Res.* **295**, 387–394 (2004).
409. Galic, M. *et al.* External push and internal pull forces recruit curvature-sensing N-BAR domain proteins to the plasma membrane. *Nat. Cell Biol.* **14**, 874–881 (2012).
410. Teo, B. K. K. *et al.* The effect of micro and nanotopography on endocytosis in drug and gene delivery systems. *Biomaterials* **32**, 9866–9875 (2011).
411. Mumm, F., Beckwith, K. M., Bonde, S., Martinez, K. L. & Sikorski, P. A transparent nanowire-based cell impalement device suitable for detailed cell-nanowire interaction studies. *Small* **9**, 263–272 (2013).
412. Persson, H. *et al.* Fibroblasts cultured on nanowires exhibit low motility, impaired cell division, and DNA damage. *Small* **9**, 4006–4016, 3905 (2013).
413. Santoro, F. *et al.* Revealing the Cell–Material Interface with Nanometer Resolution by Focused Ion Beam/Scanning Electron Microscopy. *ACS Nano* **11**, 8320–8328 (2017).
414. Beningo, K. A., Lo, C.-M. & Wang, Y.-L. Flexible polyacrylamide substrata for the analysis of mechanical interactions at cell-substratum adhesions. *Methods Cell Biol.* **69**, 325–339 (2002).
415. Saha, K. *et al.* Substrate modulus directs neural stem cell behavior. *Biophys. J.* **95**, 4426–4438 (2008).
416. Eroshenko, N., Ramachandran, R., Yadavalli, V. K. & Rao, R. R. Effect of substrate stiffness on early human embryonic stem cell differentiation. *Journal of Biological Engineering* **7**, 7 (2013).
417. Dalby, M. J. *et al.* The control of human mesenchymal cell differentiation using nanoscale symmetry and disorder. *Nat Mater* **6**, 997–1003 (2007).
418. Ji, L., LaPointe, V. L. S., Evans, N. D. & Stevens, M. M. Changes in embryonic stem cell colony morphology and early differentiation markers driven by colloidal crystal topographical cues. *Eur Cell Mater* **23**, 135–146 (2012).
419. Sonam, S., Sathe, S. R., Yim, E. K. F., Sheetz, M. P. & Lim, C. T. Cell contractility arising from topography and shear flow determines human mesenchymal stem cell fate. *Scientific Reports* **6**, 20415 (2016).
420. Kong, Y. P., Tu, C. H., Donovan, P. J. & Yee, A. F. Expression of Oct4 in human embryonic stem cells is dependent on nanotopographical configuration. *Acta Biomater* **9**, 6369–6380 (2013).
421. Abagnale, G. *et al.* Surface topography enhances differentiation of mesenchymal stem cells towards osteogenic and adipogenic lineages. *Biomaterials* **61**, 316–326 (2015).
422. Qi, L. *et al.* The Effects of Topographical Patterns and Sizes on Neural Stem Cell Behavior. *PLOS ONE* **8**, e59022 (2013).
423. Harland, B., Walcott, S. & Sun, S. X. Adhesion dynamics and durotaxis in migrating cells. *Phys. Biol.* **8**, 015011 (2011).
424. Sarvestani, A. S. On the Effect of Substrate Compliance on Cellular Motility. *Journal of*

Biosensors & Bioelectronics **2**, 1–5 (2010).
425. Ng, M. R., Besser, A., Danuser, G. & Brugge, J. S. Substrate stiffness regulates cadherin-dependent collective migration through myosin-II contractility. *J Cell Biol* jcb.201207148 (2012). doi:10.1083/jcb.201207148
426. Evans, E. B., Brady, S. W., Tripathi, A. & Hoffman-Kim, D. Schwann cell durotaxis can be guided by physiologically relevant stiffness gradients. *Biomaterials Research* **22**, 14 (2018).
427. Kanaan, Z., Qadan, M., Eichenberger, M. R. & Galandiuk, S. The actin-cytoskeleton pathway and its potential role in inflammatory bowel disease-associated human colorectal cancer. *Genet Test Mol Biomarkers* **14**, 347–353 (2010).
428. Steinestel, K., Wardelmann, E., Hartmann, W. & Grünewald, I. Regulators of Actin Dynamics in Gastrointestinal Tract Tumors. *Gastroenterology Research and Practice* (2015). doi:10.1155/2015/930157
429. Misiorek, J. O. The role of keratin intermediate filaments in the colon epithelial cells. (2016).
430. Lähdeniemi, I. A. K. *et al.* Keratins regulate colonic epithelial cell differentiation through the Notch1 signalling pathway. *Cell Death and Differentiation* **24**, 984–996 (2017).